

**University of Alberta**

**Library Release Form**

**Name of Author:** Andrew Garnet Corkum

**Title of Thesis:** Non-Linear Behaviour of Opalinus Clay Around Underground Excavations

**Degree:** Doctor of Philosophy

**Year this Degree Granted:** 2006

Permission is hereby granted to the University of Alberta Library to reproduce single copies of this thesis and to lend or sell such copies for private, scholarly or scientific research purposes only.

The author reserves all other publication and other rights in association with the copyright in the thesis, and except as herein before provided, neither the thesis nor any substantial portion thereof may be printed or otherwise reproduced in any material form whatever without the author's prior written permission.

---

Andrew Garnet Corkum

**Date:** \_\_\_\_\_

*The art of modelling lies in determining what aspects of the geology  
are essential for the model.*

– Starfield and Cundall, 1988.

**University of Alberta**

NON-LINEAR BEHAVIOUR OF OPALINUS CLAY AROUND UNDERGROUND  
EXCAVATIONS

by

**Andrew Garnet Corkum**

A thesis submitted to the Faculty of Graduate Studies and Research in partial fulfillment of the requirements for the degree of **Doctor of Philosophy**.

in

Geotechnical Engineering

Department of Civil & Environmental Engineering

Edmonton, Alberta  
Fall 2006

**University of Alberta**

**Faculty of Graduate Studies and Research**

The undersigned certify that they have read, and recommend to the Faculty of Graduate Studies and Research for acceptance, a thesis entitled **Non-Linear Behaviour of Opalinus Clay Around Underground Excavations** submitted by Andrew Garnet Corkum in partial fulfillment of the requirements for the degree of **Doctor of Philosophy**.

---

Dr. C.D. Martin

---

Dr. W.F. Bawden

---

Dr. N.R. Morgenstern

---

Dr. R.J. Chalaturnyk

---

Dr. O. Leuangthong

---

Dr. C.F. Lange

**Date:** \_\_\_\_\_

# Dedication

*To my mother Faye, my father George and  
my wife Jocelyn.*

# Abstract

Over the last 10 years argillaceous rocks (mudrocks) have gained acceptance as a potential host formation for geological disposal of nuclear waste. Much of the engineering experience with soft argillaceous rocks has been developed over the past 50 years from the civil engineering construction of dams and slopes, all of which take place at relatively shallow depths. The construction of a nuclear waste repository, however, will take place at depths greater than 400 m. With that in mind, it is essential to develop a strong understanding of the engineering behaviour of this material.

In Switzerland, the Jurassic claystone Opalinus Clay is being considered as a potential repository host formation. Observations from tunnels in Opalinus Clay at the Mont Terri rock laboratory, Switzerland, suggest that the excavation-induced response is not linear-elastic in the classic sense, and therefore, the use of linear-elasticity can lead to significant misrepresentation of rockmass deformations and yield mechanisms around underground excavations.

The fundamental nature of the Opalinus Clay's micro-structure has been identified as a source for its unique behaviour. A conceptual model of the micro-structure, including the effects of diagenetic processes, has been developed as a framework to interpret the mechanical and hydromechanical behaviour of the Opalinus Clay. This rockmass response has been captured by a phenomenological-based model, known as the stress-dependent modulus (SDM) model, and a piece-wise pore pressure formulation. This allows engineers to capture a significant portion of the observed behaviour without undue modelling complexities using data from simple unconfined and triaxial compression tests.

A comparison of the two models with geophysical measurements and piezome-

ter readings in the vicinity of excavations at the Mont Terri rock laboratory provides encouraging agreement. Furthermore, numerical back-analysis of the ED-B mine-by test, conducted at Mont Terri in 1997-98, demonstrated that the unique pore pressure response and unloading-induced large deformations could be accounted for by these models.

# Acknowledgements

The author would like to express his sincere gratitude to some of the generous individuals whose support has been greatly appreciated.

Dr. C.D. Martin provided guidance, patience and contagious enthusiasm in supervising the research effort. Dr. P. Blümling offered his insight into the Mont Terri project and the Opalinus Clay. Funding has been generously provided by NAGRA (Switzerland). Dr. N.R. Morgenstern provided a key suggestion regarding the role of diagenesis in the behaviour of argillaceous rocks.

Many professors and fellow graduate students at the University of Alberta have contributed to the value of this experience. Most notably, Jaime Jiménez Gómez took the time for many stimulating discussions. Steve Gamble provided invaluable assistance with acquiring and setting up equipment for the laboratory testing programme. The manuscript was kindly reviewed by Judith MacLean.



# Table of Contents

<b>1</b>	<b>Introduction</b>	<b>1</b>
1.1	Repository Tunnels . . . . .	1
1.2	Argillaceous Rocks . . . . .	5
1.3	Opalinus Clay . . . . .	9
1.4	Mont Terri Rock Laboratory . . . . .	13
1.5	Overview of Research Project . . . . .	17
1.6	Organization of Dissertation . . . . .	19
	Bibliography . . . . .	20
<b>2</b>	<b>Mechanical Behaviour of Weak Mudstone (Opalinus Clay) at low stresses</b>	<b>26</b>
2.1	Introduction . . . . .	26
2.2	Background . . . . .	29
	2.2.1 Properties of Opalinus Clay . . . . .	31
	2.2.2 Diagenesis and the Behaviour of Opalinus Clay . . . . .	34
2.3	Laboratory Stress-Strain Behaviour . . . . .	38
	2.3.1 Uniaxial Test Results . . . . .	39
	2.3.2 Triaxial Test Results . . . . .	45
	2.3.3 Summary . . . . .	46
2.4	Sample Stress Path . . . . .	46
	2.4.1 Sample Disturbance at Mont Terri . . . . .	47
	2.4.2 Sampling Stress Path at Mont Terri . . . . .	49
2.5	Discussion and Interpretation . . . . .	53
2.6	Conclusions . . . . .	56
	Bibliography . . . . .	57
<b>3</b>	<b>Phenomenological models for stiffness and pore pressure around tunnels in soft argillaceous rock</b>	<b>62</b>
3.1	Introduction . . . . .	62
3.2	Background . . . . .	64
3.3	SDM Model for Opalinus Clay . . . . .	68
	3.3.1 Model Development . . . . .	69
	3.3.2 Verification and Comparison . . . . .	72
	3.3.3 Discussion . . . . .	77
3.4	Simplified Model of Pore Pressure Response . . . . .	78
3.5	Summary and Conclusions . . . . .	82
	Bibliography . . . . .	82
<b>4</b>	<b>Modelling a mine-by test at the Mont Terri rock laboratory, Switzerland</b>	<b>86</b>
4.1	Introduction . . . . .	86
4.2	Background . . . . .	88

4.3	ED-B Mine-by Test . . . . .	91
4.4	Modelling the Mine-by Test . . . . .	93
4.4.1	Modelling Methodology . . . . .	93
4.4.2	Model Geometry . . . . .	95
4.4.3	In-Situ Stresses and Boundary Conditions . . . . .	96
4.4.4	Material Properties . . . . .	98
4.4.5	Constitutive Models . . . . .	99
4.4.6	Pore Pressure Formulation . . . . .	101
4.5	Modelling Results and Comparison . . . . .	102
4.5.1	Borehole Deformation Instruments . . . . .	103
4.5.2	Convergence Arrays . . . . .	106
4.5.3	Piezometer Measurements . . . . .	110
4.6	Conclusions . . . . .	112
	Bibliography . . . . .	113
<b>5</b>	<b>Summary and Conclusions</b>	<b>116</b>
5.1	Recommendations for Future Research . . . . .	118
	Bibliography . . . . .	119
<b>A</b>	<b>Modelling the Short-term Behaviour of Opalinus Clay Around a Circular Excavation</b>	<b>121</b>
A.1	Introduction . . . . .	121
A.2	Overview of Opalinus Clay . . . . .	122
A.3	Mont Terri Rock Laboratory . . . . .	123
A.3.1	Geological Setting . . . . .	123
A.3.2	In-situ Stresses . . . . .	125
A.4	Mine-by Experiment . . . . .	125
A.5	Numerical Modelling . . . . .	128
A.5.1	Modelling Methodology . . . . .	129
A.5.2	Model Parameters . . . . .	130
A.6	Results and Comparison . . . . .	130
A.7	Discussion . . . . .	134
A.8	Summary and Conclusions . . . . .	136
	Bibliography . . . . .	137
<b>B</b>	<b>In-Situ Stresses at Mont Terri Rock Laboratory</b>	<b>139</b>
	Bibliography . . . . .	144
<b>C</b>	<b>Borehole breakout development at Mont Terri rock laboratory: 2004 field study</b>	<b>146</b>
C.1	Introduction . . . . .	146
C.2	Background . . . . .	147
C.2.1	Opalinus Clay . . . . .	147
C.2.2	Mont Terri Rock Laboratory . . . . .	148
C.3	Borehole Mapping Methodology . . . . .	150
C.4	Findings and Interpretation . . . . .	151
C.5	Summary and Conclusions . . . . .	155
	Bibliography . . . . .	156

<b>D</b>	<b>Field Program: Mont Terri Report (May 2004)</b>	<b>158</b>
D.1	Introduction . . . . .	158
D.2	Mont Terri Field Programme . . . . .	160
D.2.1	Mapping of Starter Niche . . . . .	160
D.2.2	Mapping of Shotcrete Damage . . . . .	164
D.2.3	Mapping of Borehole Breakouts . . . . .	170
D.2.4	Observations from Waste Pile and Core Disking . . . . .	175
D.3	Pending Research Tasks . . . . .	178
D.4	Summary . . . . .	179
	Bibliography . . . . .	180
<b>E</b>	<b>Field Program: Shotcrete Crack Mapping</b>	<b>181</b>
<b>F</b>	<b>Field Program: Borehole Breakout Field Sketches</b>	<b>190</b>

# List of Tables

1.1	Index properties of Opalinus Clay [33]. . . . .	11
2.1	Typical mineral composition of Opalinus Clay (from Thury and Bossart [10]). . . . .	32
2.2	Index properties of Opalinus Clay (from Bock [16]). . . . .	32
2.3	Strength and deformation properties of Opalinus Clay (from Bock [16]). . . . .	33
4.1	Magnitude and orientation of the stress tensor [8]. . . . .	97
4.2	Average isotropic mechanical properties of Opalinus Clay used in the numerical model [12]. . . . .	98
A.1	Index properties of Opalinus Clay [3]. . . . .	123
A.2	Index properties of Opalinus Clay [3]. . . . .	130
B.1	Magnitude and orientation of the modified stress tensor at Mont Terri rock laboratory. . . . .	143
C.1	Index properties of Opalinus Clay [4]. . . . .	148
D.1	Boreholes mapped during field programme. . . . .	171

# List of Figures

1.1	Conceptual illustration of a high-level waste repository with surface facilities, access ramp and the main system of emplacement drifts (available at <a href="http://www.mont-terri.ch">www.mont-terri.ch</a> ). . . . .	2
1.2	The excavation disturbed (EdZ) and excavation damaged zone (EDZ) around repository tunnels result in the development of preferential flow paths. . . . .	3
1.3	The Opalinus Clay is named for the ammonite <i>Leioceras Opalinum</i> , commonly found in the formation. . . . .	10
1.4	Classification of argillaceous materials [23]. . . . .	10
1.5	Water content has a significant effect on the shear strength and the elastic Young's modulus of Opalinus Clay based on triaxial tests at high confining stress ( $\sigma_3 = 10$ MPa). Data provided by Rummel et al. [35]. . . . .	12
1.6	Looking towards the northwest along the Security Gallery. . . . .	14
1.7	Location of Mont Terri rock laboratory. . . . .	15
1.8	Cracking and debonding of shotcrete in the roof of the Starter Niche at Mont Terri more than a week after installation. This demonstrates the time-dependent behaviour of tunnels in Opalinus Clay. . . . .	16
1.9	Temperature and humidity in the Mont Terri rock laboratory during excavation of the ED-B mine-by test tunnel. Julian day 1 is January 1, 1998 (modified from Martin and Lanyon [38]). . . . .	17
2.1	Map showing Mont Terri rock laboratory near the town of St. Ursanne in northwestern Switzerland (modified from <a href="http://www.mont-terri.ch">www.mont-terri.ch</a> ). . . . .	27
2.2	Illustration of the effects of open micro-cracks on the stress-strain curve of an unconfined compression test. . . . .	28
2.3	Geological section along A16 Transjurane motorway (from Freivogel and Huggenberger [9]). Mont Terri is an asymmetrical anticline folded during the Late Miocene to Pliocene period. The rock laboratory is located within the Opalinus Clay unit that dips approximately $45^\circ$ southeast. . . . .	30
2.4	Typical mineral composition of the Opalinus Clay at Mont Terri. . . . .	32
2.5	The Opalinus Clay structure is highly oriented, parallel to bedding. Clay platelets are generally bent and the presence of quartz grains can be seen in the clay matrix. Image width is $134 \mu\text{m}$ (Möri and Bossart [17]). . . . .	33
2.6	Types of bonding for solid materials (from Diederichs [20]). The nature of bonding can determine the mode of yielding and macro-behaviour. . . . .	34
2.7	Geological history of overconsolidated clays (modified from Bjerum [24]). . . . .	36

2.8	Sedimentation compression curves compiled for normally consolidated argillaceous sediments (modified from Skempton [25]). The Opalinus Clay is at the upper limit of the original curves. Points A <sub>1</sub> and B correspond to stages of compaction for Opalinus Clay as illustrated in Fig. 2.7. Diagenetic processes resulted in a 9 % decrease in porosity (35 % change).	37
2.9	The full stress-strain response of Opalinus Clay in unconfined compression using a servo-controlled testing apparatus. The four regions of the stress-strain curve are approximately defined (Sample 2-22-2p, tested by Rummel [27]).	39
2.10	Stress-strain plots from unconfined compression tests. The samples have significant low stiffness, non-linear response at low stress levels.	41
2.11	The effect of micro-cracks on UCS relative to low stress stiffness and seismic shear wave velocity. (Data from Olalla et al. [29].)	42
2.12	Axial stress vs. axial and lateral strain for unconfined compression tests on a P-samples (parallel to bedding) with lateral strain measurements using LVDTs. (Data from Olalla et al. [29].)	44
2.13	Cyclic axial loading to increased stress levels for sample BRA-1/3b. Non-linearity at low stress levels is repeated (recoverable) in each cycle. The lack of decreased stiffness with each cycle indicates damage due to deviatoric loading is not significant.	44
2.14	Stress-strain plots for a range of $\sigma_3$ values (0-20 MPa). The increased stiffness with confinement indicates the presence of micro-cracks. All samples show a brittle post-peak response, even at $\sigma_3 = 20$ MPa. (Data from Olalla et al. [29])	46
2.15	Core diskings was generally only observed during the overcoring program. No diskings in the section where the strain gage was placed, indicating that very small confining stress can affect diskings.	48
2.16	A cutaway of the three-dimensional finite difference model (FLAC <sup>3D</sup> ) and stress field used to simulate excavation of a core at the Mont Terri rock laboratory.	50
2.17	Stress path along a core and borehole/tunnel wall during sampling from elastic stress analysis (FLAC <sup>3D</sup> ) indicates that the stress-induced cause of sample disturbance in Opalinus Clay is dominated by unloading processes.	52
2.18	Micro-structure of the Opalinus Clay based on geological history.	54
2.19	Non-linear elastic Young's modulus related to stress levels ( $\sigma_1, \sigma_3$ ). Sample 2-22-2p used for low stress $\sigma_1$ portion.	56
3.1	Stress-strain plots from unconfined compression tests carried out by Olalla et al. [4]. The samples have significant low stiffness, non-linear response at low stress levels.	63
3.2	Stress path along a circular tunnel springline and roofline calculated with linear-elasticity ( $X/D > 0$ ahead of the tunnel face). The stress path along a core sample centreline undergoes similar unloading.	65
3.3	Maximum cumulative displacements from inclinometer measurements along Borehole BED B-6 located above the ED-B tunnel.	65
3.4	System of EDZ extensional fractures oriented parallel to the tunnel observed in the FM-C Niche at Mont Terri. These fractures are typical of those observed in the EDZ around tunnels at Mont Terri.	66
3.5	Pore pressure measurements near the tunnel springline during the ED-B mine-by test show an abrupt drop in pore pressure behind the excavation face. This response cannot be predicted by conventional hydromechanical means.	67

3.6	Based on stress path, tunnel behaviour is analogous to triaxial compression testing. Engineers are typically most interested in radial strain that is analogous to triaxial extension testing and corresponds to the non-linear portion (low stress) of the stress-strain curve for Opalinus Clay. . . . .	69
3.7	The non-linear elastic constitutive behaviour was derived from the combined triaxial-uniaxial stress-modulus data. This was scaled-up to pass through the in-situ condition. Triaxial data provided by Olalla et al. [4]; UCS test data (Sample 2-22-2: used for low stress $\sigma_1$ relation) provided by Rummel [17]. . . . .	71
3.8	Ratio of unload-reload cycle stiffness to tangent modulus stiffness is representative of the relationship between dynamic to static modulus. A typical uniaxial test (Sample 2-22-2p) was used to estimate this ratio for Opalinus Clay. . . . .	73
3.9	Stress analysis of EB-Niche from 2-D finite element model (Phase <sup>2</sup> ). Borehole BED-B10 is located in a zone of unloading. . . . .	74
3.10	The effects of unloading on the distribution of stiffness properties differ significantly from the constant modulus typically used in numerical analyses. Both SDM models fit the trend of measured values while the scaled-up SDM model shows a better fit. Data provided by K. Schuster (pers. comm.). . . . .	75
3.11	Comparison of calculated tangential stresses around an excavation ( $P_o = 100$ MPa). The FLAC <sup>3D</sup> solution considers stress path and understandably differs significantly from the closed-form solution. . . . .	76
3.12	Non-linear stress-strain response and strain incompatibility resulting in extensional fractures. This non-linearity can impose up to 2 MPa of tensile stress onto the localized rockmass when completely unloaded. . . . .	77
3.13	Stress release induces micro-cracks in the rockmass resulting in a dilatant pore pressure response. Dilation is suppressed at $\sigma_3 = 2.2$ MPa, therefore, at $\sigma_3 = 0 \Rightarrow \Delta u = -2.2$ MPa. . . . .	79
3.14	A piece-wise pore pressure formulation based on the rationale behind the SDM model agrees well with the measured trends and magnitudes of pore pressure development. Pore pressures calculated at a tunnel springline with the Mont Terri stress field. . . . .	81
4.1	Map showing Mont Terri rock laboratory near the town of St. Ursanne in northwestern Switzerland (modified from <a href="http://www.mont-terri.ch">www.mont-terri.ch</a> ). . . . .	87
4.2	In-situ experiments at Mont Terri rock laboratory are conducted in isolated niches excavated into the sides of the major tunnel system (plan and elevation views). . . . .	88
4.3	Mont Terri is an asymmetrical anticline folded during the Late Miocene to Pliocene period. The rock laboratory is located within the Opalinus Clay unit that dips approximately 45° southeast. The Opalinus Clay is divided into three main facies with the ED-B tunnel located entirely within the shaly facies. One major fault intersects the rock laboratory southeast of the ED-B tunnel. . . . .	89
4.4	Layout of ED-B mine-by test instrumentation and tunnel system. The ED-B tunnel was excavated with a roadheader from the northwest to southeast. . . . .	92

4.5	For model implementation, the geometry of the Mont Terri rock laboratory was simplified to a system of two parallel tunnels (ED-B and Reconnaissance Gallery) with two instrumentation niches. The 34 x 56 x 85 m FLAC <sup>3D</sup> model contained 540,000 zones and five modelling stages were used to simulate the excavation sequence. . . . .	95
4.6	Orientations of the stress tensor from the undercoring in-situ stress measurement method (modified from Martin and Lanyon [15]). . . . .	97
4.7	Non-linear elastic Young's modulus related to stress levels ( $\sigma_1, \sigma_3$ ) that forms the basis for the SDM model developed by Corkum [8]. . . . .	100
4.8	Numerical analysis using effective stress, horizontal bedding, ubiquitous joint properties ( $c'_b = 1$ MPa, $\phi'_b = 23^\circ$ ) showing yielded zones. It can be seen that bedding plane slip occurs in roof and floor of the ED-B tunnel. Yielding is concentrated in the lower left corner of the tunnel near the invert. . . . .	103
4.9	Results of FLAC <sup>3D</sup> analyses compared with measured field data for cumulative inclinometers and sliding micrometers. The stress-dependent modulus model shows a good match of inclinometer data and a lesser fit to the micrometer data. . . . .	105
4.10	Convergence with excavation advance measured by Array CP-3 compared to the SDM model along a vertical convergence line. Orientation of convergence lines are shown in Fig. 4.12. Time-dependent deformations are significant ( $X/D < -3$ ). . . . .	106
4.11	Convergence with three-dimensional excavation advance along a vertical convergence line using the SDM model. It is estimated that approximately 50 % of convergence occurred prior to installation of a convergence array. . . . .	107
4.12	A comparison of the average convergence measurements from three arrays to the numerical model results shows a reasonable fit with the SDM model. Measurements associated with Pin 1 are under-predicted due to local yielding (see Fig. 4.8). . . . .	108
4.13	An illustration of the mechanisms of rockmass displacement around tunnels in Opalinus Clay: undisturbed zone (linear elastic), zone of unloading (non-linear) and the EDZ (dominated by dilation). . . . .	109
4.14	Change in pore pressures calculated using SDM-based piece-wise formulation adequately predicts the trends of pore pressure development with excavation advance. . . . .	111
A.1	Typical composition of Opalinus Clay. . . . .	122
A.2	Layout of Mont Terri rock laboratory (from <a href="http://www.mont-terri.ch">www.mont-terri.ch</a> ). Notice the ED-B tunnel within the New Gallery section. . . . .	124
A.3	Geological profile along Mont Terri motorway tunnel (from <a href="http://www.mont-terri.ch">www.mont-terri.ch</a> ). . . . .	124
A.4	<i>Rosas</i> 1 is the recommended in-situ stress tensor at Mont Terri (from Martin and Lanyon [5]). . . . .	126
A.5	Layout of instrumentation for ED-B mine-by test showing inclinometers/extensometers and convergence arrays. . . . .	126
A.6	Elevation view looking southeast in the direction of excavation advance. . . . .	127
A.7	FEM data and average measured convergence data. Note that significant portions of the deformations are not picked up by the instrumentation. . . . .	131
A.8	Results of FEM analysis compared with measured data for cumulative inclinometers and sliding micrometers. . . . .	132



A.9	Phase2 model looking southeast showing yielded elements and contours of deviatoric stress (MPa). . . . .	132
B.1	Orientations of the Rosas 1 stress tensor from the undercoring in-situ stress measurement method (modified from Martin and Lanyon [1]). . . . .	140
B.2	In-situ seismic measurements support $\sigma_3 = 2.2$ MPa. Data provided by K. Schuster (pers. comm.). . . . .	142
C.1	Location map of Mont Terri rock laboratory, Switzerland. . . . .	147
C.2	Layout of Mont Terri rock laboratory (from www.mont-terri.ch). . . . .	149
C.3	<i>Rosas 1</i> is the recommended in-situ stress tensor at Mont Terri (from Martin and Lanyon [6]) . . . . .	150
C.4	External view of rock laboratory looking towards the northwest (from www.mont-terri.ch). . . . .	151
C.5	Schematic of the evolution of borehole breakouts (looking southwest) based on field mapping of 110 and 250 mm diameter boreholes. . . . .	153
C.6	(a) Initial stress-induced breakout looking southwest. (b) Long-term breakout looking southwest. . . . .	154
D.1	Schedule of research project and events of 2004 field programme. . . . .	159
D.2	Plan view of Mont Terri rock laboratory. . . . .	161
D.3	Excavation of the Starter niche. . . . .	162
D.4	Cracking and debonding of shotcrete in roof of Starter niche. . . . .	163
D.5	Structurally controlled instability in the Starter niche. . . . .	165
D.6	Schematic diagram of typical excavation face of the Starter niche. . . . .	166
D.7	Looking towards the northwest along the Security Gallery. . . . .	167
D.8	Shotcrete damage in OP niche. Up to 0.5 m of outward displacement. . . . .	169
D.9	Schematic of the development of borehole breakouts from mapping and field observations. . . . .	172
D.10	Photographs illustrating borehole breakout development. . . . .	173
D.11	Disintegration of Opalinus Clay exposed to weathering in outdoor waste pile. . . . .	176
D.12	Degeneration of block sample. . . . .	177
D.13	Core dinking observed during overcoring experiment. . . . .	178
E.1	Geological plan of Mont Terri rock laboratory. (Provided by Ch. Nussbaum.) . . . . .	182
E.2	Plan view of Mont Terri rock laboratory showing the distribution of cracking along Security Gallery and typical section. . . . .	183
E.3	Shotcrete mapping with geological structure overlay. East wall of Security Gallery, first mapping section. . . . .	184
E.4	Shotcrete mapping with geological structure overlay. East wall of Security Gallery, second mapping section. . . . .	185
E.5	Shotcrete mapping with geological structure overlay. West wall of Security Gallery, first mapping section. . . . .	186
E.6	Shotcrete mapping with geological structure overlay. West wall of Security Gallery, second mapping section. . . . .	187
E.7	Shotcrete mapping with geological structure overlay. West wall of Security Gallery, third mapping section. . . . .	188
E.8	Shotcrete mapping with geological structure overlay. West wall of Security Gallery, fourth mapping section. . . . .	189
F.1	Borehole: BCP-3, Diameter: 110 mm . . . . .	191
F.2	Borehole: BCP-5, Diameter: 110 mm . . . . .	191

F.3	Borehole: BDB-1, Diameter:110 mm . . . . .	192
F.4	Borehole: BDB-2, Diameter:110 mm. . . . .	192
F.5	Borehole: BDT-1, Diameter:150 mm. . . . .	193
F.6	Borehole: BDT-2, Diameter:95 mm . . . . .	193
F.7	Borehole: BED-B13, Diameter:110 mm . . . . .	194
F.8	Borehole: BED-C5, Diameter:110 mm . . . . .	194
F.9	Borehole: BED-C9, Diameter:110 mm. . . . .	195
F.10	Borehole: BED-C10, Diameter:110 mm . . . . .	195
F.11	Borehole: BEZ-A28, Diameter:110 mm . . . . .	196
F.12	Borehole: BFD-9, Diameter:250 mm. . . . .	196
F.13	Borehole: BFD-B25, Diameter:250 mm. . . . .	197
F.14	Borehole: BFM-B2, Diameter:250 mm . . . . .	197
F.15	Borehole: BFM-B6, Diameter:110 mm . . . . .	198
F.16	Borehole: BFM-B8, Diameter:110 mm . . . . .	198
F.17	Borehole: BFP-1, Diameter:250 mm. . . . .	199
F.18	Borehole: BFP-3, Diameter:250 mm. . . . .	200
F.19	Borehole: BFP-5, Diameter:250 mm. . . . .	201
F.20	Borehole: BFP-6, Diameter:250 mm . . . . .	201
F.21	Borehole: BFP-7, Diameter:250 mm . . . . .	202
F.22	Borehole: BFP-11, Diameter:250 mm . . . . .	202
F.23	Borehole: BFP-13, Diameter:250 mm . . . . .	203
F.24	Borehole: BFP-17, Diameter:250 mm . . . . .	203
F.25	Borehole: BIS-D8, Diameter:110 mm. . . . .	204
F.26	Borehole: BLT-5, Diameter:110 mm . . . . .	204
F.27	Borehole: BLT-6, Diameter:110 mm . . . . .	205
F.28	Borehole: BLT-9, Diameter:110 mm. . . . .	205
F.29	Borehole: BPC-B3, Diameter:110 mm . . . . .	206

# Chapter 1

## Introduction

Over the last 10 years, argillaceous rocks have been extensively studied as potential host formations for deep geological storage of radioactive waste. Excavation of repository tunnels in highly stressed ground conditions will result in a zone of damaged rock around the tunnel boundary known as the excavation damaged zone (EDZ). Apart from tunnel stability, the main issue associated with the EDZ is the potentially enhanced permeability offered by this system of interconnected fractures. In order to better understand the extent and characteristics of the rockmass in the EDZ, researchers are investigating many aspects of the behaviour of argillaceous rocks.

This dissertation describes the mechanical non-linear stress-strain behaviour of the argillaceous rock Opalinus Clay around underground openings. A brief review of the geomechanical issues associated with construction of repository tunnels is presented. The Opalinus Clay and the Mont Terri rock laboratory are described, followed by an overview of the dissertation.

### 1.1 Repository Tunnels

The selection of a host formation that will perform as a natural barrier to the transport of radionuclides is a key decision. The prime candidates consist of several types of geomaterials: crystalline rock, rock salt, plastic clays, and indurated clays. These formations are being studied by various research groups around the world. Major studies of crystalline rocks have been conducted in Stripa (Sweden), Pinawa

(Canada), Aespoe (Sweden), Grimsel (Switzerland) and Kamaishi (Japan). Rock salt has been studied in Asse (Germany) and WIPP (USA), and plastic clay has been studied at Mol (Belgium). Currently, a significant effort is underway in the investigation of indurated clays in several countries. Underground rock laboratories in Meuse/Haute Marne (France), Tournemire (France) and Mont Terri (Switzerland) have undertaken the study of these indurated argillaceous rock formations.

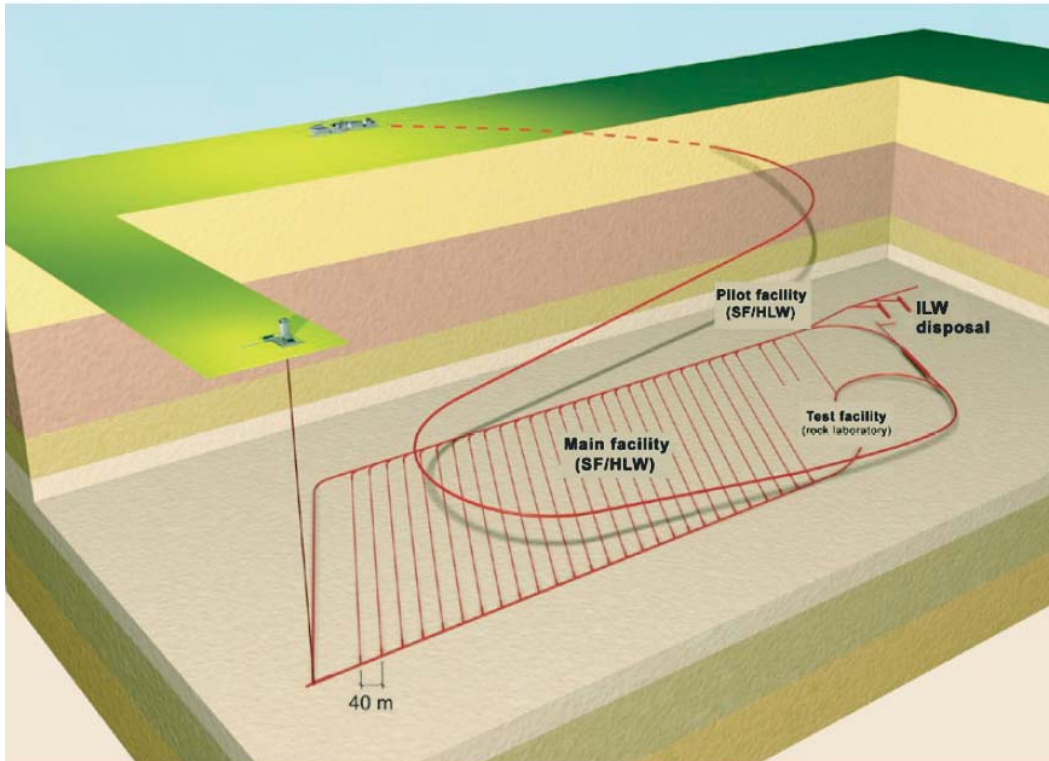


Figure 1.1: Conceptual illustration of a high-level waste repository with surface facilities, access ramp and the main system of emplacement drifts (available at [www.mont-terri.ch](http://www.mont-terri.ch)).

One of the major components of repository construction is the tunnel system itself. Fig. 1.1 shows a simple conceptual illustration of a high-level waste repository with surface facilities, access ramp and the main tunnel system of emplacement drifts. An on-site rock laboratory will be integrated into the complex to conduct site-specific in-situ experiments. Excavation of a tunnel in any pre-stressed geomaterial will result in the formation of an excavation disturbed zone (EdZ) and/or an excavation damaged zone (EDZ). According to Tsang et al. [1], differentiation between these two has been defined as:

- The EdZ is a zone with hydromechanical and geochemical modifications *without* major changes in flow and transport properties.
- The EDZ is a zone where hydromechanical and geochemical modifications induce significant changes in flow and transport properties. These changes can, for example, include one or more orders-of-magnitude increase in flow permeability.

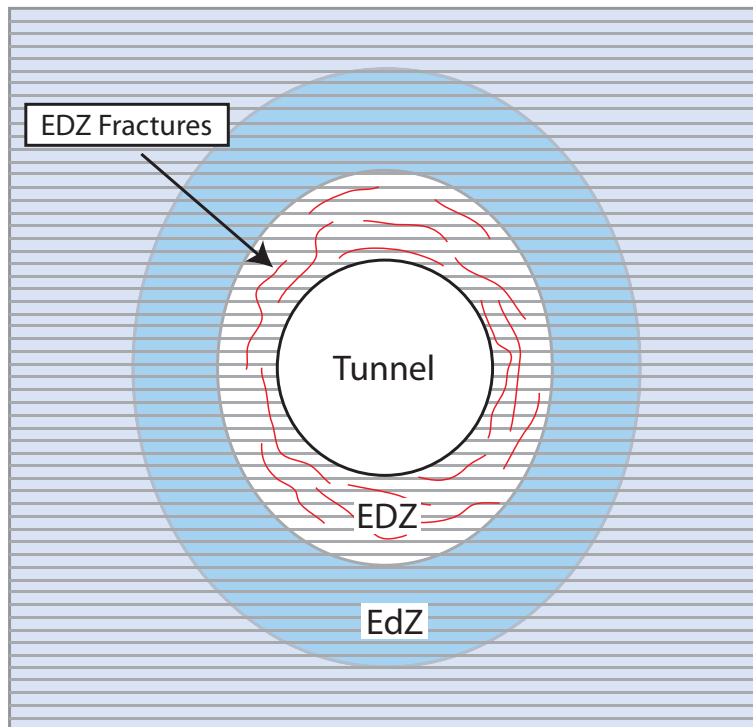


Figure 1.2: The excavation disturbed (EdZ) and excavation damaged zone (EDZ) around repository tunnels result in the development of preferential flow paths.

The nature and development of the features that make up the EDZ varies between the geomaterial-types. Generally the EDZ consists of a zone of interconnected macro- and micro-fractures that results in increased permeability and, hence, increased potential for radionuclide transport. These zones are illustrated for a horizontally bedded, indurated clay in Fig. 1.2.

In terms of man-made construction projects, the lifecycle of a radioactive waste repository gives new meaning to the concept of long-term performance. The projected time-frame of such a project is on the order of 10,000 to 100,000 years.

The performance of the storage site must be assessed for the various conditions anticipated throughout its lifecycle. The most significant issues associated with the various stages of a repository's lifecycle are [1]:

- **Excavation stage:** Excavation-induced mechanical and hydromechanical conditions, particularly the development of an EdZ and EDZ. Support systems, such as anchors or concrete liners, are installed.
- **Open-drift stage:** Evolution of the EDZ due to time-dependent processes (e.g., creep, consolidation, desaturation). Ventilation of the drifts can result in changing temperature and humidity resulting in dehydration of the rock in the tunnel near-field.
- **Early closure stage:** The drifts are backfilled and the repository is closed—the rockmass starts to become rehydrated and resaturated. Heat from the waste canisters will offset the rehydration process to some degree. Swelling pressure from the backfill material (typically bentonite pellets) will tend to close EDZ fractures, reducing the permeability.
- **Late closure stage:** The repository system is fully saturated and the induced heating dissipates with time. Long-term issues, mostly controlled by chemical and biological processes, become major factors. Tunnel support systems are degraded. Self-sealing of EDZ fractures occurs in clay formations.

The main advantages of using relatively weak (soft) argillaceous materials, as opposed to hard crystalline rock, as a host formation, are its ductile behaviour and potential self-sealing capacity. It is believed that the slaking, swelling and softening attributes of argillaceous rocks, typically considered to be negative attributes in the context of tunnel construction, offer the potential for partial, or full self-sealing of this fracture network as the material properties degrade with time. Laboratory and field experiments have shown that argillaceous rocks have a tendency to self-seal under certain conditions [2]. As a result, they have gained acceptance as a potential host formation for geological disposal of nuclear waste. Currently, the Swiss re-

search consortium NAGRA is directing studies into the behaviour and performance of a repository at a depth of 500-700 m in the Opalinus Clay.

## 1.2 Argillaceous Rocks

At least 75 % of the earth's surface is covered by sedimentary rocks. Of these, argillaceous rocks make up a large portion of those encountered near-surface and are, therefore, frequently encountered in construction projects. When intersected during tunnelling projects, they often prove to be of a troublesome nature with swelling and/or squeezing of the tunnel boundary.

Argillaceous rocks are generally soft rocks that are transitional materials between soil and rock. These materials are well known for creating a variety of civil engineering problems ranging from the diagnosis of geological and groundwater conditions, collection of undisturbed samples, the determination of representative soil properties, stability of slopes and excavations, construction of compacted shale embankments and performance of underground openings. A brief review of the mechanical behaviour, in particular processes associated with degradation with increased water content, is presented here.

Burland et al. [3] and Leroueil [4] have shown that a significant portion of the mechanical behaviour of argillaceous rocks can be attributed to the highly structured nature of these materials. A major contributor to the development of structured argillaceous rock is the formation of diagenetic bonds. The geotechnical cycle for clay sediments is described by Chandler [5] and Skempton [6] has compiled a series of sedimentation compression curves for normally consolidated argillaceous sediments. These serve to illustrate the geological history of argillaceous rocks.

During compaction, high contact stresses between particles results in recrystallization causing the contacting surfaces to physically conform to one another forming strong diagenetic bonds. This results in the development of adhesion (cohesion) from the formation of molecular bonds. Thus, under high pressure and long periods of time, the material becomes stronger and more brittle (higher cohesion). Sandstones and limestones approach equilibrium at relatively low pressure

with minor volume change while fine-grained argillaceous rocks can have a volume reduction of more than 80 % due to gravitational compaction alone [7]. Consequently, for argillaceous rocks the processes associated with burial and diagenesis are of notable importance. A mechanism involving latent strain energy and diagenetic bonding has been proposed as a contributing factor to the progressive failure of slopes in weak argillaceous rock by Bjerrum [8]. Nygård et al. [9], Shaw and Primmer [10], Ewy et al. [11] and Holt et al. [12] have also investigated the effects of diagenetic bonds on the mechanical behaviour of geomaterials.

It is difficult to determine the operational strength of argillaceous rocks. The available shear strength ranges from the peak strength of the intact material to the fully softened or residual strength. Near surface argillaceous rocks typically contain numerous fissures and discontinuities that act as weak surfaces in the material matrix. These weak planes often result in a non-linear failure envelope with a higher friction angle at low normal stresses. This is due to the fact that shear yielding tends to occur along fissures at low stresses and the interconnected fissures act similarly to a rough joint. At higher stress levels, rupture passes through the intact blocks, which results in a lower mobilized friction angle. Softening and slaking can also reduce the strength of these materials significantly. A time-dependent process of decreasing strength due to opening of fissures with resulting increased permeability was described by Terzaghi [13].

Probably the most challenging aspect of this class of materials is their propensity for degradation with increased moisture content. Swelling, slaking and softening are the main processes that comprise what is often referred to as long-term, time-dependent behaviour. These terms are often associated with weathering and are related to the structure of argillaceous rocks as mechanisms of *de-structuration*.

Morgenstern [14] outlined the processes causing swelling of clay shales as follows: (1) elastic and non-elastic rebound as measured by swelling tests; (2) change in pore fluid composition; e.g., replacement of salt-rich pore fluid by purer water increases swelling potential; (3) physical weathering by wetting and drying; (4) physical weathering by freezing and thawing; and (5) chemical weathering. In terms of tunnelling, Einstein [15] defines the swelling mechanism as a combina-



tion of physico-chemical reactions involving water and stress relief. The uptake of water (increased water content) is the major contributor to swelling, but it does not occur without accompanying stress relief. Another component of swelling consists of the release of mechanically bent clay platelets due to the breakage of diagenetic bonds. Chemical processes associated with the formation of gypsum may act as a secondary source of swelling in argillaceous rocks.

Laboratory studies, such as the Huder-Amberg test [16], can be used to assess the potential for swelling. However, there are limitations to applying these laboratory values to analytical solutions of tunnel swelling because laboratory tests do not usually properly reflect the loading conditions that a sample undergoes in the field [17].

Numerous case studies of swelling in tunnels were discussed by Einstein [15], including several dealing with the Opalinus Clay in the Jura Mountains of Switzerland. Examples include: the Czernitz tunnel, built in the 1850's; the Gotthard railroad and road tunnels in the Swiss Alps; and the Moffat, Roberts and Eisenhower tunnels in the Rocky Mountains. An extreme case was the Kappelsberg tunnel in southern Germany, constructed in 1880, with 4.7 m of invert heave. The Bozberg and Belchen tunnels in the Swiss Jura Mountains both encountered Opalinus Clay in addition to the anhydrite-rich Keuper formation.

There have been many closed form and numerical solutions to simulating swelling conditions. Two rheological models [18, 19] are described in the literature for time-dependent swelling of shales. Hawlader et al. [20] have developed a constitutive model for shaly rocks of southern Ontario, Canada that takes into account the three-dimensional stress effects using the "pseudo-Poissons ratio", and can simulate long-term swelling with anisotropic swelling potentials. They have shown this model to work well for prediction of swelling in tunnels. A relatively comprehensive model of the behaviour of Opalinus Clay, including swelling and softening, has been developed by Aristorenas [21].

Squeezing is another problematic issue for tunnelling in argillaceous rocks. Einstein [15] defines squeezing as time-dependent shear displacement of the tunnel. Mainly consisting of creep mechanisms, squeezing usually occurs at stress levels

below the short-term yield criteria. Softening of the material can degrade this yield criteria over time, increasing the effects of squeezing. Squeezing is differentiated from swelling as deformation of the rockmass into the tunnel *without* notably increased water content.

Softening is a well known issue that has been studied extensively in association with long-term slope stability [22, 14, 23]. Softening of clay shale was shown to result in up to 80 % loss of strength in some deposits after 30 to 70 years [24], and was probably responsible for the extreme variation of material strength observed at several engineering sites. Botts [24] states that there are two primary mechanisms playing important roles in the softening of argillaceous rocks:

1. Equilibration of negative pore pressures.
2. Deterioration of fissures by means of chemical alteration or slaking.

The term *slaking* usually implies the phenomena of material disruption, or dispersion, observed when dried or undisturbed chunks of argillaceous material is immersed in water. This behaviour has been attributed to several mechanisms. Nakano suggests that for some soft rocks a biological film may exist around the clay. This film resists slaking until drying induces cracks in the film allowing for slaking with re-wetting. Schmitt et al. [25] suggests that high capillary forces causes bond breakage. The pumping action of capillary air moving into and out of pores during drying and wetting cycles results in explosive slaking. Softening and slaking has been treated analytically by Yoshida [26] who has developed a constitutive model of softening in clay shales.

Physico-chemical processes can also play a significant role in combination with one or more of the above mechanisms. The change of water and sulphate into gypsum has been responsible for swelling and softening behaviour. This phenomenon has been reported for the Black Shales of Ottawa, Canada, by Quigley and Vogan [27]. Attack by sulphuric acid on other minerals present in the rock, particularly calcite, can greatly damage the cementitious bonds resulting in a softened/weathered material [28]. In the absence of calcite, sulfuric acid may react with the clay mineral illite to form jarosite. Examination of large quantities of heaved shale in the

Ottawa Region has shown that the major cause of heave is the growth of bundles of acicular crystals normal to laminations [29]. Therefore, swelling and softening would be more pronounced perpendicular to bedding and/or stress-induced fissures. This phenomena has been observed to change the anisotropy of samples in Oxford Clay [30].

Chemical weathering of Callovo-Oxfordian argillites of the Eastern part of the Paris Basin has been studied by Fouché et al. [31]. He states that the pressure of crystallisation of the newly formed phases produced by the alteration of pyrite lead to the propagation of tensile fractures. This resulted in damage to the material by the formation of micro-cracks with resulting decreased strength and stiffness. He suggested that this can result in an ultimate strength reduction of more than 10 % for the Callovo-Oxfordian argillites. The principal factor was the alteration of pyrite clusters, which resulted in gypsum and limonite neogenesis with swelling and increased porosity.

### **1.3 Opalinus Clay**

Argillaceous formations (weak rocks) are presently being studied in several countries as potential host rocks for geological disposal of radioactive waste. In Switzerland, the Opalinus Clay, named for the ammonite *Leioceras Opalinum* (see Fig. 1.3), is being investigated as a potential host formation [32]. This dry (low water content), relatively weak, Jurassic-aged argillaceous rock is found mainly in Germany and northwestern Switzerland. As shown in Fig. 1.4, it is properly classified as a claystone. In order to assess potential repository performance and the important issue of fracture self-sealing, a strong understanding of the fundamental behaviour of Opalinus Clay and the behaviour and extent of the EDZ development must be obtained. To this end, a significant amount of laboratory, field testing and numerical modelling has been conducted to investigate the behaviour of Opalinus Clay. Bock [33] has synthesized and evaluated much of this work.

The Opalinus Clay is a Lower Aalenian (middle Jurassic aged) marine deposit with past overburden estimated to have been at least 1000 m thick [34]. Based on



Figure 1.3: The Opalinus Clay is named for the ammonite *Leioceras Opalinum*, commonly found in the formation.

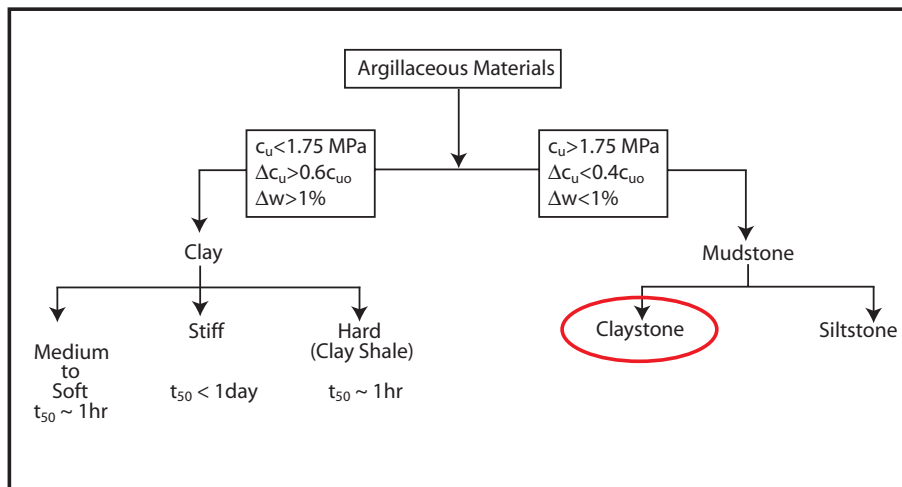


Figure 1.4: Classification of argillaceous materials [23].

the observed intensity of slaking when immersed in water, it appears to be lightly or uncemented. Like most argillaceous rocks, the laboratory properties are transversely isotropic in nature. The anisotropy can be illustrated by the Young's modulus parallel (P-samples) and perpendicular to bedding (S-samples) of 10 and 4 GPa, respectively. This anisotropy extends to many mechanical properties such as, hy-

draulic conductivity ( $k$ ) and undrained shear strength ( $c_u$ ) [33].

Compared to most argillaceous rocks, the deposit is relatively homogeneous and largely free of fissures. It has a pronounced microstructure, due to sedimentation and diagenetic processes, that consists of clay plates, or particles that are tabular-shaped and highly oriented approximately parallel to bedding. The bedding thickness is generally on the centimetre scale. This microstructure is thought to have a significant impact on the macro-behaviour of the material [33].

Typically, Opalinus Clay is composed of about 50-65 % clay particles, with the clay mineralogy consisting mostly of fairly low activity kaolinite and illite as evident from its medium plasticity. It has significant swelling potential due to its high clay content, in spite of its low activity mineralogy. A summary of the basic index properties is presented in Table 1.1.

Table 1.1: Index properties of Opalinus Clay [33].

Property	Value	Property	Value
Bulk density	2450 kg/m <sup>3</sup>	Liquid limit	38 %
Porosity	13.7 %	Plastic limit	23 %
Water content	6.1 %	Plastic index	15 %
Hydraulic conductivity	5e <sup>-13</sup> m/s	Unconfined strength	15 MPa

The claystone is a competent soft rock with an unconfined compressive strength of about 15 MPa. There have been a number of studies conducted on the stress-strain behaviour of Opalinus Clay showing that the material is generally non-linear at low stress levels and linearly-elastic in the mid-range, followed by the onset of dilatant behaviour at or near peak strength. The post-peak response is brittle with a significant reduction in strength to residual. This post-peak behaviour is typical of a large range of geomaterials from stiff over consolidated clay (such as London clay) to hard rocks (such as Lac du Bonnet granite).

Weak argillaceous rocks are often characterized by their propensity to soften and weaken with increased water content. The maximum swelling strain perpendicular to bedding is 7 % per log cycle with a swelling pressure of about 1.2 MPa. Parallel to bedding it is much lower, at 1 % per log cycle with a swelling pressure

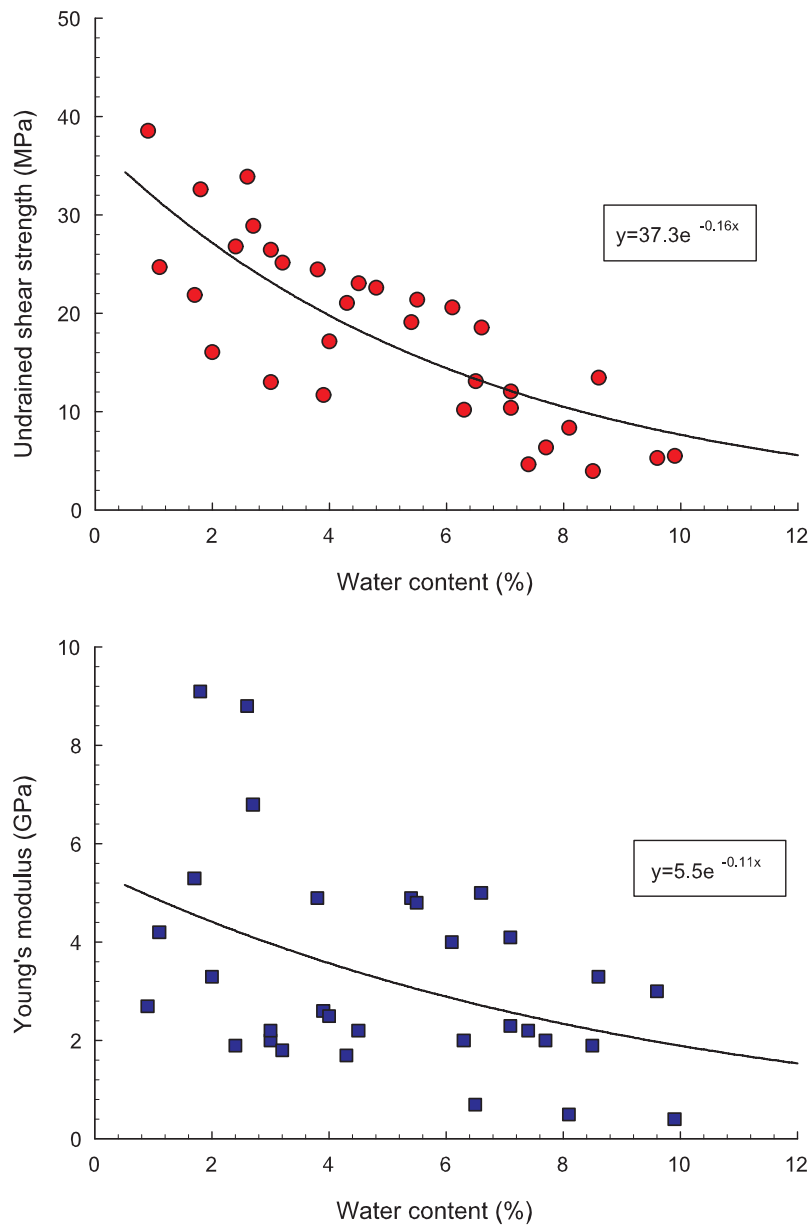


Figure 1.5: Water content has a significant effect on the shear strength and the elastic Young's modulus of Opalinus Clay based on triaxial tests at high confining stress ( $\sigma_3 = 10$  MPa). Data provided by Rummel et al. [35].

of about 0.6 MPa. Shear strength and Young's modulus are plotted against water content for Opalinus Clay in Fig. 1.5. From this plot it is clear that there is a relationship between water content, strength and stiffness. The shear strength plot shows a stronger relationship, while there is more scatter in the Young's modulus plot. Softening has been observed around excavations in-situ at Mont Terri which can be attributed to stress-induced migration of water. Softening can also be due to humidity changes in the tunnel system. According to [36], change in water content affects the mode of failure in argillaceous rocks; increased drying leads to a greater tendency for discrete tensile cracking, even in compression.

## 1.4 Mont Terri Rock Laboratory

The Mont Terri rock laboratory is located near the town of St. Ursanne in the Jura Mountains of northwestern Switzerland. It began in 1995 with the excavation of a number of niches within the Reconnaissance Gallery of the highway tunnel to carry out in-situ experiments in the Opalinus Clay. The Reconnaissance Gallery, or Security Gallery (see Fig. 1.6), was originally constructed as part of the motorway tunnel of the A16 Transjurane motorway. Over the last decade, additional experiments and expansion of the rock laboratory have been carried out. The location and an aerial view of Mont Terri are shown in Fig. 1.7.

The geological setting of Mont Terri is that of an asymmetrical anticline that was folded during the Late Miocene to Pliocene period. Stratigraphy consists of competent limestones and incompetent marly/shaly formations, dipping about  $45^\circ$  to the southeast in the area of interest [32]. Where it intersects the rock laboratory, the Opalinus Clay is about 250 m thick along the length of the tunnel. As a result of differing sedimentation, the Opalinus Clay can be grouped into three facies consisting of a shaly facies, a sandy facies and a carbonate-rich sandy facies. Only the shaly facies is considered in this research. One major fault runs through the rock laboratory and a number of discrete minor faults have been observed throughout the tunnel system. Structurally controlled instability is not believed to play a significant role at Mont Terri.

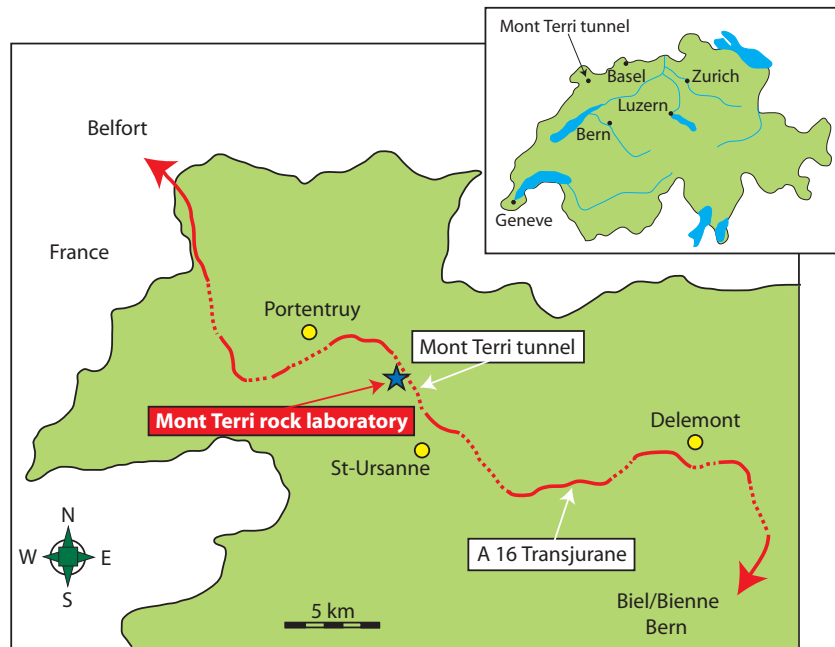


Figure 1.6: Looking towards the northwest along the Security Gallery.

Field observations and laboratory testing of samples from the rock laboratory have been a source for much of this study. In particular, observations from the ED-B mine-by test tunnel are referred to extensively. This 35 m long, 3.6 m diameter circular excavation was constructed at a depth of approximately 270 m within Mont Terri. The tunnel was instrumented prior to tunnel driving with inclinometers, micrometers, extensometers, piezometers and convergence arrays allowing for detailed monitoring of the rockmass response with tunnel advance.

The primary field observations addressed in this research project are mainly comprised of the short-term excavation response. These observations will only be described briefly here, and expanded upon in the remainder of the dissertation. The mine-by test has shown that large deformations occurred in the intact rockmass that could not be accounted for by conventional numerical analyses. Linear-elastic analysis only accounts for about half of these measured deformations. Furthermore, a field program called the Fracture Propagation (FP) study [37] has been carried out





(a) Map showing Mont Terri rock laboratory near the town of St. Ursanne in northwestern Switzerland (modified from [www.mont-terri.ch](http://www.mont-terri.ch)).



(b) Oblique aerial view of Mont Terri, Switzerland (available at [www.mont-terri.ch](http://www.mont-terri.ch)). 1. Rock laboratory location. 2. Tunnel access from southeast.

Figure 1.7: Location of Mont Terri rock laboratory.

to investigate the nature and extent of the EDZ around the ED-B tunnel. This study showed that the dominant mode of yielding around the tunnel consisted of open extensional fractures. Geophysical measurements showed that the deformation properties of the rockmass increased with distance from the tunnel boundary in regions of unloading. The measured pore pressure response appears to be strongly dilative in zones of compression where dilation of the rockmass was *not* predicted.



Figure 1.8: Cracking and debonding of shotcrete in the roof of the Starter Niche at Mont Terri more than a week after installation. This demonstrates the time-dependent behaviour of tunnels in Opalinus Clay.

The effects of time-dependent rockmass behaviour on tunnel performance was observed at Mont Terri during excavation of the 5 m diameter, horseshoe shaped *Starter* Niche in 2002. A significant crack and debonding was observed in the shotcrete lining more than a week after installation. At the time, the excavation face was about 35 m beyond this point. The shotcrete cracking coincided with increased deformation measured with a near by convergence array. The damaged shotcrete can be seen in Fig. 1.8.

The temperature and humidity recorded at the Mont Terri laboratory weather station, from June 1997 to June 2000, is shown in Fig. 1.9. There was a clear

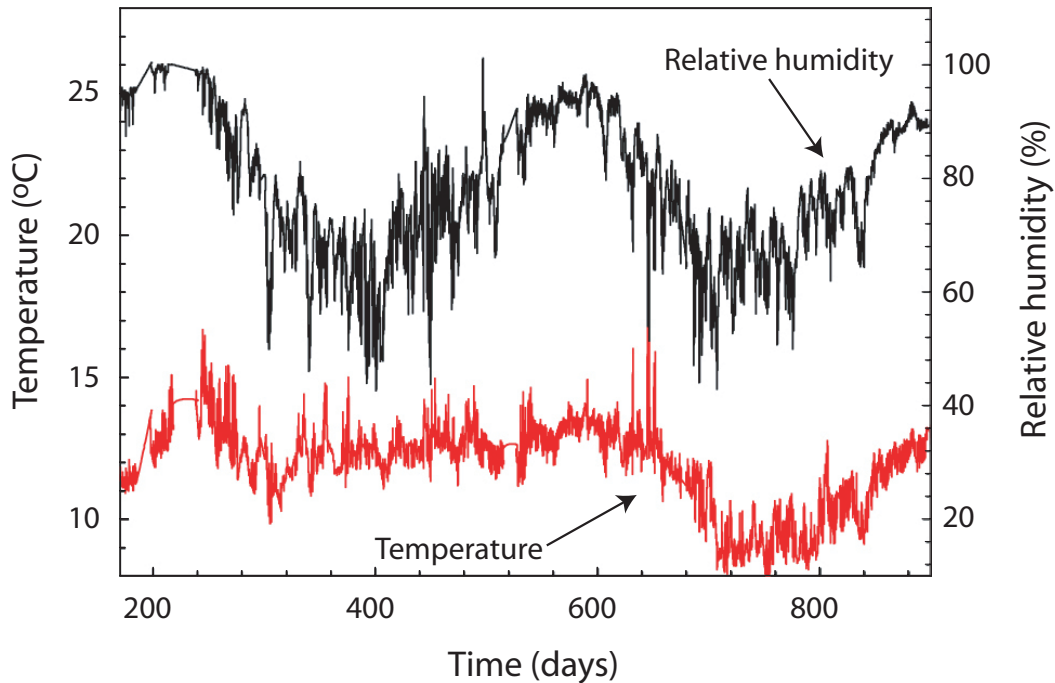


Figure 1.9: Temperature and humidity in the Mont Terri rock laboratory during excavation of the ED-B mine-by test tunnel. Julian day 1 is January 1, 1998 (modified from Martin and Lanyon [38]).

annual cycle in the humidity within the laboratory, with high humidity (close to 100 %) in Summer and low humidity (60 %) conditions in the winter. Temperature variation was small with an annual cycle ranging from about 15°C in the summer to 10°C in the winter. These changes in humidity and temperature are believed to have had an effect on the long-term moisture migration and the geochemical behaviour of tunnels in Opalinus Clay.

## 1.5 Overview of Research Project

Arguably, one of the oldest and most entrenched concepts in engineering mechanics is that of *linear-elasticity*. This assumption is valid for most forms of engineering analysis. However, observations from tunnels at the Mont Terri rock laboratory and laboratory testing suggest that the excavation-induced response of Opalinus Clay is *not* linear-elastic. Non-linearity of the stress-strain curve has been studied for many geomaterials. Yoshinkaka et al. [39] studied the non-linear behaviour of soft rocks using cyclic triaxial testing. Houlsby et al. [40] investigated the non-linear stress-

strain behaviour of soils and Kohata et al. [41] modelled the non-linear deformation properties of stiff geomaterials. The non-linear behaviour of homogeneous sandstone was studied by Morgenstern and Tamuly Phukan [42].

In engineering practice, the non-linear response of geomaterials has been addressed by several methods. The Duncan and Chang [43] model for soil mechanics has been used extensively to predict pressure-dependent stiffness properties for soils. Kulhawy [44] has developed a relationship for the pressure-dependent elastic modulus of porous rocks. The concept of pressure-dependent modulus has been used by Ewy and Cook [45] and Santarelli et al. [46] to predict the behaviour of porous rocks around deep boreholes. Nawrocki et al. [47] used uniaxial compression test results to model tunnelling in non-linear geomaterials.

This dissertation proposes that the non-linear behaviour of Opalinus Clay is a result of its micro-structure. Furthermore, that this micro-structure is a result of the composition and geological history of this argillaceous rock. This non-linear behaviour can be quantified, to some extent, for Opalinus Clay by means of simple geotechnical laboratory tests. Some of the implications of this phenomenon, such as the pore pressure response, the formation of extensional fractures and prediction of the EDZ extent around underground excavations, are explored. These findings offer a framework for interpretation of many of the unexplained observations involving tunnelling in Opalinus Clay and provide a potential “trigger mechanism” related to several time-dependent processes, such as slaking, swelling and softening.

The research study described in this dissertation consisted of field, laboratory and numerical modelling components. The author visited NAGRA’s office in Wetztingen, Switzerland to review and compile reports and data pertaining to Mont Terri and the various experiments conducted on the Opalinus Clay. A field programme was conducted at the Mont Terri rock laboratory to compile observations regarding the excavation response and time-dependent behaviour of Opalinus Clay. Laboratory testing was carried out at the University of Alberta, Canada, to examine the stress-strain behaviour of Opalinus Clay at low stress levels. Monotonic and cyclical unconfined compression tests were conducted on samples of Opalinus Clay that were provided by NAGRA. The 83 mm diameter core samples were taken parallel

to bedding and were drilled with oil and air drilling fluids, respectively. The numerical modelling component of the research was assisted by a visit to the offices of Itasca Consultants GmbH, Germany.

## 1.6 Organization of Dissertation

The dissertation consists of three main chapters that have been submitted separately as articles to peer reviewed journals, supplemented by Appendices. Because these papers have been reproduced here as they have been submitted (including citations), the dissertation itself is occasionally cited throughout the individual papers. The literature review consists of published work on argillaceous rocks and tunnelling, in addition to unpublished internal reports, referred to as Mont Terri Technical Notes, provided by NAGRA. Due to the nature of the paper-based thesis format, the literature review is interspersed throughout the dissertation.

Chapter 2 describes a laboratory study using simple unconfined and triaxial compression tests to identify and quantify the non-linear stress-strain behaviour of the Opalinus Clay. Its geological history is explored as a source of this behaviour and used to develop a conceptual micro-structure model of the argillaceous material. A numerical study of the sampling stress-path is also presented.

Chapter 3 makes use of the laboratory findings along with field observations, such as geophysical measurements, and excavation-induced deformation and pore pressure behaviour, to quantify the tunnelling response with two phenomenological-based models. A simple constitutive model to account for non-linear elasticity of Opalinus Clay is developed. In addition, a simple piece-wise pore pressure model is developed to predict the hydromechanical behaviour of Opalinus Clay due to tunnelling. These two numerical models are implemented into the three-dimensional numerical finite difference code  $FLAC^{3D}$ <sup>1</sup> in order to validate the constitutive models by back-analyzing the ED-B tunnel mine-by test conducted at the Mont Terri rock laboratory. The numerical back-analysis of this case-study is described in Chapter 4.

---

<sup>1</sup>see [www.itascacg.com](http://www.itascacg.com)

Appendix A consists of a paper presented at the Canadian Geotechnical Conference in 2004, describing the preliminary modelling of the ED-B mine-by test. Apart from the use of conventional elasto-plastic constitutive models, this preliminary analysis used an in-situ stress field that was thought to be correct at the time. However, Appendix B describes a study of the in-situ stress field at Mont Terri that concluded the stress tensor should be modified. This updated stress tensor results in little, if any, predicted plastic yielding around the ED-B tunnel. Therefore, the preliminary conventional elasto-plastic model was unable to capture the tunnel response.

Observations regarding the time-dependent development of borehole breakouts at Mont Terri are described in a paper presented at the 2004 Canadian Young Geotechnical Engineers and Geoscientists Conference. This paper, provided in Appendix C, is based on a field programme of shotcrete crack and borehole breakout mapping, mapping of the excavation advance of an extended niche, and various other field observations. A report describing the field program, that has provided insight into the short- and long-term properties of the Opalinus Clay, is provided in Appendix D. The shotcrete crack mapping and borehole breakout details are provided in Appendix E and F, respectively.

## **Bibliography**

- [1] Tsang C F, Bernier F, Davies C, Geohydromechanical processes in the Excavation Damaged Zone in crystalline rock, rock salt, and indurated and plastic clays—in the context of radioactive waste disposal. *Int J Rock Mech Min Sci* 2005, 42:109–125.
  
- [2] Blümling P, Bernier F, Lebon P, Martin C D, The Excavation Damaged Zone in clay formations – time-dependent behaviour and influence on performance assessment. In: *Proceedings of Clays in Natural & Engineering Barriers for Radioactive Waste Confinement*, Tours, France 2005 .
  
- [3] Burland J B, Rampello S, Georgiannou V N, Calabresi G, Discussion: A labo-

- ratory study of the strength of four stiff clays. *Géotechnique* 1999, 49(2):273–283.
- [4] Leroueil S, Natural slopes and cuts: movements and failure mechanisms. *Géotechnique* 2001, 5(3):197–243.
- [5] Chandler R J, Clay sediments in depositional basins: the geotechnical cycle: Third Glossop Lecture. *Q J Eng Geol & Hydro* 2000, 33:7–39.
- [6] Skempton A W, The consolidation of clays by gravitational compaction. *Quarterly Journal of the Geological Society of London* 1970, 125:373–411.
- [7] Hedberg H, Gravitational compaction of clays and shales. *Am J Sci* 1936, 31:241–287.
- [8] Bjerrum L, Progressive failure in slopes of overconsolidated plastic clay and clay shales: Third Terzaghi Lecture. *J Soil Mech Found Div, ASCE* 1967, 93(SM5):1–49.
- [9] Nygård R, Gutierrez M, Gautam R, Høeg K, Compaction behavior of argillaceous sediments as function of diagenesis. *Marine and Petroleum Geology* 2004, 21:349–362.
- [10] Shaw H F, Primmer T J, Diagenesis of mudrocks from the Kimmeridge clay formation of the Brae area, UK North Sea. *Marine and petroleum Geology* 1991, 19918:270–277.
- [11] Ewy R T, Stankovich R J, Bovberg C A, Mechanical behavior of some clays and shales from 200m to 3800m depth. In: 39th U.S. Rock Mechanics Symposium, Cambridge, USA 2003 .
- [12] Holt R M, Doornhof D, Kenter C J, Use of discrete particle modeling to understand stress-release effects on mechanical and petrophysical behavior of granular rocks. In: *Numerical Modeling in Micromechanics via Particle Methods*, Konietzky H, editor, Swets & Zeitlinger, Lisse 2003 pp. 269–276.

- [13] Terzaghi K, Stability of slopes in natural clay. In: International Conference on Soil Mechanics and Foundation Engineering, vol. 1, Cambridge, MA 1936 pp. 161–165.
- [14] Morgenstern N R, Geotechnical behaviour of clay shales - An overview. In: International Symposium on Soil Mechanics, vol. 1, Oaxaca, Mexico 1979 pp. 29–41.
- [15] Einstein H H, Design and analysis of underground structures in swelling and squeezing rocks. In: Underground Structures: Design and Instrumentation, Sinha R, editor, Developments in Geotechnical Engineering, 59A, Elsevier 1989 pp. 203–262.
- [16] Huder J, Amberg G, Quelling in mergel, Opalinuston und anhydrit. Schweiss Bauzeitung 1970, 88(43):975–980.
- [17] Steiner W, Swelling rock in tunnels: rock characterization, effect of horizontal stresses and construction procedures. Int J Rock Mech Min Sci & Geomech Abstr 1993, 30(4):361–380.
- [18] Lo K Y, Yuen C M K, Design of tunnel lining in rock for long-term effects. Can Geotech J 1981, 18:24–39.
- [19] Lo K Y, Hefny A, Design of tunnels in rock with long-term time-dependent and non-linearly stress-dependent deformation. Canadian Tunnelling 1996, pp. 179–214.
- [20] Hawlader B C, Lee Y N, Lo K Y, Three-dimensional stress effects on time-dependent swelling behaviour of shaly rocks. Can Geotech J 2003, 40:501–511.
- [21] Aristorenas G, Time-Dependent Behavior of Tunnels Excavated in Shale. Ph.D., M.I.T. 1992.



- [22] Skempton W A, The rate of softening in stiff fissured clays with special reference to London Clay. In: International Conference on Soil Mechanics and Foundation Engineering, vol. 2, Rotterdam 1948 pp. 50–53.
- [23] Eigenbrod K D, Progressive Failure in Overconsolidated Clays and Mudstones. Ph.D. thesis, University of Alberta 1972.
- [24] Botts M, The effects of slaking on the engineering behavior of clay shales. Ph.D., University of Colorado 1986.
- [25] Schmitt L, Forsans T, Santarelli F J, Shale testing and capillary phenomena. International Journal of Rock Mechanics and Geomechanics Abstracts 1994, 31(5):411–427.
- [26] Yoshida N, Time-dependent instability in fissured, over-consolidated clays and mudstones. Ph.D., University of Alberta 1990.
- [27] Quigley R M, Vogan R W, Black shale heaving in Ottawa, Canada. Can Geotech J 1970, 7:106–115.
- [28] Hawkins A B, Pinches G M, Cause and significance of heave at Llandough hospital, Cardiff - a case history of ground floor heave due to gypsum growth. Quarterly Journal of Engineering Geology, London 1987, 20:41–57.
- [29] Grattan-Bellew P E, Eden W J, Concrete deterioration and floor heave due to biogeochemical weathering of underlying shale. Can Geotech J 1975, 12:372–378.
- [30] Russell D J, Parker A, Geotechnical, mineralogical and chemical interrelationships in weathering profiles of an overconsolidated clay. Quarterly Journal of Engineering Geology, London 1979, 12:107–116.
- [31] Fouché O, Wright H, Le Cleac’h J M, Pellenard P, Fabric control on strain and rupture of heterogeneous shale samples by using a non-conventional mechanical test. Applied Clay Science 2003, 26:376–387.

- [32] Thury M, Bossart P, Mont Terri rock laboratory: Results of the hydrogeological, geochemical and geotechnical experiments performed in 1996 and 1997. In: Geological Reports No. 23, Swiss National Hydrological and Geological Survey. Bern-Ittigen 1999 .
- [33] Bock H, RA Experiment: Data report on rock mechanics - Mont Terri project. Tech. Rep. Nagra, Internal Report TN00-02, Q+S Consult, Germany 2000.
- [34] Marschall P, Croisé J, Schlickerrieder L, Boisson J Y, Vogel P, Yamamoto S, Synthesis of hydrogeological investigations at the Mont Terri site (Phases I to V). In: Mont Terri Project - Hydrogeological Synthesis, Osmotic Flow. - Reports of the Federal Office for Water and Geology (FOWG), Geology Series No 6, Bern, Heitzmann P, editor 2002 .
- [35] Rummel F, Hettkamp T, Weber U, DM experiment: Laboratory experiments for the determination of deformation mechanisms and a constitutive law for time dependent deformation behaviour of the Opalinus Clay. Tech. Rep. Nagra Internal Report TN99-35, MeSy 1999.
- [36] Schmertmann J, Osterberg J, An experimental study of the development of cohesion and friction with axial strain in saturated cohesive soils. In: Proc. ASCE Research Conference on Shear Strength of Cohesive Soils 1968 p. 643.
- [37] Möri A, Bossard P, Fracture Propagation Experiment: method, results, interpretation. Tech. Rep. TN99-72, Nagra Technical Report, Geotechnical Institute Ltd. 1999.
- [38] Martin C D, Lanyon G W, Excavation Disturbed Zone (EDZ) in clay shale: Mont Terri. Tech. Rep. TR2001-01, Nagra 2004.
- [39] Yoshinkaka R, Tran T V, Osada M, Non-linear, stress- and strain-dependent behavior of soft rocks under cyclic triaxial conditions. Int J Rock Mech Min Sci 1998, 35(7):941–955‘.
- [40] Houlsby G T, Amorosi A, Rojas E, Elastic moduli of soils dependent on pressure: a hyperelastic formulation. Géotechnique 2005, 55(5):383–392.

- [41] Kohata Y, Tatsuoka F, Wang L, Jiang G L, Hoque E, Kodaka T, Modelling the non-linear deformation properties of stiff geomaterials. *Géotechnique* 1997, 47(3):563–580.
- [42] Morgenstern N R, Tamuly Phukan A L, Non-linear stress-strain relations for a homogeneous sandstone. *Int J Rock Mech Min Sci* 1969, 6:127–142.
- [43] Duncan J, Chang C Y, Nonlinear analysis of stress and strain in soils. *J Soil Mech Found Div, ASCE* 1970, SM5:1629–1653.
- [44] Kulhawy F H, Stress deformation properties of rock and rock discontinuities. *Eng Geol* 1975, 9:327–350.
- [45] Ewy R T, Cook N G W, Deformation and fracture around cylindrical openings in rock – I. Observations and analysis of deformations. *Int J Rock Mech Min Sci* 1990, 27(5):409–427.
- [46] Santarelli F J, Brown E T, Maury V, Analysis of borehole stresses using pressure-dependent, linear elasticity: Technical Note. *Int J Rock Mech Min Sci & Geomech Abstr* 1986, 23(6):445–449.
- [47] Nawrocki P A, Dusseault M B, Bratli R K, Use of uniaxial compression test results in stress modelling around openings in nonlinear geomaterials. *J Petro Sci and Engin* 1998, 21:79–94.

# Chapter 2

## Mechanical Behaviour of Weak Mudstone (Opalinus Clay) at low stresses<sup>1</sup>

### 2.1 Introduction

A significant portion of near-surface rocks are of an argillaceous nature and their behaviour is, therefore, of wide reaching interest to engineers. Many regions are known for this challenging geomaterial, such as Italy, Japan, Switzerland and western Canada. These materials are well known for presenting a variety of engineering related problems ranging from the basic diagnosis of geological and groundwater conditions to the stability of slopes and underground excavations. These rocks tend to be sensitive to environmental changes such as water content and pore pressure variation resulting in a time-dependent response. Hence, geotechnical problems often emerge years after construction is completed as illustrated by the delayed failure of embankments discussed by Skempton [2]. In addition, severe floor heave as a result of swelling and squeezing conditions has often been reported for railway tunnels encountering Opalinus Clay [3].

Named for the ammonite *Leioceras Opalinum*, the Opalinus Clay is found mainly in Germany and northwestern Switzerland. This dry (low water content), relatively weak, Jurassic-aged argillaceous rock was formed in the Jurassic Sea around 180 million years ago [4]. Argillaceous rocks are being considered as a potential host

---

<sup>1</sup>A version of this chapter has been accepted as a paper by the *Int J Rock Mech Min Sci*.

formation for geological disposal of nuclear waste because of their low permeability and potential capacity for self-sealing of fractures. However, these same properties also present many challenges. Due to their relatively low strength and sensitivity to environmental conditions, sampling and laboratory testing procedures may significantly influence test results making interpretation difficult and determination of the laboratory properties of Opalinus Clay requires interpretation. A starting point for most engineering projects is the characterization of the material behaviour from laboratory samples.

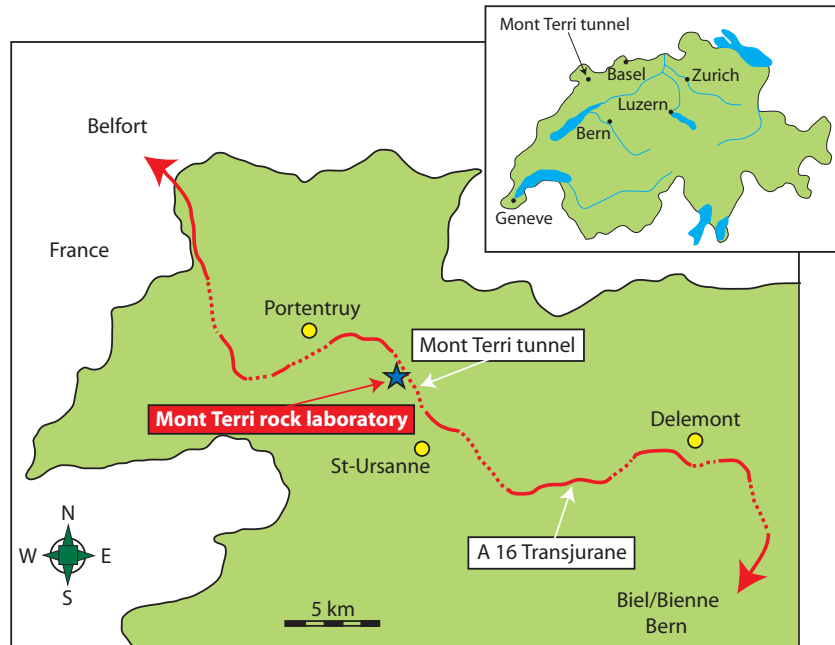


Figure 2.1: Map showing Mont Terri rock laboratory near the town of St. Ursanne in northwestern Switzerland (modified from [www.mont-terri.ch](http://www.mont-terri.ch)).

Large tunnel deformations have been observed around the well documented ED-B mine-by test conducted in Switzerland at the Mont Terri rock laboratory (see Fig. 2.1) in 1998. Conventional linear-elastic or elasto-plastic numerical analysis have generally been unsatisfactory in capturing these deformations [5]. Furthermore, Bock [6] has observed that the stress-strain curve of unconfined compression tests on samples of Opalinus Clay are unusually non-linear in the low stress region. This behaviour is illustrated by the unconfined compression test stress-strain curve for a sample of Opalinus Clay shown in Fig. 2.2.

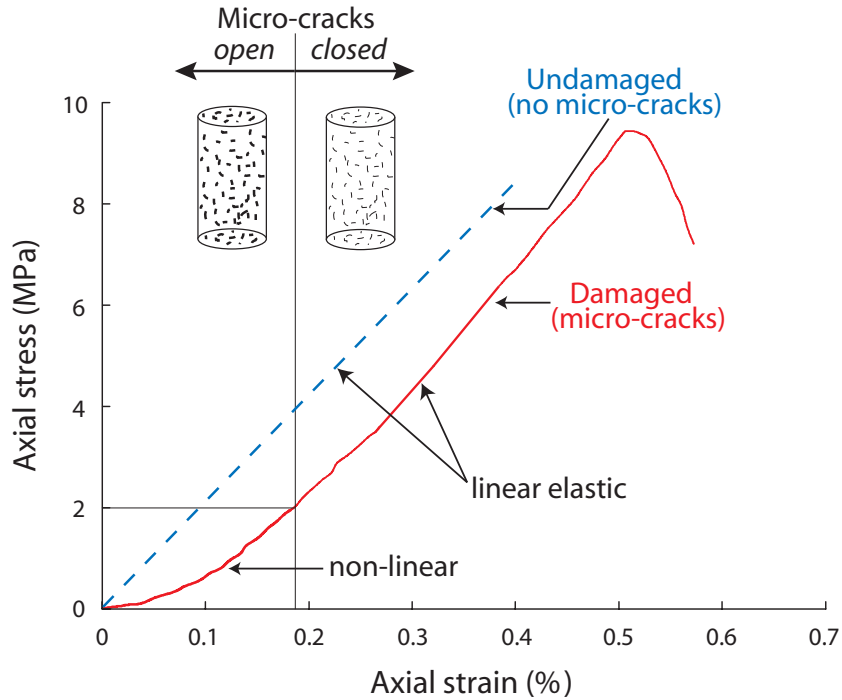


Figure 2.2: Illustration of the effects of open micro-cracks on the stress-strain curve of an unconfined compression test.

Typically, the greatest challenge of engineering numerical analysis is the implementation of an appropriate constitutive model to represent the material behaviour. There is a need to capture the stress-strain response of Opalinus Clay observed in the field and laboratory. This paper explores the highly non-linear, low stiffness stress-strain response of Opalinus Clay laboratory samples at low stress levels as part of the overall research effort to develop a simple constitutive model that captures this non-linear behaviour. The use of standard geotechnical laboratory compression tests is used to quantify this behaviour.

Diagenesis, “the chemical and physical changes occurring in sediments during and after their deposition, but before consolidation” [7], is proposed as the major factor in this observed behaviour. A model of the micro-structure, based on the diagenetic processes and the geological history of the deposit, is developed that is used as a framework for the future development of the constitutive model [8]. The likely cause of this non-linear response is proposed and its implications to underground excavations is discussed. A numerical study of the sampling stress-

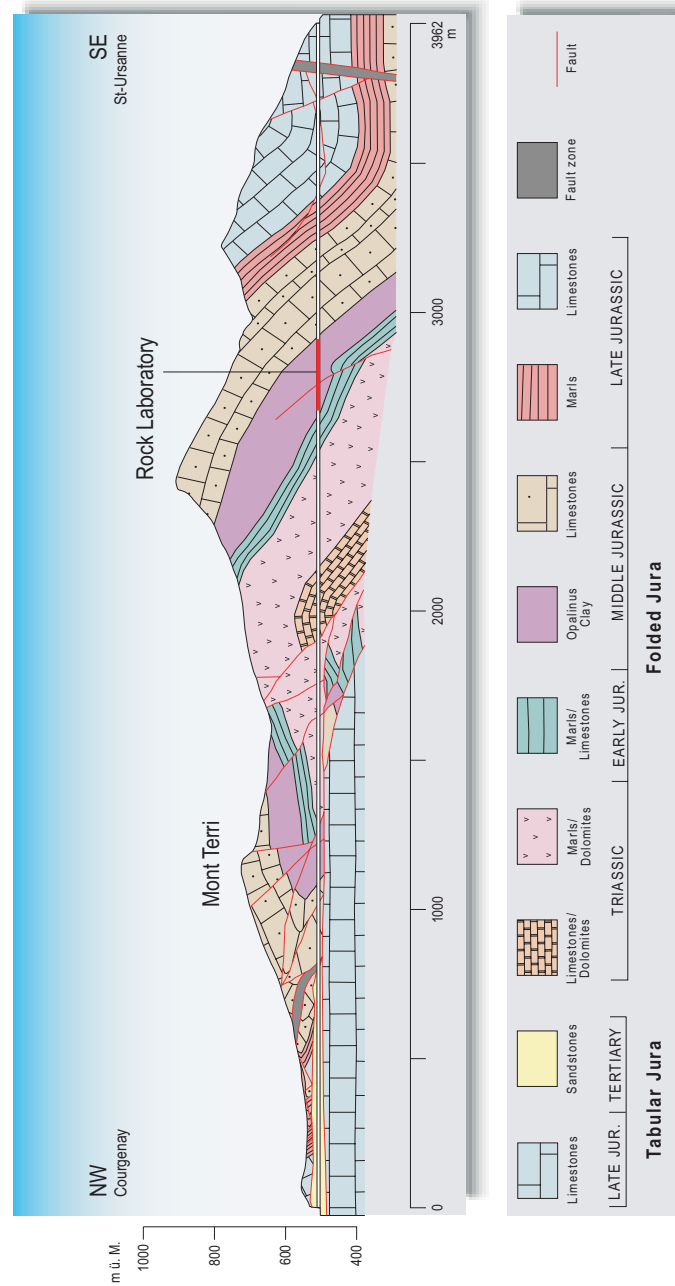
path is presented to provide insight into the processes resulting in the laboratory stress-strain response. Because this behaviour can be attributed to the composition and geological history of the material, argillaceous rocks with similar geological history and mineral composition can be expected to have a similar characteristic response to excavation and unloading.

## **2.2 Background**

Located in the Jura Mountains of northwestern Switzerland, Mont Terri is an asymmetrical anticline folded during the Late Miocene to Pliocene period, as shown in the geological section in Fig. 2.3. The stratigraphy consists of competent limestones and incompetent marly/shaly formations dipping about  $45^\circ$  to the southeast in the area of interest [10]. The Opalinus Clay is about 250 m thick along the highway tunnel where the Mont Terri rock laboratory is situated. As a result of differing sedimentation, the Opalinus Clay can be grouped into three facies consisting of a shaly facies, a sandy facies and a carbonate-rich facies.

The sequence of geological events leading to the current state of the Opalinus Clay at Mont Terri was described by Bock [6]. It was first deposited in shallow sea waters during the Dogger–Aalenian epoch of the Jurassic period [11]. Flocculation of clay particles occurred in the sea water and these particles accumulated in the form of larger aggregates while still in a state of suspension. Typical of sedimentation in marine environments, the aggregates formed an edge-to-face (card-house) texture. After sinking to the sea-floor, the aggregates were gradually buried and the steadily increased overburden weight resulted in compaction of the deposit. This process was associated with a number of major physical and structural changes, in particular:

- Consolidation and drainage of free pore water with a decrease of porosity.
- Rotation of the clay particles into a sub-horizontal flaky structure.
- Bending of clay platelets during compaction.
- Development of diagenetic bonding, locking-in this micro-structure.



Michael Freivogel (2001, University of Basel)

Figure 2.3: Geological section along A16 Transjurane motorway (from Freivogel and Huggenberger [9]). Mont Terri is an asymmetrical anticline folded during the Late Miocene to Pliocene period. The rock laboratory is located within the Opalinus Clay unit that dips approximately 45° southeast.



These mechanical processes are most pronounced for overburden depths of up to about 500 m (“burial stage”) [12]. At greater overburden depths, >500 m (“deep-burial stage”), the significance of mechanical compaction is less well developed and chemical processes such as cementation, recrystallisation and growth of new minerals become dominant [13]. The estimated maximum overburden depth of the Opalinus Clay in the Mont Terri region was in the order of 1000 m [14]; therefore, diagenetic bonding and some cementation of the clay particles is to be expected. According to Bock [6], tectonic events in connection with the Alpine orogeny lead to a tilt of the clay strata. Uplift, in combination with erosion, lead to its current state of overconsolidation. During these latter events, the texture of the clay minerals remained essentially unchanged, i.e. the clay particles were locked-in and preserved, maintaining the structure developed in the mechanical stage of compaction. The foremost result of deep burial is the transformation of smectite clay minerals into illites and chlorites [15]. This transformation is reflected in the current mineralogy of Opalinus Clay, that will be described in Sect. 2.2.1, and supports the occurrence of diagenetic processes during the burial history of the deposit.

### **2.2.1 Properties of Opalinus Clay**

Typically, Opalinus Clay is composed of 50-65 % clay particles, with clay mineralogy consisting mostly of kaolinite and illite. In spite of its low activity mineralogy, it has significant swelling potential due to its clay content. The typical mineral composition is shown in Table 2.1 and Fig. 2.4 and a summary of the basic index properties is provided in Table 2.2.

A scanning electron microscope (SEM) image from Móri and Bossart [17] is shown in Fig. 2.5 where quartz grains in a clay matrix can be seen. Void spaces between clay plates and silt grains reflect the porosity. It is clear in this image that folded and bent clay platelets are prevalent throughout the clay matrix. There is no sign of calcite crystals in the SEM image, indicating that the 7 % calcite is amorphous and a source of cementation.

As seen in the SEM image, the Opalinus Clay has a highly oriented structure with bedding on the centimetre scale. Like most argillaceous rocks, the labora-

Table 2.1: Typical mineral composition of Opalinus Clay (from Thury and Bossart [10]).

Mineral	%	Mineral	%
Kaolinite	30	Quartz	20
Illite	17	Calcite	7
Illite-smectite (mixed layer)	10	Feldspars	3
Chlorite	8	Siderite	2
		Dolomite/ankerite	1
		Pyrite	1
		Organic carbon	0.4
Total Clay	65	Total Non-Clay	35

Table 2.2: Index properties of Opalinus Clay (from Bock [16]).

Property	Value	Property	Value
Bulk Density	2450 kg/m <sup>3</sup>	Water Content	6.1 %
Liquid Limit	38 %	Liquidity Index	-1.1
Plastic Limit	23 %	Porosity	12.1 %
Plasticity Index	15 %	Void Ratio	0.19

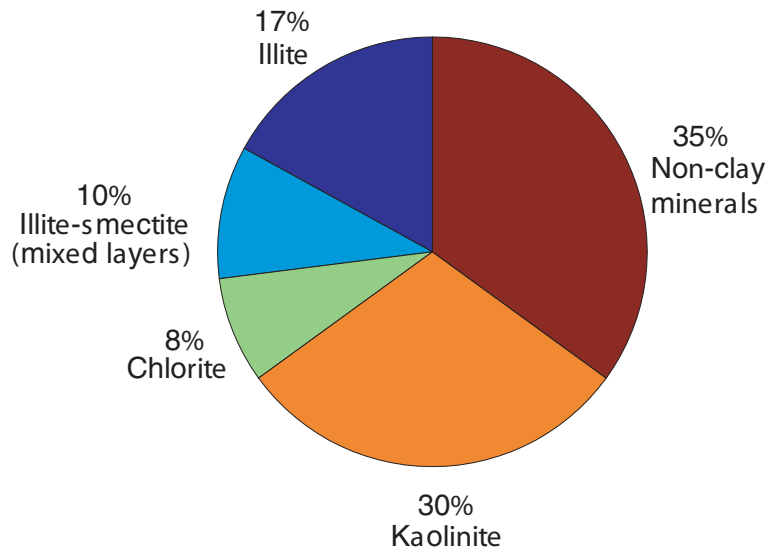


Figure 2.4: Typical mineral composition of the Opalinus Clay at Mont Terri.

tory properties are transversely isotropic in nature, as illustrated by the strength and deformation properties shown in Table 2.3. It has a comparatively high cohesive component of shear strength of 2.2 and 5 MPa parallel and perpendicular to bedding, respectively. In contrast, the London clay, which has been subjected to an estimated maximum past pressure  $\sigma_{vo} = 4$  MPa, has a cohesive strength compo-

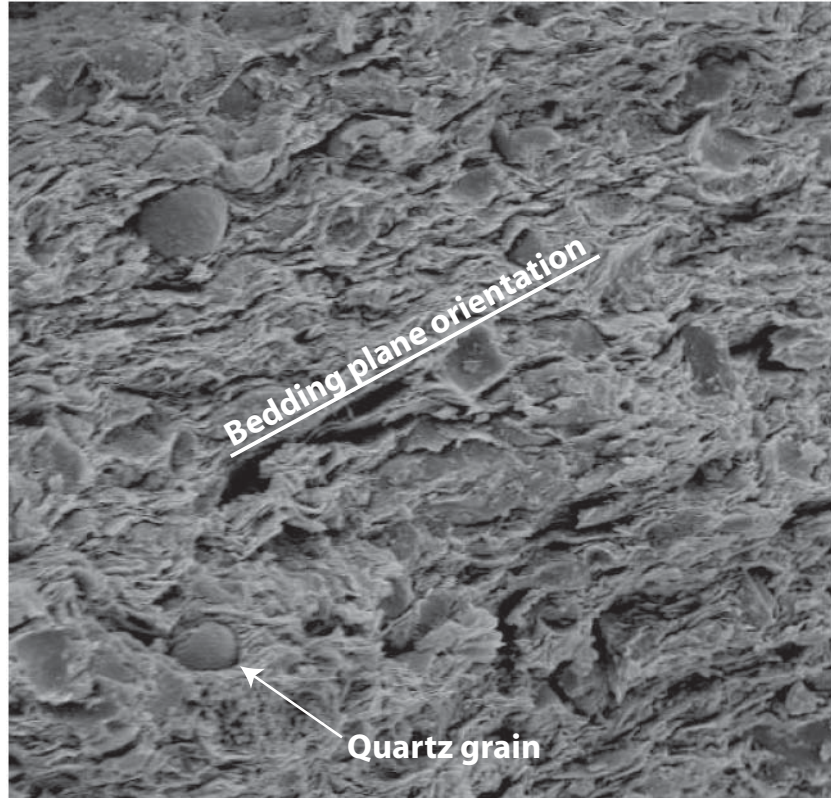


Figure 2.5: The Opalinus Clay structure is highly oriented, parallel to bedding. Clay platelets are generally bent and the presence of quartz grains can be seen in the clay matrix. Image width is 134  $\mu\text{m}$  (Möri and Bossart [17]).

Table 2.3: Strength and deformation properties of Opalinus Clay (from Bock [16]).

Parameter	Orientation to bedding	
	Parallel	Perpendicular
Uniaxial compressive strength	10 MPa	16 MPa
Tensile strength	2 MPa	1 MPa
Cohesion ( $c'$ )	2.2 MPa	5 MPa
Friction ( $\phi'$ )	25°	25°
Young's modulus (E)	10 GPa	4 GPa
Poisson's ratio ( $\nu$ )	0.33	0.24
Bedding cohesion ( $c'_b$ )	1 MPa	
Bedding friction ( $\phi'_b$ )	23°	

nent of 0.5 MPa [18]. In fully saturated soil and rock, cohesion can be attributed to physico-chemical bonding, geometrical “locking” of platelets, cementation, or some combination of these. Typical of a large range of geomaterials from stiff overconsolidated clay, such as London clay, to hard rocks, such as Lac du Bonnet

granite, the behaviour is brittle with a significant reduction to post-peak residual strength. The high level of cohesion and brittle post-peak behaviour found in the Opalinus Clay indicates the extent to which diagenetic processes have resulted in strong micro-mechanical bonds.

### 2.2.2 Diagenesis and the Behaviour of Opalinus Clay

High contact stresses between particles results in recrystallisation causing the contacting surfaces to physically conform to one another forming strong diagenetic bonds. This results in the development of adhesion (cohesion) from the formation of molecular bonds. Thus, under high pressure and long periods of time, the material becomes stronger and more brittle (higher cohesion). Sandstones and limestones approach equilibrium at relatively low pressure with minor volume change while fine-grained argillaceous rocks can have a volume reduction of more than 80 % due to gravitational compaction alone [19]. Consequently, for argillaceous rocks the processes associated with burial and diagenesis are of notable importance.

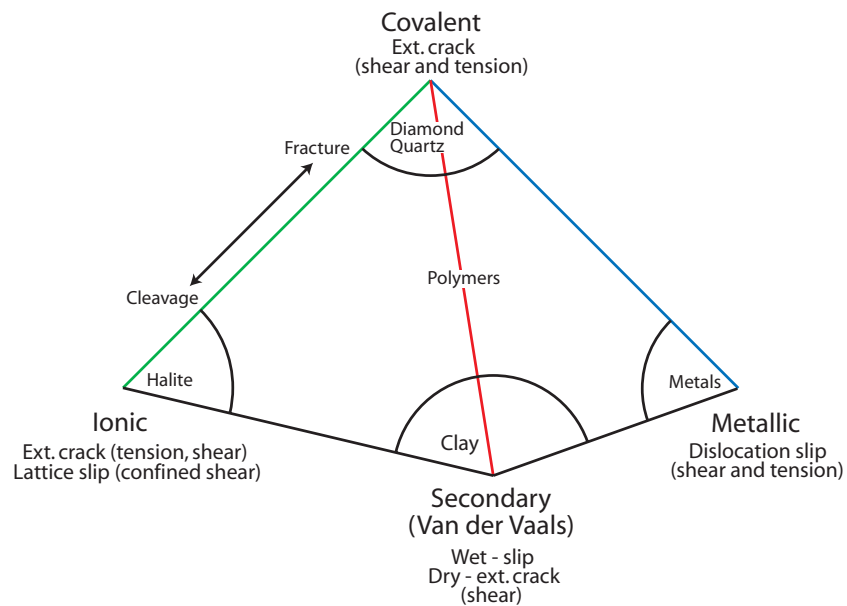
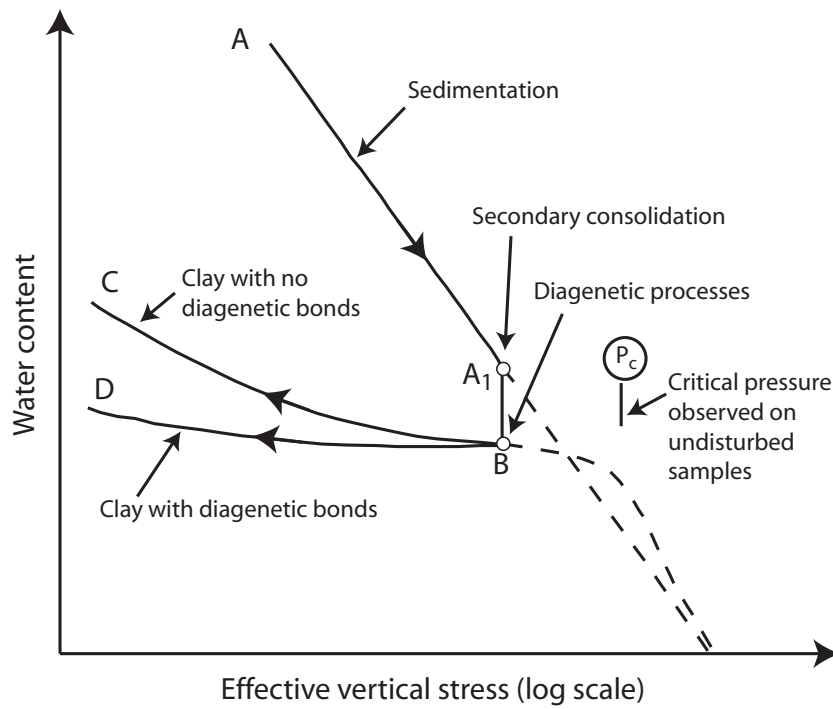


Figure 2.6: Types of bonding for solid materials (from Diederichs [20]). The nature of bonding can determine the mode of yielding and macro-behaviour.

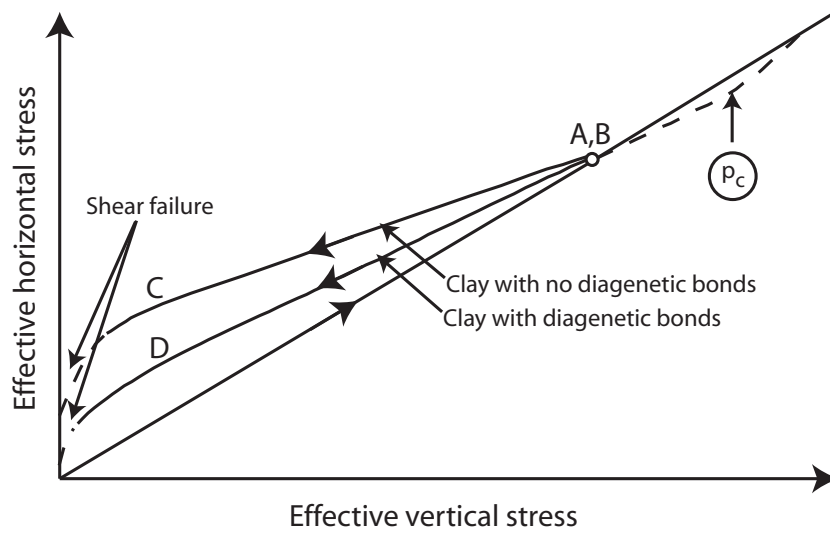
The nature of bonding determines the mode of yielding for many solid materials [21]. The type and nature of bonding for a spectrum of materials is shown

in Fig. 2.6. Cohesive soils are composed of ionic-covalent units which are in turn held together by secondary mechanisms such as Van der Waal bonding, hydrogen bonding or weak electrostatic attractions. Secondary bonding in clays may be discrete (eg. kaolinite) or distributed (eg. montmorillonite). Discrete bonds can only be broken in tension, according to Diederichs [21], and are not easily healed (damage is practically irreversible) at normal pressures and temperatures. For clays of low water content, the bonding between particles becomes more discrete and tensile cracking dominates behaviour, even in compression [22]. However, high water content clays (e.g., kaolinite) tend to yield by slip-related mechanisms. Opalinus Clay has a low water content (4 to 6 %) and consists mostly of kaolinite minerals. Therefore, it tends to yield in tension with little chance of healing without a significant increase in water content. The implication is that Opalinus Clay is lightly cemented and that the dominant portion of cohesion is physico-chemical secondary bonding with a tendency towards tensile yielding. This is in agreement with extensional fractures observed around underground excavations in Opalinus Clay at Mont Terri, particularly in zones of high deviatoric stresses where shear mode of yielding might be anticipated [23].

A mechanism involving latent strain energy and diagenetic bonding has been proposed as a contributing factor to the progressive failure of slopes in weak argillaceous rock by Bjerrum [24]. The stress-volume change history of clay with and without diagenetic bonds is shown in Fig. 2.7(a). It can be seen that the loading path associated with the processes of sedimentation and diagenesis are similar for both conditions, but the unloading behaviour is different. This is further illustrated by Fig. 2.7(b) that shows the relationship between effective vertical and horizontal stresses during the same loading history shown in Fig. 2.7(a). Unloading results in higher horizontal stresses for argillaceous rocks without diagenetic bonds. This is because the strain energy is locked into the structure by the diagenetic bonds. Bjerrum referred to this as latent strain energy. The recoverable part of compression is believed primarily to come from the bending of the flexible tabular-shaped clay particles. As such, the magnitude of latent strain energy is related to clay plasticity with higher plasticity clay minerals having more potential strain energy. Breakage



(a) Consolidation behavior.



(b) Horizontal-vertical stress relationship.

Figure 2.7: Geological history of overconsolidated clays (modified from Bjerrum [24]).

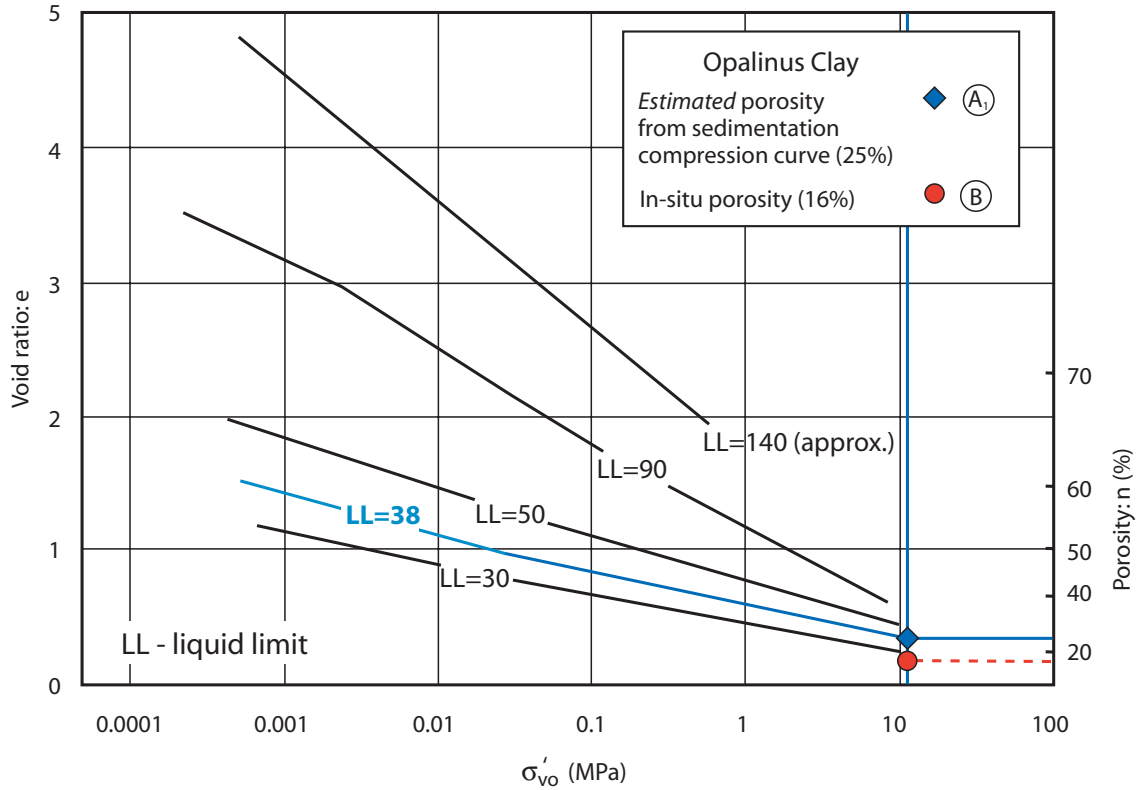


Figure 2.8: Sedimentation compression curves compiled for normally consolidated argillaceous sediments (modified from Skempton [25]). The Opalinus Clay is at the upper limit of the original curves. Points A<sub>1</sub> and B correspond to stages of compaction for Opalinus Clay as illustrated in Fig. 2.7. Diagenetic processes resulted in a 9 % decrease in porosity (35 % change).

of these bonds results in a lower strength and stiffness material.

According to Bjerrum, strain is the major agent in the destruction of diagenetic bonds, but weathering may also play a significant role. As the bonds which attempt to maintain the original structure of the clay are destroyed due to strain or weathering, the locked-in recoverable strain energy is liberated. Bjerrum suggested that the released latent strain energy can act as a driving force in the instability of slopes.

Diagenetic processes over the last 180 Ma have been responsible for chemical and mechanical changes occurring in the Opalinus Clay since its deposition. The estimated effective vertical maximum past pressure ( $\sigma_v$ ), based on at least 1000 m of overburden, is  $\sigma_{vo} = 12$  MPa. Skempton's compilation of sedimentation compression curves for normally consolidated argillaceous sediments is plotted in Fig. 2.8 [25]. The Opalinus Clay is at the upper stress limit of the original curves; however,

it can be seen that the estimated normally consolidated porosity would be about 25 %.

Gravity-induced mechanical compaction alone should not be sufficient to reduce the porosity in the Opalinus Clay to that measured in-situ at Mont Terri of 14 %. This reduction from its sedimentation compression curve value to its final porosity was due to diagenetic processes (from Point A<sub>1</sub> to B in Figs. 2.7(a) and 2.8). This provides evidence that significant diagenetic alteration of the Opalinus Clay has occurred, resulting in an 11 % decrease in porosity.

## 2.3 Laboratory Stress-Strain Behaviour

The stress-strain response of geomaterials is required when analyzing underground excavations. When analyzing these problems the inappropriate use of simple linear elastic models may introduce significant errors. The full response of brittle rock has been investigated by many authors who have shown that the stress-strain curve can be divided into five regions [26].

- Region I – closure of existing micro-cracks and crushing of asperities.
- Region II – linear elastic.
- Region III – onset of dilation (crack initiation).
- Region IV – unstable crack growth.
- Region V – post-peak.

The stress-strain curve of Opalinus Clay, although it is considered to be a relatively weak rock, is similar to that of brittle rock. The approximate divisions of the five regions of the stress-strain curve are shown in Fig. 2.9 for a typical uniaxial test on Opalinus Clay with unload-reload cycles. It can be seen that the deformation behaviour of Opalinus Clay at low stress levels is characterized by a shallow sloping stress-strain curve near the origin ( $0 < \sigma < 2$  MPa). The low-stress Region I is of most interest in the context of unloading around tunnels.



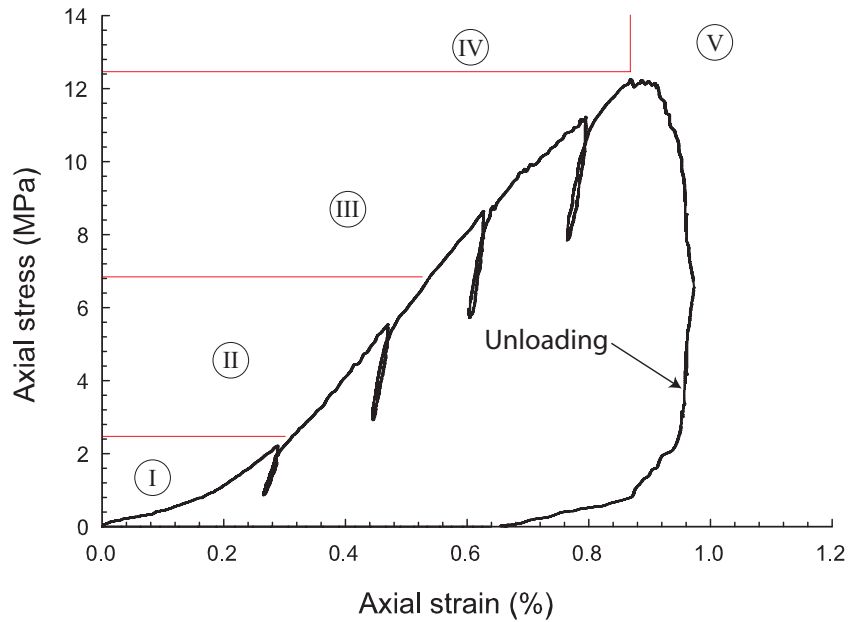


Figure 2.9: The full stress-strain response of Opalinus Clay in unconfined compression using a servo-controlled testing apparatus. The four regions of the stress-strain curve are approximately defined (Sample 2-22-2p, tested by Rummel [27]).

This section presents the stress-strain response of Opalinus Clay in relatively simple uniaxial and triaxial compression tests in order to characterize the non-linear response and the effects of various levels of confining stress. Furthermore, these tests are used to quantify this behaviour. Numerous laboratory programs have been carried out to investigate the properties of Opalinus Clay. This paper makes use of this data along with supplemental testing carried out at the University of Alberta to examine the stress-strain behaviour of Opalinus Clay at low stress levels.

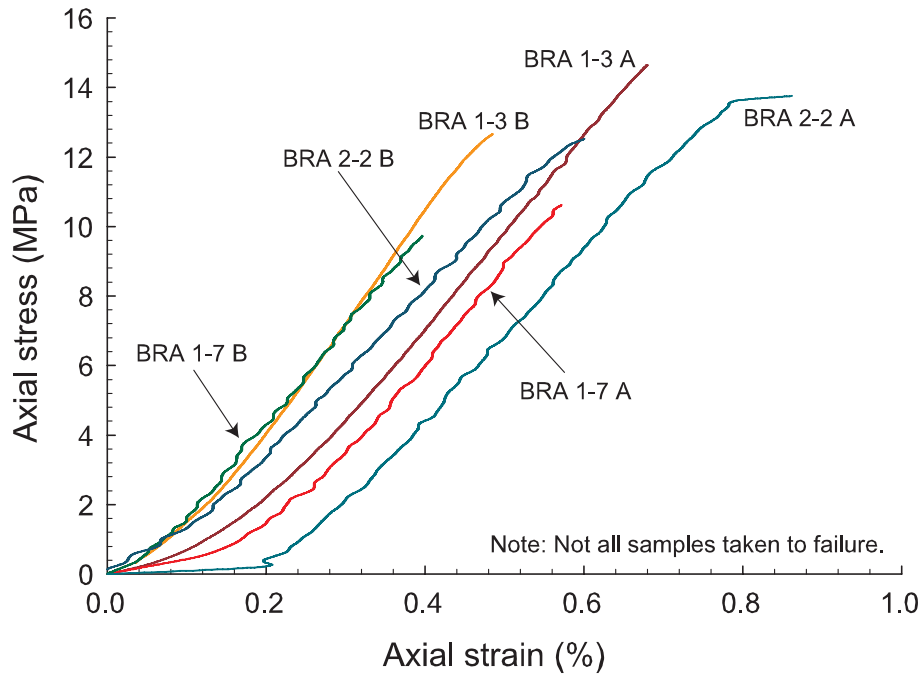
### 2.3.1 Uniaxial Test Results

The effect of testing equipment on the measured properties must be addressed to determine if the observed behaviour is a result of the testing procedure or representative of the in-situ material. Korinets and Alehossein [28] state that for hard rocks, non-linearity at low stresses can be the result of boundary asperities rather than the closure of internal voids, flaws or fractures in the sample. Their experiments were conducted using granite and norite samples, supplemented by numerical modelling. Typically an external measuring system, with LVDTs mounted on

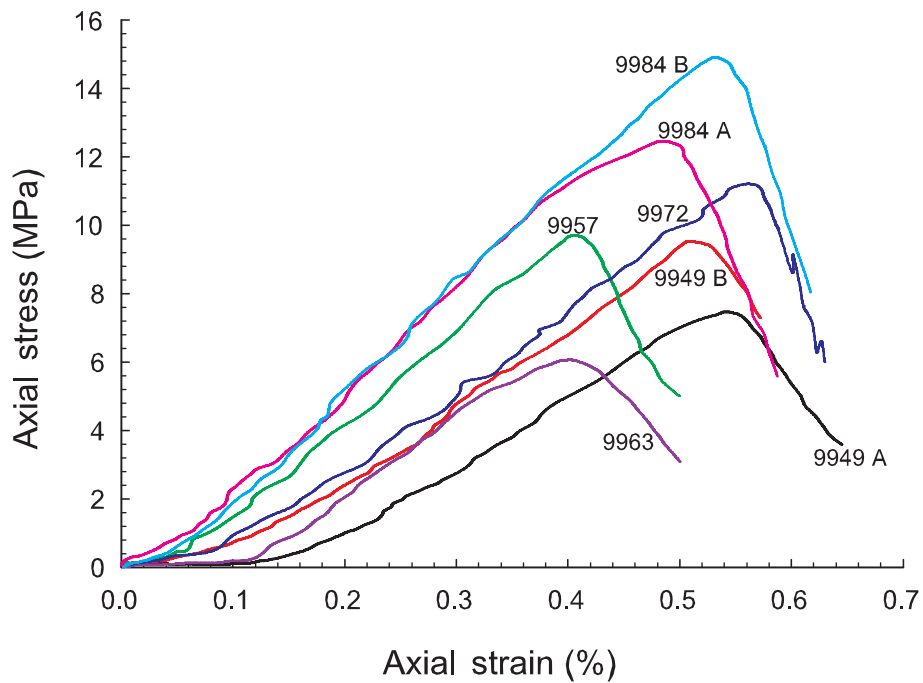
the platens, is used for cylindrical compression tests. An internal measuring system with LVDTs mounted directly onto the sample can remove the effects of asperities, but Korinets and Alehossein [28] state that for more porous and softer rocks the edge effect may totally disappear. The data presented here for Opalinus Clay was measured by external means (LVDT between the end platens). The Opalinus Clay would be considered “soft” in this context, measurements by external means alone should adequately represent the behaviour of the sample. Data presented in this paper has been compiled from three independent laboratory programs utilizing different loading equipment and measuring systems. This shows that the behaviour is observed independently using different platens and seating conditions.

Uniaxial tests were performed at the University of Alberta on 83 mm diameter saw-cut core samples from Boreholes BRA-1 and BRA-2 drilled with oil and air drilling fluids, respectively. Apart from the difference in colour (oil-drilled samples were darker), there was no real indication that the drilling fluid had a significant effect on the strength and stiffness of the samples. Stress-strain plots for the six samples are shown in Fig. 2.10(a) showing significant low stiffness, non-linear response at low stress levels typical of Region I behaviour. Only samples oriented parallel to bedding, referred to as “P-samples”, were provided for the laboratory program. The tests were conducted at constant stress rate of 0.25 MPa per minute (a strain rate of about  $2 \times 10^{-6}$  per second). Because the initial portion of the stress-strain curve was of greatest interest, some of these samples were loaded cyclically and were not all taken to failure. Only the initial loading curve is shown for cyclically loaded samples and the post-peak response was not recorded. An additional seven unconfined uniaxial compression tests carried out on P-samples by Olalla et al. [29] are shown in Fig. 2.10(b). These samples were generally 78 mm diameter and were also saw-cut directly from the core samples.

Further uniaxial tests were carried out by Rummel [27] using mini-core samples (30 mm diameter, 65 mm length) tested in a 30 tonne servo-controlled loading machine at a constant strain rate of  $1 \times 10^{-6}$  per second. The axial load was measured using a calibrated strain-gauge type load cell and axial deformation was measured using two inductive displacement transducers placed parallel to the sample on op-

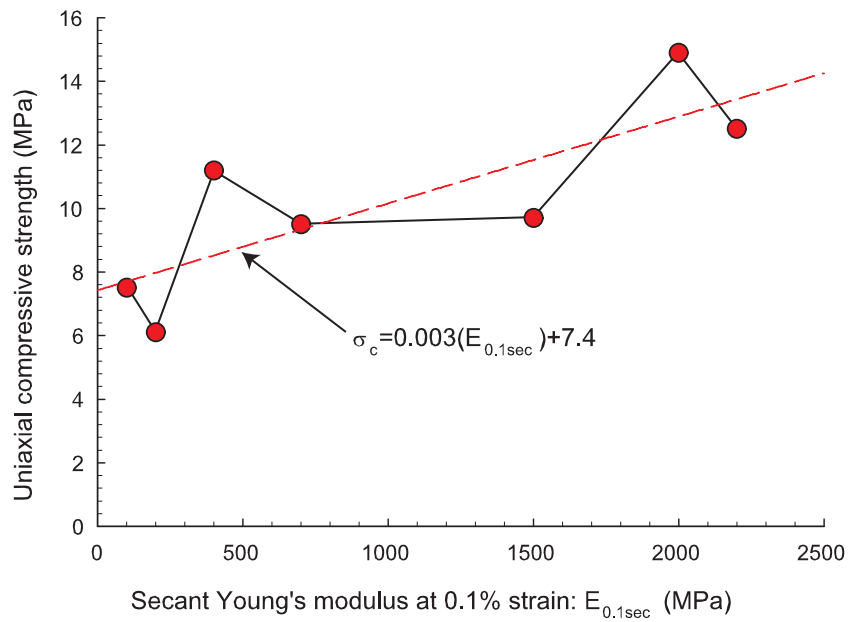


(a) Unconfined compression tests conducted at University of Alberta.

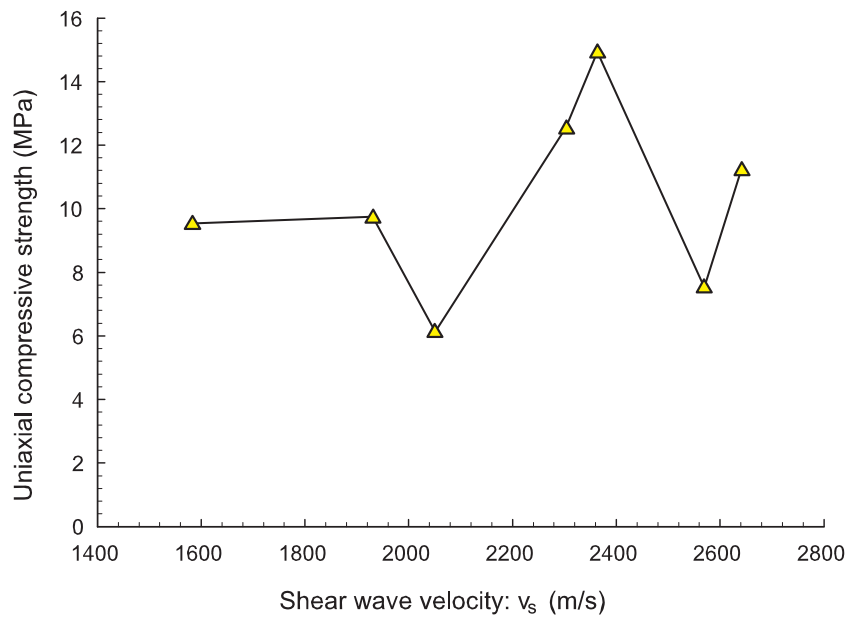


(b) Unconfined compression tests carried out by Olalla et al. [29].

Figure 2.10: Stress-strain plots from unconfined compression tests. The samples have significant low stiffness, non-linear response at low stress levels.



(a) There is a positive correlation between  $E_{0.1sec}$  and UCS. Strength and low stress stiffness properties are affected by the formation of micro-cracks.



(b) Seismic shear wave velocity ( $v_s$ ) measurements are less sensitive to the effects of micro-cracks in the Opalinus Clay.

Figure 2.11: The effect of micro-cracks on UCS relative to low stress stiffness and seismic shear wave velocity. (Data from Olalla et al. [29].)

posite sides. A typical stress-strain curve from this program is shown in Fig. 2.9 for Sample 2-22-2p which again shows low stress non-linearity. Sample 2-22-2p (P-sample) yielded at a peak stress of 12.1 MPa and had a Young's modulus of 4.2 GPa. The Young's modulus from unloading-reloading cycles was 15.7 GPa, significantly stiffer than the virgin loading curve. This response is often observed for unload-reload cycles and Jaeger and Cook [30] have attributed this behaviour to the work done against friction between the crack surfaces during loading and unloading. The unload-reload loop stiffness is representative of the small strain stiffness of the material which Atkinson [31] considered to be comparable to the dynamic stiffness properties obtained from seismic velocity measurements.

A plot of the secant Young's modulus at 0.1 % axial strain ( $E_{0.1sec}$ ) versus the uniaxial compressive strength (UCS) of the seven uniaxial tests shown previously (Fig. 2.10(b) can be seen in Fig. 2.11. The plot shows that a linear relationship exists between  $E_{0.1sec}$  and UCS; the degraded stiffness at low stress correlates with decreased strength. The relationship also gives further validity to the low stiffness non-linearity of the stress-strain curve as a "true" material response, as opposed to seating or other testing-induced issues. Shear wave velocities ( $v_s$ ) for the seven samples are also plotted. A weaker correlation exists between  $v_s$  and UCS for the samples, but it serves to further support the relationship.

Dilation has been shown to be an important issue in underground construction. For example: the onset of dilation (or dilational boundary) has been associated with the long-term strength which controls yielding and the extent of EDZ development [32]. From true triaxial testing of Opalinus Clay with ultrasonic monitoring, Popp and Salzer [33] concluded that onset of dilation occurs significantly below peak strength. Fig. 2.12 shows stress-strain curves for two unconfined compression tests on samples of Opalinus Clay conducted by Olalla et al. [29] that include lateral strain measurements using LVDTs. Although dilation has been measured consistently in the post-peak range, to this point there is no clear evidence of the onset of dilation in triaxial or uniaxial testing of Opalinus Clay in the pre-peak range (Blümling, pers. comm.).

The stress-strain curve of a P-sample loaded uniaxially in a cyclic manner with

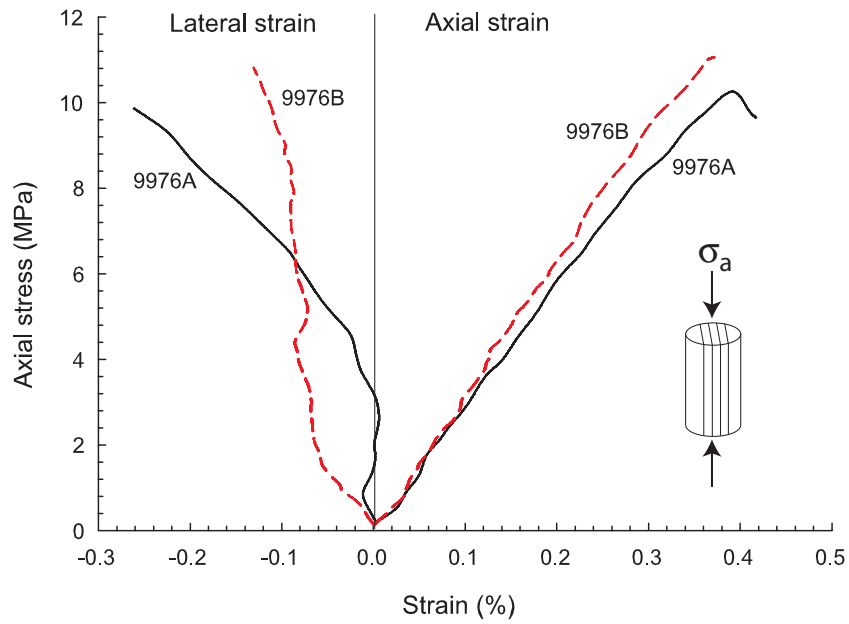


Figure 2.12: Axial stress vs. axial and lateral strain for unconfined compression tests on a P-samples (parallel to bedding) with lateral strain measurements using LVDTs. (Data from Olalla et al. [29].)

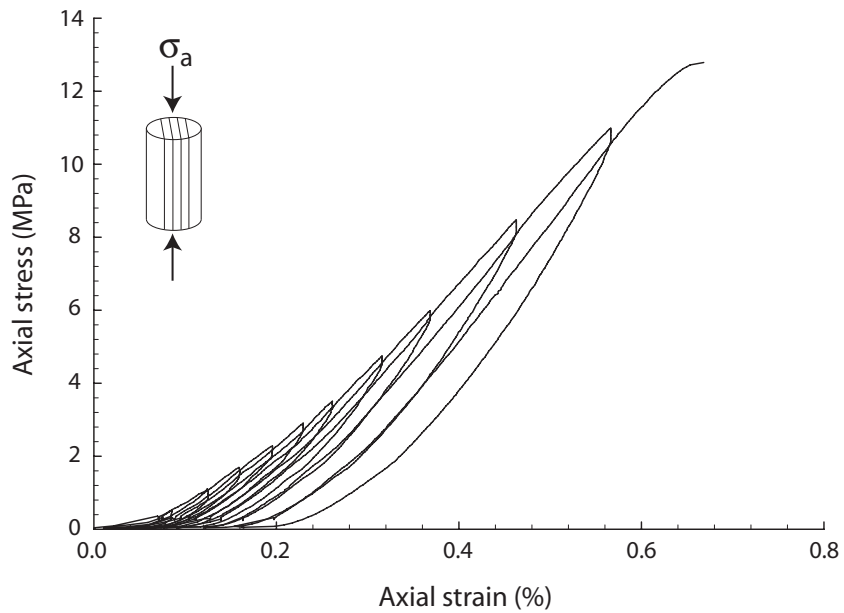


Figure 2.13: Cyclic axial loading to increased stress levels for sample BRA-1/3b. Non-linearity at low stress levels is repeated (recoverable) in each cycle. The lack of decreased stiffness with each cycle indicates damage due to deviatoric loading is not significant.

increasing levels of axial stress is shown in Fig. 2.13. Interestingly, the region of non-linearity, or crack closure, is repeatedly seen with each cycle. Therefore, the non-linear behaviour is recoverable and repeatable to some degree. This cannot be described as purely elastic or purely plastic behaviour, but may be described as anelastic behaviour. There was no observed decrease in stiffness with cycling, or due to increased loading, indicating that significant damage has not occurred as a result of cyclic loading or deviatoric stress levels. A better quantification of the effects of sample damage can be achieved by cyclically loading the sample to a repeated, constant, relatively high stress level (into Region IV). At a given stress level the initial portion of each unloading cycle was significantly more steep than the corresponding portion of the loading cycle with resulting hysteresis. This was similar to the small unload-reloading loops measured on Sample 2-22-2p (see Fig. 2.9) discussed previously.

### **2.3.2 Triaxial Test Results**

Consolidated undrained triaxial tests have been used to assess the effects of confining stress on the shape of the stress-strain curve. Stress-strain plots for consolidated undrained triaxial tests of samples of Opalinus Clay at confining stresses of 0, 6, 10 and 20 MPa are shown in Fig 2.14. These tests, conducted by Olalla et al. [29], were carried out at a strain-rate of  $1 \times 10^{-6}$  per second on samples that were originally 78 mm diameter and lathed down to 75 mm diameter for triaxial testing. At low confining stress, the low stiffness non-linearity is similar to that of unconfined compression tests. This behaviour is diminished with increased confining stress. A positive correlation between stiffness and confining stress was found by observing that the Young's modulus at 0.2 % strain showed increased stiffness with increased confining stress. Below 0.2 % strain, the stiffness increase with confining stress was notably even more significant due to the effects of micro-cracks. At high confining stress (20 MPa) the high non-linear small-strain stiffness typical of many bonded argillaceous materials can be seen. The samples show brittle response at all confining stress levels. Surprisingly, no indication of a brittle-ductile transition was observed up to 20 MPa (twice the estimated maximum past pressure).

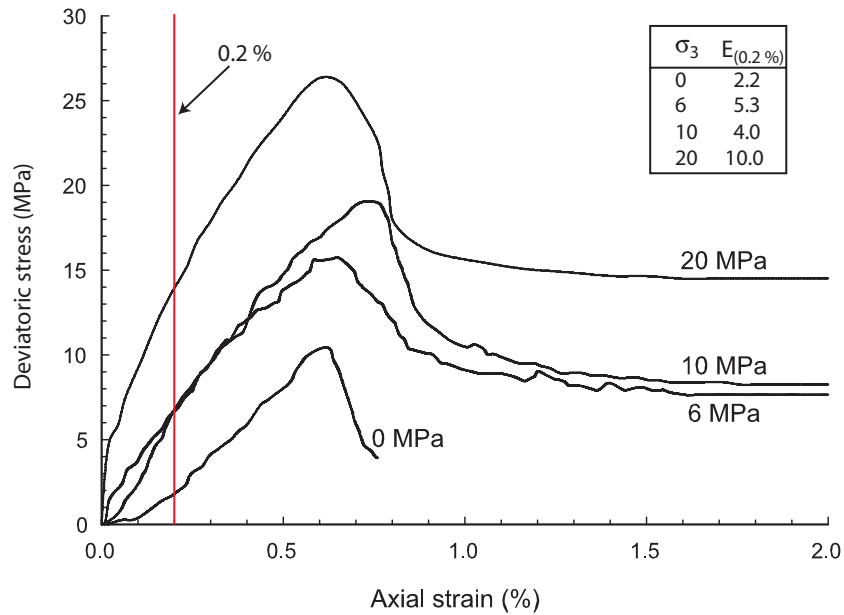


Figure 2.14: Stress-strain plots for a range of  $\sigma_3$  values (0-20 MPa). The increased stiffness with confinement indicates the presence of micro-cracks. All samples show a brittle post-peak response, even at  $\sigma_3 = 20$  MPa. (Data from Olalla et al. [29])

### 2.3.3 Summary

Stress-strain data from several independent sources, using different equipment, has been presented here. All tests show mild to strong non-linear behaviour up to an axial stress of between 1 and 2 MPa. Above this stress threshold, samples are linear elastic with slight non-linearity after about 80 to 90 % of peak strength. The stiffness in the linear range was found to increase with increased confining stress, indicative of the closure of micro-cracks. The extremely flat slope of the stress-strain curve at low stress indicates that the micro-cracks are not only extensive, but that they may be substantially open. It is interesting to note that the stress level associated with crack closure corresponds approximately with the minimum in-situ stress at Mont Terri ( $\sigma_3=2.2$  MPa [8]).

## 2.4 Sample Stress Path

Soil and rock samples removed from their in-situ state by coring can be affected by a process referred to as sample disturbance. Martin and Stimpson [26] showed



the effect of sample disturbance on the properties of Lac du Bonnet granite and Santarelli and Dusseault [34] discussed the influence of sample disturbance on core samples in the petroleum industry. More specifically to argillaceous rocks, Barla et al. [35] described the need to scale-up laboratory properties in order to match tunnel deformations in an Italian clay shale, i.e., the damaged sample properties significantly over-estimated deformations. The stress-induced damage caused by sample disturbance is often characterized by degradation of the sample's mechanical properties (i.e. strength and stiffness) due mostly to the formation and opening of micro-cracks in samples. Once confining stress is applied to the samples, this stress-induced damage is partially recovered as the open micro-cracks close and the stiffness of the material is partially restored. However, as pointed out by Martin and Stimpson [26], the application of confining stress can never fully recover the cohesion of the damaged rock and the laboratory properties can never fully attain the true properties of the in-situ rock. This section describes the use of numerical modelling to quantify the most significant processes that result in the observed stress-strain response of Opalinus Clay, and illustrates that the rockmass near tunnel boundaries undergoes similar processes and can be expected to respond similarly.

#### **2.4.1 Sample Disturbance at Mont Terri**

Thury and Bossart [10] evaluated the properties of samples cored with single-, double- and triple-tube core barrels at Mont Terri. It was found that the use of a double core barrel was sufficient to limit disturbance. Experiments were made with a number of drilling fluids with the conclusion that compressed air resulted in the least damage to cores and the most stable boreholes. Cores were sealed immediately with a number of measures, such as vacuum sealing in plastic with or without enclosure in a pressure cell. The Opalinus Clay is a fairly strong and brittle soft rock, and even with these precautions the stress-strain data shown previously in Figs. 2.10(a), 2.11 and 2.14 indicate that the samples tested were indeed significantly affected by micro-crack generation and opening.

Martin and Stimpson [26] noted that these stress-induced flaws reduced the uniaxial strength of the Lac du Bonnet granite from approximately 220 MPa to

155 MPa when the ratio of far-field maximum stress to the undisturbed uniaxial strength was approximately 0.25. This ratio would be approximately 0.55 for the Opalinus Clay at Mont Terri, using a vertical stress of 6.5 MPa. Hence, if a similar reduction occurred in the Opalinus Clay samples, the uniaxial compressive strength of undisturbed samples would increase to 14 and 22 MPa for samples parallel and perpendicular to bedding, respectively, based on the strength values shown in Table 2.3 [36].

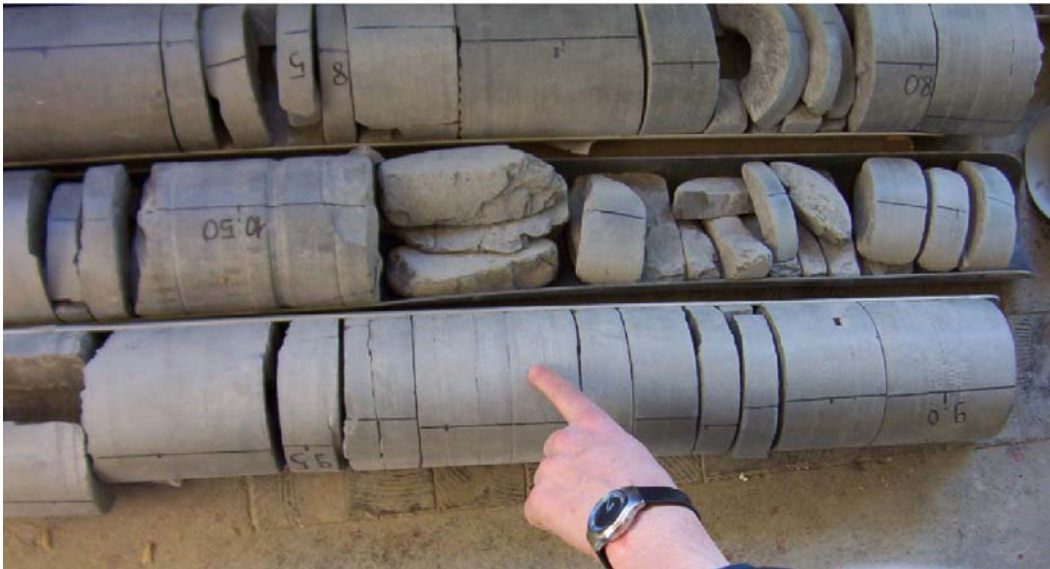


Figure 2.15: Core dinking was generally only observed during the overcoring program. No dinking in the section where the strain gage was placed, indicating that very small confining stress can affect dinking.

Core dinking (disk-like breakage of core samples) is a common sign of sample disturbance. Core dinking rarely has been observed at Mont Terri for typical solid coring (Blümling, pers. comm.). However, core dinking was observed during an in-situ stress measurement programme at Mont Terri using the overcoring method as shown in Fig 2.15. The measuring device for these tests was a CSIRO hollow-inclusion stress gage (containing many strain gages) installed in a 25 mm diameter inner hole that was later overcored by a 150 mm outer hole. The core dinking was observed along the entire length of the borehole except in the zone where the strain gage was located. The gage is made of a fairly compliant material and glued onto the side of the inner borehole wall. This suggests that even minimal confining stress

can reduce the tendency to disk, further evidence that minimal confining stresses may have a disproportionate effect on the response of Opalinus Clay.

## 2.4.2 Sampling Stress Path at Mont Terri

It has been shown that processes occurring during sampling have a significant effect on the laboratory properties of Opalinus Clay. A linear-elastic analysis of the sampling stress path was used to investigate whether unloading (tensile strain) or deviatoric loading (shear strain) was the most dominant aspect leading to the stress-induced formation and opening of micro-cracks in samples from Mont Terri.

A three-dimensional finite difference method (FDM) model using *FLAC<sup>3D</sup>*<sup>2</sup> was used to investigate the stress path of sampling at Mont Terri. This model simulates only the behaviour due to release of the core from the in-situ stress field. It does not include detachment of the core end from the formation. The model was not capable of simulating complete detachment, nevertheless, most of the stress changes occur prior to detachment. The effects of cooling fluid (air or oil), the drilling process (heat and vibration) and handling and storage effects were not considered by the model. Given these limitations, the model was effective in capturing the most dominant aspects of the stress path that occurred during sampling. This can be compared directly to the stress path of the rockmass during tunnel excavation.

The stress field used in the model had the following magnitudes and orientations:

- $\sigma_1 = 6.5$  MPa – vertical
- $\sigma_2 = 4.0$  MPa – horizontal (parallel to borehole)
- $\sigma_3 = 2.2$  MPa – horizontal (perpendicular to borehole)

The stress field at the Mont Terri rock laboratory [8] with a simplified orientation to the stress field (horizontal sampling parallel to  $\sigma_2$ ) was used in the model. This orientation results in the maximum deviatoric stress conditions around the excavation and is similar to that observed around a circular test tunnel. Stresses can be

---

<sup>2</sup>see [www.itascacg.com](http://www.itascacg.com)

significantly higher in the vicinity of existing excavations due to three-dimensional effects.

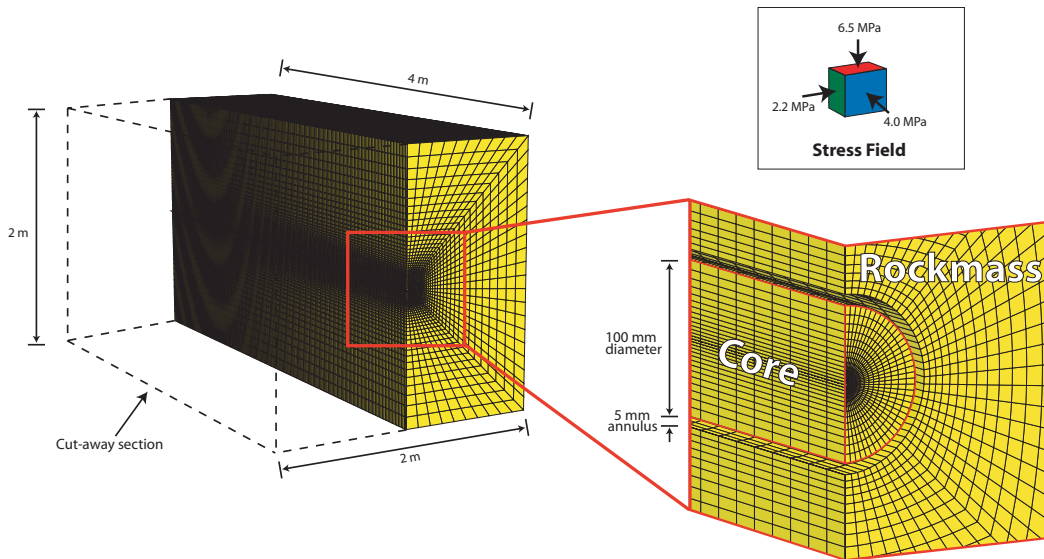


Figure 2.16: A cutaway of the three-dimensional finite difference model (FLAC<sup>3D</sup>) and stress field used to simulate excavation of a core at the Mont Terri rock laboratory.

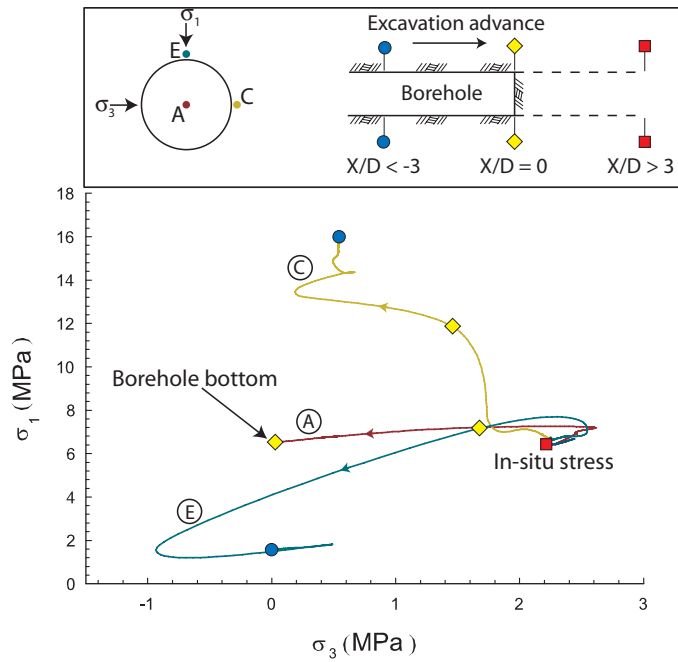
The model geometry consisted of a 2 m x 4 m brick-shaped grid with a central borehole aligned parallel to the long axis. The 100 mm diameter core with a 5 mm annulus was built into the mesh which had a grid spacing of about 4 mm at the excavation boundary, grading larger away from the excavation. The model geometry and stress field are shown in Fig. 2.16. Initially, roller boundary conditions (fixed in 1 direction and free in 2 directions) were applied to all sides of the model. This type of boundary condition is considered appropriate for modelling a rockmass in an infinite elastic medium where adequate distance has been provided from the excavation to the model boundaries [37].

Two model simulations were run for comparison: one to simulate sampling (without detachment from the rockmass), and one that simulates the fully excavated borehole alone. Instead of sequentially advancing the borehole excavation, the annulus was instantaneously excavated for a length of 2 m. When the annulus of the borehole was excavated, the end of the core at the outer boundary was

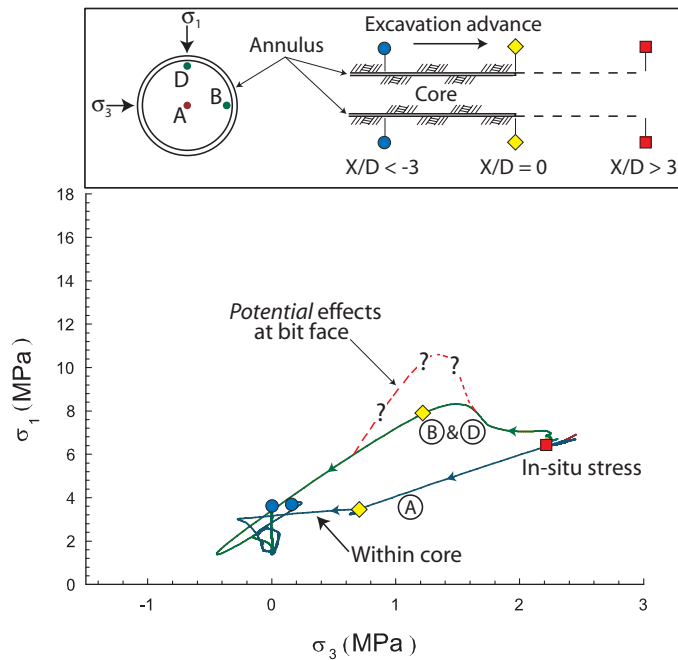
released (free boundary condition) simulating release of the top end of the core. Stresses along a line running the length of the borehole were recorded relative to the excavation face to track the stress path at a given point with excavation advance.

Typical of the elastic stress distribution around a circular opening in an anisotropic stress field, the rockmass was compressive in the sidewalls perpendicular to the  $\sigma_1$  direction and unloading occurred in the top and bottom of the borehole, parallel to the  $\sigma_1$  direction. The core itself experienced complete unloading to a uniform stress state throughout. The stress paths followed by the rockmass and core during excavation are shown in Fig. 2.17. Stress paths within the core while still attached to the formation are shown along the centreline (Point A), along the side/sample boundary (Point C), and along the top (Point E). The stress path for the fully excavated borehole along the same orientation is plotted with corresponding points along the boundary: centreline (Point A), side (Point B) and top (Point D). Points on the top and side core boundary followed identical stress paths. The stress path for a point at the centreline of the core was slightly different than at the centreline of the borehole because the borehole was fully excavated (with free excavation face) while the core remained attached to the formation. A model capable of tracking detachment of the sample from the formation would simply show further unloading near the sample end.

Fig. 2.17 shows that the dominant stress-path is unloading, particularly in the core, borehole roof and excavation face. Deviatoric loading is only a factor along a line corresponding to Point C. The effects at the bit-face may result in some yielding near the core boundary and the minor effects of heat, vibration, handling and storage may result in minor sample disturbance. Therefore, the degree and nature of micro-crack formation and opening in samples exhibiting strong, non-linear deformations at low stress levels is a consequence of the unloading process. This agrees well with the geological model and implies that damage is likely due to the breaking of diagenetic bonds from tensile strain, with release of latent strain energy. It should be noted that the fully excavated borehole is analogous to a tunnel excavated in the same stress field. This suggests that the stress path of sampling is similar to that in the tunnel roof/floor and that high deviatoric stresses accompany unloading along



(a) Borehole stress path with inside core removed.



(b) Sample stress path prior to detachment of core end from formation.

Figure 2.17: Stress path along a core and borehole/tunnel wall during sampling from elastic stress analysis (FLAC<sup>3D</sup>) indicates that the stress-induced cause of sample disturbance in Opalinus Clay is dominated by unloading processes.

the tunnel springline.

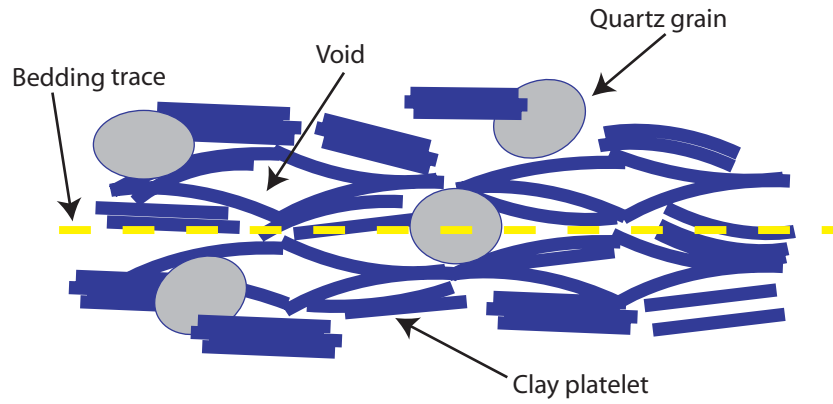
## 2.5 Discussion and Interpretation

It has been shown that the stress-strain curve of Opalinus Clay behaves in a manner that is highly non-linear with low stiffness at low stresses. The nature of diagenetic bonding explains why tensile strain (e.g. from unloading) results in the formation and opening of micro-cracks. This behaviour is more pronounced in Opalinus Clay than with other geomaterials because the locked-in strain energy is an inherent property of the Opalinus Clay micro-structure.

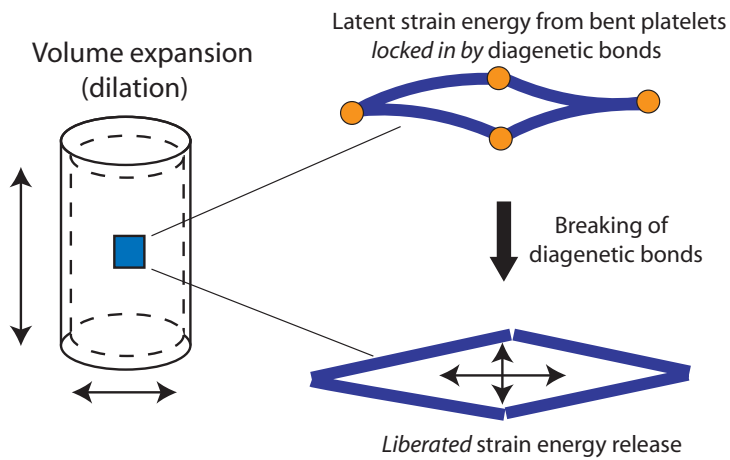
A conceptual model of the Opalinus Clay micro-structure as a matrix of bent clay platelets with quartz silt grains interspersed is shown in Fig. 2.18(a). This conceptual model includes the effects of locked-in latent strain energy and diagenetic bonding as described by Bjerrum [24]. It agrees well with the observed phenomena and is physically consistent with the geological history of the Opalinus Clay. The breakage of bonds with the release of strain energy and resultant micro-crack opening has an observable effect on the stress-strain curve. Although not directly verified in this study, the anticipated initial response upon unloading would be volumetric dilation (see Fig. 2.18(b)) as the broken bonds provide the kinematic freedom to allow the clay platelets to straighten. This effect is illustrated by Fig. 2.18(b).

The reduced strength and stiffness properties due to bond breakage may be dealt with numerically using damage mechanics by means of a damage variable and associated function. In reality this behaviour is probably due to a combination of the factors discussed. The damage of greatest significance appears to be induced by unloading, as opposed to deviatoric loading. Therefore, once bonds are broken, the stress-strain response appears to be nearly fully recoverable (not plasticity). In practical terms, it can probably be described best as a relationship where stiffness is a function of stress or as a stress-dependent modulus. Such a stress-dependent modulus has been proposed by Ewy and Cook [38] and Santarelli et al. [39] for deep boreholes in the petroleum industry.

Based on a wide range of experimental data, Kulhawy [40] concluded that non-



(a) Conceptual model of Opalinus Clay micro-structure with horizontal bedding. See Fig. 2.5 for comparison.



(b) Release of latent strain energy due to breakage of diagenetic bonds results in dilation and reduced cohesion and stiffness.

Figure 2.18: Micro-structure of the Opalinus Clay based on geological history.



linearity and pressure dependence of the rock modulus are significant factors in porous, clastic or closely jointed rock. It has been observed that porous rock often exhibits a relationship between confining stress and elastic modulus due to decreased porosity from consolidation at higher stress levels or closure of micro- and macro-fractures. The stress-strain curves presented in Sect. 2.3 show this to be consistent with the behaviour of the Opalinus Clay in terms of micro-fracture closure (Region I).

Triaxial tests consolidated hydrostatically initially often have relatively high axial stresses with resulting initial micro-crack closure. Therefore, the stress-strain curve for triaxial tests at low deviatoric stress can not be expected to exhibit the same characteristics as a uniaxial test at low deviatoric stresses. For example, a sample consolidated hydrostatically to 5 MPa actually has the full 5 MPa acting on it axially at zero deviatoric stress. Although there is no confining stress ( $\sigma_3$ ) applied to unconfined tests, this simple index test provides a way to quantify stiffness at true low stress, particularly in the direction of loading (axial). This implies that modulus is a function of stress in the direction of a given applied stress, or that an anisotropic stress field results in an anisotropic stiffness field. This has significant implication to tunnelling deformations.

The stress-strain curve for Sample 2-22-2p (see Fig. 2.9) was fairly typical of unconfined compression tests, particularly in the range below 2 MPa, and was conducted with axial deformations measured using two LVDTs by Rummel [27]. The incremental secant modulus at low axial stress levels ( $\sigma_1$ ) are shown as circles for Sample 2-22-2p in Fig. 2.19. Triaxial data of confining stress ( $\sigma_3$ ) and Young's modulus (E) at 0.2 % strain, from Olalla et al. [29], are shown as diamonds. From this plot it can be seen that a relationship between E and  $\sigma$  exists. A curve can be fitted to the combined data with an equation of the same form as that found by Santarelli et al. [39] for carboniferous sandstone. The fitted curve has an  $r^2 = 0.89$  with the equation:

$$E(\sigma) = -0.7 + 2.2(\sigma)^{0.48} \quad (2.1)$$

It is reasonable to assume that the severity of stress-strain non-linearity can be

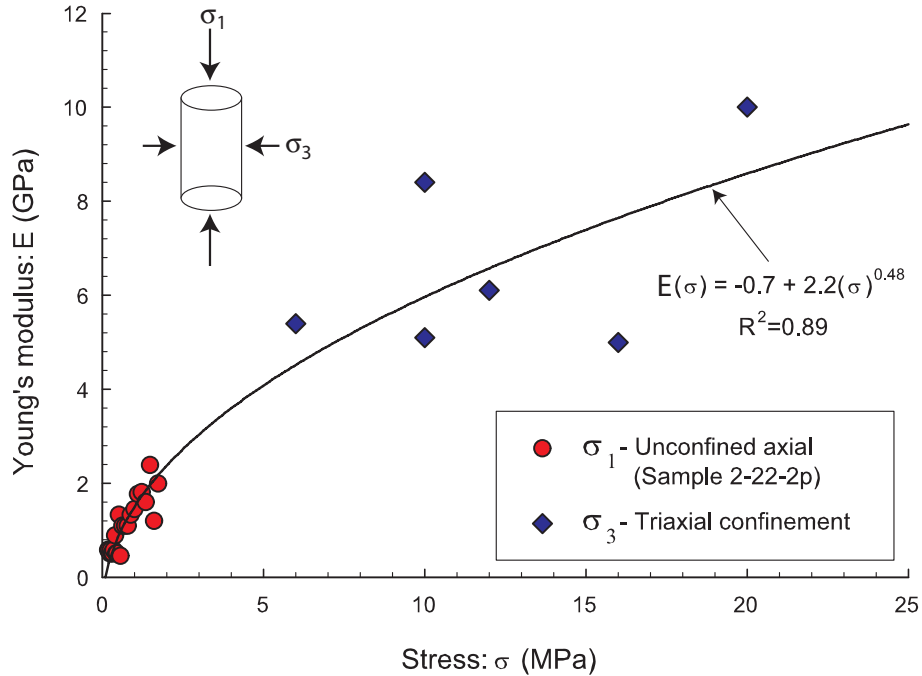


Figure 2.19: Non-linear elastic Young's modulus related to stress levels ( $\sigma_1, \sigma_3$ ). Sample 2-22-2p used for low stress  $\sigma_1$  portion.

affected by numerous processes. Processes that result in increased bond breakage, such as tensile strain, shear strain, or time-dependent processes would amplify this non-linear elastic behaviour. If bond breakage is severe (e.g. unloading and high deviatoric stress), and involve large volumes of material with greater energy release, strain localization can be expected resulting in the development of macro-fractures in addition to micro-cracking (i.e. EDZ extensional fractures in a compressive stress field). It seems evident that damage associated with excavation induced strain results in the breakage of diagenetic bonds and liberation of latent strain energy. Potentially, in samples most of the strain associated with the release of diagenetic bonds will occur as a result of the initial stress release due to sampling.

## 2.6 Conclusions

Laboratory testing of samples recovered at Mont Terri rock laboratory indicate that the stress-strain behaviour of Opalinus Clay is highly non-linear at low confining stresses. The UCS tests, confirmed by laboratory seismic measurements, showed

that a correlation exists between the degree of non-linearity and peak strength. Tri-axial data also showed that stiffness increased with increased confining stress.

An investigation of this non-linearity has shown that it is a material property linked to the geological history, in particular, diagenesis of the Opalinus Clay. Diagenetic processes over the last 180 Ma have been responsible for chemical and mechanical changes since deposition of the Opalinus Clay. This alteration has resulted in a decrease in porosity and increase in stiffness and cohesive strength. SEM imaging shows that folded and bent clay platelets are prevalent throughout the clay matrix. The breakage of diagenetic bonds results in the liberation of strain energy stored within the bent clay platelet structure and is responsible for the highly non-linear behaviour at low confining stresses.

Numerical modelling demonstrated that the stress-path followed during sampling is very similar to the stress path experienced at the boundary of a tunnel. Hence, the non-linear response observed in laboratory samples is also likely to be a characteristic of the tunnel response. Based on the laboratory test results, the non-linear stiffness has been quantified as a function of stress levels. This relationship serves to explain observed large radial elastic deformations in tunnels excavated in soft argillaceous rock at Mont Terri rock laboratory [8]. The findings from this laboratory study have been used by the author to develop a phenomenological-based constitutive model of the non-linear elastic behaviour to successfully model the unloading response of Opalinus Clay to tunnelling at Mont Terri rock laboratory [8].

## **Bibliography**

- [1] Corkum A G, Martin C D, The mechanical behaviour of weak mudstone (Opalinus Clay) at low stresses. *Int J Rock Mech Min Sci* 2006, In Progress.
- [2] Skempton W A, Long-term stability of clay slopes: Fourth Rankine Lecture. *Géotechnique* 1964, 14:77–101.
- [3] Steiner W, Swelling rock in tunnels: rock characterization, effect of horizontal stresses and construction procedures. *Int J Rock Mech Min Sci & Geomech Abstr* 1993, 30(4):361–380.

- [4] Lambert A, Clay: small particles with a large impact. In: From building bricks to repositories: the allrounder material clay, Nagra Bulletin, vol. 31 1997 .
- [5] Corkum A G, Martin C D, Modelling the short-term behaviour of Opalinus Clay around a circular excavation. In: Canadian Geotechnical Conference 2004 .
- [6] Bock H, RA Experiment: Rock mechanics analysis and synthesis: Conceptual model of the Opalinus Clay. Tech. Rep. Nagra, Internal Report TN01-03, Q+S Consult, Germany 2001.
- [7] Parker S P, editor, Dictionary of Geology & Mineralogy. McGraw-Hill 1997.
- [8] Corkum A G, Non-Linear Behaviour of Opalinus Clay Around Underground Excavations. Ph.D. thesis, Dept. Civil & Environmental Engineering, University of Alberta, Canada 2006.
- [9] Freivogel M, Huggenberger P, Modellierung bilanzierter Profile im Gebiet Mont Terri La Croix (Kanton Jura). Tech. Rep. 4 (Switzerland), FOWG, Geology Series 2003.
- [10] Thury M, Bossart P, Mont Terri rock laboratory: Results of the hydrogeological, geochemical and geotechnical experiments performed in 1996 and 1997. In: Geological Reports No. 23, Swiss National Hydrological and Geological Survey. Bern-Ittigen 1999 .
- [11] Ziegler P A, Geological Atlas of Western and Central Europe - 2nd edition. Shell International, Amsterdam (Elsevier) 1990.
- [12] Müller G, Diagenesis in Argillaceous Sediments. Elsevier Publishing Company 1967 pp. 127–177.
- [13] Wolf K H, Chilingarian G V, Diagenesis, III. Elsevier 1992, 674 pp.
- [14] Marschall P, Croisé J, Schlickerieder L, Boisson J Y, Vogel P, Yamamoto S, Synthesis of hydrogeological investigations at the Mont Terri site (Phases

- I to V). In: Mont Terri Project - Hydrogeological Synthesis, Osmotic Flow. - Reports of the Federal Office for Water and Geology (FOWG), Geology Series No 6, Bern, Heitzmann P, editor 2002 .
- [15] Potter P E, Maynard J B, Depetris P J, Mud & Mudstones: Introduction and Overview. Springer 2005.
- [16] Bock H, RA Experiment: Data report on rock mechanics - Mont Terri project. Tech. Rep. Nagra, Internal Report TN00-02, Q+S Consult, Germany 2000.
- [17] Möri A, Bossart P, DM Experiment: Thin section and REM analyses on deformed drillcores from rock mechanical lab experiments. Tech. Rep. TN99-76, Nagra Technical Note 2001.
- [18] Bishop A, Undisturbed samples of London clay from the Ashford Common shaft: strength-effective stress relationships. *Géotechnique* 1965, pp. 1–31.
- [19] Hedberg H, Gravitational compaction of clays and shales. *Am J Sci* 1936, 31:241–287.
- [20] Diederichs M S, Instability of hard rockmasses: the role of tensile damage and relaxation. Ph.D. thesis, University of Waterloo 1999.
- [21] Diederichs M S, Rock fracture and collapse under low confinement conditions. *Rock Mech and Rock Engin* 2003, 36(5):339–381.
- [22] Schmertmann J, Osterberg J, An experimental study of the development of cohesion and friction with axial strain in saturated cohesive soils. In: Proc. ASCE Research Conference on Shear Strength of Cohesive Soils 1968 p. 643.
- [23] Martin C D, Lanyon G W, Measurement of in-situ stress in weak rocks at Mont Terri rock laboratory, Switzerland. *Int J Rock Mech Min Sci* 2003, 40:1077–1088.
- [24] Bjerrum L, Progressive failure in slopes of overconsolidated plastic clay and clay shales: Third Terzaghi Lecture. *J Soil Mech Found Div, ASCE* 1967, 93(SM5):1–49.

- [25] Skempton A W, The consolidation of clays by gravitational compaction. Quarterly Journal of the Geological Society of London 1970, 125:373–411.
- [26] Martin C D, Stimpson B, The effects of sample disturbance on laboratory properties of lac du bonnet granite. Can Geotech J 1994, 31:692–702.
- [27] Rummel F, RA Experiment: Rock mechanics testing and characterization on drillcores of Boreholes BRA-1 and BRA-2, TN 2004-38. Tech. Rep., Nagra 2004.
- [28] Korinets A, Alehossein H, On the initial non-linearity of compressive stress-strain curves for intact rock: Technical Note. Rock Mech and Rock Engin 2002, 35(4):319–328.
- [29] Olalla C, Martin M, Sáez J, ED-B Experiment: Geotechnical laboratory testing on Opalinus Clay rock samples. Tech. Rep. TN98-57, Mont Terri Project 1999.
- [30] Jaeger J C, Cook N G W, Fundamentals of rock mechanics, 3rd Edition. Chapman & Hall 1979.
- [31] Atkinson J, Non-linear soil stiffness in routine design. Géotechnique 2000, 50(5):487–508.
- [32] Martin C D, Seventeenth Canadian Geotechnical Colloquium: The effect of cohesion loss and stress path on brittle rock strength. Can Geotech J 1997, 34(5):698–725.
- [33] Popp T, Salzer K, Triaxial deformation tests in a multi-anvil apparatus with ultrasonic monitoring. Tech. Rep., Nagra 2005.
- [34] Santarelli F J, Dusseault M B, Core quality control in petroleum engineering. In: Rock Mechanics as a Multidisciplinary Science, Roegiers, editor 1991 pp. 111–120.

- [35] Barla G, Barla M, Bonini M, Characterisation of Italian clay shales for tunnel design, CD-ROM, Paper 1B 05A - SINOROCK2004 Symposium. *Int J Rock Mech Min Sci* 2004, 41(3).
- [36] Martin C D, Lanyon G W, Blümling P, Mayor J C, The excavation disturbed zone around a test tunnel in the Opalinus Clay. In: *Proc. 5th North American Rock Mechanics Symposium and 17th Tunnelling Association of Canada Conference: NARMS/TAC 2002*, Hammah R, Baden W, Curran J, Telesnicki M, editors, Toronto: University of Toronto Press 2002 pp. 1581–1588.
- [37] Itasca Consulting Goup I, *FLAC (Fast Lagrangian Analysis of a Continua), Users Manual, Version 5.0*. Minneapolis, Minnesota 2005.
- [38] Ewy R T, Cook N G W, Deformation and fracture around cylindrical openings in rock – I. Observations and analysis of deformations. *Int J Rock Mech Min Sci* 1990, 27(5):409–427.
- [39] Santarelli F J, Brown E T, Maury V, Analysis of borehole stresses using pressure-dependent, linear elasticity: Technical Note. *Int J Rock Mech Min Sci & Geomech Abstr* 1986, 23(6):445–449.
- [40] Kulhawy F H, Stress deformation properties of rock and rock discontinuities. *Eng Geol* 1975, 9:327–350.

# Chapter 3

## Phenomenological models for stiffness and pore pressure around tunnels in soft argillaceous rock<sup>1</sup>

### 3.1 Introduction

The Opalinus Clay, named for the ammonite *Leioceras Opalinum*, is an argillaceous rock formed in the Jurassic Sea around 180 million years ago [2]. Because of its low conductivity and potential for self-sealing of excavation-induced fractures, this relatively weak claystone is being considered as a potential host formation for geological disposal of nuclear waste. According to Hudson et al. [3], the coherent choice of engineering design in rock mechanics depends on the predictive capability of numerical modelling. In keeping with this, numerical analyses, based on rock mechanics principles, will play a significant role in performance predictions of the natural barrier system for a repository excavated in Opalinus Clay at depths of between 300 to 700 m.

Most rocks are not elastic in the classic manner; for example, stress-strain curves show non-linearity, hysteresis, and apparent permanent strain [5]. It has been demonstrated from laboratory data, that the stress-strain curve for Opalinus Clay is highly non-linear (anelastic), with low stiffness at low stress levels [6]. This response is illustrated by unconfined compression tests shown in Fig. 3.1. Although the approximation of linear elasticity is suitable for most natural rocks, the use of

---

<sup>1</sup>A version of this chapter has been submitted as a paper to the *Rock Mech and Rock Engin.*



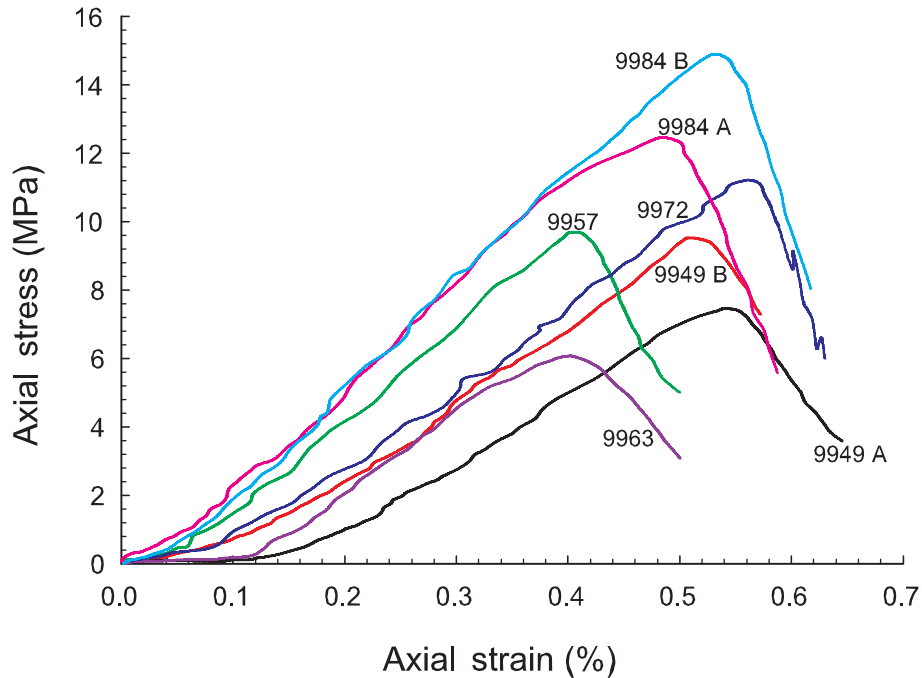


Figure 3.1: Stress-strain plots from unconfined compression tests carried out by Olalla et al. [4]. The samples have significant low stiffness, non-linear response at low stress levels.

linear-elasticity can result in significant misrepresentation in the prediction of deformations, pore pressures and yield mechanisms around underground excavations in Opalinus Clay.

Several researchers have dealt with the non-linear response of geomaterials in engineering practice. The Duncan and Chang [7] model for soil mechanics has been used extensively to predict pressure-dependent stiffness properties for soils. Kulhawy [8] developed a relationship for the pressure-dependent elastic modulus of porous rocks. The concept of pressure-dependent modulus has been used by Ewy and Cook [9] and Santarelli et al. [10] to predict the behaviour of porous rocks around deep boreholes.

For Opalinus Clay, the source of non-linearity is its micro-structure and, therefore, a model to accurately describe this behaviour warrants further study. A conceptual model of the micro-structure of Opalinus Clay, modified for the effects of locked-in latent strain energy and diagenetic bonding, has been presented by Corkum and Martin [6]. This model agrees well with the observed phenomena and

is physically consistent with the geological history of the Opalinus Clay. Because this behaviour can be attributed to the composition and geological history of the material, argillaceous rocks with similar geological history and mineral composition can be expected to have a similar characteristic response to excavation and unloading.

Two separate phenomenological-based models, to represent the stiffness (and resulting deformation) and pore pressure response around underground excavations in Opalinus Clay, have been proposed. This paper describes the development of these models and their implementation into the continuum finite difference code FLAC<sup>3D</sup><sup>2</sup>. Some verification of the models is also provided.

## 3.2 Background

A brief description follows of observations that highlight the impact of non-linear stress-strain behaviour on deformations, the development of the excavation disturbed zone (EDZ) and pore pressure response to tunnelling in Opalinus Clay. Many of these stem from the well documented ED-B mine-by test conducted in Switzerland at the Mont Terri rock laboratory in 1998 [11]. Laboratory data and observations of this non-linear behaviour have been described in detail by Corkum [12].

Corkum and Martin [6] showed that non-linearity of the stress-strain curve for Opalinus Clay is a result of diagenetic bond-breakage due to unloading (extensional strain) and the release of latent strain energy. Fig. 3.2 illustrates the stress path undergone by the rockmass along the centreline of a core during sampling, and that of the immediate tunnel boundary along the springline and roofline at the Mont Terri rock laboratory. The stress field at Mont Terri is:  $\sigma_1 = 6.5$  MPa,  $\sigma_2 = 4.0$  MPa and  $\sigma_3 = 2.2$  MPa [6]. It can be seen that in zones of unloading around tunnels, the rockmass follows a similar stress path as a core during sample retrieval. Therefore, the characteristic response observed in samples could be anticipated to be similar to that of the rockmass around a tunnel and, therefore, non-linearity of the stress-strain

---

<sup>2</sup>see [www.itascacg.com](http://www.itascacg.com)

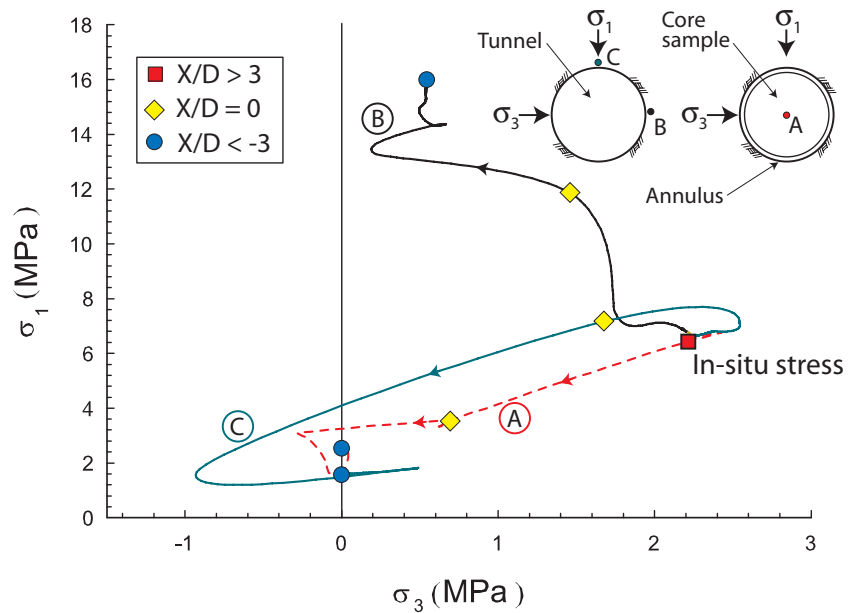


Figure 3.2: Stress path along a circular tunnel springline and roofline calculated with linear-elasticity ( $X/D > 0$  ahead of the tunnel face). The stress path along a core sample centreline undergoes similar unloading.

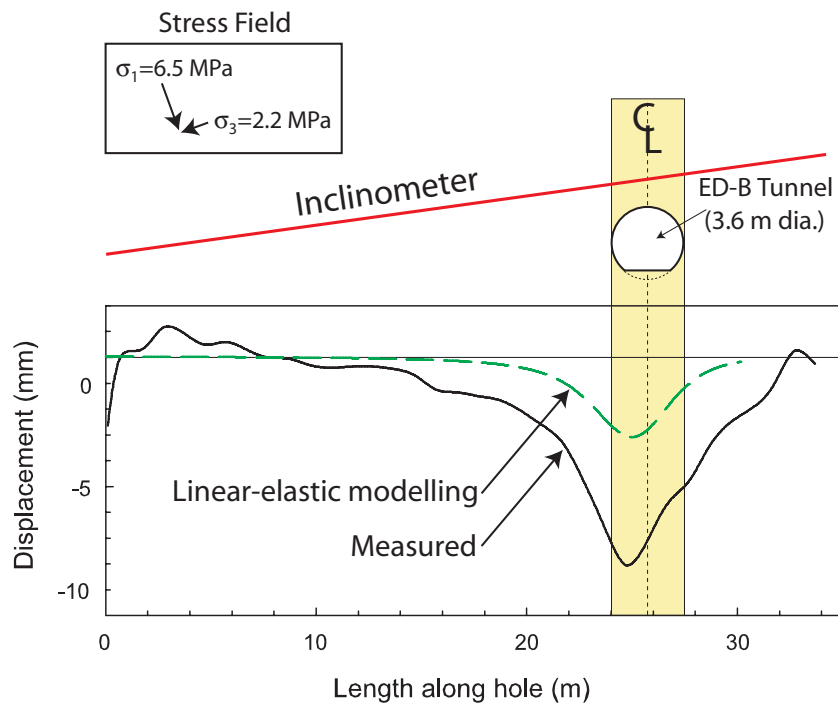


Figure 3.3: Maximum cumulative displacements from inclinometer measurements along Borehole BED B-6 located above the ED-B tunnel.

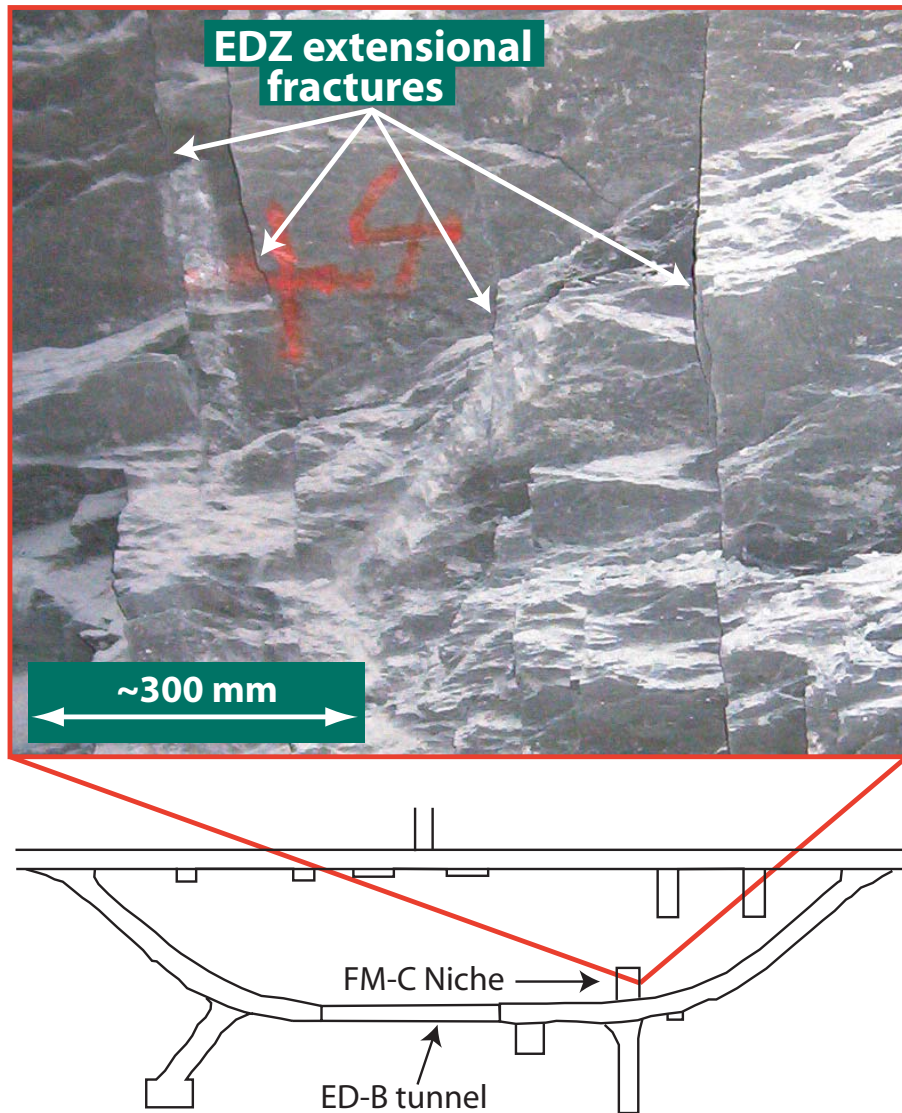


Figure 3.4: System of EDZ extensional fractures oriented parallel to the tunnel observed in the FM-C Niche at Mont Terri. These fractures are typical of those observed in the EDZ around tunnels at Mont Terri.

curve should not be overlooked.

The maximum cumulative inclinometer measurements along Borehole BED-B6 located above the 3.6 m diameter circular ED-B tunnel is shown in Fig. 3.3. The finite difference numerical code  $FLAC^{3D}$  was used to back-analyse the mine-by test [12] showing that linear-elasticity accounts for only about half of the measured deformations in this location. Furthermore, a field program called the Fracture Propagation (FP) study [13], carried out to investigate the nature and extent of the EDZ around the ED-B tunnel, showed that the dominant mode of yielding around the tunnel consisted of open extensional fractures. Where the EDZ has been intersected by another tunnel, these fractures have been observed on excavation walls, as shown for the FM-C Niche in Fig. 3.4.

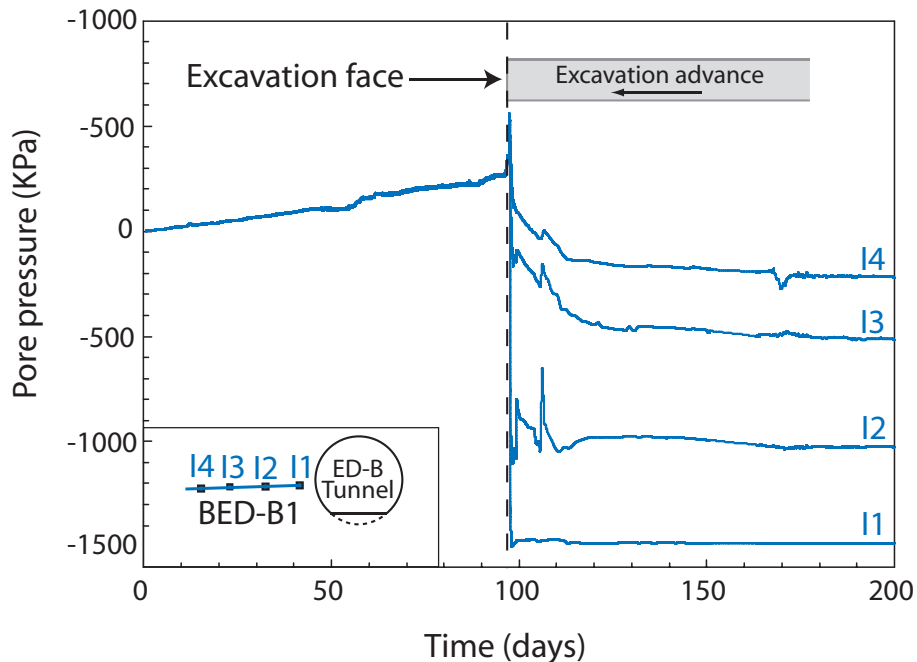


Figure 3.5: Pore pressure measurements near the tunnel springline during the ED-B mine-by test show an abrupt drop in pore pressure behind the excavation face. This response cannot be predicted by conventional hydromechanical means.

The pore pressure response due to excavation, measured during the ED-B mine-by test, indicated an unusual hydromechanical response. As an example, pore pressure measurements near the tunnel springline during the ED-B mine-by test are shown in Fig. 3.5. A moderate but steady rise in pore pressures was observed

prior to excavation while the piezometers equilibrated. As the excavation face approached the piezometers, the pore pressures rose, corresponding to excavation induced stress changes, with an abrupt spike at the excavation face. Immediately behind the excavation face, as excavation passed the piezometers, pore pressures dropped dramatically. The abrupt drop in pore pressure behind the excavation face differs significantly from typical hydromechanical analyses that predict steadily increasing pore pressures with increased mean stress [14, 15]. The distinct difference in pore pressure response in front and behind the excavation face indicates that different mechanisms are controlling the coupling response.

### 3.3 SDM Model for Opalinus Clay

Analytical methods to account for stress-dependent non-linear elasticity are reviewed in this section, followed by the development of a constitutive model for the Opalinus Clay, with some field verification.

Based on a wide range of experimental data, Kulhawy [8] concluded that non-linearity and pressure dependence of the rockmass elastic modulus are significant in porous, clastic or closely jointed rock. This can be due to decreased porosity from consolidation at higher stress levels or closure of micro- and macro-fractures. This concept may be represented numerically using variations of a pressure/stress-dependent modulus. Such a pressure-dependent modulus (PDM) has been proposed by Ewy and Cook [9] and Santarelli et al. [10] for deep boreholes in the petroleum industry.

Santarelli et al. [10] derived the closed form PDM solution for the case of a deep circular excavation in a simple plane-strain, homogeneous, isotropic elastic rockmass initially subjected to hydrostatic in-situ stress. The best-fit analytical equation to complete the closed form solution for  $E(\sigma_3)$  found by linear regression analysis of tangent modulus at 50 % peak strength measured in triaxial compression tests on dry Carboniferous sandstone was:

$$E = E_o(1 + 0.043\sigma_3^{0.78}) \quad (3.1)$$

The confining stress around a circular excavation typically increases with distance from the excavation boundary, especially with an in-situ stress ratio close to unity. Therefore, for materials with an  $E(\sigma)$  function, the pressure-dependent modulus approach has been simplified by Nawrocki and Dusseault [16] to a radius-dependent modulus (RDM). This allows for a simplified implementation into closed-form solutions and/or numerical modelling codes. The development of a model for Opalinus Clay similar to that used for the PDM will be described.

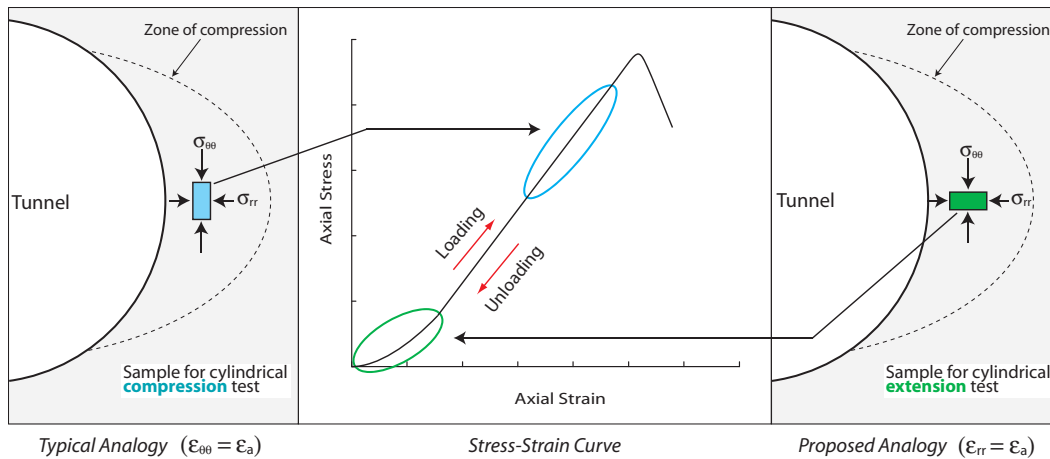


Figure 3.6: Based on stress path, tunnel behaviour is analogous to triaxial compression testing. Engineers are typically most interested in radial strain that is analogous to triaxial extension testing and corresponds to the non-linear portion (low stress) of the stress-strain curve for Opalinus Clay.

### 3.3.1 Model Development

Engineers are primarily concerned with deformations and yielding parallel to the tunnel boundary. In the radial direction, the rockmass undergoes unloading and it is this low stress response that dominates radial deformations around underground excavations in an elastic rockmass. Fig. 3.6 shows a tunnel excavated in a stress field with maximum and minimum principal stresses acting vertically and horizontally, respectively, that results in maximum deviatoric stresses acting in the tangential direction near the tunnel springline. This can be considered analogous to the stress path of a cylindrical compression test. The stress path is of great importance in tunnelling, however, this tool can be misleading in regard to the mode of yielding.

Looking at the problem at 90° from the typical analogy of triaxial loading, in the orientation of most interest around tunnels (radial), we could use the analogy of a triaxial extensional test (unloading) in the zone of compression (see Fig. 3.6). In the case of triaxial extension, for a highly non-linear material at low stress levels, it can be reasonably anticipated that deformations are dominated by the radial (lower) stress levels. The implications in terms of the development of extensional fracture and pore pressure response around excavations will be discussed later.

Triaxial testing at different confining stress levels indicates that a relationship exists between confining stress and the elastic Young's modulus for Opalinus Clay. At zero deviatoric stress, triaxial test samples consolidated to hydrostatic conditions often have significant true axial stresses prior to deviatoric loading. For example, a sample consolidated hydrostatically to 5 MPa actually has the full 5 MPa acting on it axially at zero deviatoric stress. This makes it difficult to evaluate material stiffness with triaxial testing at true low stress. Although there is no confining stress ( $\sigma_3$ ) applied to unconfined tests, they provide a practical means to quantify the stiffness at truly low stresses, particularly in the direction of loading (axial). The stress-strain response of Opalinus Clay in unconfined compression is characterized by a distinct low stiffness non-linear behaviour at low stresses (below about 2 MPa).

The combined use of unconfined and triaxial test stress-strain data can be used to capture the stiffness around excavations throughout a range of stresses of practical importance. The low stress behaviour is described by the non-linear response of unconfined compression tests and high confining stress behaviour is represented by triaxial test data.

In the vicinity of underground excavations at confining stresses greater than about 2 MPa (compression zone), the Young's modulus is a function of confining stress ( $\sigma_3$ ). At lower stresses, below about 2 MPa, the modulus in the direction of loading/unloading (radial direction) is most important and is, therefore, a function of the radial stress ( $\sigma_1$ ) which, for this model, corresponds to the unconfined axial stress. There are limitations associated with this logic that limits its range of applicability, but it can be effective with respect to tunnelling analysis. Some discretion is required when applying this model.



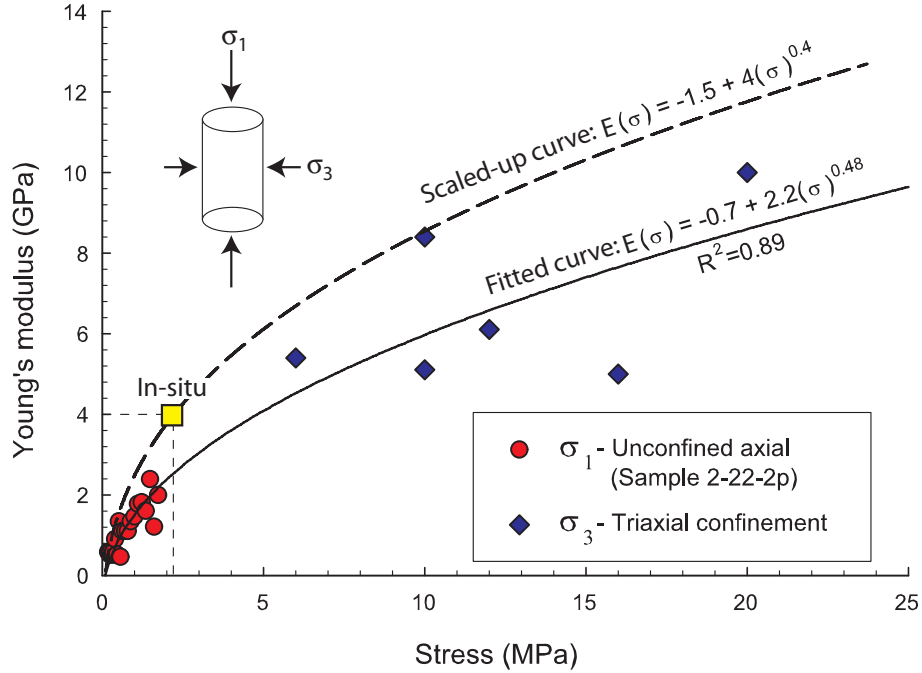


Figure 3.7: The non-linear elastic constitutive behaviour was derived from the combined triaxial-uniaxial stress-modulus data. This was scaled-up to pass through the in-situ condition. Triaxial data provided by Olalla et al. [4]; UCS test data (Sample 2-22-2: used for low stress  $\sigma_1$  relation) provided by Rummel [17].

The stress-strain curve for Sample 2-22-2p (see Fig. 3.7) was fairly typical of unconfined compression tests, particularly in the range below 2 MPa, and was conducted with axial deformations measured using two LVDTs. The incremental secant modulus at low axial stress levels ( $\sigma_1$ ) are shown as circles for Sample 2-22-2p in Fig. 3.7. The stress-strain curve for Sample 2-22-2p is shown in Fig. 3.8. Triaxial data of confining stress ( $\sigma_3$ ) and Young's modulus ( $E$ ) at 0.2 % strain, from Rummel [17], are shown as diamonds. From this plot, it can be seen that a relationship between  $E$  and  $\sigma$  exists. A curve can be fitted to the combined data with an equation of the same form as that found by Santarelli et al. [10] for carboniferous sandstone. The fitted curve has an  $r^2 = 0.89$  with the equation:

$$E(\sigma) = -0.7 + 2.2(\sigma)^{0.48} \quad (3.2)$$

Samples that have been completely unloaded during retrieval, and prior to reloading in uniaxial compression, suffer the full extent of unloading-induced non-linearity.

The stress path during tunnel excavation in the stress field at Mont Terri can be quite complex, however, the majority of the rockmass around underground excavations typically undergoes only partial unloading to its final stress level. Therefore, the degree of non-linearity reflected by Eq. 3.2 may not be fully achieved in the rockmass. In addition, the estimated equivalent isotropic in-situ rockmass modulus of 4 GPa at  $\sigma_3 = 2.2$  MPa does not correspond according to Eq. 3.2. Keeping the equation in the same form as that reported by Santarelli et al. [10], the SDM equation parameters were scaled-up to achieve  $E=4$  GPa at  $\sigma_3 = 2.2$  MPa. The scaled-up SDM equation is:

$$E(\sigma) = -1.5 + 4(\sigma)^{0.4} \quad (3.3)$$

It should be noted that while both curves rise infinitely, the data they are derived from only goes up to 20 MPa. The main focus of this study is the behaviour of Opalinus Clay at low stresses where most of the deformation around the tunnel occurs. The behaviour at high stress levels is unknown and it may not be suitable to continue to extrapolate these relationships to stress levels beyond 20 MPa.

### 3.3.2 Verification and Comparison

Confidence in the SDM model can only be achieved by back-analysis and comparison to observed material behaviour. A program of in-situ seismic measurements along an array of boreholes in the EB Niche was conducted at Mont Terri by Schuster (pers. comm.). The dynamic elastic modulus calculations from seismic velocity measurements ( $E_d$ ) are significantly higher than those measured by static means ( $E_s$ ), i.e., cylindrical compression testing [18]. Fig. 3.8 shows a stress-strain curve with four unloading-reloading cycles for Sample 2-22-2p used to develop the SDM model. The unloading-reloading portions of the curve show significantly higher stiffness than the overall trend of the curve. The difference is often attributed to friction along closed micro-cracks that induce hysteresis of the stress-strain curve. The micro-cracks close during initial loading, bringing the micro-crack faces into frictional contact. The micro-cracks re-open (unloading) at a slower rate than they closed (loading) resulting in increased Young's modulus due to this frictional work.

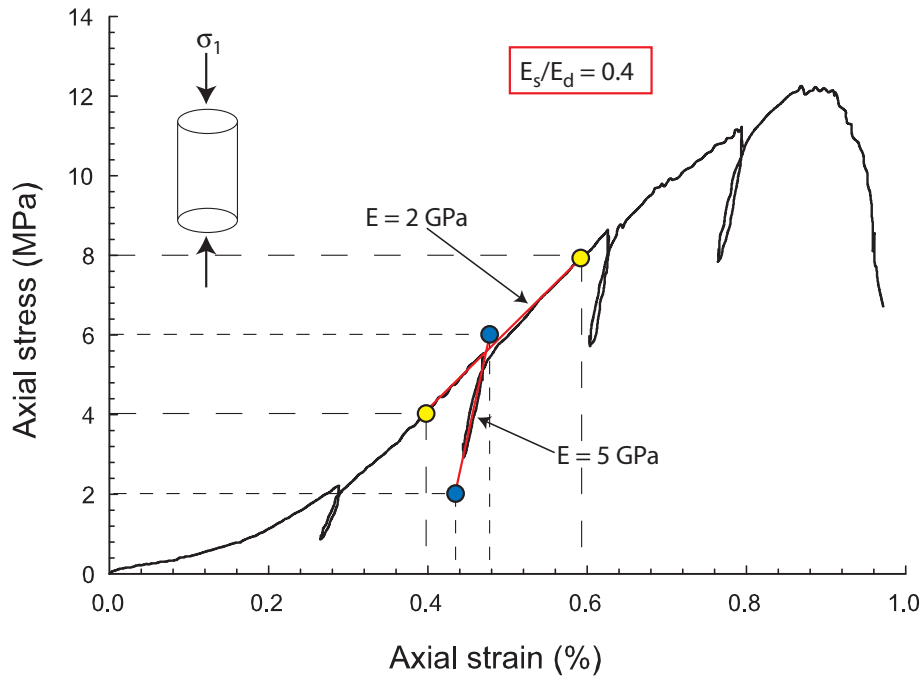


Figure 3.8: Ratio of unload-reload cycle stiffness to tangent modulus stiffness is representative of the relationship between dynamic to static modulus. A typical uniaxial test (Sample 2-22-2p) was used to estimate this ratio for Opalinus Clay.

The unload-reload stiffness may represent the small strain, or stiffness, measured by dynamic methods. From this stress-strain curve the ratio of  $E_s/E_d = 0.4$ .

In order to investigate the stress distribution and potential for yielding around the EB Niche at Mont Terri, a simple two-dimensional FEM analysis of the niche was conducted (see Fig. 3.9). The analysis indicated that yielding in shear, tension or bedding plane slip is not anticipated in the vicinity of Borehole BED-B10 located in the roof of the EB Niche at an orientation of  $45^\circ$ . This is a zone of unloading where confining stresses are low.

The plot shown in Fig. 3.10 shows the measured static Young's modulus using the ratio of  $E_s/E_d = 0.4$  calculated from seismic measurements along the borehole. The Young's modulus was about 1 GPa near the excavation boundary, significantly below the in-situ value of 4 GPa, and recovered to about 4 GPa after less than 1 m from the tunnel boundary. It is evident that the field measurements agree with the highly non-linear, low stiffness behaviour at low confining stress observed in laboratory samples subjected to unloading. The stresses from the FEM analysis were

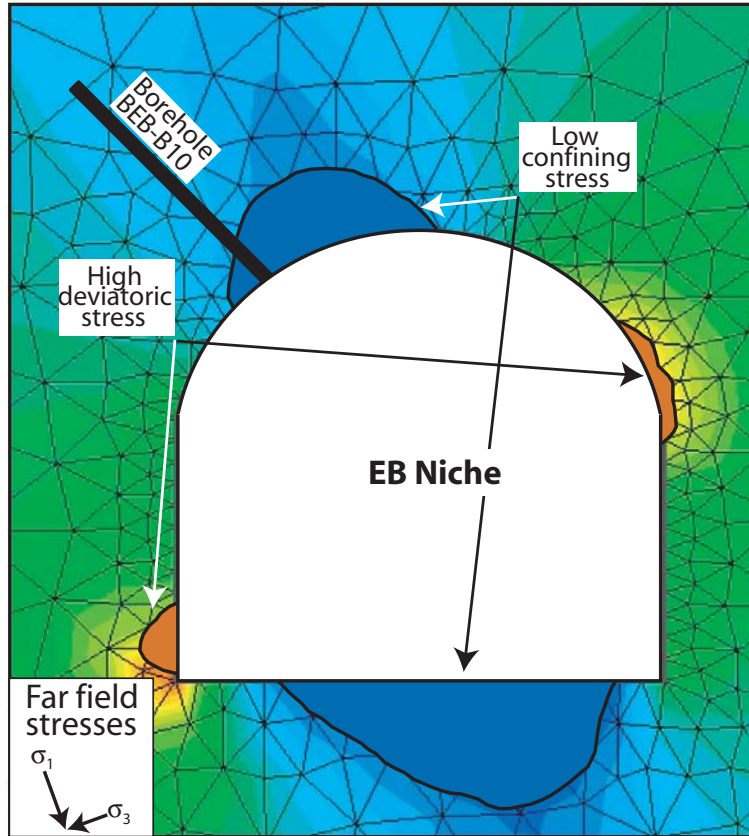


Figure 3.9: Stress analysis of EB-Niche from 2-D finite element model (Phase<sup>2</sup>). Borehole BEB-B10 is located in a zone of unloading.

used to calculate Young's modulus according to the SDM function and the scaled-up SDM function shown in Eq. 3.2 and 3.3, respectively. Both of the functions show a good match to the trend of Young's modulus distribution, but the scaled-up version shows a better fit to the magnitudes. The measured Young's modulus rises more steeply with length along the borehole than the calculated modulus using either equation.

In order to evaluate the implementation of a stress-dependent model, a comparison of Santarelli's closed form solution to the finite difference analysis was conducted. Santarelli's equation (Eq. 3.1) was implemented into the numerical code *FLAC<sup>3D</sup>* using its internal programming language *FISH*. After each time step the stress levels in all of the elements were checked and the Young's modulus was updated according to Santarelli's formulation. A three-dimensional problem was set up with a circular excavation through the centre. The boundaries were fixed

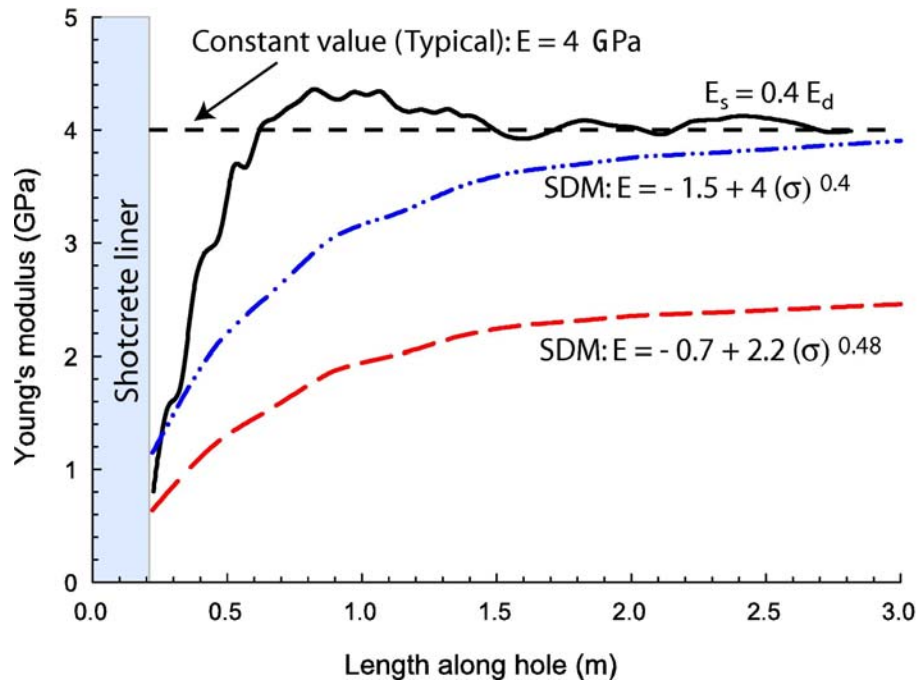


Figure 3.10: The effects of unloading on the distribution of stiffness properties differ significantly from the constant modulus typically used in numerical analyses. Both SDM models fit the trend of measured values while the scaled-up SDM model shows a better fit. Data provided by K. Schuster (pers. comm.).

at a distance of seven times the tunnel diameter and an isotropic stress field of  $P_o = 100$  MPa was applied. A simple elastic constitutive model was used for the rockmass. Fig. 3.11 shows the radial distribution of tangential stresses around a circular excavation calculated by:

- Kirsch's [19] elastic closed-form solution
- Santarelli's closed-form solution (PDM)
- Elastic  $FLAC^{3D}$  analysis
- Santarelli's equation implemented in  $FLAC^{3D}$  (SDM model)

The most notable feature of the PDM is the stress distribution around an excavation. Santarelli's pressure-dependent modulus closed-form solution predicts a stress distribution with  $\sigma_{\theta\theta} = P_o = 100$  MPa at the excavation boundary, rising and then dissipating away from the tunnel. The maximum stress predicted by the closed-form PDM was about 1/3 of that predicted by the other methods and the

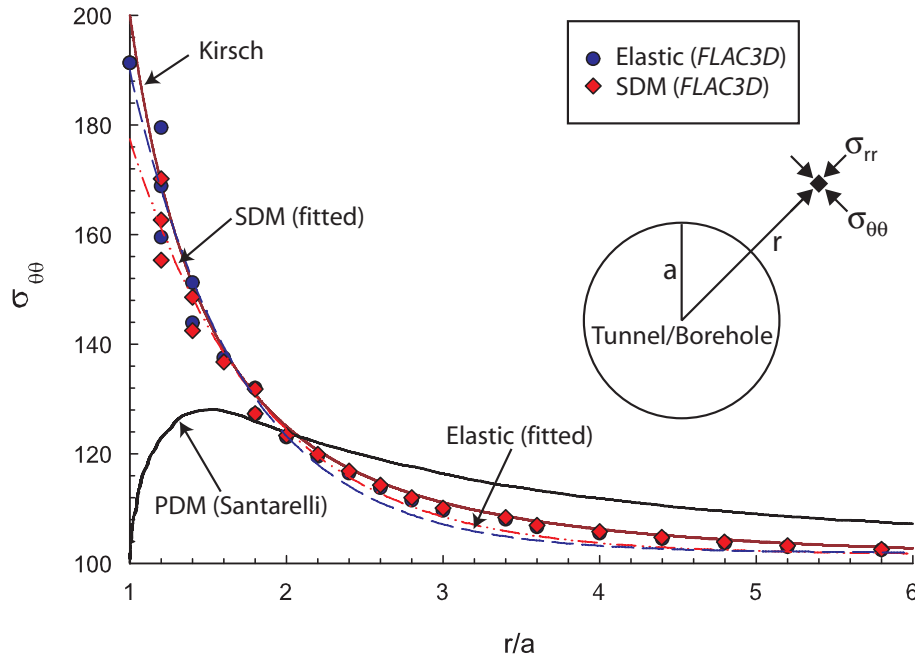


Figure 3.11: Comparison of calculated tangential stresses around an excavation ( $P_o = 100$  MPa). The  $FLAC^{3D}$  solution considers stress path and understandably differs significantly from the closed-form solution.

peak stress occurs some distance away from the excavation boundary. The  $FLAC^{3D}$  implementation of the SDM model clearly disagrees with the closed-form solution.

The reason for this discrepancy is that the closed form solution maintains the distribution of modulus at final equilibrium throughout the entire excavation process. Incremental strains and associated modulus changes are not considered by this pressure-dependent, linear-elastic, closed form solution. This explains the fact that there is no change in the calculated stress at the excavation boundary. The SDM model takes into consideration the stress path as the model goes from pre-excavation equilibrium through to post-excavation equilibrium. It seems likely that the boundary tangential stress would change with excavation advance. Therefore, the SDM model  $FLAC^{3D}$  implementation appears to have been properly implemented. It is important to note that the distribution of Young's modulus from the SDM model has a minor effect on the stress distribution.

### 3.3.3 Discussion

The greatest limitation of the SDM approach in the analysis of underground excavations is that it does not properly account for dilation. The formation of extensional fractures in the EDZ (spalling-like behaviour) has long been recognized as a mode of yielding around underground excavations under high deviatoric stresses. The SDM model treats the rockmass around a tunnel in the same way that a sample released from the in-situ stress conditions would react. The resulting non-linear low-stress, low-stiffness behaviour does not include the anticipated dilatant component.

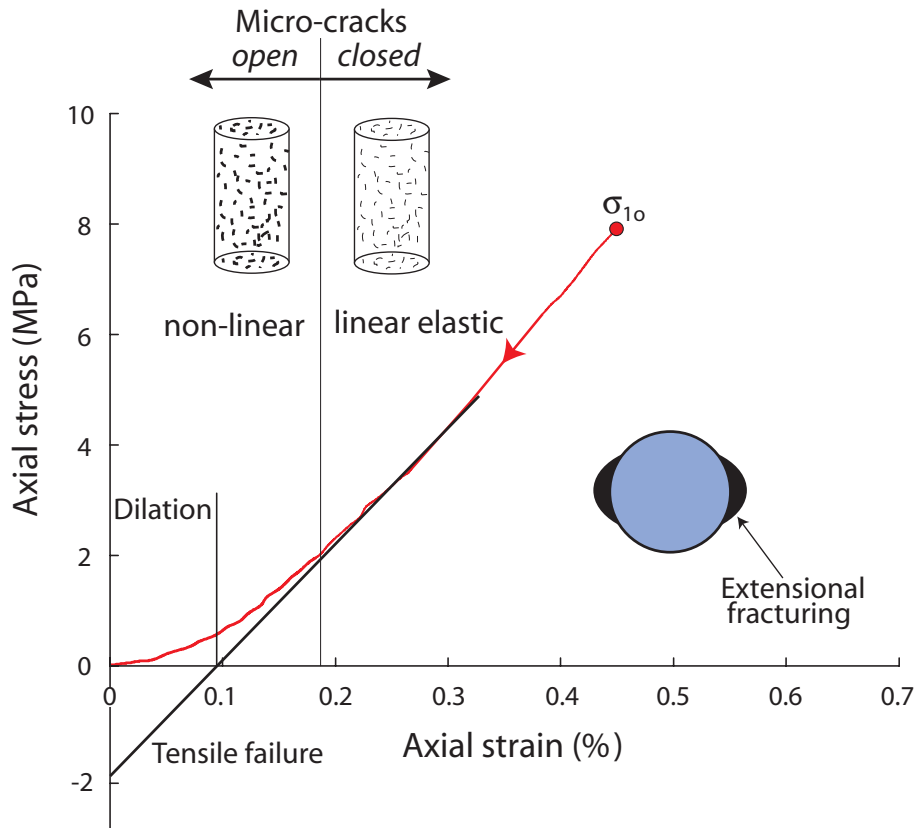


Figure 3.12: Non-linear stress-strain response and strain incompatibility resulting in extensional fractures. This non-linearity can impose up to 2 MPa of tensile stress onto the localized rockmass when completely unloaded.

Kaiser et al. [20] described large calculated tensions due to stress-strain non-linearity during unloading in hard rock mining. Fig. 3.12 shows the stress-strain curve of a typical uniaxial compression test of the Opalinus Clay. It can be seen that

for a non-linear material, an equivalent linear-elastic material would be required to resist nearly 2 MPa of tensile stress to achieve the corresponding linear-elastic magnitude of strain at complete unloading. The non-linear stress-strain response could induce up to 2 MPa of tensile stress in the completely unloaded localized material that is intact and responding linearly. This exceeds the tensile strength of Opalinus Clay and could explain the observed tensile yielding around tunnels. Geomaterials are generally characterized by some level of material property heterogeneity that can further exacerbate this strain incompatibility. These large strains cannot be accommodated by the rockmass which results in the formation of extensional fractures perpendicular to the direction of maximum strain.

### 3.4 Simplified Model of Pore Pressure Response

The pore pressure response to tunnelling in Opalinus Clay has not been in agreement with conventional analytical methods. Hydromechanical coupled formulations, such as Skempton's approach [14] or the theory of linear poroelasticity [15], predict increased pore pressure associated with an increase in the mean stress level with some shear-induced dilation in heavily overconsolidated materials. Non-linear stress-strain behaviour, or dilation, of the rockmass is not considered by these conventional methods. Skempton's [14] formulation for stress-induced pore pressure change is:

$$\Delta u = B[\Delta\sigma_3 + A(\Delta\sigma_1 - \Delta\sigma_3)] \quad (3.4)$$

The  $B$  parameter represents the change in pore pressure due to mean stress and the  $A$  parameter takes into consideration the effects of shear-induced pore pressure change. Based on the results of several laboratory studies, it has been concluded that shear-induced dilation does not generally occur in samples of Opalinus Clay until at, or near, peak strength [6]. This implies that Skempton's  $A$  parameter can be neglected for the pre-peak strength range. Neglecting dilation, a mean stress relation can be used as a simplified pore pressure equation:



$$\Delta u = B \frac{\Delta\sigma_1 + \Delta\sigma_2 + \Delta\sigma_3}{3} \quad (3.5)$$

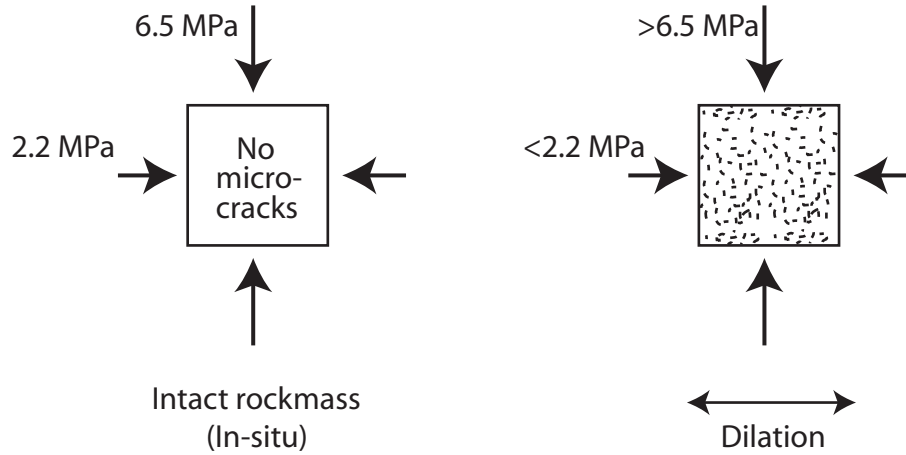


Figure 3.13: Stress release induces micro-cracks in the rockmass resulting in a dilatant pore pressure response. Dilation is suppressed at  $\sigma_3 = 2.2$  MPa, therefore, at  $\sigma_3 = 0 \Rightarrow \Delta u = -2.2$  MPa.

A conceptual model of dilation-like non-linear unloading, and resulting pore pressure response to unloading is illustrated in Fig. 3.13. Due to the release of latent strain energy, these micro-fractures tend to open or dilate during unloading. The SDM model has been developed to quantify the effects of non-linear stress-strain behaviour, but no true correlation exists for the determination of the degree of volumetric strain, and pore pressure change, in relation to stresses. Laboratory testing data does allow some correlation between stress levels and the relative degree of dilation. The stress levels can then, in turn, be related to pore pressure changes in accordance with the principles of effective stress ( $\sigma' = \sigma - u$  [21]). Because of the low permeability of the Opalinus Clay, the short-term change in pore pressure is approximately (Skempton's  $B < 1$ ) equal to the change in total stress  $\Delta u = \Delta\sigma$ .

It has been demonstrated that during unloading, non-linear behaviour of the rockmass begins at approximately  $\sigma_3 = 2$  MPa. Non-linear deformation increases until the rockmass is completely unloaded (behaviour in tension is not considered). At  $\sigma_3 = 0$ , the non-linear deformation due to unloading is at its maximum and it is known that the rockmass requires approximately 2 MPa of pressure to restore it to its un-dilated, intact form. Put another way, at  $\sigma_3 = 0$ , the latent strain energy

locked into the micro-structure of the Opalinus Clay would apply an internal stress of approximately 2 MPa from within the rockmass. Therefore, at  $\sigma_3 = 0$ , approximately 2 MPa of pressure would be applied to the pore water. A simple linear function can be extrapolated between the two known conditions where:

$$\begin{aligned}\sigma_3 &= 2 \text{ MPa at } \Delta u = 0 ; \text{ and} \\ \sigma_3 &= 0 \text{ MPa at } \Delta u = 2 \text{ MPa}\end{aligned}$$

The measured data indicates that pore pressure responses ahead of and behind the excavation face are dominated by different mechanisms (see Fig. 3.5). Therefore, a piece-wise formulation is appropriate to describe hydromechanical coupling for tunnel excavation. For practical usage, because  $\sigma_{3o} = 2.2 \text{ MPa}$ , the change in pore pressure associated with unloading dilation can be expressed simply as:

$$\Delta u = B \frac{\Delta \sigma_1 + \Delta \sigma_2 + \Delta \sigma_3}{3} \quad ; \text{ for } X/D > 0 \quad (3.6)$$

$$\Delta u = \sigma_3 - \sigma_{3o} = \Delta \sigma_3 \quad ; \text{ for } X/D < 0 \quad (3.7)$$

Behind the excavation face ( $X/D < 0$ ), the effects of the maximum principal stress ( $\sigma_1$ ), intermediate principal stress ( $\sigma_2$ ) and mean stress ( $\sigma_m$ ) are significantly less relevant than in the conventional hydromechanical formulations and are not considered in this simplified pore pressure model.

The piece-wise pore pressure formulation was implemented into the numerical code  $\text{FLAC}^{3D}$  using the internal programming language *FISH*. A simple circular excavation has been modelled with the stress tensor at Mont Terri rock laboratory (see Sect. 3.2). Fig. 3.14 shows the plotted pore pressure development with excavation advance based on hydromechanical formulations along with the individual components of the pore pressure formulation and the combined piece-wise formulation. A value for Skempton's  $B=0.85$  was used.

The mean stress formulation greatly over-predicts the pore pressure behind the excavation face, while that based on the change in minimum stress under-predicts the pore pressures in front of the excavation face. The piece-wise formulation shows

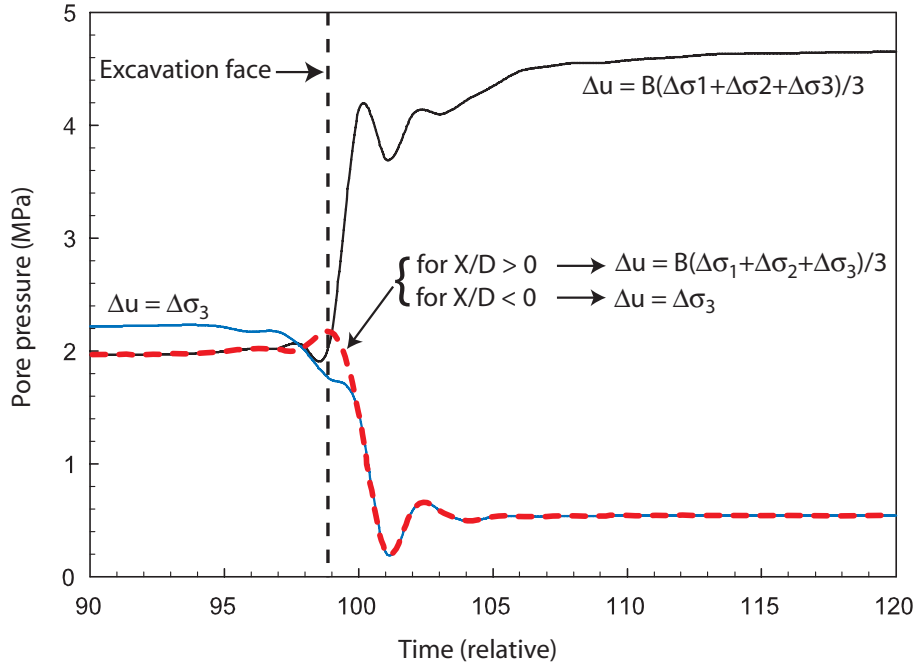


Figure 3.14: A piece-wise pore pressure formulation based on the rationale behind the SDM model agrees well with the measured trends and magnitudes of pore pressure development. Pore pressures calculated at a tunnel springline with the Mont Terri stress field.

a good match of the trends and magnitudes of pore pressure development measured during the ED-B mine-by test (see Fig. 3.5). A more detailed analysis of this case study is presented by Corkum [12].

The practical implication of the unique piece-wise pore pressure response to short-term tunnel behaviour is that pore pressures do not rise behind the excavation face as a function of the mean stress. As a result, it can be stated that hydromechanically coupled behaviour is not responsible for yielding of the rockmass. In fact, because a form of dilation-like behaviour has been induced, the material is stronger due to increased effective stress, with a tendency to increase in moisture content with time. Delayed yielding, similar to that observed in natural cuts by Skempton [14], or softening and/or swelling is likely to occur and may be more severe due to the non-linear deformation characteristics of the Opalinus Clay. The simplified pore pressure model presented here does not include the effects of time-dependent behaviour.

### 3.5 Summary and Conclusions

A practical method to predict the constitutive behaviour of Opalinus Clay is needed in order to assess tunnel performance. Observations from laboratory and field studies have been synthesized to develop a model of the micro-structure within the context of the geological history of the Opalinus Clay. This framework has served as a guide for development of two separate phenomenological-based models to capture the stiffness and pore pressure behaviour around underground excavations by utilizing data from simple unconfined and triaxial compression tests. Based on the premise that the tunnel walls undergo processes similar to those of samples removed from the stress field, these simple models allow engineers to capture a significant portion of the observed behaviour without undue modelling complexities.

The authors are aware that the simplified approach taken for pore pressure interpretation is based on one set of field measurements only, plus extrapolation of laboratory stress-strain behaviour. Significant research remains in order to acquire direct evidence regarding the breakage of diagenetic bonds and release of latent strain energy, and for quantification of the fundamental physical processes. In addition, further investigation is needed to identify the mechanisms responsible for the two discrete components of the piece-wise hydromechanical model.

The models presented in this paper are in agreement with field observations of the variation of stiffness around tunnels from geophysical measurements and the measured pore pressure response. Furthermore, the FLAC<sup>3D</sup> implementation of the SDM model and simplified pore pressure model were used to successfully analyze the pore pressures and unloading-induced deformations of the ED-B mine-by test, as described by Corkum [12]. Less quantitatively, the SDM model can be used to predict non-linear behaviour around tunnels that may be useful in defining the extent of the EDZ and conditions associated with the onset of softening and/or swelling processes.

## Bibliography

- [1] Corkum A G, Martin C D, Phenomenological models for stiffness and pore pressure around tunnels in soft argillaceous rock. *Rock Mech and Rock Engin* 2006, In Progress.
- [2] Lambert A, Clay: small particles with a large impact. In: *From building bricks to repositories: the allrounder material clay*, Nagra Bulletin, vol. 31 1997 .
- [3] Hudson J A, Stephansson O, Andersson J, Guidance on numerical modelling of thermo-hydro-mechanical coupled processes for performance assessment of radioactive waste repositories. *Int J Rock Mech Min Sci* 2005, 42:850–870.
- [4] Olalla C, Martin M, Sáez J, ED-B Experiment: Geotechnical laboratory testing on Opalinus Clay rock samples. Tech. Rep. TN98-57, Mont Terri Project 1999.
- [5] Walsh J B, Brace W F, Elasticity of rock: a review of some recent theoretical studies. *Rock Mech and Eng Geol* 1966, 4:283–297.
- [6] Corkum A G, Martin C D, The mechanical behaviour of weak mudstone (Opalinus Clay) at low stresses. *Int J Rock Mech Min Sci* 2006, In Progress.
- [7] Duncan J, Chang C Y, Nonlinear analysis of stress and strain in soils. *J Soil Mech Found Div, ASCE* 1970, SM5:1629–1653.
- [8] Kulhawy F H, Stress deformation properties of rock and rock discontinuities. *Eng Geol* 1975, 9:327–350.
- [9] Ewy R T, Cook N G W, Deformation and fracture around cylindrical openings in rock – I. Observations and analysis of deformations. *Int J Rock Mech Min Sci* 1990, 27(5):409–427.
- [10] Santarelli F J, Brown E T, Maury V, Analysis of borehole stresses using pressure-dependent, linear elasticity: Technical Note. *Int J Rock Mech Min Sci & Geomech Abstr* 1986, 23(6):445–449.

- [11] Corkum A G, Martin C D, Modelling the short-term behaviour of Opalinus Clay around a circular excavation. In: Canadian Geotechnical Conference 2004 .
- [12] Corkum A G, Non-Linear Behaviour of Opalinus Clay Around Underground Excavations. Ph.D. thesis, Dept. Civil & Environmental Engineering, University of Alberta, Canada 2006.
- [13] Möri A, Bossard P, Fracture Propagation Experiment: method, results, interpretation. Tech. Rep. TN99-72, Nagra Technical Report, Geotechnical Institute Ltd. 1999.
- [14] Skempton A W, The pore pressure coefficients A and B. *Géotechnique* 1954, 4:143–147.
- [15] Wang H, Theory of Linear Poroelasticity with Applications to Geomechanics and Hydrogeology. Princeton University Press 2000.
- [16] Nawrocki P A, Dusseault M B, Modelling of damaged zones around openings using radius-dependent Young's modulus: Technical Note. *Rock Mech and Rock Engin* 1995, 28(4):227–239.
- [17] Rummel F, RA Experiment: Rock mechanics testing and characterization on drillcores of Boreholes BRA-1 and BRA-2, TN 2004-38. Tech. Rep., Nagra 2004.
- [18] Stagg K G, Zienkiewicz O C, editors, Rock mechanics in engineering practice. John Wiley & Sons 1968.
- [19] Kirsch G, Die theorie der elastizitat und die bedürfnisse der festigkeitslehre. *Veit Ver Deut Ing* 1898, 42:797–807.
- [20] Kaiser P K, Yazici S, Maloney S, Mining-induced stress change and consequences of stress path on excavation stability—a case study. *Int J Rock Mech Min Sci* 2001, 38:167–180.

- [21] Terzaghi K, The shearing resistance of saturated soils and the angles between the planes of shear. In: 1st Int Conf on Soil Mech and Found Eng, vol. 1, Cambridge, Mass 1936 pp. 54–56.

# Chapter 4

## Modelling a mine-by test at the Mont Terri rock laboratory, Switzerland<sup>1</sup>

### 4.1 Introduction

The behaviour of the Opalinus Clay around deep underground excavations is of interest to many organizations currently studying argillaceous rocks for potential geological disposal of nuclear waste. In 1997-98, a mine-by test tunnel was excavated at the Mont Terri rock laboratory, Switzerland (see Fig. 4.1) to assess the issues associated with tunnel excavation in Opalinus Clay. The 35 m long, 3.6 m diameter circular excavation, known as the ED-B tunnel, was excavated at a depth of approximately 270 m. The rockmass was instrumented prior to tunnel driving, allowing for monitoring of the rockmass response with tunnel advance. The instrumentation records contain unique deformation signatures that provide insight into the mechanical response of the Opalinus Clay to unloading and the formation of the excavation damaged zone (EDZ).

Past researchers have modelled the well-documented ED-B mine-by test at Mont Terri with various conventional approaches [2, 3] that generally have proven to be unsatisfactory. In particular, the elastic deformations and mode of yielding (extensional fractures) in the EDZ have not been adequately matched. Large near-field deformations and EDZ fractures have been attributed to plasticity. Based on the stress field at Mont Terri and recommended strength data, only limited plasticity is anticipated around the ED-B tunnel. Corkum and Martin [4] have demonstrated

---

<sup>1</sup>A version of this chapter has been submitted as a paper to the *Int J Rock Mech Min Sci*.



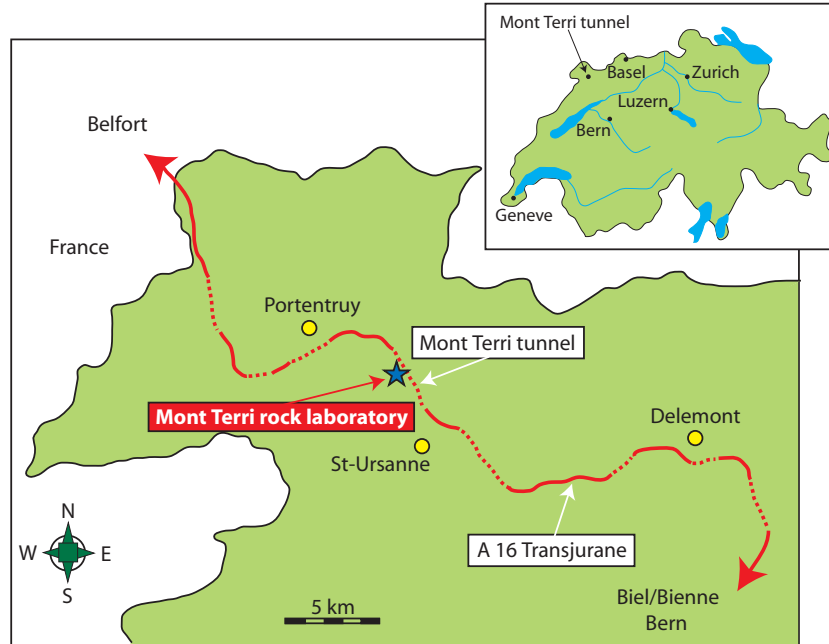


Figure 4.1: Map showing Mont Terri rock laboratory near the town of St. Ursanne in northwestern Switzerland (modified from [www.mont-terri.ch](http://www.mont-terri.ch)).

that the mechanical response of Opalinus Clay is unique and reflective of a micro-structure that is dominated by diagenetic bonding and stored latent strain energy. They showed that the low stress, low stiffness non-linear (anelastic) stress-strain response of laboratory samples is a real material behaviour that can have a significant impact on the rockmass response to excavation.

From a wide range of experimental data, Kulhawy [5] concluded that non-linearity and pressure dependence of the rock modulus are significant in porous, clastic or closely jointed rock. It has been observed that porous rock often exhibits a non-linear relationship between confining stress and elastic modulus. For deep boreholes in the petroleum industry this issue has been addressed by Ewy and Cook [6] and Santarelli et al. [7] using a pressure-dependent modulus (PDM) model. A stress-dependent modulus (SDM) phenomenological model for the Opalinus Clay has been developed based on a rational interpretation of the physical properties and geological history of the Opalinus Clay as described by Corkum [8]. This model has been implemented into the finite difference method (FDM) code  $FLAC^{3D}$ <sup>2</sup> and

<sup>2</sup>see [www.itascacg.com](http://www.itascacg.com)

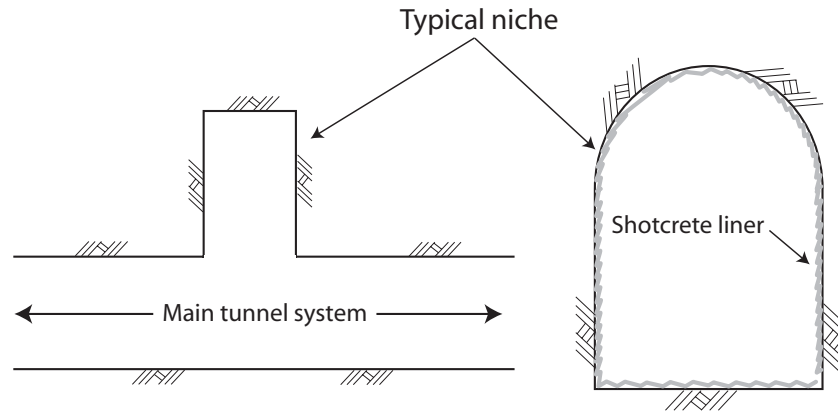


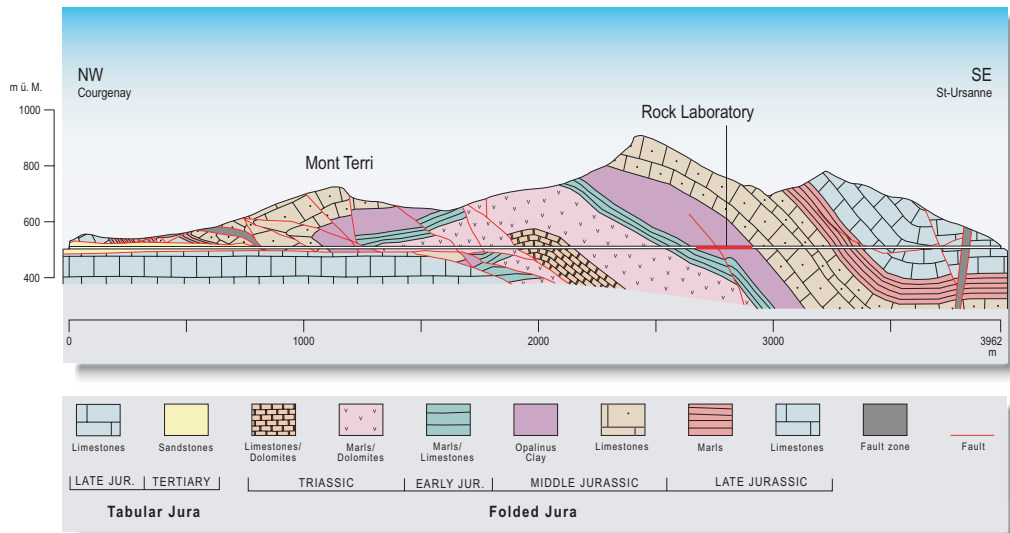
Figure 4.2: In-situ experiments at Mont Terri rock laboratory are conducted in isolated niches excavated into the sides of the major tunnel system (plan and elevation views).

used to model the ED-B mine-by test. In this paper we compare the measured short-term excavation-induced mechanical and pore-pressure response with the predicted response using five modelling approaches, including the SDM model.

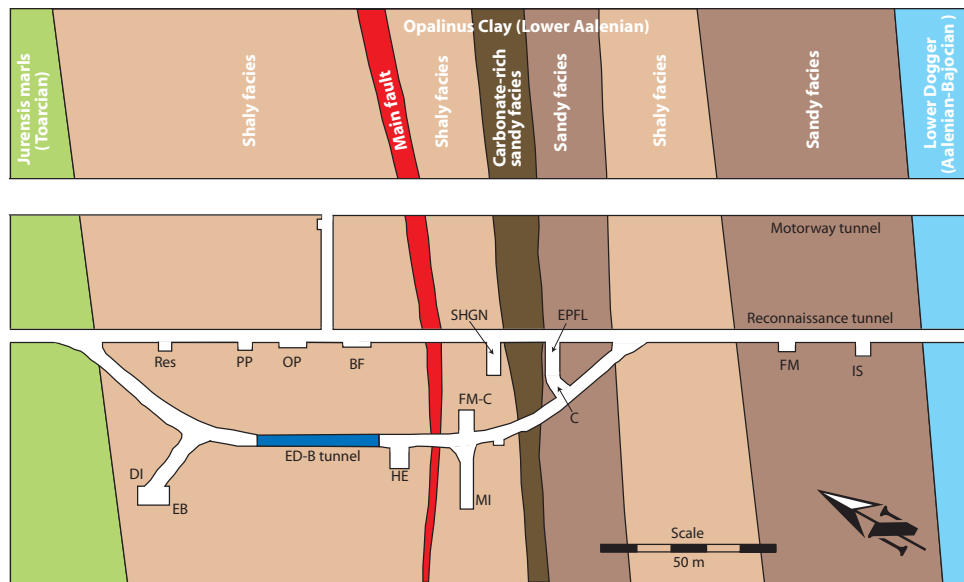
## 4.2 Background

The Mont Terri rock laboratory is located near the town of St. Ursanne in the Jura Mountains of northwestern Switzerland (see Fig. 4.1). The Reconnaissance Gallery (or Security Gallery) was originally constructed as part of the motorway tunnel of the A16 Transjurane motorway. A number of niches were excavated within the Reconnaissance Gallery in 1995 to conduct various experiments in the Opalinus Clay formation. The layout of a typical niche is shown in Fig. 4.2. Over the last decade expansion of the rock laboratory and additional experiments have been carried out.

Mont Terri is an asymmetrical anticline folded during the late Miocene to Pliocene period as shown in the geological section in Fig. 4.3(a). The stratigraphy of Mont Terri consists of competent limestones and incompetent marly/shaly formations. The rock laboratory is located within the southeastern limb of the anticline where the stratigraphy generally dips about  $45^\circ$  to the southeast [10]. The Opalinus Clay is immediately overlain by a limestone layer and underlain by marly units. Where it intersects the rock laboratory, the Opalinus Clay is about 250 m thick along the



(a) Geological section along A16 Transjurane motorway (from Freivogel and Huggenberger [9]).



(b) Geological plan of the Mont Terri rock laboratory (modified from [www.mont-terri.ch](http://www.mont-terri.ch)).

Figure 4.3: Mont Terri is an asymmetrical anticline folded during the Late Miocene to Pliocene period. The rock laboratory is located within the Opalinus Clay unit that dips approximately  $45^\circ$  southeast. The Opalinus Clay is divided into three main facies with the ED-B tunnel located entirely within the shaly facies. One major fault intersects the rock laboratory southeast of the ED-B tunnel.

length of the tunnel. As a result of differing sedimentation, the Opalinus Clay can be grouped into three facies: a sandy facies, a carbonate-rich sandy facies and a shaly facies, the latter being of most interest for repository construction. The ED-B tunnel is located entirely within the shaly facies. One major fault zone runs through the rock laboratory south of the ED-B tunnel (see Fig. 4.3(b)) and a number of discrete minor faults and joint sets have been observed throughout the tunnel system. Structurally controlled instability does not generally play a significant role at the rock laboratory.

The Opalinus Clay is a weak argillaceous rock, classified as a claystone, found mainly in Germany and northwestern Switzerland. Named for the ammonite *Leioceras Opalinum*, it is a Lower Aalenian (middle Jurassic age) marine deposit with past overburden estimated to have been at least 1000 m thick [11]. The claystone is a competent soft rock with an average unconfined compressive strength of about 15 MPa. Typically, Opalinus Clay is composed of 50-65 % clay particles, with the clay mineralogy consisting mostly of low activity kaolinite and illite which results in medium plasticity. It is very dry with low water content and porosity and, like most argillaceous rocks, many of the mechanical properties are sensitive to changing water content. Based on the observed intensity of slaking when immersed in water, it appears to be lightly- or un-cemented.

Opalinus Clay has a pronounced microstructure, due to sedimentation and diagenetic processes, that consists of clay plates (or particles) that are tabular-shaped and highly oriented approximately parallel to bedding. The bedding thickness is generally on the centimetre scale. As with most argillaceous rocks, the laboratory properties are transversely isotropic in nature. The anisotropy can be illustrated by the Young's modulus parallel (P-samples) and perpendicular to bedding (S-samples) of 10 and 4 GPa, respectively. This anisotropy extends to many mechanical properties such as hydraulic conductivity ( $k$ ) and undrained shear strength ( $c_u$ ) [12].

### 4.3 ED-B Mine-by Test

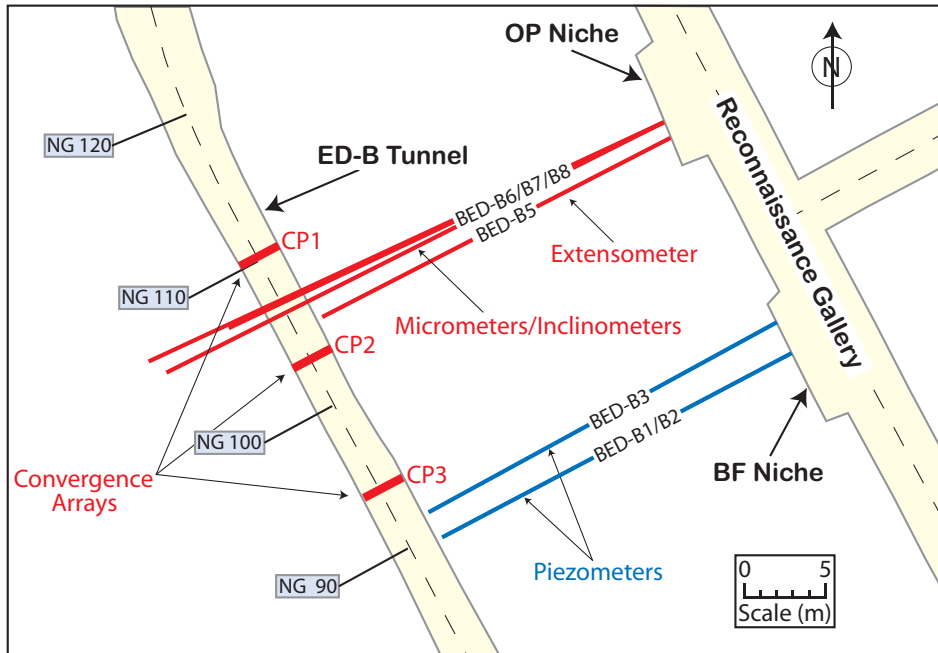
The ED-B mine-by experiment was conducted at Mont Terri in 1997-98. Consisting of a 36 m long, 3.6 m diameter circular excavation, this experiment has provided measurements from a number of instruments such as piezometers, inclinometers, extensometers and convergence arrays, with excavation advance [13]. Most of the instrumentation was installed prior to excavation from the OP Niche in the Reconnaissance Gallery, located approximately 24 m away from the ED-B tunnel.

The instrumentation layout is shown in plan and section in Fig. 4.4(a) and Fig. 4.4(b), respectively. Borehole deformation instrumentation consisted of one multipoint extensometer, installed in Borehole BED-B5, and three sliding micrometers/horizontal inclinometers installed in Borehole BED-B6 through -B8. The borehole deformation instruments were measured 19 times between September 1997 and June 1999. Near-field deformations were measured using three sets of five-point convergence arrays installed in the ED-B tunnel approximately 1 to 2 m behind the excavation face.

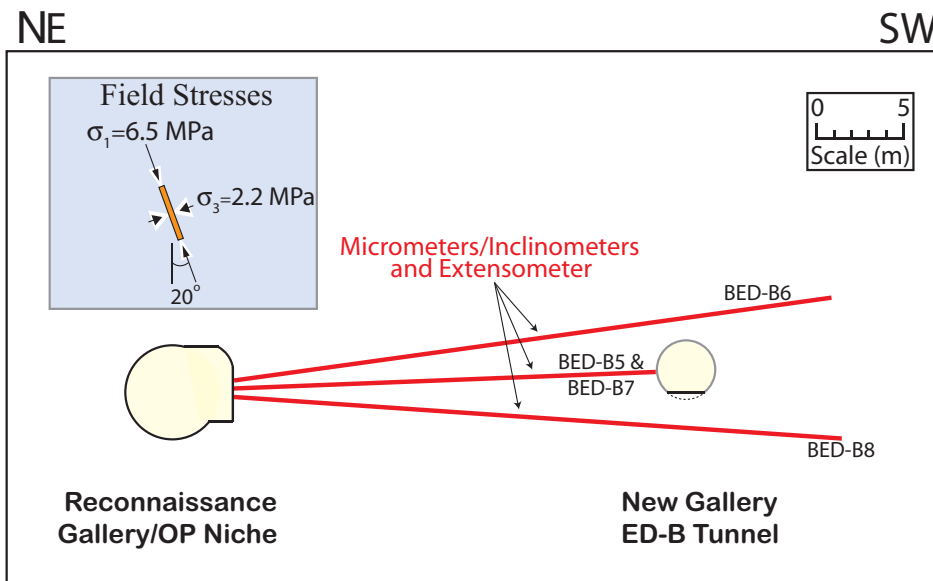
Following the installation of instrumentation, the ED-B tunnel was excavated full face using a roadheader from a northwest to southeast direction. The tunnel was stable during excavation and 200 mm thick steel fibre reinforced shotcrete support was installed approximately 7 m behind the excavation face.

Multi-point micrometers and inclinometers measure the incremental displacement at discrete intervals along the borehole. These are integrated along the instrument length to get the cumulative displacements that represent the total displacement of the instrument in the ground. A major assumption is that there is at least one known fixed point along the instrument to act as a datum. In the case of the inclinometers and sliding micrometers, it was initially assumed that the borehole collars, located greater than 24 m from the new excavation, would be the fixed point datum. However, the instrumentation data clearly shows that large deformations were recorded at these points as the ED-B excavation advanced (see Sect. 4.5).

Careful observation of the instrumentation data revealed a point 8 m from the Reconnaissance Gallery to have the least amount of relative movement. The amount



(a) Plan view of instrumentation for ED-B mine-by test showing piezometers, inclinometers/micrometers, extensometer and convergence arrays.



(b) Elevation view of tunnel/niche sections and instrumentation. The stress field is shown in plane.

Figure 4.4: Layout of ED-B mine-by test instrumentation and tunnel system. The ED-B tunnel was excavated with a roadheader from the northwest to southeast.

of movement that did occur at this point is unknown, but finite element method (FEM) modelling [3] indicated it would be negligible in comparison with the magnitude of movement typically measured along the instruments. Therefore, the 8 m point was used as the new “zero-movement” datum. The deformation data was readjusted with the new datum using the following sign convention when looking towards the southeast (direction of excavation):

- Inclinometers: positive movement was upward and negative was downward; and
- Micrometers: positive movement was to the right (towards ED-B tunnel from Reconnaissance Gallery) and negative was to the left.

## 4.4 Modelling the Mine-by Test

The goal of the analysis was to use the SDM phenomenological model to simulate the short-term rockmass deformation and pore pressure around a circular excavation in the Opalinus Clay. This model has been developed and described by Corkum [8] and will be reviewed briefly in Sect. 4.4.5.

### 4.4.1 Modelling Methodology

A three-dimensional model was selected because of such geometrical issues associated with tunnel modelling as potential tunnel interaction, orientation of the stress tensor relative to the tunnel, and the nature of tunnel advancement. The well-established FDM code  $FLAC^{3D}$  was used because of the flexibility it offers in programming constitutive models and other user defined modifications, in addition to its native ability to conduct plasticity analyses. A methodology was adopted to simulate the boundary conditions and construction sequence of the ED-B mine-by test as closely as possible. The chronology of events associated with the mine-by experiment consisted of a five-staged model as follows:

- **Stage 1:** Generation of the geometry in modular form providing adequate distance between excavations and boundaries.

- **Stage 2:** Application of boundary conditions and far-field stresses.
- **Stage 3:** Excavation of Reconnaissance Gallery pilot-tunnel (to simulate three-dimensional tunnel advance).
- **Stage 4:** Full excavation of the Reconnaissance Gallery and niches allowing the liner and ground to come into equilibrium. In real time this point corresponded to installation of instrumentation.
- **Stage 5:** Excavation of the ED-B tunnel, leaving it temporarily unsupported. The invert was left in place at this stage.

It was not known how far behind the excavation face the shotcrete support was installed in the Reconnaissance Gallery, but it was most likely installed prior to full convergence. Elastically, full convergence occurs approximately three tunnel diameters behind excavation face. For the numerical simulation, it was assumed that 50 % of convergence occurred prior to installation of shotcrete. The modulus softening method is often used in numerical codes to simulate partial convergence in a given modelling stage [14]. Re-initialization of the model stress field is required by this approach. Significant adaptation of the existing FLAC<sup>3D</sup> code would be needed to accomplish this. Therefore, a pilot-tunnel was excavated with a diameter suitable to allow 50 % of elastic displacement of the tunnel boundary to occur (5.6 m and 3.6 m diameter tunnel and pilot-tunnel, respectively). The model was cycled to equilibrium, then the Reconnaissance Gallery was fully excavated, 200 mm of shotcrete support installed and cycled again to allow the rockmass and support to come to equilibrium together.

As mentioned previously, during excavation of the ED-B tunnel shotcrete support was not required at the tunnel face and lagged excavation by up to 7 m. At this point the majority of the deformation had occurred. Therefore, most of the deformation measured by instrumentation occurred between model Stages 4 and 5 and these deformations were compared to the measured instrumentation data.



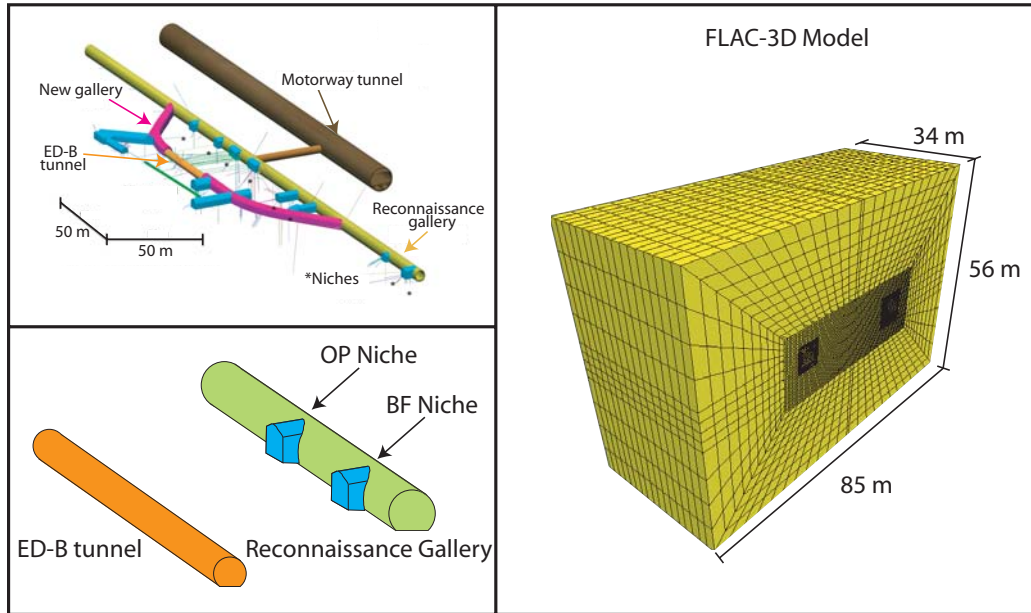


Figure 4.5: For model implementation, the geometry of the Mont Terri rock laboratory was simplified to a system of two parallel tunnels (ED-B and Reconnaissance Gallery) with two instrumentation niches. The 34 x 56 x 85 m  $FLAC^{3D}$  model contained 540,000 zones and five modelling stages were used to simulate the excavation sequence.

#### 4.4.2 Model Geometry

The model geometry consisted of the two main tunnels: the 3.6 m diameter ED-B tunnel and the 5.6 m diameter Reconnaissance Gallery. Two niches (OP and BF) were located closest to the instrumented section of the mine-by test. Neither the Highway tunnel, located 33 m northeast of the Reconnaissance Gallery, nor the Highway-Reconnaissance connector tunnel were included in the model. Preliminary FEM modelling indicated that inclusion of these two tunnels would have minor influence on the rockmass near the ED-B tunnel while increasing run times to impractical levels. The Z-axis was vertical in the model, while the horizontal Y and X-axes were aligned parallel and perpendicular to the tunnels, respectively. The dimensions of the model were 85 m in the X-direction, 34 m in the Y-direction and 56 m in the Z-direction.

As with most geomechanical models, some simplifications of the problem geometry were required to model the ED-B mine-by test. These simplifications were

selected to minimize their impact on the areas of interest in the model while limiting the number of model elements to a reasonable size. The basic model contained 540,000 zones and took approximately four days of computer time to achieve equilibrium for a single excavation stage. The model consisted of five stages and took three weeks to solve the problem. An overview of the FLAC<sup>3D</sup> model geometry can be seen in Fig. 4.5. Some of these simplifications were as follows:

- The lower portion of the ED-B tunnel was slightly less circular than the actual excavation in order to maintain adequate aspect ratios in the model zones.
- The Reconnaissance Gallery geometry was excavated into a square grid. As a result the excavation boundaries are rough as opposed to smooth. This was done so the niches—which have some influence on instrumentation measurements—could be included with consistency.
- The Motorway tunnel and the tunnel connecting the Motorway tunnel and Reconnaissance Gallery were omitted because of the difficulty in achieving a reasonable geometrical representation without increasing the number of model elements to impractical levels.
- The angled tunnel sections that connect the New Gallery (ED-B) with the Reconnaissance Gallery were omitted. These sections were quite far removed from the instrumented sections so the main tunnel system was simply further extruded.

#### **4.4.3 In-Situ Stresses and Boundary Conditions**

An understanding of the in-situ stress conditions is important for the analysis of underground excavations. These boundary conditions are particularly significant when the objective is to understand the rockmass response to excavation and conduct experiments that are sensitive to stress levels. Therefore, the in-situ stress conditions at Mont Terri were measured during a number of campaigns utilizing an assortment of techniques such as undercoring, slotter and hydrofracturing methods. Martin and Lanyon [15] have investigated the various stress measurement programs

and pertinent observations, and Corkum [8] has further constrained the value of  $\sigma_{3o}$ . The orientation and magnitudes of the stress tensor, obtained using the undercoring method, modified with  $\sigma_{3o} = 2.2$  MPa is considered the most likely stress field at Mont Terri.

Table 4.1: Magnitude and orientation of the stress tensor [8].

Principal Stress	Magnitude (MPa)	Dip Direction (°)	Dip (°)
$\sigma_1$	6 - 7 (6.5)	210	70
$\sigma_2$	4 - 5 (4.0)	52	18
$\sigma_3$	2 - 3 (2.2)	320	7

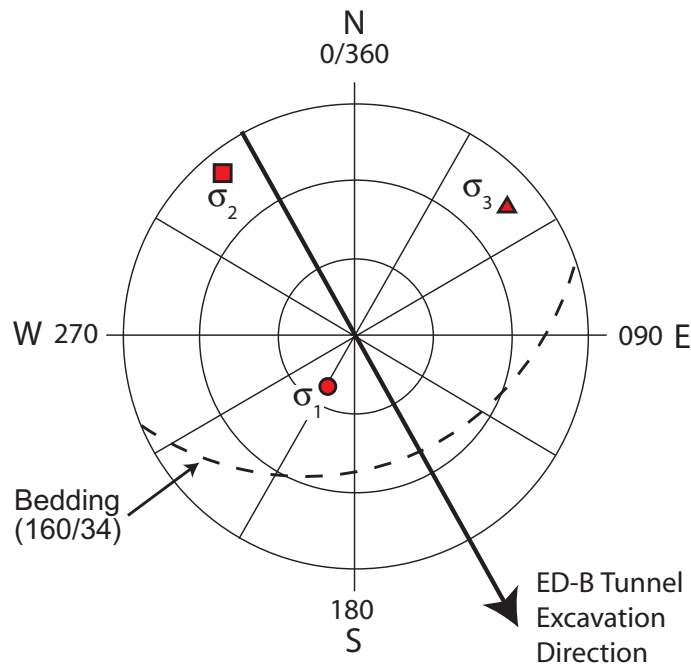


Figure 4.6: Orientations of the stress tensor from the undercoring in-situ stress measurement method (modified from Martin and Lanyon [15]).

The measured maximum principal stress ( $\sigma_{1o} = 6.5$  MPa) was sub-vertical and agrees well with the estimated vertical stress due to overburden ( $\sigma_v = \gamma z = 6.6$  MPa). The intermediate principal stress ( $\sigma_{2o} = 4.0$  MPa) was oriented sub-parallel, while the minimum principal stress ( $\sigma_{3o} = 2.2$  MPa) was sub-perpendicular to the ED-B tunnel axis. The magnitudes of the stress tensor are listed in Table 4.1 and the orientations are shown in Fig. 4.6.

The measured in-situ pore pressure at Mont Terri was between 1.5 and 2 MPa. Pore pressures were not directly incorporated into the numerical model. Instead, excavation-induced pore pressures were calculated as described in Sect. 4.4.6.

Boundary conditions (far-field stresses) based on the recommended stress tensor were applied to the model periphery and initialized throughout the model. For a three-dimensional model, the boundary locations have a greater impact on model run times than comparable two-dimensional models. The boundaries were set at a distance of approximately 50 m from the edge of each tunnel, or 10 times the individual excavation diameters, or two times the distance between the two tunnels. Roller fixidity conditions were applied on all six exterior faces of the model.

#### 4.4.4 Material Properties

Significant field and laboratory testing has been conducted on the Opalinus Clay and the mechanical properties were known with a relative high level of confidence. Like most bedded materials, the Opalinus Clay is strongest in shear and tension parallel to bedding.

Table 4.2: Average isotropic mechanical properties of Opalinus Clay used in the numerical model [12].

Property	Value
Bulk density ( $\rho$ )	2450 kg/m <sup>3</sup>
Poisson's ratio ( $\nu$ )	0.3
Young's modulus (E)	4 GPa
Cohesion ( $c_u$ )	8 MPa
Friction ( $\phi$ )	0 (undrained)
Tension (t)	1.5 MPa
Bedding cohesion ( $c_b'$ )	1 MPa
Bedding friction ( $\phi_b'$ )	23°

Given the stress field discussed previously, any shear yielding would be expected in the tunnel sidewall (highest deviatoric stress) and tensile yielding would be expected in the roof and floor. Both of these modes of failure and locations correspond to the stronger parallel-to-bedding orientation. Therefore, the higher parallel-to-bedding strength values would be appropriate for the isotropic model.

The recommended Young's modulus from laboratory testing was 10 and 4 GPa parallel and perpendicular to bedding, respectively. Geophysical measurements reported by Schuster (pers. comm.), and discussed by Corkum [8], indicate an average isotropic Young's modulus for the rockmass of 4 GPa. As a result, an elastic Young's modulus (E) of 4 GPa was used for all analyses with isotropic linear-elastic and elasto-plastic constitutive models (not including the SDM model). The mechanical properties used in the numerical model are summarized in Table 4.2.

The average isotropic hydraulic conductivity of the Opalinus Clay is about  $5 \times 10^{-13}$  m/s. According to Anagnostou and Kovari [16], a total stress undrained analysis is appropriate for tunnel advancement in materials of this permeability. Therefore, total stress (undrained) properties were used in the analyses. The exception was in bedding plane slip analysis where effective stress shear strength parameters were used for bedding planes.

#### **4.4.5 Constitutive Models**

Laboratory testing indicated that the stress-strain behaviour of Opalinus Clay was highly non-linear with low stiffness at low stress levels. There has been significant evidence that the low stress non-linearity is inherent to the material itself and not a result of testing equipment or procedures. This is probably the single most important aspect of material behaviour that is not adequately captured by conventional elasto-plastic analyses. A phenomenological-based model has been developed based on observations from field and laboratory studies and the geological history of the Opalinus Clay. It should be noted that the stress-dependent modulus (SDM) model is not truly a constitutive model but a modification of the linear elastic model to represent the SDM behaviour. The development and implementation of this phenomenological model into  $FLAC^{3D}$  is described by Corkum [8]. Some background is provided here to orientate the reader.

The incremental secant modulus at low axial stress levels ( $\sigma_1$ ) are shown as circles for Sample 2-22-2p in Fig. 4.7. Triaxial data of confining stress ( $\sigma_3$ ) and Young's modulus (E) at 0.2 % strain are shown as diamonds (original data provided by Rummel [17]). From this plot it can be seen that a relationship exists between

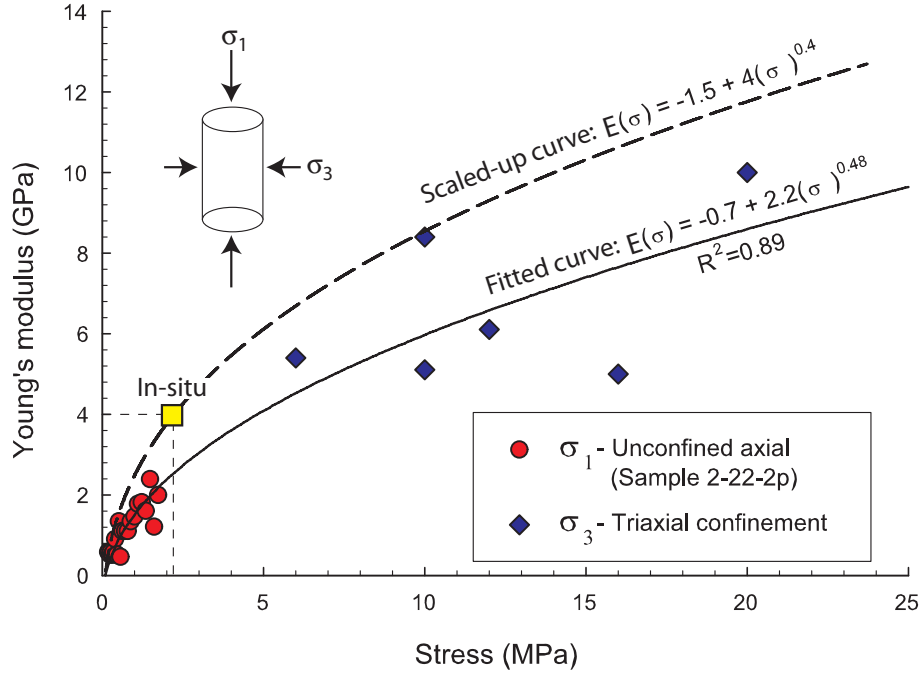


Figure 4.7: Non-linear elastic Young's modulus related to stress levels ( $\sigma_1, \sigma_3$ ) that forms the basis for the SDM model developed by Corkum [8].

$E$  and  $\sigma$ . A curve can be fitted to the combined data with an equation of the same form used by Santarelli et al. [7] for carboniferous sandstone. The fitted curve has an  $r^2 = 0.89$  with the equation:

$$E(\sigma) = -0.7 + 2.2(\sigma)^{0.48} \quad (4.1)$$

Samples that have been completely unloaded during sampling, and prior to reloading in uniaxial compression, display the maximum non-linear strains. The stress path during tunnel excavation in the stress field at Mont Terri can be quite complex. The rockmass around underground excavations typically undergoes only partial unloading to its final stress level during excavation. Therefore, the degree of stiffness non-linearity reflected by Eq. 4.1 may not be fully achieved in-situ. In addition, the estimated equivalent isotropic in-situ rockmass modulus was 4 GPa at  $\sigma_3 = 2.2$  MPa. Keeping the equation in the same form as that reported by Santarelli et al. [7], the equation parameters were scaled-up to achieve  $E=4$  GPa at  $\sigma_3 = 2.2$  MPa.

$$E(\sigma) = -1.5 + 4(\sigma)^{0.4} \quad (4.2)$$

Although the Opalinus Clay is bedded and anisotropic a simplified isotropic constitutive model was used because the effects of SDM on stiffness properties are more dominant than the natural anisotropy alone.

#### 4.4.6 Pore Pressure Formulation

Hydromechanical coupled formulations, such as Skempton's approach [18] or linear poroelasticity [19], generally predict increased pore pressure associated with an increase in the mean stress level with some shear-induced dilation in heavily over-consolidated materials. The pore pressure response due to excavation was measured during the ED-B mine-by test using piezometers that were installed in boreholes prior to excavation. These specially designed multi-interval packer piezometers were constructed with sintered steel filters that are able to withstand borehole squeezing [20].

Corkum [8] demonstrated that pore pressure measured during excavation of the ED-B tunnel was not predicted by conventional approaches and developed a simplified hydromechanical formulation for the Opalinus Clay to account for the non-linear behaviour observed in laboratory samples during unloading.

The pore pressure response ahead of and behind the excavations face are dominated by completely different mechanisms. Therefore, a piece-wise formulation was considered appropriate to describe hydromechanical coupling during tunnel excavation. A conventional mean stress formulation was used to estimate the pore pressure response ahead of the excavation face ( $X/D > 0$ ), and a confining stress dependent pore pressure relation was used behind the excavation face ( $X/D < 0$ ). Ahead of the tunnel face:

$$\Delta u = B \frac{\Delta\sigma_1 + \Delta\sigma_2 + \Delta\sigma_3}{3} \quad ; \text{for } X/D > 0 \quad (4.3)$$

Where  $\Delta u$  is the change in pore pressure,  $\Delta\sigma_i$  is the change in principal stress  $i$  and  $B$  is Skempton's pore pressure parameter. Significant dilation of the rockmass

has been observed below about 2 MPa [4] and because  $\sigma_{3o} = 2.2$  MPa the change in pore pressure when dilation is kinematically possible ( $X/D < 0$ ) can be expressed as:

$$\Delta u = \sigma_3 - \sigma_{3o} = \Delta \sigma_3 \quad ; \text{ for } X/D < 0 \quad (4.4)$$

It should be noted that the pore pressure model does *not* include time-dependent effects such as pore pressure dissipation.

## 4.5 Modelling Results and Comparison

The data obtained from the ED-B mine-by test provided a comprehensive set of measurements and observations for comparison with the numerical model. In general, the deformations measured around the ED-B tunnel show unique signatures with all deformations trending inwards towards the tunnel. The deformations away from the tunnel boundary, measured using borehole instrumentation, will be discussed first, followed by the convergence measurements that capture deformations in the near field at the tunnel boundary, and finally, the pore pressure measurements.

A total of five constitutive models were used in the analyses to simulate the ED-B mine-by test:

1. Linear-elastic model.
2. Elasto-perfectly plastic model.
3. Ubiquitous joint anisotropic elasto-plastic model.
4. SDM phenomenological model.
5. Scaled up SDM model.

Total stress, undrained analyses ( $\phi' = 0$ ) were used to model the Opalinus Clay. The ubiquitous joint perfectly plastic model, showing yielded elements and the location of the borehole instruments, is shown in Fig. 4.8. There was some yielding along joints, but very little yielding of rockmass elements. The instrumentation deformations for the elasto-plastic and ubiquitous joint elasto-plastic analyses were



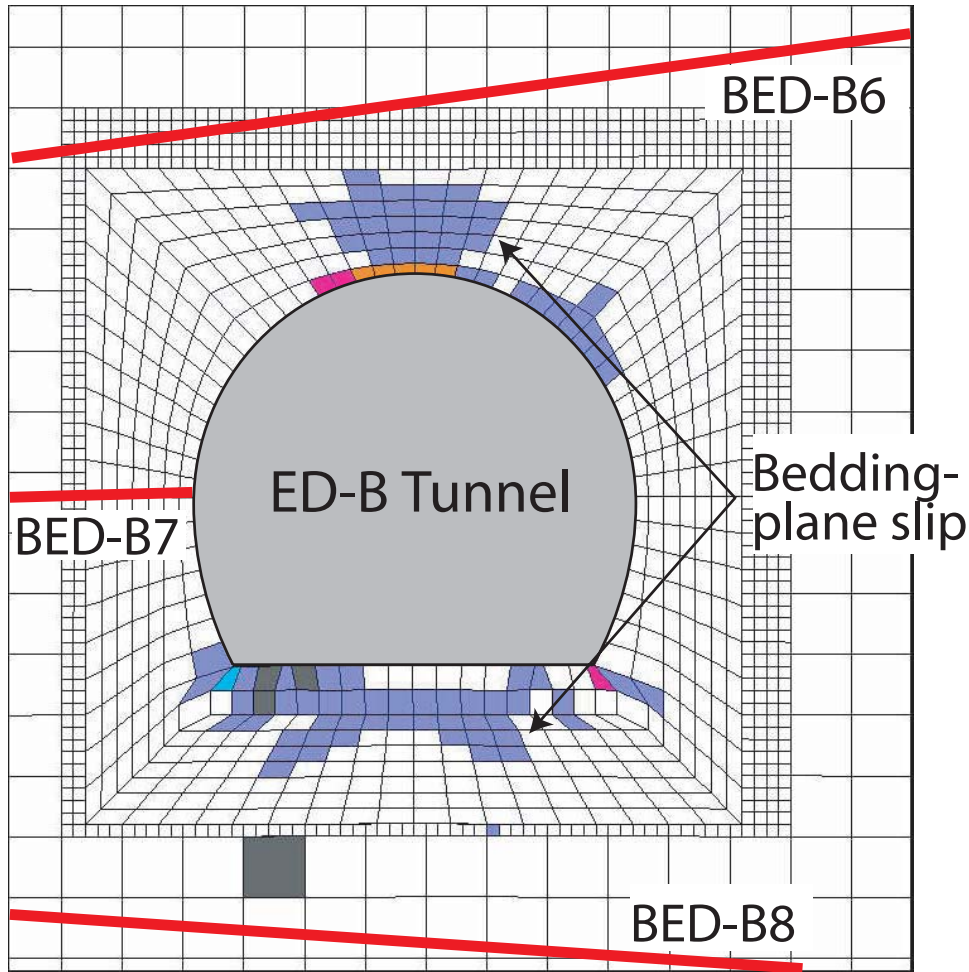


Figure 4.8: Numerical analysis using effective stress, horizontal bedding, ubiquitous joint properties ( $c'_b = 1 \text{ MPa}$ ,  $\phi'_b = 23^\circ$ ) showing yielded zones. It can be seen that bedding plane slip occurs in roof and floor of the ED-B tunnel. Yielding is concentrated in the lower left corner of the tunnel near the invert.

similar (within about 10 %) to the linear-elastic results. Therefore, only elastic model results are shown in the deformations plots for comparison.

#### 4.5.1 Borehole Deformation Instruments

The borehole instrumentation installed from the OP Niche provides excellent data over a large extent of the rockmass outside of the EDZ around the ED-B tunnel during excavation. As mentioned previously, in order to directly compare the results of modelling data to actual instrumentation data, the model data was transposed into deformation components that correspond to the instrumentation orientations.

This was done using the sign convention that deformations to the right (away from Reconnaissance Gallery) and upward are positive displacements.

The cumulative deformations for sliding micrometers and inclinometers in Boreholes BED-B6 through -B8, along with the model predictions, are shown in Fig. 4.9. Linear-elastic, the SDM and the scaled-up SDM constitutive model results are all represented. The inclinometers above and below the tunnel recorded a maximum of about 8 mm of inward movement with the maximum deformation approximately in line with the direction of  $\sigma_1$  as it passes through the tunnel centre. Similarly, the micrometers show a maximum of about 3 mm of horizontal movement towards the tunnel, with a transition between positive and negative movement again in line with the direction of  $\sigma_1$ . The proximity of the flat invert near BED-B8 explains the asymmetrical response of the borehole instruments above and below the tunnel.

The linear-elastic analysis was unable to capture the magnitude of deformations. The SDM model was able to match both the trend and magnitude of the inclinometer data well and the scaled-up SDM model fell somewhere in between the elastic and SDM models. In general, the micrometer field measurements were not matched particularly well by any of the constitutive models. The shape of the curves in the immediate tunnel vicinity was adequately matched, particularly the change from positive to negatively sloping deformations, but the horizontal deformations to the left of the tunnel were over-predicted by the model in BED-B6 and under-predicted in BED-B8.

Due to deformations at the borehole collar, there is greater uncertainty with the quality of the micrometer data compared to the inclinometer data, as discussed in Sect. 4.3. There are clear discrepancies between the model and measured micrometer data. Martin and Lanyon [2] showed that the sidewall was subjected to deviatoric stresses capable of inducing extensional fractures. This was also confirmed by the field mapping [21]. The SDM model used a nonlinear stiffness response to capture strains in the zones not subjected to these deviatoric stresses. It is clear from Fig. 4.9 that the SDM model does not capture the deformations associated with the zone of extensional fracturing and hence an alternative approach is required. This is the subject of on-going research.

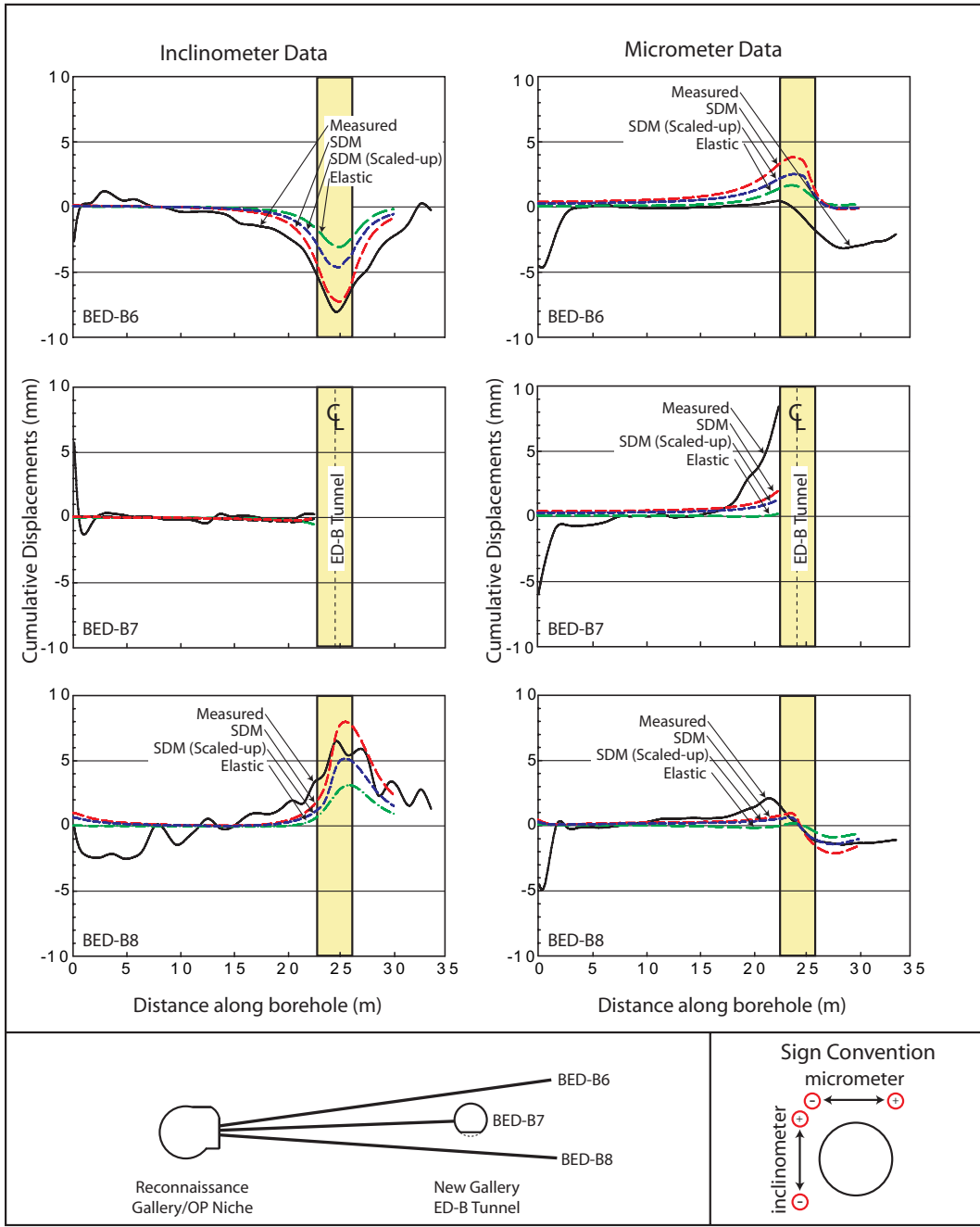


Figure 4.9: Results of  $FLAC^{3D}$  analyses compared with measured field data for cumulative inclinometers and sliding micrometers. The stress-dependent modulus model shows a good match of inclinometer data and a lesser fit to the micrometer data.

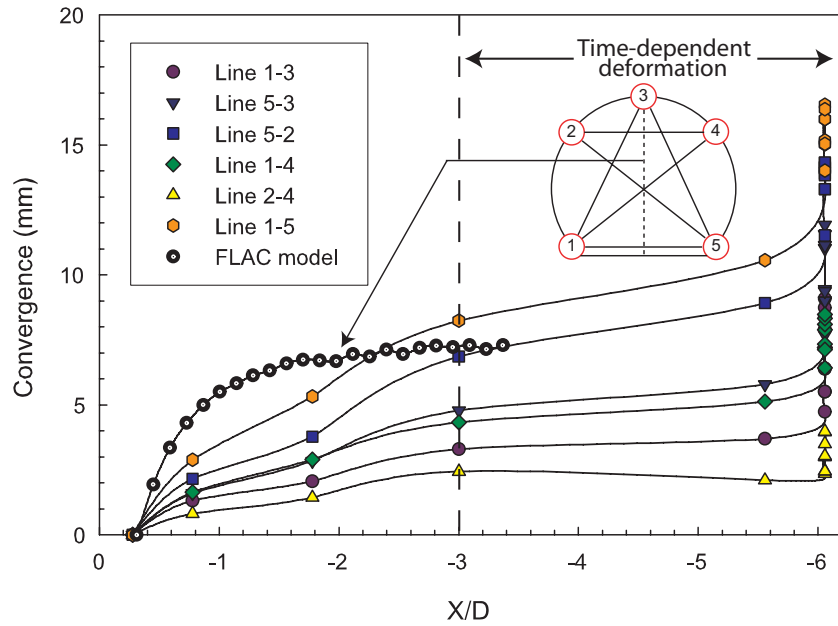


Figure 4.10: Convergence with excavation advance measured by Array CP-3 compared to the SDM model along a vertical convergence line. Orientation of convergence lines are shown in Fig. 4.12. Time-dependent deformations are significant ( $X/D < -3$ ).

A notable inconsistency between the model and measured data was the significant field deformations measured near the borehole collars as shown in Fig. 4.9. Corkum [8] described a mechanism of swelling associated with bio-geo-chemical processes as a potential cause of these large, unexplained deformations.

#### 4.5.2 Convergence Arrays

Convergence arrays provide a relatively simple and reliable form of directly measuring tunnel wall deformations, with the convention that inward rockmass deformation between two pins is positive convergence. A total of three convergence arrays were installed during the mine-by test, as shown in Fig. 4.4. The deformation magnitudes and trends were similar for all three sets of convergence arrays and an average convergence from the three arrays was used for comparison with numerical results. Fig. 4.10 shows measured convergence with excavation advance for Array CP-3 and model convergence along a vertical line.

The convergence arrays were installed approximately 1 to 2 m behind the excavation face; therefore, significant deformations that occurred prior to their instal-

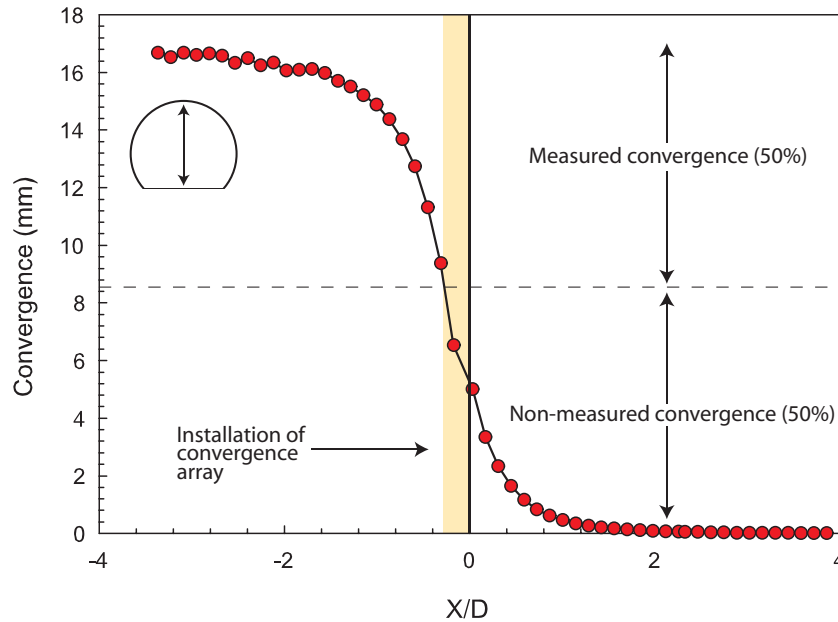


Figure 4.11: Convergence with three-dimensional excavation advance along a vertical convergence line using the SDM model. It is estimated that approximately 50 % of convergence occurred prior to installation of a convergence array.

lation were not picked-up by the field measurements. This issue was addressed by using the numerical model to estimate the deformation component that occurred prior to installation of the instrumentation. Convergence along a vertical line using the SDM model is shown in Fig. 4.11. The convergence curve is typical for tunnel advancement and it can be seen that 50 % of maximum convergence had occurred before the convergence arrays were installed (at  $X=1$  m or  $X/D=0.3$ ). Initially, the calculated convergence measurements included all deformation and the calculated convergence measurements were reduced by 50 % for direct comparison with field measurements.

Typically, elastic deformations stabilize approximately three tunnel diameters behind the excavation face ( $X/D=-3$ ). Deformations beyond this are dominated mainly by time-dependent processes, particularly evident in the Opalinus Clay. Measured and modelled convergence, excluding the time-dependent component (at  $X/D=-3$ ), is plotted in Fig. 4.12.

The calculated vertical convergence line (Fig. 4.11) is nearly aligned with the maximum principal stress and therefore agrees well with the diagonal convergence

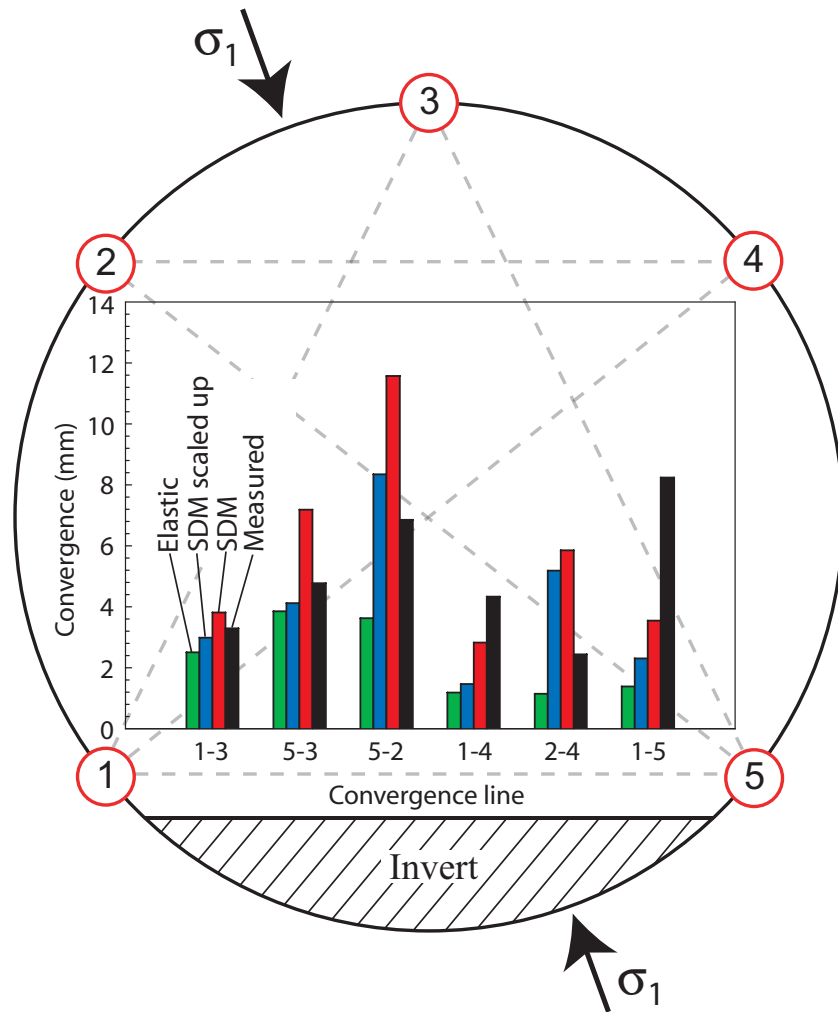


Figure 4.12: A comparison of the average convergence measurements from three arrays to the numerical model results shows a reasonable fit with the SDM model. Measurements associated with Pin 1 are under-predicted due to local yielding (see Fig. 4.8).

line (Line 5-2). However, because the SDM is very sensitive to both confining and deformation driving stresses, the model over-predicts the deformations aligned with the maximum principal stress (Line 5-2 in Fig. 4.12).

Deformations from the elastic analysis do not match in magnitude, but have somewhat similar trends to the measured values. This supports non-linear elasticity, as opposed to plasticity, as the source of these deformation magnitudes. The SDM model shows a fair fit to the data in terms of both magnitude and trend, while the scaled-up SDM fell somewhere in between. The most notable exception was

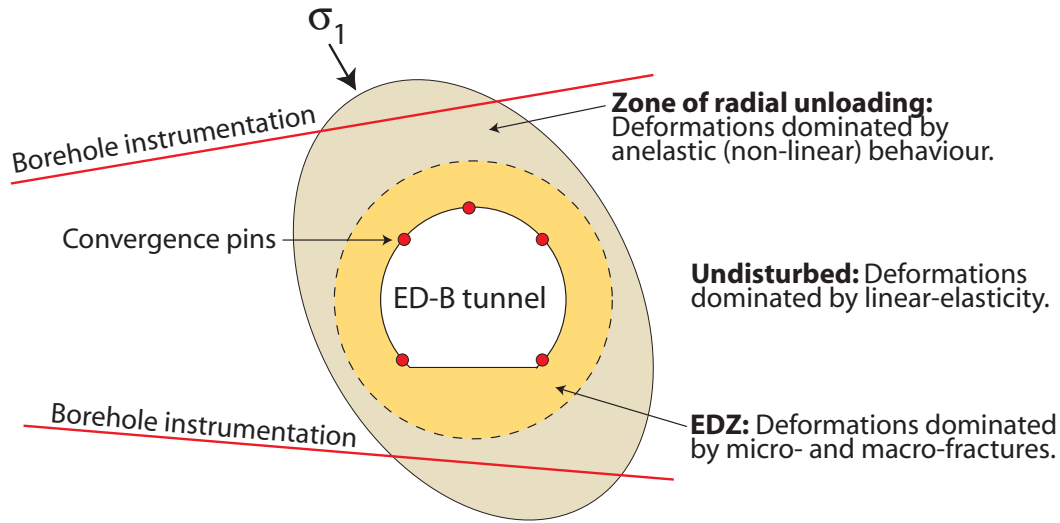


Figure 4.13: An illustration of the mechanisms of rockmass displacement around tunnels in Opalinus Clay: undisturbed zone (linear elastic), zone of unloading (non-linear) and the EDZ (dominated by dilation).

Convergence Line 1-5, along the bottom of the tunnel, which was significantly under-predicted by all models. Line 5-2 shows a good fit, while Line 1-4 shows a lesser fit indicating that the modelling deficiency is associated more with Pin 1 than Pin 5. Pin 1 is located near the sharp corner of the invert in a zone of high deviatoric stress and it is likely that the effects of dilation and/or plastic yielding associated with high deviatoric stresses results in larger than predicted inward deformations in this area. This notion is also supported by the distribution of yielded elements shown in Fig. 4.8.

The SDM model generally over-predicts deformations in zones of low deviatoric stresses (scaled-up works best here) and under-predicts deformations in zones of high deviatoric stresses. This indicates that deviatoric stresses induce increased dilation in the rockmass by opening fractures. Although this is not accounted for adequately by the SDM model, it is in agreement with the concepts of the micro-structure model. Fig. 4.13 illustrates the different modes of behaviour around tunnels in Opalinus Clay.

### 4.5.3 Piezometer Measurements

All of the sintered steel interval piezometers were installed on the northeast side of the ED-B tunnel as shown in Fig. 4.4. Piezometers BED-B1 and -B3 were located in a similar location/orientation while Piezometer BED-B2 was located slightly lower and farther away from the tunnel. The latter location corresponded to a zone of lower stress changes but higher deviatoric stresses than the other piezometer locations.

The initial pre-tunnelling piezometric measurements were between 1500 and 2000 KPa. The general pore pressure response can be described as a gradual rise prior to excavation, followed by an abrupt rise, or “spike”, as the excavation face approached the piezometers. Immediately behind the excavation face, pore pressures dropped off dramatically with the lowest values approaching zero. Similar trends were observed in all piezometers, although this trend was more pronounced closer to the tunnel where stress changes are greatest as shown in Fig. 4.14. The measured pore pressure in Intervals I1 and I2 in BED-B3 were very similar and a leak in the packer system was suspected between these intervals. These readings did not appear to differ substantially from those of the other instruments.

Fig. 4.14 shows the measured and calculated change in pore pressure using the piece-wise relationship described in Sect. 4.4.6 and implemented into FLAC<sup>3D</sup>. Because the numerical code does not directly account for real time for purely mechanical analyses, the value of time for the model data is based on tunnel advance rates recorded during excavation. Behind the excavation face, pore pressures were adequately matched, including the spike in pore pressures at the excavation face. The abrupt decrease in pore pressure as the excavation face passed the piezometer locations is also captured. However, the calculated pore pressure magnitudes under-predicted the measured field data in the dilatant stage. The model does not include the additional effects of deviatoric loading on rockmass dilation and this underestimation of the pore pressure drop was consistent throughout. Although it is applicable to a narrow range of problems (zones of unloading), and there are clearly observable shortcomings compared to conventional hydromechanical formulations, this level of agreement presents a compelling argument for application



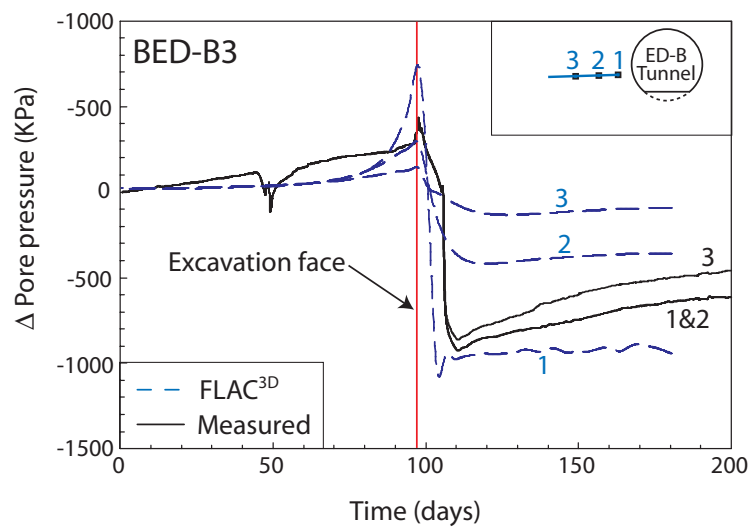
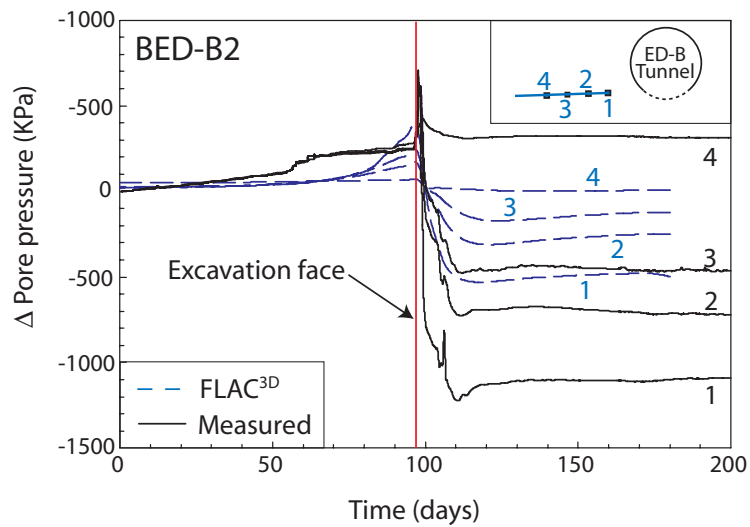
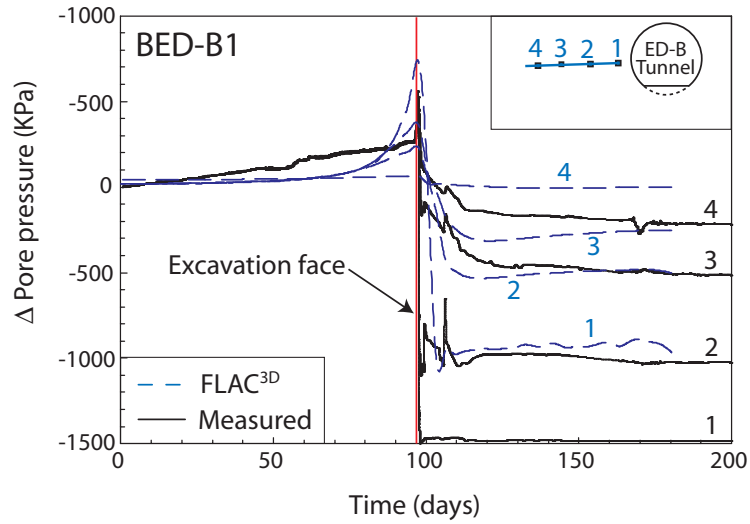


Figure 4.14: Change in pore pressures calculated using SDM-based piece-wise formulation adequately predicts the trends of pore pressure development with excavation advance.

of the proposed pore pressure response model.

It is interesting to note that the measured spike in pore pressure at the excavation face was between 300 to 700 KPa. This is significantly below the intact tensile strength of the Opalinus Clay (1 to 1.5 MPa) and therefore, even at  $\sigma_3 = 0$ , pore pressure-induced tensile yielding would not be anticipated as a cause of EDZ fractures.

## 4.6 Conclusions

From field and laboratory observations it has been observed that Opalinus Clay exhibits responses that are often not adequately represented by simple linear-elastic or elasto-plastic models. A stress-dependent modulus (SDM) model has been formulated to capture the highly non-linear response as the Opalinus Clay is unloaded under laboratory and/or field conditions. The concepts of the SDM model have been extended to a piece-wise pore pressure formulation that describes the hydromechanical rockmass response. The SDM model and pore pressure formulation were implemented into  $\text{FLAC}^{3D}$  in order to analyze the ED-B mine-by test case study.

Five constitutive models were used to analyze the ED-B tunnel response. The construction of the ED-B test tunnel produced relatively large displacements for the size of the opening, yet the construction experience suggested an essentially elastic response (i.e., no support was required near the face). The response from elastic and elastic ubiquitous joint (used to simulate bedding) analyses, significantly under-predicted the measured displacements. A traditional elasto-plastic analysis was also conducted and gave deformations similar to the elastic model. The SDM approach provided better agreement with the measured response; however, the model was unable to match the micrometer and convergence data correctly. Both of these are likely due to the same predictive shortcoming: the inability to include the effects of dilation associated with deviatoric loading.

The goal of this work was to assess if the short-term development and behaviour of the excavation damaged zone around underground openings in Opalinus Clay could be approximated using non-linear elastic modelling. This approach is in

keeping with the understanding of the geological history of the Opalinus Clay and its unloading behaviour. Observations regarding the behaviour of Opalinus Clay around underground openings are mutually supportive and present a compelling argument for the non-linear elastic model incorporated in the SDM model.

While the mine-by test was heavily instrumented, the authors are aware that this is only one case study and that further refinement and validation of the proposed model is required. Nonetheless, these findings suggest that while an excavation damaged zone will develop around underground openings in the Opalinus Clay, the damaged zone need not be analyzed using complex constitutive models.

## **Bibliography**

- [1] Corkum A G, Martin C D, Modelling a mine-by test at the Mont Terri rock laboratory, Switzerland. *Int J Rock Mech Min Sci* 2006, In Progress.
- [2] Martin C D, Lanyon G W, Excavation Disturbed Zone (EDZ) in clay shale: Mont Terri. Tech. Rep. TR2001-01, Nagra 2004.
- [3] Corkum A G, Martin C D, Modelling the short-term behaviour of Opalinus Clay around a circular excavation. In: *Canadian Geotechnical Conference 2004* .
- [4] Corkum A G, Martin C D, The mechanical behaviour of weak mudstone (Opalinus Clay) at low stresses. *Int J Rock Mech Min Sci* 2006, In Progress.
- [5] Kulhawy F H, Stress deformation properties of rock and rock discontinuities. *Eng Geol* 1975, 9:327–350.
- [6] Ewy R T, Cook N G W, Deformation and fracture around cylindrical openings in rock – I. Observations and analysis of deformations. *Int J Rock Mech Min Sci* 1990, 27(5):409–427.
- [7] Santarelli F J, Brown E T, Maury V, Analysis of borehole stresses using pressure-dependent, linear elasticity: Technical Note. *Int J Rock Mech Min Sci & Geomech Abstr* 1986, 23(6):445–449.

- [8] Corkum A G, Non-Linear Behaviour of Opalinus Clay Around Underground Excavations. Ph.D. thesis, Dept. Civil & Environmental Engineering, University of Alberta, Canada 2006.
- [9] Freivogel M, Huggenberger P, Modellierung bilanzierter Profile im Gebiet Mont Terri La Croix (Kanton Jura). Tech. Rep. 4 (Switzerland), FOWG, Geology Series 2003.
- [10] Thury M, Bossart P, Mont Terri rock laboratory: Results of the hydrogeological, geochemical and geotechnical experiments performed in 1996 and 1997. In: Geological Reports No. 23, Swiss National Hydrological and Geological Survey. Bern-Ittigen 1999 .
- [11] Marschall P, Croisé J, Schlickerrieder L, Boisson J Y, Vogel P, Yamamoto S, Synthesis of hydrogeological investigations at the Mont Terri site (Phases I to V). In: Mont Terri Project - Hydrogeological Synthesis, Osmotic Flow. - Reports of the Federal Office for Water and Geology (FOWG), Geology Series No 6, Bern, Heitzmann P, editor 2002 .
- [12] Bock H, RA Experiment: Data report on rock mechanics - Mont Terri project. Tech. Rep. Nagra, Internal Report TN00-02, Q+S Consult, Germany 2000.
- [13] Fierz T, ED-B Experiment: Deformation measurements during Phase 4. Inclinator and sliding micrometer measurements in BED-B6, BED-B7 and BED-B8. Tech. Rep. Nagra, Internal Report TN99-25, Solexperts, AG. 1999.
- [14] Curran J, Hammah R, Yacoub T, A two-dimensional approach for designing tunnel support in weak rock. In: Can Geotech Conf 2003 .
- [15] Martin C D, Lanyon G W, Measurement of in-situ stress in weak rocks at Mont Terri rock laboratory, Switzerland. Int J Rock Mech Min Sci 2003, 40:1077–1088.
- [16] Anagnostou G, Kovari K, Face stability conditions with earth-pressure-balanced shields. Tunn Undergr Sp Tech 1996, 11(2):165–173.

- [17] Rummel F, RA Experiment: Rock mechanics testing and characterization on drillcores of Boreholes BRA-1 and BRA-2, TN 2004-38. Tech. Rep., Nagra 2004.
- [18] Skempton A W, The pore pressure coefficients A and B. *Géotechnique* 1954, 4:143–147.
- [19] Wang H, *Theory of Linear Poroelasticity with Applications to Geomechanics and Hydrogeology*. Princeton University Press 2000.
- [20] Volckaert G, Fierz T, Results of the Hydrogeological, Geochemical and Geotechnical Experiments Performed in 1996 and 1997. Swiss National Hydrological and Geological Survey 1999 pp. 91–93.
- [21] Bossart P, Nussbaum C, Mayoraz J, Niederberger B, Zingg A, Engineered barrier experiment: Structural mapping of tectonic fractures and artificial features of the EB niche. Tech. Rep., Nagra 2002.

# Chapter 5

## Summary and Conclusions

Most rocks are not linearly-elastic in the classic manner; for example, stress-strain curves show non-linearity, hysteresis, and apparent permanent strain [1]. Laboratory testing of samples recovered at Mont Terri rock laboratory indicates that the stress-strain behaviour of Opalinus Clay is highly non-linear (anelastic) at low confining stresses. An investigation of this non-linearity has shown that it is a material property linked to the geological history, in particular, diagenesis of the Opalinus Clay. Diagenetic processes over the last 180 Ma have been responsible for chemical and mechanical changes since deposition of the Opalinus Clay. Numerical modelling has been used to demonstrate that the stress-path followed during sampling is very similar to the stress path experienced at the boundary of a tunnel. Hence, the non-linear response observed in laboratory samples is also likely to be a characteristic of the tunnel response.

A practical method to predict the constitutive behaviour of Opalinus Clay is needed in order to predict repository tunnel performance. Observations from laboratory and field studies have been synthesized to develop a model of the microstructure within the context of the geological history of the Opalinus Clay. This framework has served as a guide for development of two separate phenomenological-based models to capture the stiffness and pore pressure behaviour around underground excavations by utilizing data from simple unconfined and triaxial compression tests. Based on the premise that the tunnel walls undergo processes similar to those of samples removed from the stress field, these simple models allow engineers to capture a significant portion of the observed behaviour without undue modelling

complexities.

The construction of the ED-B test tunnel produced relatively large displacements for the size of the opening, yet the construction experience suggested only minor rockmass yielding occurred (i.e., no support was required near the face). Five constitutive models were used to analyze the ED-B tunnel response, including the SDM model and pore pressure formulation, implemented into FLAC<sup>3D</sup>. The ED-B case study has demonstrated that the SDM model is adept at capturing the deformations and pore pressure change as a result of unloading during tunnel excavation. The greatest shortcoming observed in the back-analysis was due to the inability to include the effects of dilation-induced behaviour. These mechanisms were not accounted for by the SDM model and will need to be addressed in order to capture the full spectrum of the rockmass response to tunnelling. Furthermore, because the SDM model varies stiffness as a function of  $\sigma_3$  to represent the general unloading response, care must be taken to ensure that the method is appropriate for a given problem.

Observations regarding the behaviour of Opalinus Clay around underground openings are mutually supportive and present a compelling argument for the non-linear elastic SDM model and pore pressure model. The models presented in this thesis are in agreement with field observations of the variation of stiffness around tunnels from geophysical measurements and the measured pore pressure response. Less quantitatively, the stress-dependent modulus (SDM) model can be used to predict non-linear behaviour around tunnels that may be useful in defining the extent of the EDZ.

This research has provided insight into the engineering behaviour of the Opalinus Clay that is needed in the assessment of repository tunnel performance. In addition, it has provided a framework that can be used to interpret various observations and experiments conducted on the Opalinus Clay. Furthermore, in terms of the direct implications towards a radioactive waste repository, the findings of this study may have their greatest impact by the identification of a mechanism that may ultimately trigger long-term behaviour processes, such as slaking, softening and swelling. This will impact the behaviour of micro- and macro-fractures around

repository tunnels and play a significant role in the self-sealing of such fractures.

The SDM constitutive behaviour model could be developed to a higher level of sophistication. However, development of a model to a level of complexity that is not justified by the current state of understanding of the fundamental properties is not necessarily of great benefit to engineers. Instead, it is hoped that this thesis provides compelling evidence that many aspects of the behaviour of argillaceous rocks, in particular the Opalinus Clay, are dominated by diagenetic bonding. Furthermore, that the relatively simple, yet effective, phenomenological-based constitutive models for stiffness and pore pressure described here can be quantified, to a reasonable extent, by conventional geotechnical means. Essentially this thesis serves as a middle-ground in the topic of micro-structure controlled non-linear stress-strain behaviour of argillaceous rock. Direct evidence of the presence and behaviour of diagenetic bonds is desirable and there is further need for more research into the micro-mechanical behaviour on a fundamental level.

## **5.1 Recommendations for Future Research**

It is clear that research into the fundamental behaviour of argillaceous rock is very demanding. For example, it can take several months to properly conduct a drained triaxial test. In many cases, the act of measuring a given property value for these sensitive materials, *in itself* can result in changes to that very value. Nevertheless, research efforts over the last 10 years have resulted in many interesting and promising developments in our understanding of the Opalinus Clay. Most notably, in regard to issues such as self-sealing behaviour, gas migration and micro-mechanical behaviour.

Clearly, there are many areas where significant additional research could be of great benefit. Just a few examples are: hydromechanical coupled behaviour, geochemical behaviour, the role of dilation, and extensional fracture generation in the EDZ around tunnels. In addition, time-dependent processes, such as swelling and softening, are probably the most troublesome to engineers. Many of these challenges have been recognized for decades [2, 3, 4].



As with many geotechnical problems, the fundamental root of the issue often lies in the geological history of the deposit. The findings in this dissertation have highlighted the role of diagenetic bonds and latent strain energy in the behaviour of Opalinus Clay. It has been shown that a phenomenological-based continuum model can be used to capture a significant portion of the non-linear elastic deformations. Based on this, the development of a more robust and generalized constitutive model is warranted. At this time, the main limitation is the accurate calibration and determination of engineering properties for such a model.

With the ever-increasing speed and capacity of computing, numerical modelling of geomaterials on the micro-scale is becoming more routine in geotechnical research and practice. Holt et al. [5] have demonstrated that the mechanical effects of sample release from in-situ stress conditions, and its effect on the behaviour of granular rocks, could be simulated using discrete particle modelling techniques. Bock et al. [6] have used distinct element formulations to simulate the mechanical behaviour of the Opalinus Clay on the micro-mechanical scale. A similar, but more extensive approach, that would include the unique depositional processes undergone by argillaceous rocks could be carried out for the Opalinus Clay.

Distinct element formulations could be used to simulate the geomaterial from initial sedimentation, through the various stages of diagenesis. This could include sampling and even the direct simulation of laboratory testing. The findings of such a study would provide significant insight into the development of the micro-structure of the Opalinus Clay and could be used to calibrate large-scale continuum models.

## **Bibliography**

- [1] Walsh J B, Brace W F, Elasticity of rock: a review of some recent theoretical studies. *Rock Mech and Eng Geol* 1966, 4:283–297.
- [2] Skempton W A, Long-term stability of clay slopes: Fourth Rankine Lecture. *Géotechnique* 1964, 14:77–101.
- [3] Terzaghi K, Stability of slopes in natural clay. In: *International Conference on*

Soil Mechanics and Foundation Engineering, vol. 1, Cambridge, MA 1936 pp. 161–165.

- [4] Morgenstern N R, Geotechnical behaviour of clay shales - An overview. In: International Symposium on Soil Mechanics, vol. 1, Oaxaca, Mexico 1979 pp. 29–41.
- [5] Holt R M, Doornhof D, Kenter C J, Use of discrete particle modeling to understand stress-release effects on mechanical and petrophysical behavior of granular rocks. In: Numerical Modeling in Micromechanics via Particle Methods, Konietzky H, editor, Swets & Zeitlinger, Lisse 2003 pp. 269–276.
- [6] Bock H, Blümling P, Konietzky H, Study of the micro-mechanical behaviour of the Opalinus Clay: an example of co-operation across the ground engineering disciplines. Bull Eng Geol Env 2006, 65:195–207.

# Appendix A

## Modelling the Short-term Behaviour of Opalinus Clay Around a Circular Excavation<sup>1</sup>

### A.1 Introduction

The behaviour of the Opalinus Clay claystone around deep underground excavations is of great interest to many organizations currently studying argillaceous rocks for potential geological disposal of nuclear waste. Argillaceous rocks are often described as the transition material between soil and soft rock and are well known for presenting challenges to civil engineers from identification of basic laboratory parameters to difficult tunnel construction. The research discussed in this paper is a portion of the larger research project underway on the behaviour of Opalinus Clay around deep underground openings.

A mine-by test tunnel was excavated through Opalinus Clay at the Mont Terri rock laboratory in 1997-98. The 3.6 m diameter circular excavation, known as the ED-B tunnel, was modelled using a simplified finite element method (FEM) analysis. Modelling this class of material is particularly challenging. The construction sequence, problem geometry, in-situ stresses, constitutive model, material properties and behaviour were the main issues investigated. A plane strain, two-dimensional, isotropic, elasto-plastic FEM analysis was carried out using Phase2<sup>2</sup>. Pore pressures were not directly considered in the hydromechanically uncoupled

---

<sup>1</sup>This chapter has been presented as a paper at the 2004 Canadian Geotechnical Conference.

<sup>2</sup>Information available at [www.roscience.com](http://www.roscience.com)

analyses, but because of the low permeability and relatively rapid rate of excavation, undrained conditions are believed to control the short-term behaviour.

## A.2 Overview of Opalinus Clay

The Opalinus Clay, found mainly in Germany and northwestern Switzerland, is a relatively weak argillaceous rock classified as a claystone. Named for the ammonite *Leioceras Opalinum*, it is a Lower Aalenian (middle Jurassic aged) marine deposit with past overburden estimated to have been at least 1000 m thick [2]. Based on the observed intensity of slaking when immersed in water, it appears to be lightly or uncemented. Like most argillaceous rocks, the laboratory properties are transversely isotropic in nature, with bedding on the centimetre scale. It has a pronounced microstructure that consists of clay plates, or particles that are tabular shaped and highly oriented approximately parallel to bedding. This microstructure is thought to have a significant impact on the macro-behaviour of the material [3].

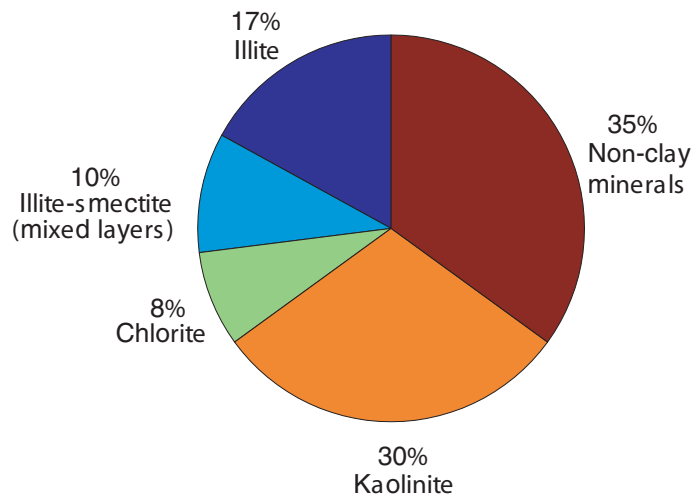


Figure A.1: Typical composition of Opalinus Clay.

Typically, Opalinus Clay is composed of about 50-65 % clay particles, with the clay mineralogy consisting mostly of fairly low activity kaolinite and illite. It has significant swelling potential due to its high clay content, regardless of the low activity mineralogy. Fig. A.1 shows the typical mineral composition of Opalinus Clay and a summary of the basic index properties is tabulated in Table A.1. The most

Table A.1: Index properties of Opalinus Clay [3].

Property	Value	Property	Value
Bulk density	2450 kg/m <sup>3</sup>	Liquid limit	38 %
Porosity	13.7 %	Plastic limit	23 %
Water content	6.1 %	Plastic index	15 %
Hydraulic conductivity	5e <sup>-13</sup> m/s	Unconfined strength	13 MPa

notable mechanical properties are the very low water content and porosity as well as the highly anisotropic nature. There have been a number of studies conducted on the shear strength of Opalinus Clay showing that the material is fairly linearly elastic, followed by the onset of dilatant behaviour at or near peak strength. It is very brittle with a significant reduction in post-peak strength. This behaviour is typical of a large range of geomaterials from stiff over consolidated clay, such as London clay, to hard rocks, such as Lac du Bonnet granite.

### A.3 Mont Terri Rock Laboratory

The Reconnaissance Gallery, also referred to as the Security Gallery, was originally constructed as part of the motorway tunnel of the A16 Transjurane motorway near the town of St. Ursanne, Switzerland. The rock laboratory began in 1995 with the excavation of a number of Niche's within the Reconnaissance Gallery to carry out various experiments in the Opalinus Clay. Over the last decade additional experiments and expansion of the rock laboratory have been carried out. A layout of the rock laboratory and the ED-B tunnel, which is the focus of this paper, can be seen in Fig. A.2.

#### A.3.1 Geological Setting

Located in the Jura Mountains of northwestern Switzerland, Mont Terri is an asymmetrical anticline which was folded during the Late Miocene to Pliocene period. Stratigraphy consists of competent limestones and incompetent marly/shaly formations, dipping about 45 to the southeast in the area of interest [4]. Where it intersects the rock laboratory, the Opalinus Clay is about 250 m thick. Fig. A.3 shows a ge-

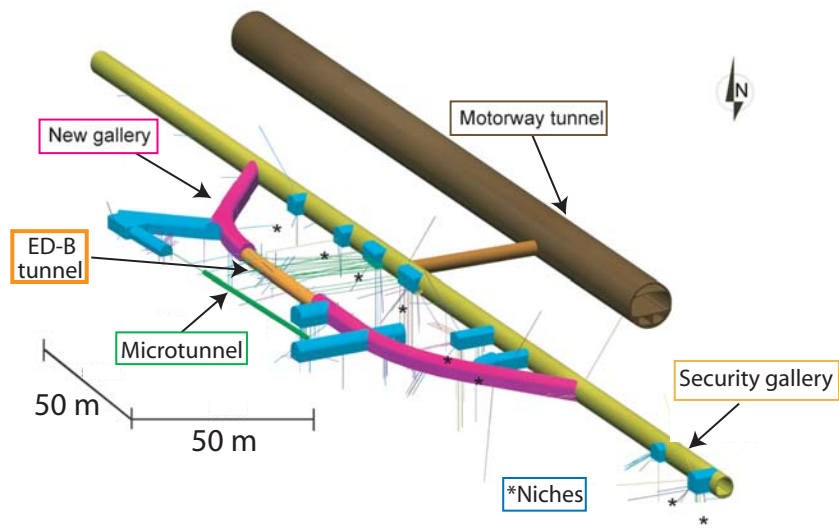
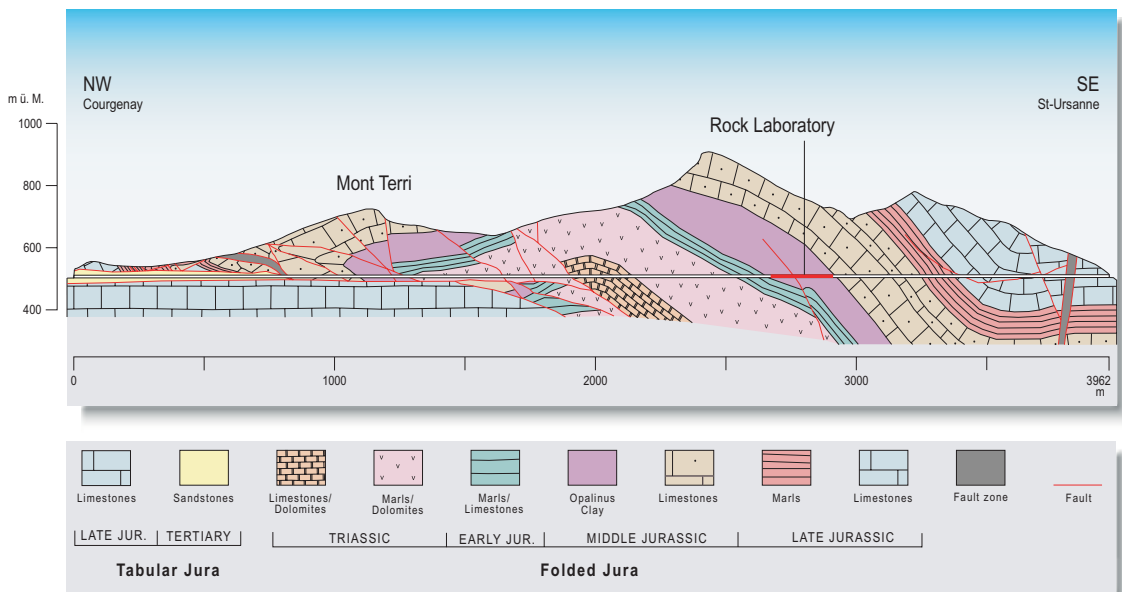


Figure A.2: Layout of Mont Terri rock laboratory (from [www.mont-terri.ch](http://www.mont-terri.ch)). Notice the ED-B tunnel within the New Gallery section.



Michael Freivogel (2001, University of Basel)

Figure A.3: Geological profile along Mont Terri motorway tunnel (from [www.mont-terri.ch](http://www.mont-terri.ch)).

ological section along the motorway tunnel. As a result of differing sedimentation, the Opalinus Clay can be grouped into three facies consisting of a shaly facies, a sandy facies and a carbonate-rich facies. The ED-B tunnel is located entirely within the shaly facies. One major fault runs through the rock laboratory south of the ED-B tunnel and a number of discrete minor faults have been observed throughout the rock laboratory. Structurally controlled instability is not believed to play a significant role in the ED-B tunnel.

### **A.3.2 In-situ Stresses**

The in-situ stress conditions were measured during a number of campaigns utilizing an assortment of techniques such as undercoring, slotter and hydrofracture. However, the results were somewhat unclear as some of the findings were not in agreement, and occasionally appear to conflict. Martin and Lanyon [5] have investigated the various stress measurement programs and pertinent observations and have recommended the stress tensor known as the *Rosas 1* tensor, obtained using the undercoring method. The magnitude and orientation of this stress tensor is shown in Fig. A.4. The maximum principal stress (6.5 MPa) is sub-vertical and agrees well with the estimated vertical stress due to overburden ( $\sigma_v = \gamma z = 6.6$  MPa). The orientation of  $\sigma_2$  is approximately parallel to the ED-B tunnel axis, while  $\sigma_3$  is nearly perpendicular.

The magnitude of  $\sigma_3$  is very low and results in an extreme horizontal to vertical stress ratio ( $k$ ) of 0.09 in the plane perpendicular to the tunnel (i.e. plane strain orientation). It should be noted that there is some uncertainty associated with the magnitude of  $\sigma_3$ .

## **A.4 Mine-by Experiment**

In addition to the many other field tests carried out at Mont Terri, a mine-by experiment was conducted during excavation of the 3.6 m diameter ED-B tunnel in 1997-98. This experiment has provided deformation data from a number of instruments, such as inclinometers, extensometers and convergence arrays, with time as

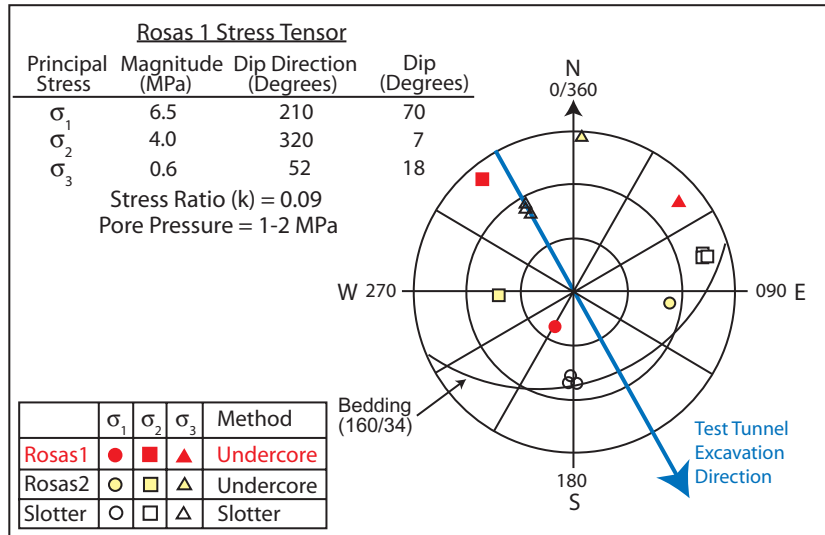


Figure A.4: *Rosas 1* is the recommended in-situ stress tensor at Mont Terri (from Martin and Lanyon [5]).

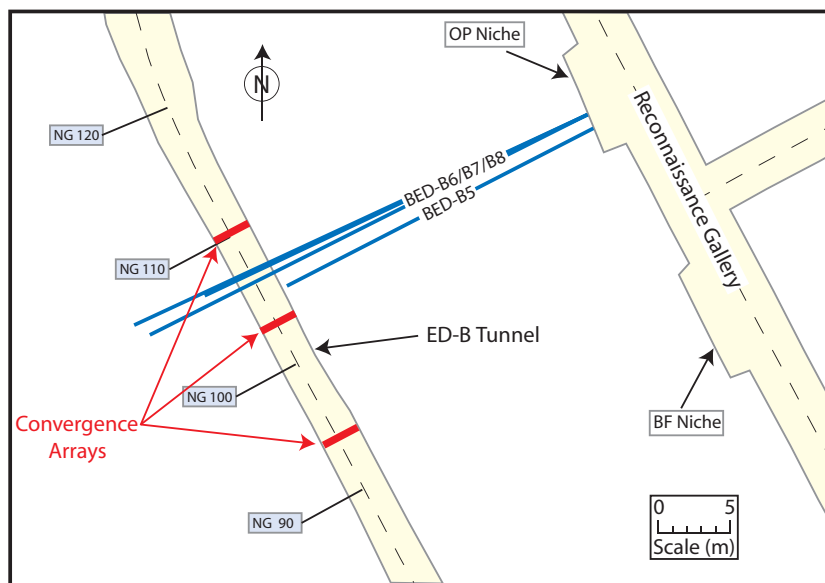


Figure A.5: Layout of instrumentation for ED-B mine-by test showing inclinometers/extensometers and convergence arrays.

the excavation advanced [6]. Most of the instrumentation was installed from the Security Gallery located approximately 24 m away from the ED-B tunnel prior to excavation (see Fig. A.5). One multipoint extensometer was installed in Borehole BED-B5. In addition, 3 instrumentation casings capable of acting as both sliding micrometers and horizontal inclinometers were installed in Borehole BED-B6



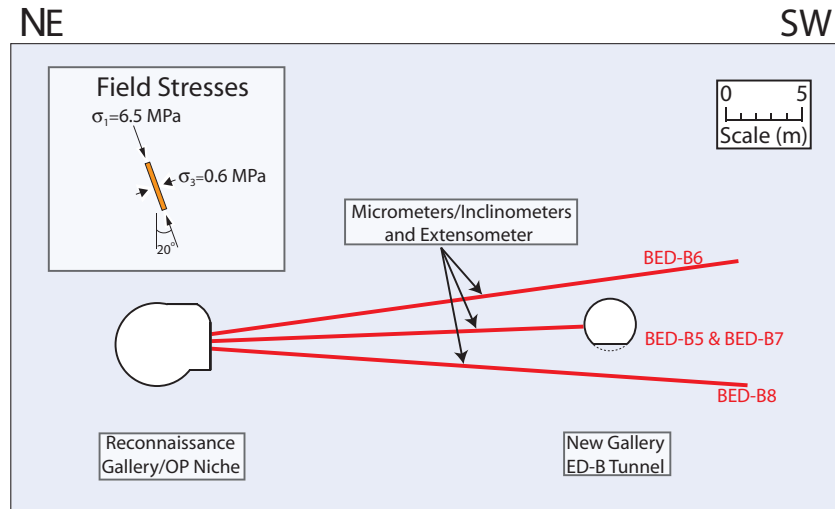


Figure A.6: Elevation view looking southeast in the direction of excavation advance.

through -B8. Three sets of five point convergence arrays were installed in the ED-B tunnel just behind the excavation face as it advanced. The instrumentation layout is shown in plan and section in Figs. A.5 and A.6, respectively. The deformation instruments were measured 19 times between September 1997 and June 1999.

A number of piezometers were installed as part of the mine-by experiment. Unfortunately, it appears that mechanical effects, such as squeezing and fracture initiation, dominate measurements near the tunnel, thus greatly reducing their applicability.

Following instrumentation, the ED-B tunnel was excavated full face using mechanical methods with a roadheader. Excavation was carried out from a northwest to southeast direction. The tunnel was stable during excavation and about 200 mm thick steel fibre reinforced shotcrete support was installed. The excavation was generally stable and shotcrete was installed approximately 7 m behind the excavation face.

Instruments such as micrometers and inclinometers measure the incremental displacement at discrete intervals along the instrument. These are integrated along the instrument length to get the cumulative displacements that represent (after appropriate corrections) the total displacement of the instrument in the ground. A major assumption is that there is at least one known fixed point along the instru-

ment to act as a datum. In the case of the inclinometers and sliding micrometers for the mine-by test, it was assumed that the collars, located greater than 24 m from the new excavation, would be the fixed points. However, the instrumentation data clearly shows that large deformations were recorded at these points as the ED-B excavation advanced.

Upon careful observation of the instrumentation data, a point approximately 8 m from the Security Gallery showed the least amount of relative movement. The amount of movement that did occur at this point is unknown, but FEM modelling indicated it would be negligible in comparison with the magnitude of movement typically measured along the instruments. As such, the 8 m point was used as the new datum assuming zero movement here. The deformation data was readjusted with the new datum using the following convention when looking towards the southeast (direction of excavation): positive movement is upward and negative is downward for inclinometers; and positive is to the right and negative is to the left for micrometers. This removes the more difficult concept of instrument "extension" and "contraction" for the micrometers and presents a more intuitive meaning to the inclinometer and micrometer data.

## **A.5 Numerical Modelling**

A two-dimensional, isotropic, elasto-plastic analysis using the FEM code Phase2 was used for the analysis. A total stress (undrained) analysis was used to model the Opalinus Clay. According to Anagnostou and Kovari [7], tunnelling in materials of this permeability and rate of advancement are considered undrained conditions. An effective stress (drained) analysis was also carried out for comparison because the extent of applicability of effective stress concepts to some argillaceous materials like the Opalinus Clay may be questionable [5]. Purely elastic, elastic perfectly-plastic and elastic brittle-plastic constitutive models were used for both total and effective stress analyses.

### A.5.1 Modelling Methodology

A simplified methodology was adopted to simulate the known physical conditions and construction sequence of the ED-B mine-by test as closely as possible. A three-noded graded mesh was automatically generated by Phase2 around the user defined excavation, stage and exterior boundaries of the problem. The nodal spacing for the mesh was approximately 0.1 m in the vicinity of the ED-B tunnel and decreased with distance. The boundary nodes were fixed (zero displacement) in both "x" and "y" and constant far-field stresses corresponding to the *Rosas* 1 tensor were initiated throughout the model. The chronology of events associated with the mine-by experiment was simulated using a six-staged model. These stages consisted of:

Stage 1: The initial stage where far-field stresses (*Rosas* 1) and boundary conditions were applied.

Stage 2: In order to simulate installation of the shotcrete liner prior to full convergence of the Reconnaissance Gallery, the modulus softening method was used [8]. This consisted of reducing the elastic Young's modulus by 50 %, then installing the 200 mm shotcrete liner.

Stage 3: Excavation of the Reconnaissance Gallery allowing the liner and ground to come into equilibrium.

Stage 4: The OP niche was excavated and lined with shotcrete. This point corresponded in real time to installation of instrumentation.

Stage 5: Excavation of ED-B tunnel, leaving it temporarily unsupported. The invert was left in place at this stage.

Stage 6: Installation of the shotcrete support and cutting through of the invert (later replaced by a concrete invert).

As mentioned previously, during excavation shotcrete support was not required at the tunnel face and lagged excavation by up to 7 m. By this time the majority of the deformation had occurred. Therefore, most of the deformation measured by instrumentation occurred between Stages 4 and 5 in the model. It is these deformations that are compared to the measured instrumentation data.

## A.5.2 Model Parameters

Model parameters are based on a summary of rock mechanics data compiled by Bock [3] for the Opalinus Clay at Mont Terri. As mentioned previously, the Opalinus Clay is highly anisotropic and averaged properties were used for the isotropic model discussed here. Table A.2 below shows the parameters used for the Opalinus Clay in the elastic brittle-plastic models. The constitutive model used was characterized by cohesion dominated peak strength and frictional residual properties, as suggested for weak rock by Hoek et al. [9].

Table A.2: Index properties of Opalinus Clay [3].

Analysis	Peak strength		Post-peak strength	
	$\phi$ (Deg.)	c (MPa)	$\phi_r$ (Deg.)	$c_r$ (MPa)
Total stress	0	6.5	23	0
Effective stress	25	1	23	0

## A.6 Results and Comparison

The data obtained from the ED-B mine-by test provided a very comprehensive set of measurements and observations for comparison with the FEM model. The deformation measured around the ED-B tunnel by the instrumentation show fairly unique signatures with all deformations tending inwards towards the tunnel. However, as already discussed it presented some challenges in interpretation.

To gage the results of various constitutive models, elastic and perfectly-plastic models have been conducted in addition to the brittle-plastic analysis. The deformation magnitudes from the elastic and perfectly-plastic analyses do not approach those observed in the field. For clarity of comparison, only the results of the brittle-plastic analysis are shown in the various plots in this section.

Convergence arrays provide a relatively simple and reliable form of directly measuring tunnel wall deformations, with the sign convention that positive convergence is inward tunnel deformation. Because the convergence arrays were installed behind the excavation face, approximately 1/3 to 1/2 of deformations occurred be-

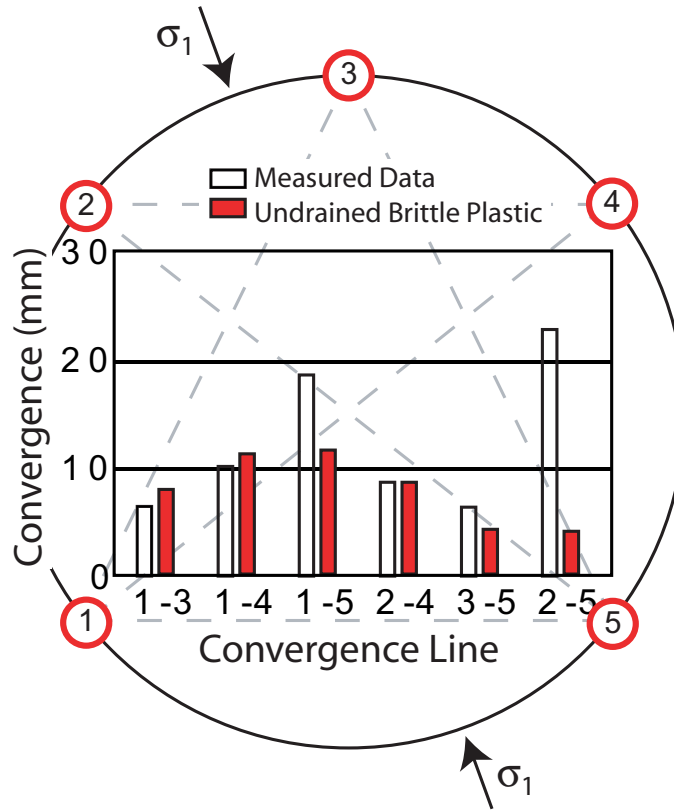


Figure A.7: FEM data and average measured convergence data. Note that significant portions of the deformations are not picked up by the instrumentation.

fore their installation and were not included in the measurements. This means total convergence from tunnel excavation is significantly discounted. The deformation magnitudes and trends were very similar for all three sets of convergence arrays and average convergence from the three arrays is shown on Fig. A.7 with the results from the FEM modelling. Due to the nature of the two-dimensional staged model, the data from the model includes all of the deformation associated with the ED-B tunnel excavation. Fig. A.7 also shows the layout of a typical convergence array looking in the direction of excavation advance (southeast). By far the largest deformations occur along convergence line 2-5 which are roughly in the direction of  $\sigma_1$ . Apart from convergence line 2-5, the trends of convergence show a reasonable match although the magnitudes from the model are not achieved, especially considering that the field measurements only pick up a portion of total deformation.

The instrumentation installed from the OP Niche provides excellent data over a large extent of the rockmass around the ED-B tunnel. In order to directly com-

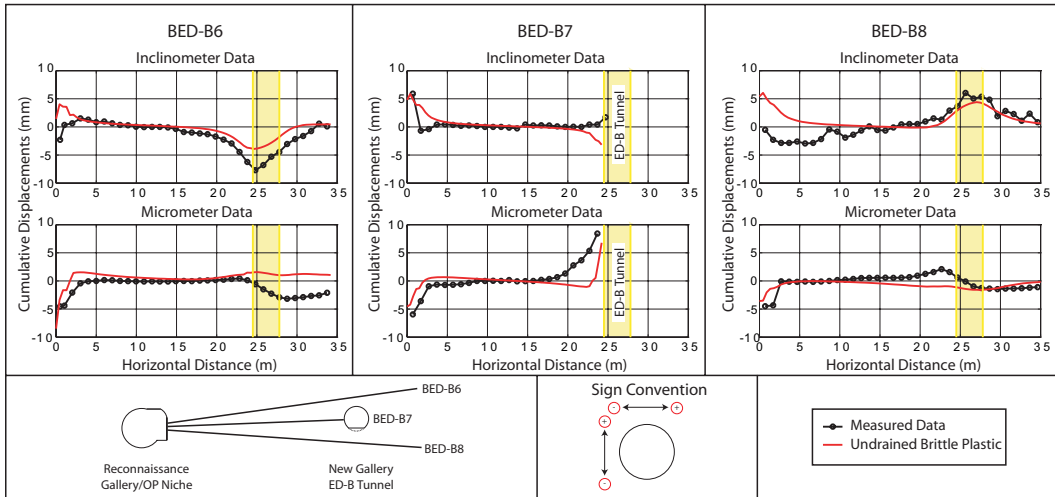


Figure A.8: Results of FEM analysis compared with measured data for cumulative inclinometers and sliding micrometers.

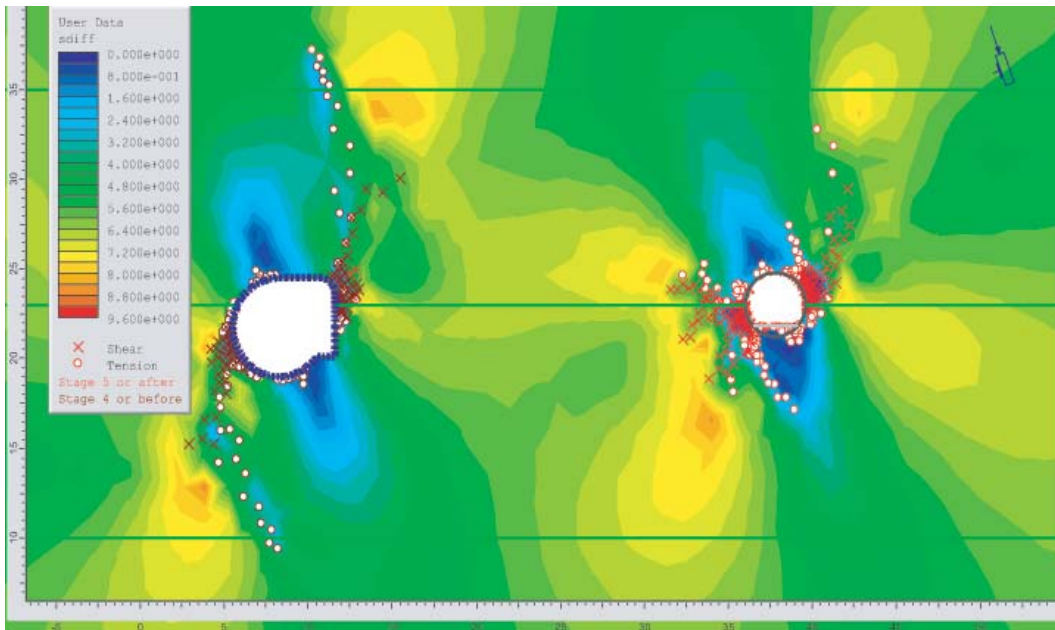


Figure A.9: Phase2 model looking southeast showing yielded elements and contours of deviatoric stress (MPa).

pare the results of modelling data to actual instrumentation data, the model data was transposed into deformation components that correspond to the instrumentation orientations. This was done using the same sign convention discussed previously. The cumulative deformations for sliding micrometers and inclinometers in Boreholes BED-B6 through -B8, along with the corresponding model data, are shown in Fig. A.8. The inclinometers above and below the tunnel show a maximum of about 8 mm of inward movement with the maximum deformation approximately in line with the direction of  $\sigma_1$ . Similarly, the micrometers show a maximum of about 3 mm of horizontal movement towards the tunnel with a transition between positive and negative movement approximately in the direction of  $\sigma_1$ .

Inclinometer data generally show a good fit to the model data for all instruments throughout their length except BED-B7. The modelling data for inclinometer BED-B7 shows good agreement with the measured data near the collar, but has the opposite orientation near the ED-B tunnel. This is understandable because it occurs along the neutral axis of the tunnel in a zone of transition between positive and negative vertical displacement. In general micrometers show a good fit near the collar, but the most notable deficiency is the poor fit of the micrometer data above and below the ED-B tunnel (BED-B6 and -B8). A multipoint extensometer was installed in Borehole BED-B5 from the OP Niche to the ED-B tunnel in the same orientation as BED-B7. Both instruments show a good fit to the model data throughout their length. Data from this extensometer show similar deformation magnitudes and trends as micrometer BED-B7, except the deformations occur over a more discrete zone closer to the tunnel.

Deformations in Fig. A.8 demonstrate that a good match of the deformation signatures was achieved by the simple brittle-plastic model. Inclinometer data appears to be modelled better than micrometer data. This could be due to anisotropy in the material that was not captured by the purely isotropic FEM model. Interestingly, the best match occurred near the collar of the boreholes around the OP Niche, as opposed to the ED-B tunnel itself. These indicate outward movement of the OP Niche wall with excavation of the ED-B tunnel. This movement was predicted by the model, measured by the instrumentation and observed by severe damage to the

shotcrete in the OP Niche [10]. According to the instrumentation and modelling, the zone of damage is isolated within the first 3 m of the borehole collars/niche wall.

The pattern of yielded elements observed around the ED-B tunnel from the FEM analysis is shown in Fig. A.9. It consists mainly of shear failure mode near the tunnel wall and develops into tensile yielding away from the tunnel. These yielded elements are concentrated along the sidewalls of the tunnel in the direction of the minimum principal stress where the maximum deviatoric stress occurs. The failure pattern extends greater than a tunnel diameter in a diagonal direction before trending towards a more vertical orientation away from the tunnel wall. The pattern of yielded elements is unsymmetrical, probably because of the affects of the invert in the floor of the ED-B tunnel.

## **A.7 Discussion**

The goal of the analysis presented in this paper has been to identify the major issues contributing to the behaviour of Opalinus Clay around a circular excavation. The main limitations were that the following were not given direct consideration:

- Hydromechanical coupling.
- Material anisotropy.
- Time dependent behaviour.
- Three-dimensional geometry.
- Excavation advance.

There is some debate regarding the in-situ stress tensor at Mont Terri, in particular the low value of  $\sigma_3$ . The recommended value of 0.6 MPa is lower than the measure value of pore pressure (2 MPa). A parametric study varying the value of  $\sigma_3$  between 0.6 and 2.2 MPa was conducted as part of this programme. This study found that as the value of  $\sigma_3$  increased (increased k), the magnitudes of deformation



decrease, but the deformation trends remained fairly constant for the range of in-situ stresses considered. Unfortunately, this study was unable to further constrain the stress tensor at Mont Terri.

For most soft rocks, the in-situ stress ratio is often close to one. With these stress ratios, a typical elastic deformation pattern has inward movement all around the circular excavation with maximum deformation in the direction of the maximum principal stress. However, with stress ratios below 0.3, such as that measured at Mont Terri ( $k=0.09$ ), the stress pattern again has maximum inward deformation in the direction of the maximum principal stress, but in the direction of the minimum principal stress deformations move away from the excavation. As mentioned, all measured data show inward movement all around the tunnel.

A field study called the Fracture Propagation (FP) study [11] was carried out to investigate the extent of the EDZ around the ED-B tunnel. Resin was injected into the formation under controlled pressure and then core samples were taken. This allowed for careful observation of the frequency, orientation and mode of failure. The results show that the EDZ extended around the ED-B tunnel approximately 0.5-1 m from the tunnel boundary. The dominant mode of yielding identified consisted of open extensional fractures. These fractures have also been observed on excavation walls where the EDZ has been intersected. Interestingly, these extensional features have not been identified in the excavation face.

The location, if not the correct mode, of yielded elements within the first 1 m of the tunnel wall has been adequately matched by the model. However, a significant disagreement between field conditions and model results was the difference in the failure pattern and mode of yielding away from the tunnel wall. There has been much speculation on the physical processes that result in the failure pattern observed in the field. Deformations were more accurately matched away from the tunnel wall, but the magnitudes of deformation were not achieved in the near-field. These observations indicate that near-field deformations were dominated by non-elastic behaviour associated with the failure mode identified in the FP study.

Deformations observed at the instrumentation borehole collars (see Fig. A.8) indicated inward movement of the OP Niche. This observation has been further

verified by significant shotcrete damage in this area. During cementation of the instruments in the OP Niche, water was released into the network of EDZ fractures around the niche (Peter Blümling, pers. comm.). A short time after this, (also corresponding to the excavation of the ED-B tunnel) significant deformations of up to 0.5 m were observed in the OP Niche. This was accompanied by extensive shotcrete damage. Water continues to be observed slowly dripping out of the formation along cementation lines. A sampling programme conducted in this area showed only slightly increased in-situ water content. This indicates that swelling alone would probably not be sufficient to explain the large deformations.

The neighbouring BF and PP Niche's have not experienced shotcrete damage to the same extent as the OP Niche, indicating that the phenomenon is somewhat isolated. Whether it is the inherently less competent rockmass, degradation of the rockmass properties due to ingress of water, or formation water travelling along the borehole, is not apparent. From elastic analysis alone, no movement of these borehole collars would be predicted, but based on the instrumentation, it appears that the trigger mechanism for this displacement was indeed excavation of the ED-B tunnel. The observations regarding the impact of the ED-B tunnel on the OP Niche show that three-dimensional geometry is an issue at Mont Terri even at significant distances. During tunnel driving there are other geometrical features involved, such as corners and intersections and face advancement itself is a three-dimensional problem. Finally, the recommended stress tensor is not in exact alignment with the tunnel direction adding another three-dimensional component to the problem.

## **A.8 Summary and Conclusions**

This paper has presented preliminary results of modelling the behaviour of Opalinus Clay (claystone) around a circular excavation at the Mont Terri rock laboratory, Switzerland. Field data from a mine-by test of the ED-B tunnel has provided a fairly comprehensive set of data with time and excavation advance. The analysis presented in this paper has demonstrated that a simplified total stress model, using the recommended stress tensor and material properties, was able to achieve a rea-

sonable match to field measurements. This provided insight into the major issues that require further consideration to accurately capture the behaviour of Opalinus Clay around underground openings.

Three-dimensionality is a strong issue in this problem for a number of reasons and must be given consideration in any future modelling of the ED-B tunnel. Modelling and field observations from the ED-B mine-by test have shown that tunnel interaction at Mont Terri can occur over distances much greater than would be expected based on elastic solutions. The analysis described in this paper was able to predict this interaction. The continually increasing frequency of openings at Mont Terri may require interpretation of the system-wide response for future analyses.

The fracture propagation study has shown that the EDZ was dominated by frequent open extensional fractures within the first 1 m of the tunnel wall. Near-field deformations were dominated by non-elastic behaviour. Although reasonably successful in modelling the instrumentation response, the FEM model was unable to accurately capture this mode of failure.

## **Bibliography**

- [1] Corkum A G, Martin C D, Modelling the short-term behaviour of Opalinus Clay around a circular excavation. In: Canadian Geotechnical Conference 2004 .
- [2] Marschall P, Croisé J, Schlickenrieder L, Boisson J Y, Vogel P, Yamamoto S, Synthesis of hydrogeological investigations at the Mont Terri site (Phases I to V). In: Mont Terri Project - Hydrogeological Synthesis, Osmotic Flow. - Reports of the Federal Office for Water and Geology (FOWG), Geology Series No 6, Bern, Heitzmann P, editor 2002 .
- [3] Bock H, RA Experiment: Data report on rock mechanics - Mont Terri project. Tech. Rep. Nagra, Internal Report TN00-02, Q+S Consult, Germany 2000.
- [4] Thury M, Bossart P, Mont Terri rock laboratory: Results of the hydrogeological, geochemical and geotechnical experiments performed in 1996 and 1997.

- In: Geological Reports No. 23, Swiss National Hydrological and Geological Survey. Bern-Ittigen 1999 .
- [5] Martin C D, Lanyon G W, Excavation Disturbed Zone (EDZ) in clay shale: Mont Terri. Tech. Rep. TR2001-01, Nagra 2004.
- [6] Fierz T, ED-B Experiment: Deformation measurements during Phase 4. Inclinator and sliding micrometer measurements in BED-B6, BED-B7 and BED-B8. Tech. Rep. Nagra, Internal Report TN99-25, Solexperts, AG. 1999.
- [7] Anagnostou G, Kovari K, Face stability conditions with earth-pressure-balanced shields. *Tunn Undergr Sp Tech* 1996, 11(2):165–173.
- [8] Curran J, Hammah R, Yacoub T, A two-dimensional approach for designing tunnel support in weak rock. In: *Can Geotech Conf 2003* .
- [9] Hoek E, Marinos P, Marinos V, Characterization and engineering properties of tectonically undisturbed but lithologically varied sedimentary rock masses. *Int J Rock Mech Min Sci* 2005, 42(2):277–285.
- [10] Corkum A G, Field Report: 2004 Mont Terri site visit. Tech. Rep., Nagra internal report 2004.
- [11] Möri A, Bossard P, Fracture Propagation Experiment: method, results, interpretation. Tech. Rep. TN99-72, Nagra Technical Report, Geotechnical Institute Ltd. 1999.

## Appendix B

# In-Situ Stresses at Mont Terri Rock Laboratory

An understanding of the in-situ stress conditions is of great importance for underground excavations. These boundary conditions are particularly significant when the objective is to understand the rockmass response to excavation and conduct experiments that are sensitive to stress levels. Therefore, the in-situ stress conditions at Mont Terri were measured during a number of campaigns utilizing an assortment of techniques such as: undercoring, slotter and hydrofracture. The results were somewhat unclear and some of the findings were not in agreement and, occasionally, appear to conflict. Martin and Lanyon [1] have investigated the various stress measurement programs and pertinent observations, and have recommended the stress tensor known as the Rosas 1 tensor, obtained using the undercoring method.

According to this stress tensor, the measured maximum principal stress ( $\sigma_{1o} = 6.5$  MPa) is sub-vertical and agrees well with the estimated vertical stress due to overburden ( $\sigma_v = \gamma z = 6.6$  MPa).  $\sigma_{2o} = 4.0$  MPa is oriented sub-parallel, while  $\sigma_{3o} = 0.6$  MPa and is sub-perpendicular to the ED-B tunnel axis, respectively. The orientation of this stress tensor is shown in Fig. B.1. While there is sufficient confidence in the orientation of the stress tensor, there is some uncertainty associated with the magnitude of  $\sigma_{3o}$  with the greatest reservation that the measured value of  $\sigma_{3o} = 0.6$  MPa is lower than the measure value of pore pressure ( $u_o = 2$  MPa). The remainder of this section will be devoted to constraining the value of  $\sigma_{3o}$  of

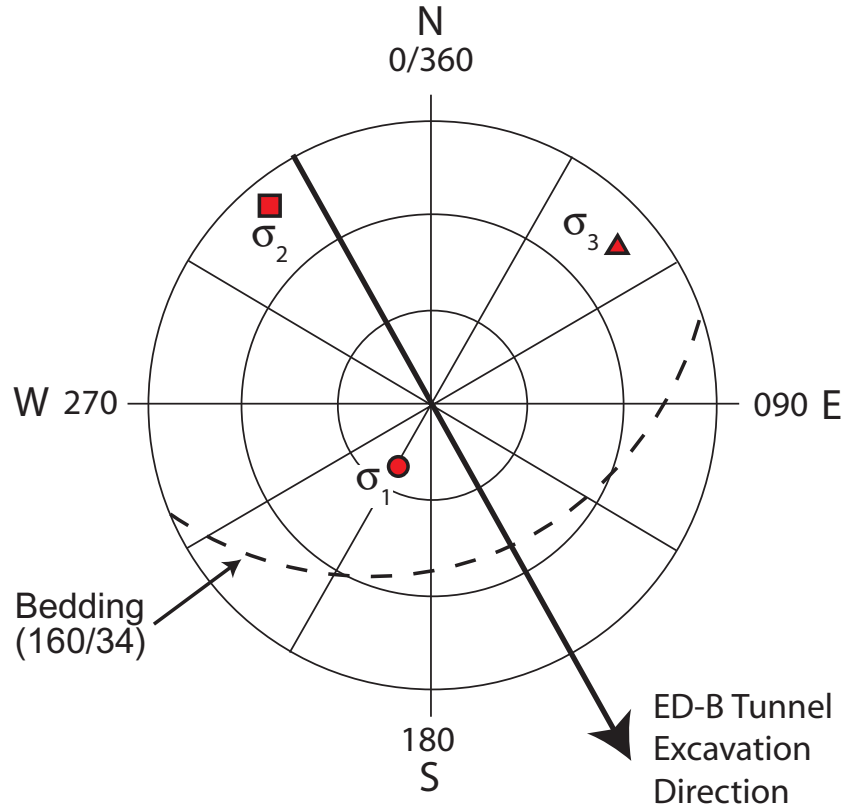


Figure B.1: Orientations of the Rosas 1 stress tensor from the undercoring in-situ stress measurement method (modified from Martin and Lanyon [1]).

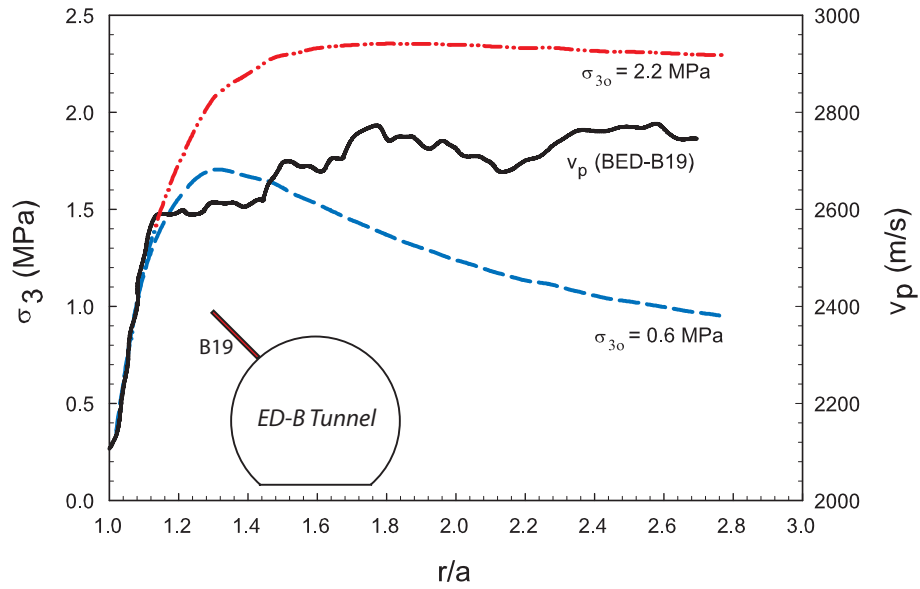
the stress tensor. Hydrofracture testing conducted in 1999 by Evans et al. [2] measured an in-situ stress normal to bedding of 4.2 MPa and indicated an upper-bound value of  $\sigma_{3o} = 2.9$  MPa. Given the relatively high level of confidence in the orientations and measured values of  $\sigma_{1o}$  and  $\sigma_{2o}$ , the hydrofracture results indicate that  $\sigma_{3o} \geq 0.6$  MPa is more likely.

At the time of publication of their work, Martin and Lanyon [3] stated there was no strong reason to disregard, or dismiss out-of-hand, the measured value of  $\sigma_{3o}$  from the Rosas 1 stress tensor. Evidence from the behaviour of laboratory samples described in this thesis showed that the Opalinus Clay behaves in a non-linear manner at low confining stress, such as in the radial direction around a borehole. This is in contrast to a significant assumption central to many in-situ stress measuring methods and presents some doubt regarding the reliability of measured stresses, particularly at low stress levels.

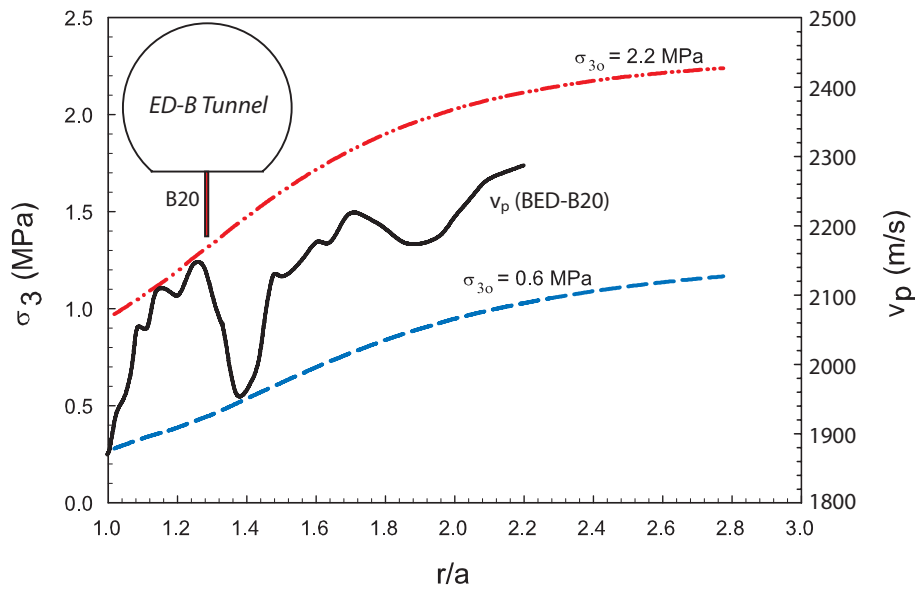
For most soft rocks, the in-situ stress ratio is often close to one. A value of  $\sigma_{3o} = 0.6$  MPa results in an extreme horizontal to vertical stress ratio (K) of approximately 0.09 in the plane perpendicular to the ED-B and Security Gallery tunnels (i.e. plane strain orientation). Preliminary numerical modelling of the ED-B tunnel was conducted by Corkum and Martin [4] using the Rosas 1 stress tensor with  $\sigma_{3o} = 0.6$  MPa. With this stress field, the calculated zone of yielding extended for several tunnel diameters away from the tunnel. The extent of the EDZ has been identified by several methods (fracture mapping study, geophysics, etc) and it appears to extend only about 1 m around the tunnel boundary.

Borehole breakouts have been used successfully to indicate the orientation of principal stresses [5] and this approach can be extended to tunnels. Fig. B.2 shows seismic compression wave velocity ( $v_p$ ) along a vertical borehole (B19) in the roof of the ED-B tunnel [6]. It shows that  $v_p$  rises quickly away from the tunnel wall and stabilizes at a fairly constant level after about 1.4 m from the tunnel wall. These measurements have been used to delineate the extent of the EDZ around the ED-B tunnel. It is well known that a relationship exists between  $\sigma_3$  and seismic velocity in a rockmass. The  $\sigma_3$  calculated from a finite element method (FEM) analysis of the ED-B tunnel with  $\sigma_{3o}=0.6$  and 2.2 MPa is superimposed on the plot of  $v_p$ . Near the tunnel boundary (within the EDZ) there is little discrepancy for the different values of  $\sigma_{3o}$ . There is some difficulty in making a direct comparison, as the fractured rockmass affects the geophysical readings in the EDZ, but away from the tunnel boundary (outside of the EDZ) the  $v_p$ - $\sigma_3$  correlation clearly agrees more strongly with the case of  $\sigma_{3o}=2.2$  MPa.

Further evidence for a magnitude of  $\sigma_{3o}$  greater than that of the in-situ pore pressure stems from the geological history of Mont Terri. According to Bossard and Wermeille [7], at the elevation of the rock laboratory, Mont Terri passed from an infiltration system to an exfiltration system between 1 and 3 million years (My) ago. This was based on an erosion model that indicated the erosion level reached the top of the Opalinus Clay at  $1.2 \pm 0.6$  My ago and reached the base of the unit about  $0.35 \pm 0.15$  My ago. This indicates that the Opalinus Clay has been dissipating excess pore pressure induced from the erosional process for approximately



(a) Borehole BED-B19.



(b) BED-B20

Figure B.2: In-situ seismic measurements support  $\sigma_3 = 2.2$  MPa. Data provided by K. Schuster (pers. comm.).

the last 1.2 My. Fenelli and Picarelli [8] have shown a case study of pore pressure dissipation in Italian argillaceous rock. In a deposit where the erosion rate exceeds the swelling rate in an actively eroded area, it was observed that negative pore pres-



sure was unable to dissipate and measured pore pressures were extremely low. This resulted in the effective stress decreasing to approximately equal the total stress.

This indicates that at Mont Terri the result of unloading due to valley erosion would be a suppressed pore pressure, as opposed to an unusually low value of total stress. The measured pore pressure at Mont Terri ranges between approximately 1-2 MPa, which agrees with the approximate hydrostatic pressure [9]. It is unlikely that the pore pressure is less than the minimum total stress. There are other geological and hydrological scenarios that could result in very low total and effective stress, but none have been identified at Mont Terri to date.

Finally, in a more subjective manner, there are many observations of the behaviour of Opalinus Clay being sensitive to a stress level of about 2 MPa. Examples include: the non-linearity of uniaxial samples at stress levels below about 2 MPa; the observation of significantly reduced flow in the EDZ fracture system (self-sealing) with 2 MPa of applied stress [10]; and increased laboratory self-sealing at 2 MPa [11]. These observations may not be particularly convincing on their own, but the combined weight of all of these additional observations results in a compelling argument for a stress tensor with  $\sigma_{3o}$  in the vicinity of 2 MPa.

Given the above evidence, and a reason to question the measured value, it is most likely that the true value of  $\sigma_{3o}$  is between 2 and 3 MPa. A value just above the highest measured pore pressure of 2.2 MPa is often used by researchers at the Mont Terri rock laboratory. Therefore, it is concluded that the Rosas 1 stress tensor orientations are correct, but the value of  $\sigma_{3o}$  should be adjusted upwards from 0.6 to approximately 2.2 MPa. The modified stress tensor is shown in Table B.1. This research, in particular the numerical modelling, has been conducted under the assumption of this stress tensor.

Table B.1: Magnitude and orientation of the modified stress tensor at Mont Terri rock laboratory.

Principal Stress	Magnitude (MPa)	Dip Direction (°)	Dip (°)
$\sigma_1$	6.5 (6 - 7)	210	70
$\sigma_2$	4.0 (4 - 5)	52	18
$\sigma_3$	2.2 (2 - 3)	320	7

## Bibliography

- [1] Martin C D, Lanyon G W, Measurement of in-situ stress in weak rocks at Mont Terri rock laboratory, Switzerland. *Int J Rock Mech Min Sci* 2003, 40:1077–1088.
- [2] Evans K, Piederach M, Portmann F, Hydrofracture stress test in Boreholes BIS-C1 and BIS-C2. Tech. Rep., Unpubl. Mont Terri Internal Report, Geot. Inst. Ltd. Bern 1999.
- [3] Martin C D, Lanyon G W, Excavation Disturbed Zone (EDZ) in clay shale: Mont Terri. Tech. Rep. TR2001-01, Nagra 2004.
- [4] Corkum A G, Martin C D, Modelling the short-term behaviour of Opalinus Clay around a circular excavation. In: *Canadian Geotechnical Conference 2004* .
- [5] Bell J, Gough D, Intraplate stress orientations from Alberta oil wells. *Evolution of the Earth, Geodynamics Series*, Geophysics Union, Washington, DC 1980, 5:96–104.
- [6] Schuster K, Alheid H J, Böddener D, Seismic investigation of the excavation damaged zone in Opalinus Clay. *Eng Geol* 2001, 61:189–197.
- [7] Bossard P, Wermeille S, Mont Terri Project - Geology, Paleohydrology and Stress Field of the Mont Terri Region. Report of the Federal Office for Water and Geology (FOWG), vol. 4 of Geology Series 2003 pp. 65–92.
- [8] Fenelli G B, Picarelli L, The pore pressure field built up in a rapidly eroded soil mass: Notes. *Can Geotech J* 1990, 27:387–392.
- [9] Marschall P, Croisé J, Schlickenrieder L, Boisson J Y, Vogel P, Yamamoto S, Synthesis of hydrogeological investigations at the Mont Terri site (Phases I to V). In: *Mont Terri Project - Hydrogeological Synthesis, Osmotic Flow. - Reports of the Federal Office for Water and Geology (FOWG), Geology Series No 6*, Bern, Heitzmann P, editor 2002 .

- [10] Blümling P, Bernier F, Lebon P, Martin C D, The Excavation Damaged Zone in clay formations – time-dependent behaviour and influence on performance assessment. In: Proceedings of Clays in Natural & Engineering Barriers for Radioactive Waste Confinement, Tours, France 2005 .
- [11] Ortiz L, Van Geet M, Self-healing capacity of argillaceous rocks: Review of laboratory results obtained from the SELFRAC project. In: Proceedings of Clays in Natural & Engineering Barriers for Radioactive Waste Confinement, Tours, France 2005 .

# Appendix C

## **Borehole breakout development at Mont Terri rock laboratory: 2004 field study<sup>1</sup>**

### **C.1 Introduction**

Borehole breakouts consist of slabbing/spalling and yielding in the direction perpendicular to the orientation of the maximum principal stress. This orientation coincides with the zone of maximum deviatoric stress. Therefore, borehole breakouts have been used successfully to indicate the orientation of principal stresses [2]. In addition, insight into the material behaviour around openings can be gained from borehole observations.

This paper describes the findings and interpretation from a field study of borehole breakouts at the Mont Terri rock laboratory near St. Ursanne, Switzerland (Fig. C.1). The field programme consisted of mapping 48 boreholes at various stages in the evolution of borehole breakouts. The intent was to gain an understanding of the development of breakouts with time and to assess the factors affecting borehole breakouts in Opalinus Clay. This field programme was conducted as part of the larger research study on the behaviour of Opalinus Clay around underground openings.

---

<sup>1</sup>This chapter has been presented as a paper at the 2004 Canadian Young Geotechnical Engineers and Geoscientists Conference.

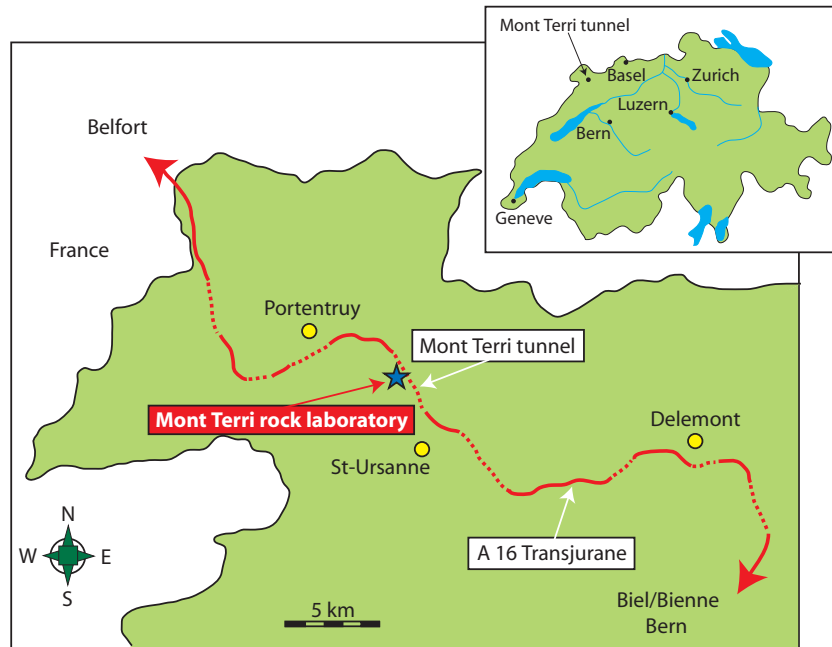


Figure C.1: Location map of Mont Terri rock laboratory, Switzerland.

## C.2 Background

### C.2.1 Opalinus Clay

Argillaceous rocks, such as the Opalinus Clay, are often described as transition materials between soil and soft rock. The Opalinus Clay, found mainly in Germany and northwestern Switzerland, is a relatively weak argillaceous rock classified as a claystone. Named for the ammonite *Leioceras Opalinum*, it is a Lower Aalenian (middle Jurassic aged) marine deposit with past overburden estimated to have been at least 1000 m thick [3]. Based on the observed intensity of slaking when immersed in water, it appears to be lightly or uncemented. Like most argillaceous rocks, the laboratory properties are transversely isotropic in nature, with bedding on the centimetre scale. It has a pronounced microstructure that consists of clay plates, or particles that are tabular shaped and highly oriented approximately parallel to bedding.

Typically, Opalinus Clay is composed of about 50-65 % clay particles, with the clay mineralogy consisting mostly of fairly low activity kaolinite and illite. It has significant swelling potential due to its high clay content, regardless of the low

activity mineralogy. A summary of the basic index properties of Opalinus Clay are tabulated in Table C.1. The most notable mechanical properties are the very low water content and porosity as well as the highly anisotropic nature. There have been a number of studies conducted on the shear strength of Opalinus Clay showing that the material is fairly linearly elastic, followed by the onset of dilatant behaviour at or near peak strength. It is very brittle with a significant reduction in post-peak strength. This behaviour is typical of a large range of geomaterials from stiff overconsolidated clay, such as London clay, to hard rocks, such as Lac du Bonnet granite.

Table C.1: Index properties of Opalinus Clay [4].

Property	Value	Property	Value
Bulk density	2450 kg/m <sup>3</sup>	Liquid limit	38 %
Porosity	13.7 %	Plastic limit	23 %
Water content	6.1 %	Plastic index	15 %
Hydraulic conductivity	5e <sup>-13</sup> m/s	Unconfined strength	13 MPa

## C.2.2 Mont Terri Rock Laboratory

The Mont Terri rock laboratory is the centre for in-situ testing of Opalinus Clay. The Reconnaissance Gallery, also referred to as the Security Gallery, was originally constructed as part of the motorway tunnel of the A16 Transjurane motorway near the town of St. Ursanne, Switzerland. The rock laboratory began in 1995 with the excavation of a number of Niche's within the Reconnaissance Gallery to carry out various experiments in the Opalinus Clay. Over the last decade additional experiments and expansion of the rock laboratory have been carried out. A layout of the rock laboratory can be seen in Fig. C.2.

Located in the Jura Mountains of northwestern Switzerland, Mont Terri is an asymmetrical anticline which was folded during the Late Miocene to Pliocene period. Stratigraphy consists of competent limestones and incompetent marly/shaly formations, dipping about 45 to the southeast in the area of interest [5]. Where it intersects the rock laboratory, the Opalinus Clay is about 250 m thick along the

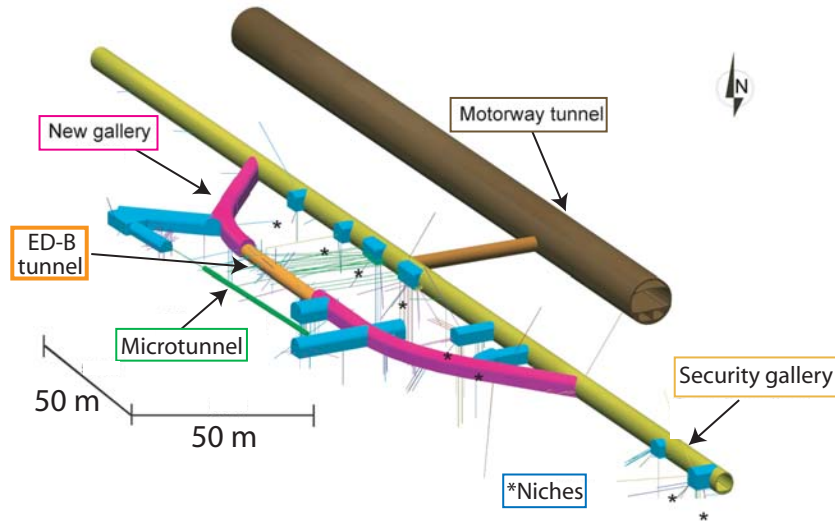


Figure C.2: Layout of Mont Terri rock laboratory (from [www.mont-terri.ch](http://www.mont-terri.ch)).

length of the tunnel. One major fault runs through the rock laboratory south of the ED-B tunnel and a number of discrete minor faults have been observed throughout the rock laboratory. Apart from bedding, naturally occurring discontinuities are not believed to play a significant role in the development of borehole breakouts.

The in-situ stress conditions were measured during a number of campaigns utilizing an assortment of techniques such as undercoring, slotter and hydrofracture. However, the results were somewhat unclear as some of the findings were not in agreement, and occasionally appear to conflict. Martin and Lanyon [6] have investigated the various stress measurement programs and pertinent observations, including borehole breakouts, and have recommended the stress tensor known as the *Rosas 1* tensor, obtained using the undercoring method. The magnitude and orientation of this stress tensor is shown in Fig. C.3. The maximum principal stress (6.5 MPa) is sub-vertical and agrees well with the estimated vertical stress due to overburden ( $\sigma_v = \gamma z = 6.6$  MPa). It should be noted that there is some uncertainty associated with the magnitude of  $\sigma_3$ .

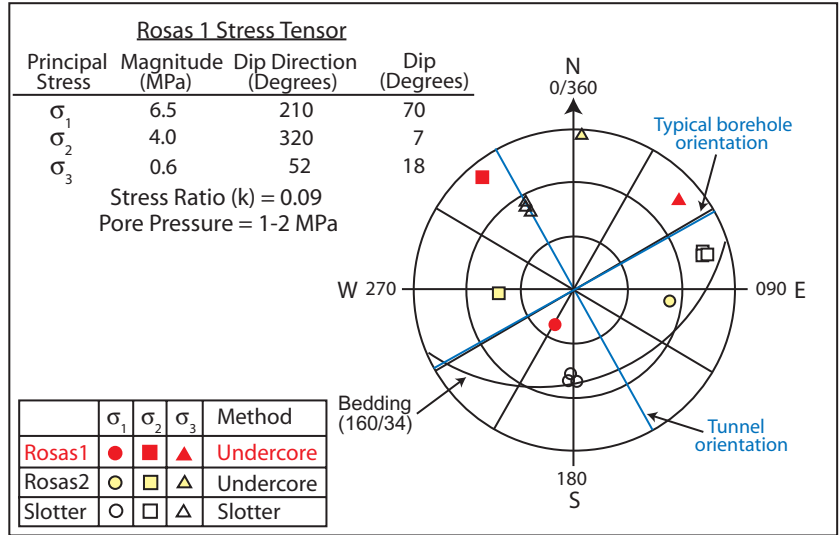


Figure C.3: *Rosas 1* is the recommended in-situ stress tensor at Mont Terri (from Martin and Lanyon [6])

### C.3 Borehole Mapping Methodology

A systematic programme of borehole mapping was carried out in 2004. The intent was to gain an understanding of the development of breakouts with time and to assess the factors affecting borehole breakouts in Opalinus Clay. Mapping of boreholes along the Security Gallery was done followed by mapping of most of the accessible boreholes in the New Gallery section. A total of 48 boreholes were mapped. Differing drilling methods, instrumentation, environmental conditions (moisture) and experimental usage has had a large impact on the individual borehole behaviour. The original usage of the boreholes was not always known and it was difficult to give full consideration to these issues. However, every attempt was made to give weighted consideration to boreholes that appeared to be air drilled and showed few signs of the breakout being strongly affected by drilling methods or experimental procedures.

Borehole orientation in regard to the stress field and bedding was significant. The vast majority of boreholes were oriented sub-horizontally in the direction perpendicular to the Security Gallery. Based on the stress tensor recommended by Martin and Lanyon [2003a], this is in the  $\sigma_1 - \sigma_2$  plane. This alignment corresponds to drilling parallel to bedding which dips approximately 45 towards the



southeast. Borehole diameters at Mont Terri ranged from about 25 mm to greater than 300 mm, but mapping was done with most of the boreholes having a diameter of 110 or 250 mm. The complex geometry and borehole density can be appreciated from Fig. C.4 showing the as-built layout of the rock laboratory.

## C.4 Findings and Interpretation

Borehole breakouts generally occur in the wall of the borehole in the direction perpendicular to the maximum stress in the plane of the borehole. This corresponds to the zone of maximum deviatoric stress. The boreholes observed at Mont Terri were drilled from existing tunnels and niche openings and there is a complex three-dimensional component to the stress field around most (see Fig. C.4). Therefore, the stresses around the borehole are superimposed upon the stresses induced from the larger tunnel excavations. According to Martin and Lanyon [6], breakouts are only observed when stresses around the borehole are elevated by the influence of three-dimensional geometry, such as an existing tunnel. This indicates that in-situ stresses at Mont Terri are not high enough to exceed the peak yield strength of the

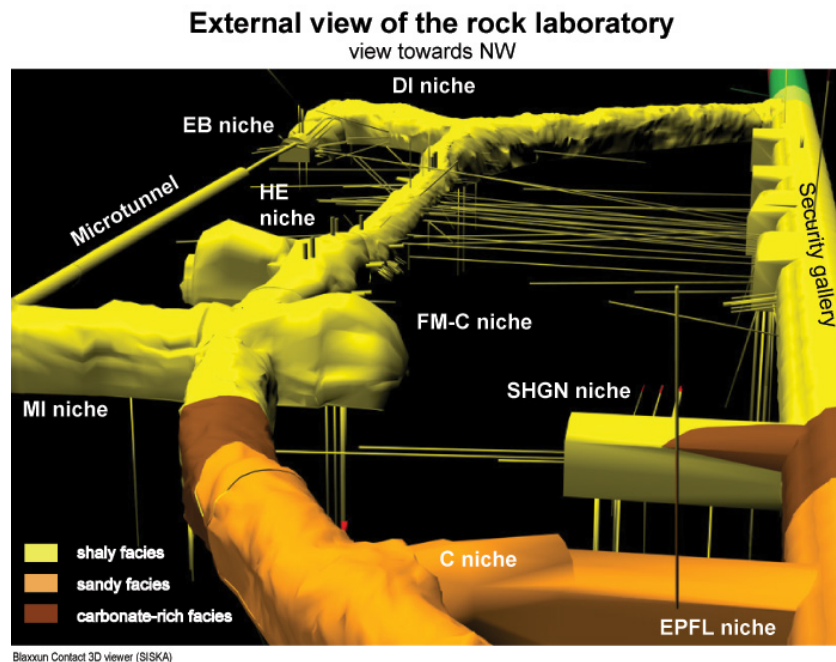


Figure C.4: External view of rock laboratory looking towards the northwest (from [www.mont-terri.ch](http://www.mont-terri.ch)).

rock. These observations hold true for the current study. The most significant breakouts occur close to the collar, usually within the first 1 m where the influence of the associated tunnel is highest, and decreases in severity along the borehole length.

EDZ fractures around tunnel openings are concentrated around the first 1 m of the tunnel wall [7]. There were few observations of geological or tunnelling induced fractures having a strong influence on the breakout, but these fractures were occasionally observed to influence the borehole breakouts in the early stress-induced stage of breakout development.

As mentioned above, the vast majority of borehole orientations are sub-horizontal, drilled perpendicular to the direction of the main tunnel system. Very few boreholes were oriented in the direction parallel to the tunnel and the few that were, would be significantly influenced by tunnel geometry induced stresses. Therefore, there was no direct evidence to assist in further constraining the in-situ stress tensor from borehole breakouts. However, it may be possible to use the data compiled here along with modelling and other observations to do so. The few vertical boreholes appear to be very stable, but occasionally they appear to be affected by swelling and squeezing mechanisms.

The 250 mm diameter boreholes display more significant breakouts than the smaller boreholes, particularly in the advanced stages where strength degradation and bedding planes dominate the breakout development. Therefore, scale has some affect on breakout development. There were a number of boreholes where complete collapse had occurred, but it is believed that these were cases where the borehole was strongly affected by the experimental use of the borehole. Many boreholes were covered leading to increased humidity and moisture over time. In a few of these covered boreholes, condensation was observed in the borehole or borehole cover. Frequent observations of gypsum deposits on the surface within the borehole and on breakout debris in covered boreholes indicates the presence of air; meaning that these boreholes were connected to the tunnel via a network of EDZ fractures.

In a previous review of borehole breakouts at Mont Terri, Bossard and Wermeille [8] categorized three types of breakouts:

1. Mechanically-induced breakouts, observed where the bedding is tangential to

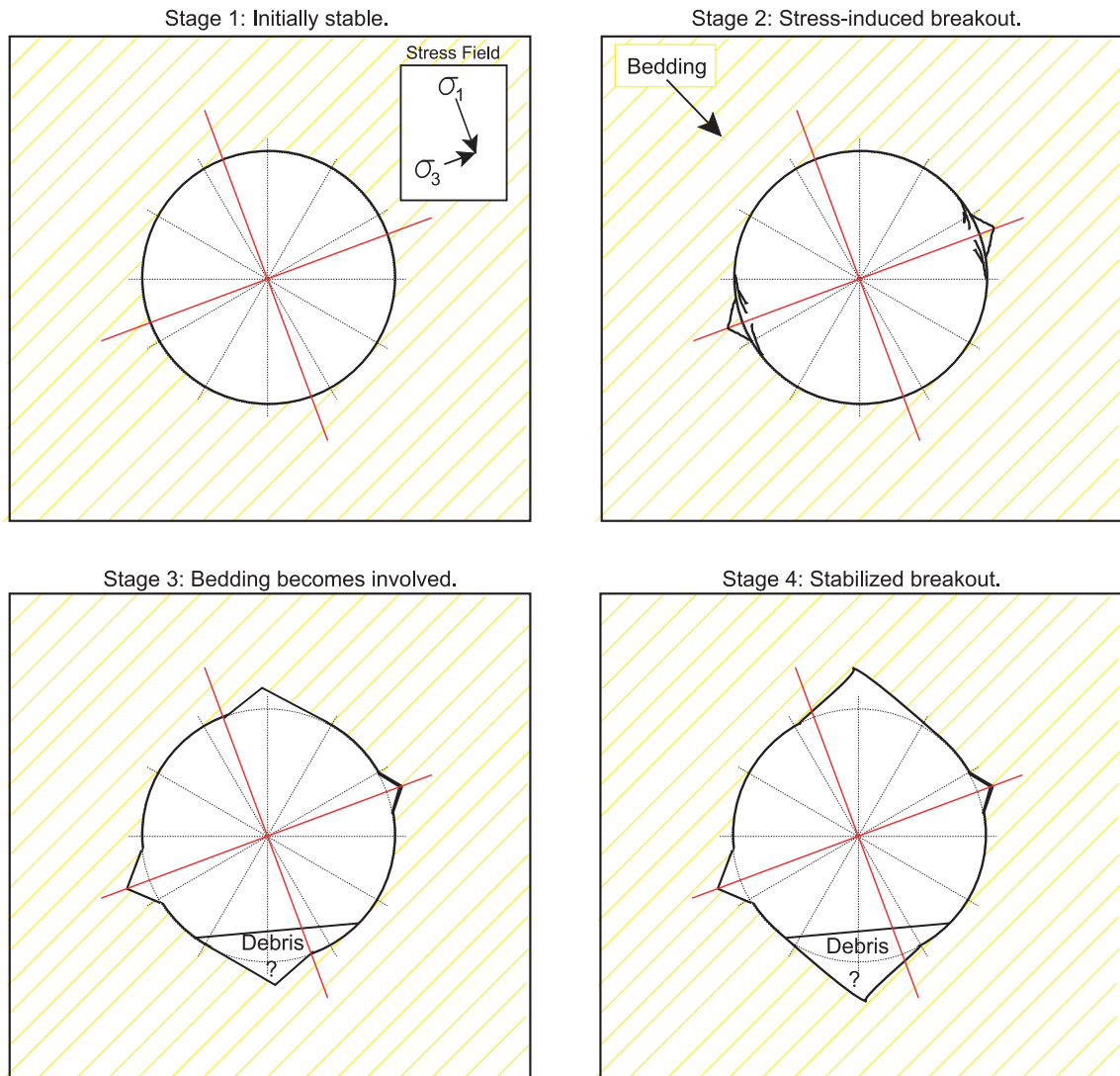


Figure C.5: Schematic of the evolution of borehole breakouts (looking southwest) based on field mapping of 110 and 250 mm diameter boreholes.

the borehole circumference, and which are related to the mechanical strength anisotropy of the Opalinus Clay. Statistically, they constituted about 75 % of the breakouts.

2. Stress-induced breakouts related to the stress anisotropy of the Opalinus Clay.
3. Breakouts influenced by steeply-inclined unloading fractures of the excavation disturbed zone (EDZ). They are restricted to the first metre in the gallery wall.

The current field program takes into consideration the breakout development with time. This was done by comparing boreholes by approximate relative age. Based on the borehole breakout data collected during the 2004 field programme, there are enough observations at various stages of breakout evolution to propose a typical breakout development. The typical breakout, for relatively undisturbed boreholes oriented perpendicularly to the main tunnel system, can be described as a four-stage process. The general sequence of borehole breakout development is shown in the schematic in Fig. C.5 and can be described as:

Stage 1: Post drilling there is very little if any breakout evidence for boreholes except when natural or EDZ fractures are encountered. However, large convergence has been measured at this stage (Peter Blümling, pers. comm.).

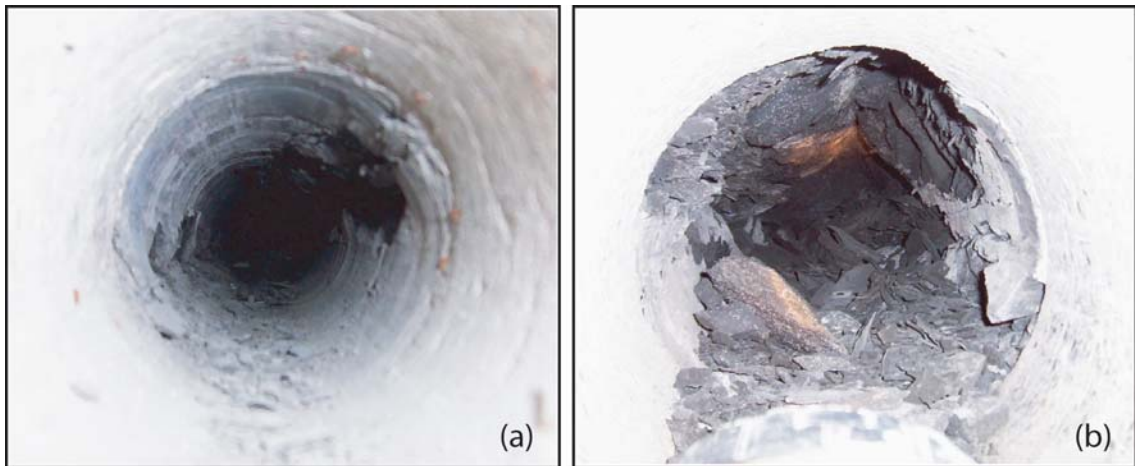


Figure C.6: (a) Initial stress-induced breakout looking southwest. (b) Long-term breakout looking southwest.

Stage 2: Soon after drilling, stress-induced breakouts can be observed in the zone of maximum deviatoric stress (in the direction of the minimum in-plane principal stress). This can be seen in the photograph in Fig. C.6(a).

Stage 3: Time-dependent processes, such as; pore pressure dissipation, strength degradation, creep, etc, start to have a significant effect on the breakout. The bedding planes become involved leading to the development of a breakout in the crown/invert which was not in alignment with the major principal stress direction.

Stage 4: Bedding plane degradation dominates the breakout which enlarges until long-term stabilization of the borehole occurs. Most likely the ultimate depth of the breakout is governed by geometrical conditions as opposed to stress/strength conditions. Fig. C.6(b) shows the long-term breakout geometry.

## **C.5 Summary and Conclusions**

Borehole breakouts can be used to indicate in-situ principal stresses and material response to excavation. A field programme of borehole mapping has been conducted at the Mont Terri rock laboratory in 2004 with the intent of gaining an understanding of the development of breakouts with time and to assess the factors affecting borehole breakouts in Opalinus Clay. This paper has presented the findings of the study and interpretation of the observations.

The complex stress field around boreholes and various other openings have contributed strongly to breakout development. Although stress field effects have not been quantified as part of this study, numerical modelling may be used to more thoroughly account for the actual stress field around individual boreholes and any changes to stress fields associated with additional excavations or experimental procedures at the Mont Terri rock laboratory.

The relative age of boreholes was used to quantify the time frame of the breakout process in this study. Further observations may be drawn from a more precise study that may include direct consideration of the drilling methods, borehole usage and more precise temporal observations as the breakout develops. In the opinion of the author, there are enough observations at various stages of breakout evolu-

tion to propose a typical breakout development. The typical breakout, for relatively undisturbed boreholes oriented perpendicularly to the main tunnel system, can be described as a time-dependent four-stage process. Initially stress-induced breakouts are prevalent, with time-dependent degradation of material properties and bedding plane behaviour dominating the long-term breakout pattern. The time-dependent behaviour can be attributed mainly to pore pressure dissipation and softening mechanisms associated with argillaceous materials.

Although observations from the borehole breakouts are consistent with the recommended stress tensor in terms of the maximum principal stress, it was inconclusive in terms of the more elusive intermediate and minimum principal stresses. There was no strong direct evidence to assist in further constraining the in-situ stress tensor from this study of borehole breakouts. Further mapping of boreholes in other orientations would be helpful to constrain the stress tensor. Alternatively, if the stress tensor were constrained further by other means (i.e. future in-situ measurements) the borehole data could be used with numerical modelling as a means of calibrating the time-dependent behaviour of Opalinus Clay.

## **Bibliography**

- [1] Corkum A G, Borehole breakout development at Mont Terri rock laboratory: 2004 field study. In: Canadian Young Geotechnical Engineers and Geoscientists Conference 2004 .
- [2] Bell J, Gough D, Intraplate stress orientations from Alberta oil wells. Evolution of the Earth, Geodynamics Series, Geophysics Union, Washington, DC 1980, 5:96–104.
- [3] Marschall P, Croisé J, Schlickenrieder L, Boisson J Y, Vogel P, Yamamoto S, Synthesis of hydrogeological investigations at the Mont Terri site (Phases I to V). In: Mont Terri Project - Hydrogeological Synthesis, Osmotic Flow. - Reports of the Federal Office for Water and Geology (FOWG), Geology Series No 6, Bern, Heitzmann P, editor 2002 .

- [4] Bock H, RA Experiment: Data report on rock mechanics - Mont Terri project. Tech. Rep. Nagra, Internal Report TN00-02, Q+S Consult, Germany 2000.
- [5] Thury M, Bossart P, Mont Terri rock laboratory: Results of the hydrogeological, geochemical and geotechnical experiments performed in 1996 and 1997. In: Geological Reports No. 23, Swiss National Hydrological and Geological Survey. Bern-Ittigen 1999 .
- [6] Martin C D, Lanyon G W, Excavation Disturbed Zone (EDZ) in clay shale: Mont Terri. Tech. Rep. TR2001-01, Nagra 2004.
- [7] Martin C D, Lanyon G W, Blümling P, Mayor J C, The excavation disturbed zone around a test tunnel in the Opalinus Clay. In: Proc. 5th North American Rock Mechanics Symposium and 17th Tunnelling Association of Canada Conference: NARMS/TAC 2002, Hammah R, Baden W, Curran J, Telesnicki M, editors, Toronto: University of Toronto Press 2002 pp. 1581–1588.
- [8] Bossard P, Wermeille S, Mont Terri Project - Geology, Paleohydrology and Stress Field of the Mont Terri Region. Report of the Federal Office for Water and Geology (FOWG), vol. 4 of Geology Series 2003 pp. 65–92.

# Appendix D

## Field Program: Mont Terri Report (May 2004)<sup>1</sup>

### D.1 Introduction

A field visit to the Mont Terri rock laboratory near St. Ursanne, Switzerland was made by the author in March-April 2004. The field visit was a component of the larger Ph.D. research project being conducted at the University of Alberta, Edmonton, Canada, under the supervision of Dr. C.D. Martin. Funding for the research project has been provided by Nagra, Switzerland under the direction of Dr. Peter Blümling, Nagra. The schedule of the research project and the field portion discussed in this report, are shown in Fig. D.1.

The main goal of participation in experiments at Mont Terri was to provide hands-on experience during tunnel projects in claystone (Opalinus Clay). As outlined by Dr. Blümling, four different projects were addressed:

1. Tunnel mapping of a newly excavated tunnel at Mont Terri in cooperation with geologists from the Geotechnical Institute (GI). The leader of the mapping team is Dr. Christophe Nussbaum, who defined the specific work for the team members and coordinated the work on-site. Emphasis was placed on the collection of data leading to an understanding of deformation mechanisms in the vicinity of a tunnel.
2. Mapping of existing shotcrete failure in the security tunnel. The failure pat-

---

<sup>1</sup>This chapter has been submitted for internal publication as a Technical Note to Nagra, Switzerland.



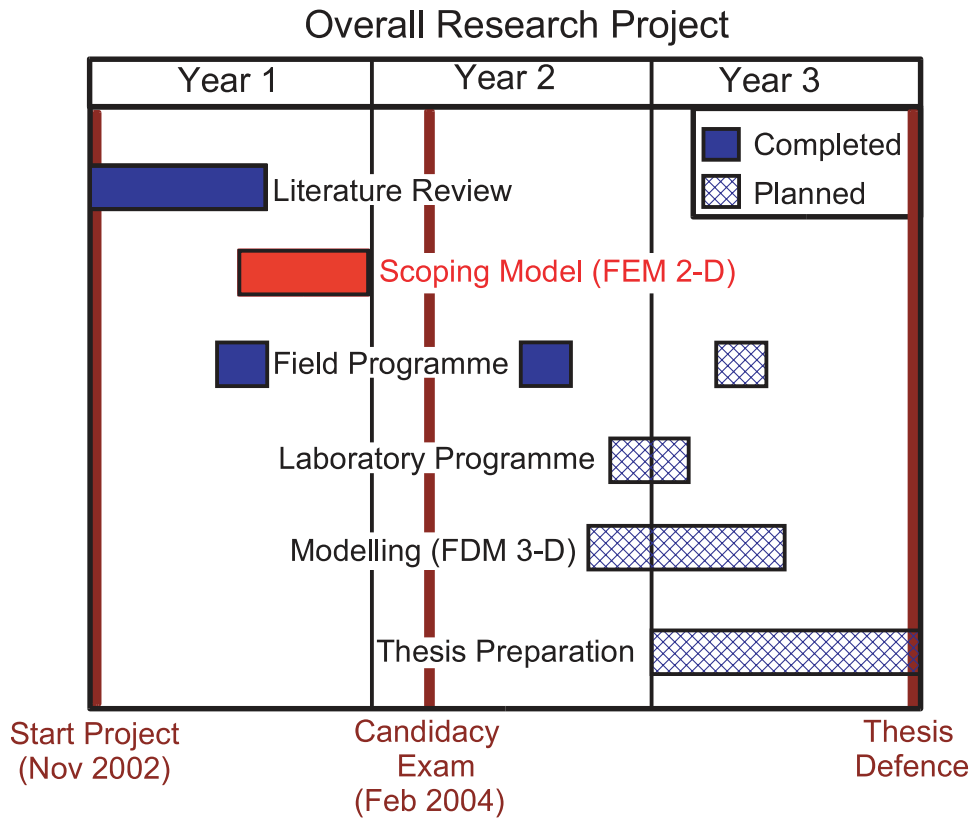


Figure D.1: Schedule of research project and events of 2004 field programme.

terns and possible failure mechanisms were evaluated. Possible reasons for failure were to be investigated such as stress concentrations near intersections or niches, water transport along boreholes, etc.

3. Investigation of borehole breakout behaviour of boreholes at Mont Terri. The following questions were addressed: How did the borehole cross-section develop? Up to what distance from the tunnel wall are breakouts observed? How do they relate to bedding plane orientations? Are they associated with induced fractures of the tunnel EDZ or to natural features (check core logging from GI)?
4. Semi-quantitative investigation of the weathering of Opalinus Clay dumped outside of the caverns. Can one observe differences of weathering with depth? Do originally open spaces between blocks indicate onset of closure? What could be the associated process.

At the conclusion of the site visit a three day series of meetings were arranged with a number of participants associated with different phases of the project. The objective was to promote discussion and provide input about tunnelling and rock mechanics at Mont Terri. Present for all or part of the discussions were:

- Dr. Peter Blümling, Nagra
- Dr. Peter Kaiser, Laurentian University
- Dr. Derek Martin, University of Alberta
- Dr. Paul Bossard, Geotechnical Institute
- Salina Yong, ETH
- Andrew Corkum, University of Alberta (author of this report)

These technical meetings concluded with a review of the author's site visit, for which this report is a formalized version, as well as a discussion of the overall research project.

## **D.2 Mont Terri Field Programme**

### **D.2.1 Mapping of Starter Niche**

A major expansion of the tunnel system at Mont Terri is underway to provide access for future experiments in the Opalinus Clay. At this time the Starter niche, a short 30 m section of this expansion, was undertaken. Excavation to the target length of 30 m was carried out in March 2004. The highest priority task of the site visit was to observe and contribute to mapping the excavation of the Starter niche in order to observe the response of Opalinus Clay to excavation first hand. The Mont Terri rock laboratory and the location of the Starter niche, as well as other pertinent features discussed in this report, are shown in Fig. D.2.

#### **Construction Sequence**

The Starter niche is located off the Security Gallery with a heading orientation towards the southwest, as shown in Fig. D.2. The heading was excavated full face,

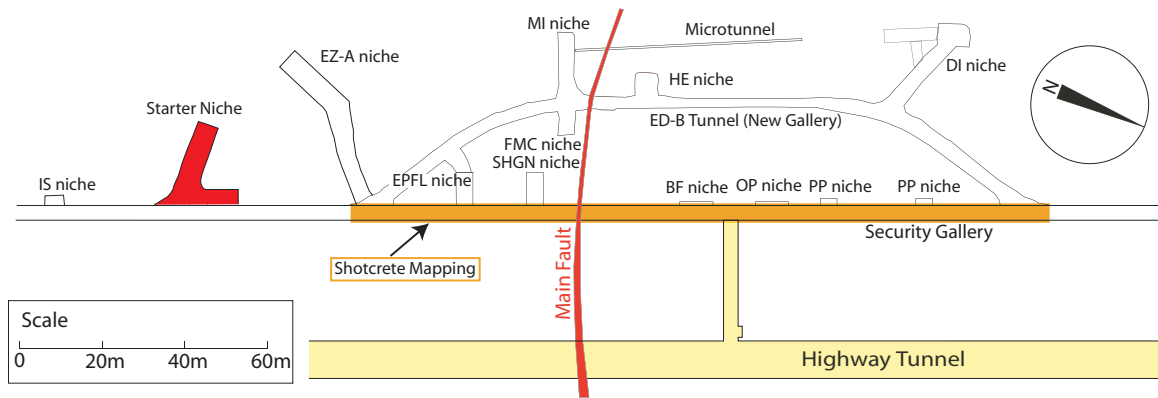


Figure D.2: Plan view of Mont Terri rock laboratory.

leaving a temporary invert that was cut through after the Starter niche reached its full excavation length of 30 m. The horseshoe shaped Starter niche, with 4.6 m height and 5 m width, was excavated with the road header shown in Fig. D.3(a).

Much of the equipment for the many ongoing experiments at Mont Terri is sensitive to dust; therefore, excavation was carried out slowly in order to minimize the dust accumulation in the tunnel. Instability in an adjacent excavation known as the EZ-A niche, which had a similar orientation as the Starter niche, was also cause for concern. These issues, plus the desire to perform careful mapping, provided further incentive to excavate slowly. The typical construction cycle consisted of excavating a length of 1.5 m over the course of 2 days. During this time, the 1.5 m excavation round was left unsupported. Mapping of the newly exposed face and walls was carried out prior to installing a thin (25-50 mm) layer of shotcrete along the roof and walls of the excavation. The shotcrete consisted of a synthetic fibre reinforced dry-mix. A convergence array was installed at the tunnel entrance at the beginning of the excavation. Measurements were taken once or twice per week.

During excavation there were signs of instability in the upper left corner (looking towards the tunnel face) of the tunnel that required bolting support. Two rows of resin bolts were installed at 1 m spacing along the excavation in this corner. Upon completion of the current phase of the expansion (Starter niche), a greater thickness of shotcrete consisting of about 150-200 mm was placed on the roof and walls. The floor was unsupported leaving an unclosed shotcrete support.



(a) A roadheader was used for mechanized excavation.



(b) Some structurally controlled instability in upper left corner, but none in the excavation face.

Figure D.3: Excavation of the Starter niche.



Figure D.4: Cracking and debonding of shotcrete in roof of Starter niche. Face of excavation is approximately 25 m beyond this location.

On March 17, 2004 cracking was observed on the right (north) wall of the Starter niche at the corner of the excavation opening. The crack was subvertical and extended about 2.5 m from the invert. This cracking coincided with increased deformation measured at the convergence pin located in the bottom right corner of the niche. On March 22, 2004 large cracks and shotcrete debonding were observed in the roof of the Starter niche also at the entrance to the niche. At this time the excavation face was about 25 m beyond this point. These fractures can be seen in Fig. D.4. The damage was repaired when the final 150-200 mm thick layer of shotcrete was applied to the entire excavation.

### **Mapping and Observations**

Mapping of the geological structure and excavation induced features was carried out under the supervision of Dr. Ch. Nussbaum of GI. Apart from the instability observed in the upper left corner of the excavation, few excavation induced features

were observed. There were no signs of significant face instability. The most notable finding from the geological mapping of the Starter niche was the frequency of geological discontinuities. In addition to the bedding planes that dip  $45^\circ$ , two sets of discontinuities were observed in the excavation. One set dipping approximately subparallel to bedding, tracing  $50^\circ$  in the excavation face, and another set that tends to cross-cut these dipping steeply at about  $70^\circ$  in the face. These discontinuities can be described as faults because striations and slickensided surfaces were observed on their surfaces, indicating past deformations nearly parallel to the dip direction as shown in Fig. D.5(a). These observations of historic deformations, along with occasional observations of fault-infilling, identify the discontinuities as geological in origin, as opposed to excavation induced. Fig. D.6 shows a schematic representation of the features observed in the excavation face. All mapping was documented and will be compiled and reported by GI separately from this report.

It appears that discontinuities play a significant role in the stability of excavations at Mont Terri. In particular when excavations have an unfavourable orientation such as the Starter niche and adjacent EZ-A niche where it has been suggested (Ch. Nussbaum, pers. comm.) that these discontinuities contributed to the instability and resulting collapse of the EZ-A excavation.

## **D.2.2 Mapping of Shotcrete Damage**

### **Security Gallery Mapping**

Mapping of shotcrete failure patterns in the Security Gallery was done to investigate mechanisms of failure that might add to a fuller understanding of tunnelling in Opalinus Clay. Originally excavated as part of the Highway tunnel project, the shotcrete in the Security Gallery has been subject to damage and repairs. The mapping was done along the Security Gallery between Stations RG 870 and RG 1020 (see Fig. E.1, Appendix E), corresponding approximately with the length of the New Gallery. The Security Gallery can be seen in Fig. D.7.

All zones of significant cracking and/or shotcrete debonding were carefully mapped taking note of any physical signs of the mechanism of damage. The shotcrete mapping overlaid by geological data provided by GI, can be seen in Figs. E.3



(a) Surface of a fault subparallel to bedding observed in the right sidewall. Note the striations indicating movement along the dip direction.



(b) Anchored support was required for upper left corner of excavation.

Figure D.5: Structurally controlled instability in the Starter niche.

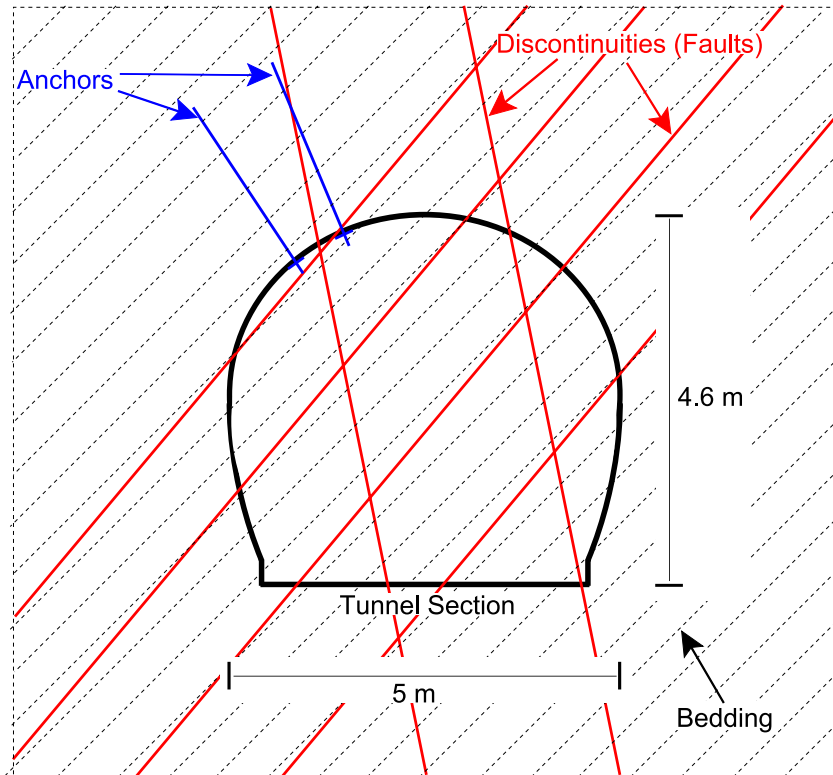


Figure D.6: Schematic diagram of typical excavation face of the Starter niche. Bedding planes and discontinuities intersect in the face of the excavation resulting in instability in the upper left corner.

through E.8 in Appendix E. This geological data was collected from mapping during original tunnel driving and supplemented by borehole data. It can be seen in Figs. E.3 through E.8 that in most cases shotcrete damage occurs in zones where significant geological features are mapped.

Damage consisted mainly of long open cracks, up to 12 m long with openings from millimetres to centimetres in width. There were locations where shotcrete had become debonded and “drummy”, with either the surface layer or the entire shotcrete layer becoming debonded from the surface. In places the debonded materials were completely broken away leaving wire mesh or bare rock. Based on the mapping carried out, it appears that approximately 25 % of the east wall and 40 % of the west wall of the Security Gallery was suffering from noticeable to significant shotcrete cracking and/or damage. There appears to be two main reasons





Figure D.7: Looking towards the northwest along the Security Gallery.

for shotcrete damage; the presence of geological structures, and stress concentrations associated with niche corners or other tunnels. Severe damage is most often related to geological features (OP niche). There was almost always significant shotcrete damage in zones where mapping showed major and/or numerous discontinuities. Additional, but less severe cracking was observed at most of the corner locations along the Security Gallery, where stress concentration or stress relaxation are heightened. Damage is particularly noticeable when both conditions are present.

There were a number of locations where shotcrete had been repaired. There are also locations where shotcrete was placed as a result of a new excavation. The extent of damage that was present prior to the repair work is unknown. It is difficult to draw too many conclusions regarding damage mechanisms without a significant understanding of the development with time of the cracking in relation to excavation activities and the impact of experiments, particularly those involving the use of

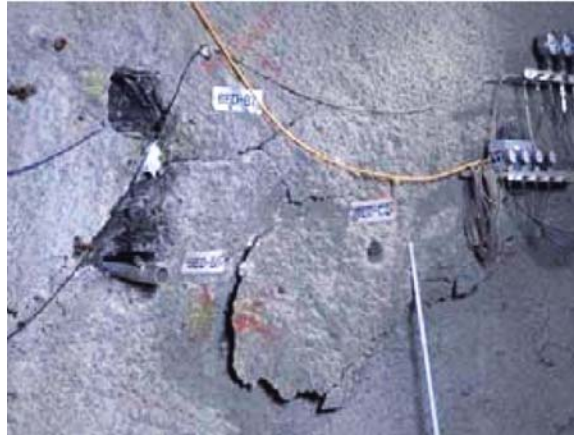
water.

### **OP Niche**

Located on the west wall of the Security Gallery, in approximate alignment with the ED-B section of the New Gallery, the OP niche is a particularly severely damaged shotcrete section at Mont Terri. The mechanisms responsible for this damage has not yet been identified. Numerous instruments were installed in the OP niche as part of the ED-B mine-by test. During installation of the instruments, it is believed (Peter Blümling, pers. comm.) that some amount of water was released into the network of EDZ fractures in the formation. A short time after this, (also corresponding to the excavation of the ED-B tunnel) significant deformations of up to 0.5 m were observed in the OP niche as shown in Fig. D.8(a). This was accompanied by extensive damage to the shotcrete. Inclinometers and extensometer measurements are based on the assumption of zero displacement at the collar, meaning that collar movement was a notable instrumentation issue as well as tunnelling observation. This instrumentation data clearly shows that large deformations were recorded here as the ED-B excavation advanced.

These large deformations were investigated by cutting out the shotcrete for careful observation and mapping as shown in Fig. D.8(b). Sampling from resin impregnated boreholes and removal of a large block sample were also carried out. Moisture contents measured from samples were only slightly higher than the *in-situ* values (Peter Blümling pers. comm.). This indicates that swelling alone was most likely not responsible for such large deformations.

Mapping of the OP niche and the corresponding area on the opposite side of the Security Gallery point out that this is an area of significant geological disturbance. Faulting and discontinuities are pervasive and the rockmass appears highly folded and disturbed compared to other zones of Opalinus Clay, excluding the Main fault zone. Therefore, this area was inherently less competent than most of the Security Gallery. In addition, a shallow dipping discontinuity tracing sub-horizontally was observed at the base of the zone of damaged shotcrete that was identified essentially as a sliding plane.



(a) Large displacements lead to major shotcrete cracking in OP niche.



(b) Shotcrete was cut out in OP niche for investigation. A large block sample was removed from centre area of picture.

Figure D.8: Shotcrete damage in OP niche. Up to 0.5 m of outward displacement.

The neighbouring BF and PP niche's have not experienced shotcrete damage to the same extent as the OP niche, indicating that the phenomenon is somewhat isolated. Whether it is the inherently less competent rockmass, degradation of the rockmass properties due to ingress of water, or formation water travelling along the borehole, is not apparent. However, based on the instrumentation, it appears that the trigger mechanism for this displacement was indeed excavation of the ED-B tunnel. This hypothesis is further demonstrated by finite element analysis carried

out by the author which has shown the potential for excavation of the ED-B tunnel to induce deformations of this magnitude in the OP niche.

### **D.2.3 Mapping of Borehole Breakouts**

#### **Methodology**

A systematic programme of borehole mapping was carried out during the site visit. The intent was to gain an understanding of the development of breakouts with time and to assess the factors affecting borehole breakouts in Opalinus Clay. Mapping of boreholes along the Security Gallery was done followed by mapping of most of the accessible boreholes in the New Gallery section. A total of 48 boreholes were mapped and these boreholes are listed in Table D.1. Differing drilling methods, instrumentation, environmental conditions (moisture) and experimental usage has had a large impact on the individual borehole behavior. The original usage of the mapped boreholes was not always known and it was difficult to give full consideration to these issues. However, every attempt was made to give weighted consideration to boreholes that appeared to be air drilled and showed few signs of the breakout being strongly affected by drilling methods or experimental procedures.

Borehole diameters at Mont Terri ranged from about 25 mm to greater than 300 mm, but mapping was done with most of the boreholes having a diameter of 110 or 250 mm. The vast majority of boreholes were oriented sub-horizontally in the direction perpendicular to the Security Gallery. Based on the stress tensor recommended by Martin and Lanyon [1], this is in the  $\sigma_1$ - $\sigma_2$  plane. This alignment corresponds to drilling parallel to bedding which dips approximately 45° towards the southwest.

#### **Findings and Interpretation**

According to Martin and Lanyon [2], breakouts are only observed when stresses around the borehole are elevated by the influence of three-dimensional geometry, such as an existing tunnel. This indicates that *in-situ* stresses at Mont Terri are not high enough to exceed the peak yield strength of the rock. These observations hold true for the current study. The most significant breakouts occur close to the collar

Table D.1: Boreholes mapped during field programme.

Borehole	Diameter (mm)	Borehole	Diameter (mm)	Borehole	Diameter (mm)
BCP-2	110	BED-B26	110	BFM-B2	250
BCP-3	110	BED-B31	110	BFM-B7	110
BCP-5	110	BED-C4	110	BFM-B6	110
BDT-1	150	BED-C5	110	BFM-B8	110
BDT-2	95	BED-C8	110	BFP-1	250
BDB-1	110	BED-C9	110	BFP-3	250
BDB-2	110	BED-C10	110	BFP-5	250
BED-B4	110	BED-C12	110	BFP-6	250
BED-B13	110	BEZ-A28	110	BFP-17	250
BED-B14	110	BFD-4	250	BHE-B3	110
BED-B15	110	BFD-7	250	BIS-D8	110
BED-B17	110	BFD-9	250	BLT-5	110
BED-B18	110	BFD-11	250	BLT-6	110
BED-B20	110	BFD-13	250	BLT-7	110
BED-B22	110	BFD-15	250	BLT-9	110
BED-B25	250	BFD-17	250	BPC-B3	110

of the borehole, usually within the first 1 m and decreases in severity with depth. This is where the influence of the associated tunnel is highest.

As mentioned above, the vast majority of borehole orientations are sub-horizontal, drilled perpendicular to the direction of the main tunnel system. Very few boreholes were oriented in the direction parallel to the tunnel and the few that were, were in locations that would be significantly influenced by stresses induced by tunnel geometry. Therefore, there was no direct evidence to assist in further constraining the *in-situ* stress tensor from borehole breakouts. However, it may be possible to use the data compiled here along with modelling and other observations to do so. The few vertical boreholes appear to be very stable, but occasionally they appear to be affected by swelling and squeezing mechanisms.

Based on the borehole breakout data collected during this field programme, there are enough observations at various stages of breakout development to propose a typical breakout development. The typical breakout, for relatively undisturbed boreholes oriented perpendicularly to the main tunnel system, can be described as a four-stage process. The general sequence of borehole breakout development is shown in the schematic in Fig. D.9 and can be described as:

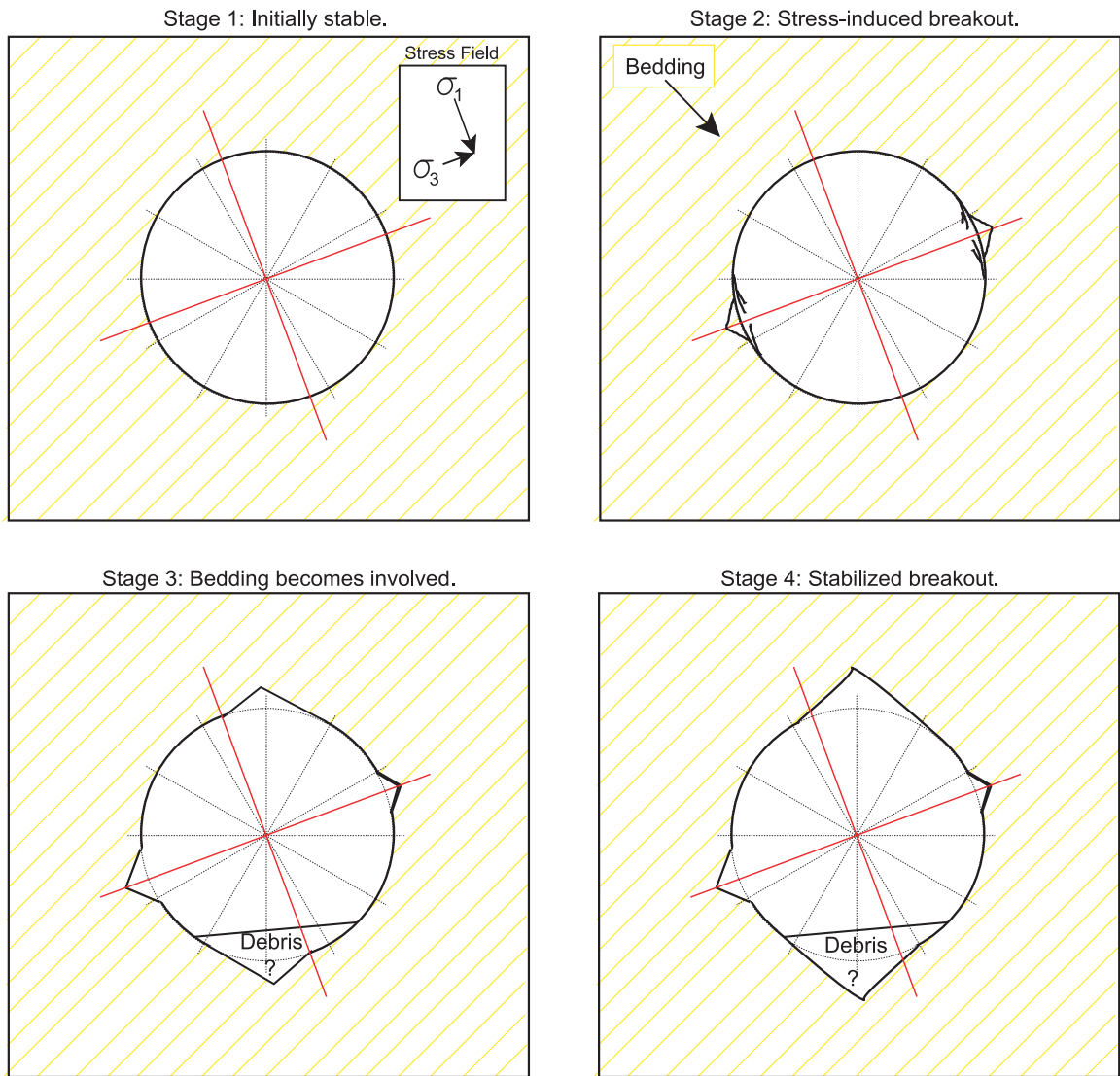


Figure D.9: Schematic of the development of borehole breakouts from mapping and field observations.



(a) Initially stable borehole.



(b) Developed stress induced breakout in the direction of  $\sigma_3$



(c) Long-term development associated with strength degradation of bedding.



(d) Unique shape of long-term breakout for a borehole parallel to tunnel axis.

Figure D.10: Photographs illustrating borehole breakout development.

- **Stage 1:** Post drilling there is very little if any breakout evidence for boreholes (see Fig. D.10(b)), although large convergence has been measured at this stage (Peter Blümling, pers. comm.).
- **Stage 2:** Soon after drilling, stress-induced breakouts can be observed in the zone of maximum deviatoric stress (in the direction of the minimum in-plane principal stress). This can be seen in the photograph in Fig. D.10(b).
- **Stage 3:** Time-dependent processes, such as; pore pressure dissipation, strength degradation, creep, etc, start to have a significant effect on the breakout. This results in the bedding planes becoming involved resulting in the development of a breakout in the crown/invert. Notably, *not* in alignment with the major principal stress direction.
- **Stage 4:** Bedding plane degradation dominates the breakout which enlarges until long-term stabilization of the borehole occurs. Most likely the ultimate depth of the breakout is governed by geometrical conditions as opposed to stress/strength conditions. Fig. D.10(c) shows the long-term breakout geometry.

There does seem to be a scale effect. The 250 mm diameter boreholes display more significant breakouts than the smaller boreholes, particularly in the advanced stages where strength degradation and bedding planes dominate the breakout development. There were a number of boreholes where complete collapse had occurred, but it is believed that these were cases where the borehole was strongly affected by the experimental use of the borehole. There were few observations of geological or tunnelling induced fractures having a strong influence on the breakout.

One of the few boreholes aligned parallel to the major tunnel system is shown in Fig. D.10(d). Long-term degradation of the borehole walls and collapse along bedding have resulted in a large breakout without the development of a breakout notch geometry. Many boreholes were covered leading to increased humidity and moisture over time. In a few of these covered boreholes, condensation was observed in the borehole or borehole cover. Frequent observations of gypsum deposits on the



surface within the borehole and on breakout debris in covered boreholes indicates the presence of air; meaning that the boreholes were connected to the tunnel via a network of EDZ fractures.

#### **D.2.4 Observations from Waste Pile and Core Disking**

A semi-quantitative study of the weathering response of Opalinus Clay was carried out in the waste pile. Located outside of the caverns, waste rock was dumped here in an uncontrolled manner where it accumulated in a steep pile governed by the angle of repose of the material, which is approximately 25°.

Although the material appeared to remain more intact with depth, upon further investigation, this was really just a superficial observation. Minor disturbance revealed complete weathering of almost all material in the waste pile. Interestingly, it was observed that the material tends to maintain some kind of structural integrity as it degenerates (see Fig. D.11(a)). Possibly reflecting micro-scale structural characteristics. Flat, tabular particles are prevalent and with advancing stages of disintegration these particles simply become smaller while maintaining very similar geometrical shapes (see Fig. D.11(b)). Large blocks remain relatively intact structurally, but upon minor disturbance reveal complete degradation, in particular along bedding where there is essentially no tensile resistance remaining. It has been observed that the material tends to develop fissures that “suck in” water along some bedding planes. When split, free water can be observed along these bedding planes.

Although this study was helpful in providing insight into the slaking mechanisms and the structure of Opalinus Clay, no real conclusions can be made in regard to self-sealing. The degree of degradation is so severe and pervasive that the material in the waste pile cannot be compared in a meaningful way to any anticipated natural process occurring in the tunnel system.

A simple experiment was carried out to observe the advancement of weathering. A small block of Opalinus Clay (shown in Fig. D.12) that was previously sheltered was placed outside. Within days it had softened to nearly the strength of soil. After about two weeks of exposure to sun and significant precipitation, it was completely destroyed. After two weeks the material could be easily remoulded by hand into a



(a) Disintegration of a block of Opalinus Clay.



(b) Typical remains due to weathering. Only a short time required to achieve this level of degradation.

Figure D.11: Disintegration of Opalinus Clay exposed to weathering in outdoor waste pile.



Figure D.12: Degeneration of block sample. A block of material was placed outside and carefully observed over a two week period. Maintained structure to some degree, but nearly *total* loss of strength.

ball, having little resemblance to a rock. However, it still maintained its structure. Also note in Fig. D.12 the incompatibility of swelling strain along the different beds. This behavior may influence the loss of strength along bedding even with the relatively small environmental effects, such as those observed within the tunnel.

While at Mont Terri the author was able to observe the execution of an overcoring experiment. A 25 mm inner diameter and 150 mm overcore was observed. The measuring device was a CSIRO cell with 3 strain rosetts. This probe was very compliant (to match the formation) and was glued onto the side of the inner borehole wall. A trial hole was overcored *without* the presence of a strain cell. As shown in Fig. D.13, the retrieved core experienced severe diskings on the centimetre scale. Core samples do not generally have a diskings problem at Mont Terri (Peter Blümling pers. comm.). Further overcoring *with* the cell glued in place resulted in

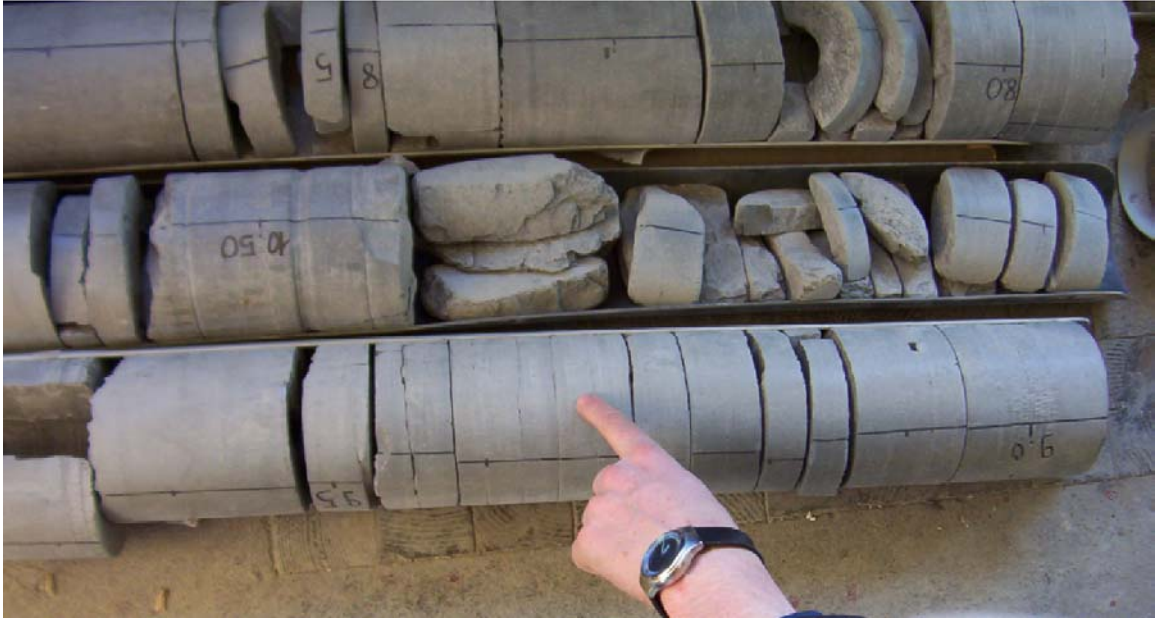


Figure D.13: Core disking observed during overcoring experiment. Note the small inner hole along core axis for insertion of strain cell.

cores that were again disked *except* in the zone where the strain cell was present. This crudely demonstrates that a very small reaction force may be sufficient to maintain a stable hole in Opalinus Clay.

### D.3 Pending Research Tasks

The completion of this field study comes at approximately halfway through the three year Ph.D. research programme. The proposed upcoming tasks required to complete the research over the next 18 months, as shown on Fig. D.1, consist of:

- Compilation and interpretation of the field data reported here.
- Acquisition, synthesis and interpretation of data from other sources that relate directly to this research project. Specifically:
  - Geometrical and geological data from borehole information system.
  - Core sample and borehole convergence measurements related to sampling disturbance.
  - Triaxial and uniaxial strength degradation data.

- Laboratory programme to investigate and quantify the response of Opalinus Clay to damage induced release of strain energy. This will be done using stress-path controlled, high capacity triaxial testing.
- Three-dimensional modelling of the Mont Terri rock laboratory, in particular the ED-B tunnel using FLAC-3D.
- Preparation of thesis.

## **D.4 Summary**

This report has presented the findings of a field study carried out by the author as a component of the larger Ph.D. research project on the behavior of Opalinus Clay around deep tunnels. It has provided valuable hands-on experience with tunnelling in Opalinus Clay and an increased appreciation for the response of Opalinus Clay to excavation and time dependent behavior. Data has been collected from the Starter niche excavation, mapping of shotcrete damage in the Security Gallery, borehole breakout development and the severe material degradation observed in the waste pile. Finally, the field visit has allowed the author to make contacts with personnel directly involved in experiments and day to day operation of the Mont Terri rock laboratory.

Mapping of the Starter niche revealed the presence of geological discontinuities and the significance of structurally controlled stability around excavations at Mont Terri. This was also demonstrated by the instability and ultimate collapse of the EZ-A niche. The single most important observation from this field study was the pervasiveness and implications of geological discontinuities at Mont Terri.

Mapping of shotcrete damage in the Security Gallery showed a strong connection between the presence of discontinuities and liner performance. The accumulation of shotcrete damage located in the vicinity of corners and intersections, and the increased severity of borehole breakouts near the collar where the effects of tunnel induced stresses are most significant, demonstrated the strong three-dimensionality of the Mont Terri rock laboratory.

The damage observed at the OP niche, whether a direct or indirect effect of excavation of the ED-B tunnel, demonstrates that a system-wide response to excavation is a significant factor in damage to the rockmass and shotcrete support at Mont Terri.

The study of borehole breakouts allowed for deduction of a typical breakout development as a four-stage process. Initially starting with minor stress induced breakout in the zone of maximum deviatoric stress, to a final mature breakout that is dominated by degradation of material properties and bedding plane strength and orientation.

Observations from the waste pile illuminated the strong slaking response of the Opalinus Clay and provided some insight into the structural integrity of the material. The time-dependent material properties of Opalinus Clay have played some role in all of these studies and has emphasized the need to appreciate this aspect of behavior for excavation performance.

## **Bibliography**

- [1] Martin C D, Lanyon G W, Measurement of in-situ stress in weak rocks at Mont Terri rock laboratory, Switzerland. *Int J Rock Mech Min Sci* 2003, 40:1077–1088.
- [2] Martin C D, Lanyon G W, Excavation Disturbed Zone (EDZ) in clay shale: Mont Terri. Tech. Rep. TR2001-01, Nagra 2004.

## **Appendix E**

### **Field Program: Shotcrete Crack Mapping**

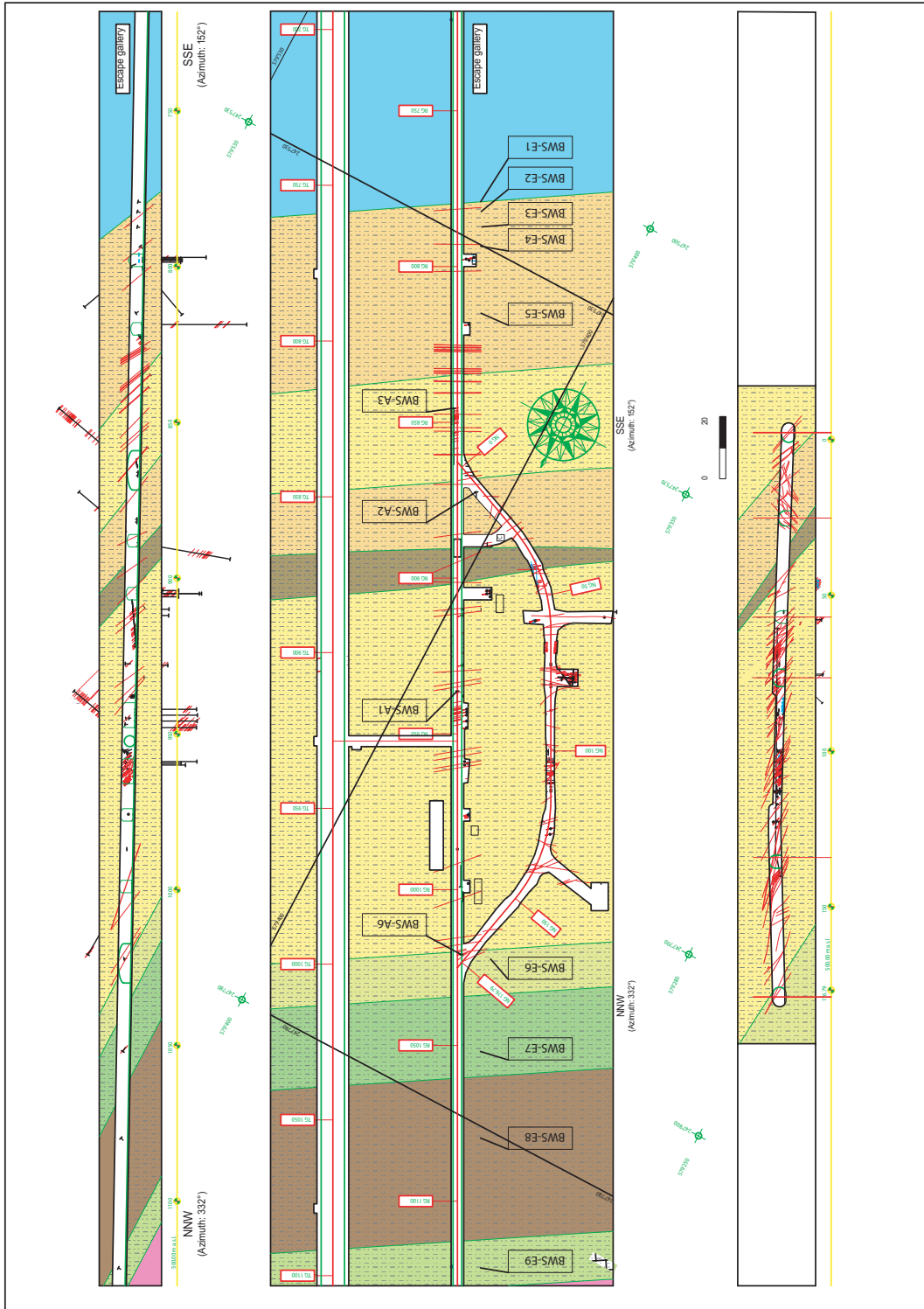


Figure E.1: Geological plan of Mont Terri rock laboratory. (Provided by Ch. Nussbaum.)



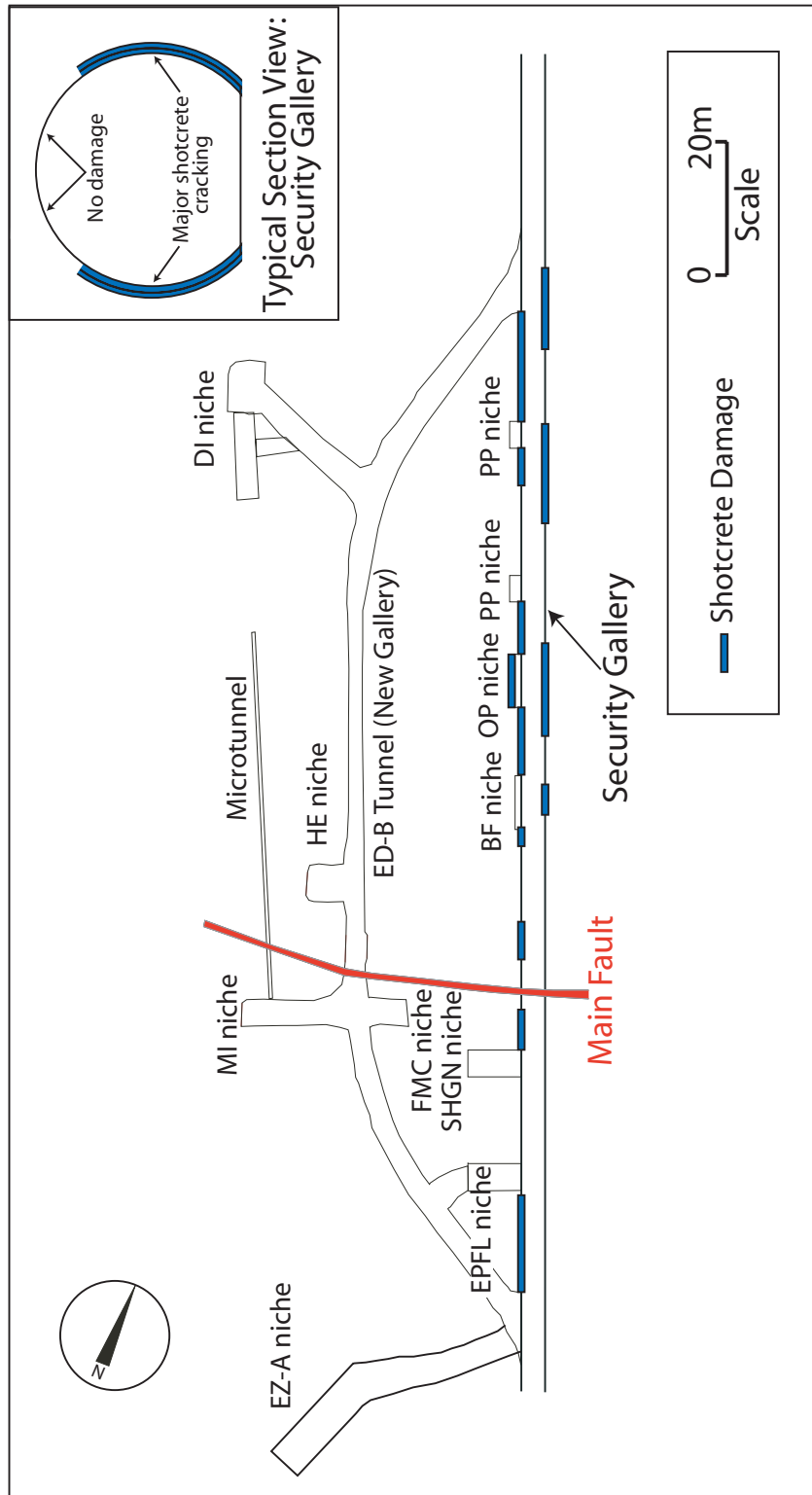


Figure E.2: Plan view of Mont Terri rock laboratory showing the distribution of cracking along Security Gallery and typical section.

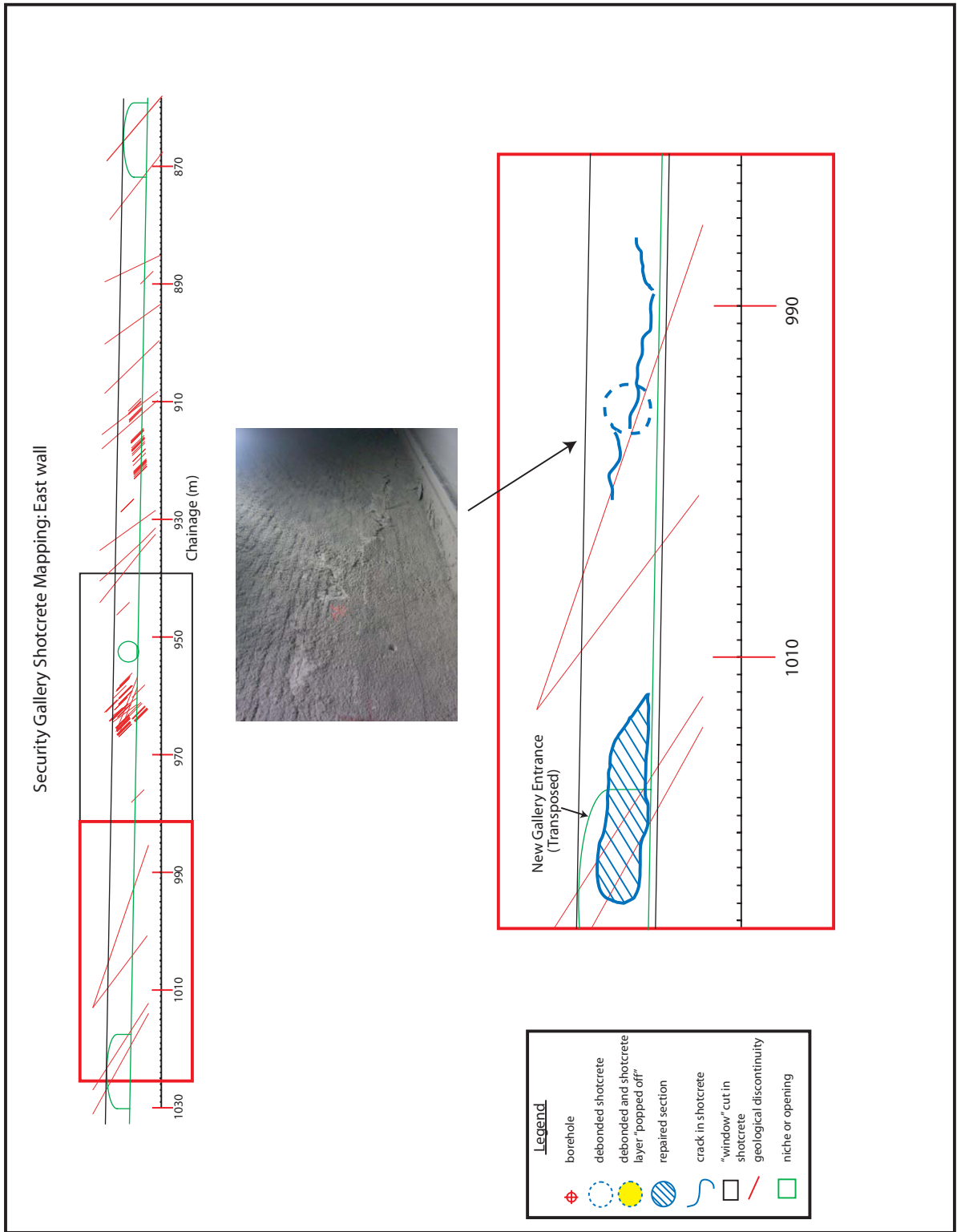


Figure E.3: Shotcrete mapping with geological structure overlay. East wall of Security Gallery, first mapping section.

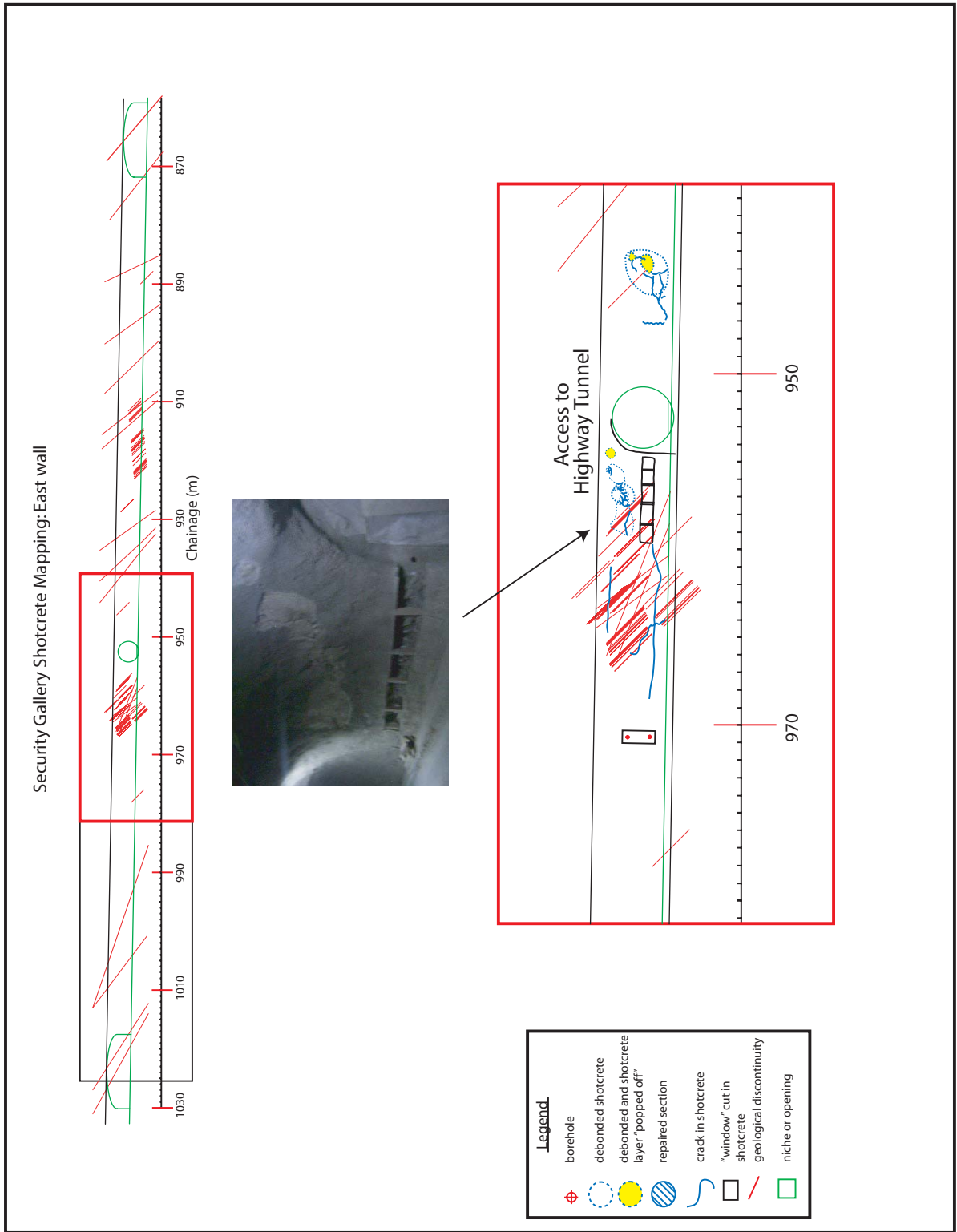


Figure E.4: Shotcrete mapping with geological structure overlay. East wall of Security Gallery, second mapping section.

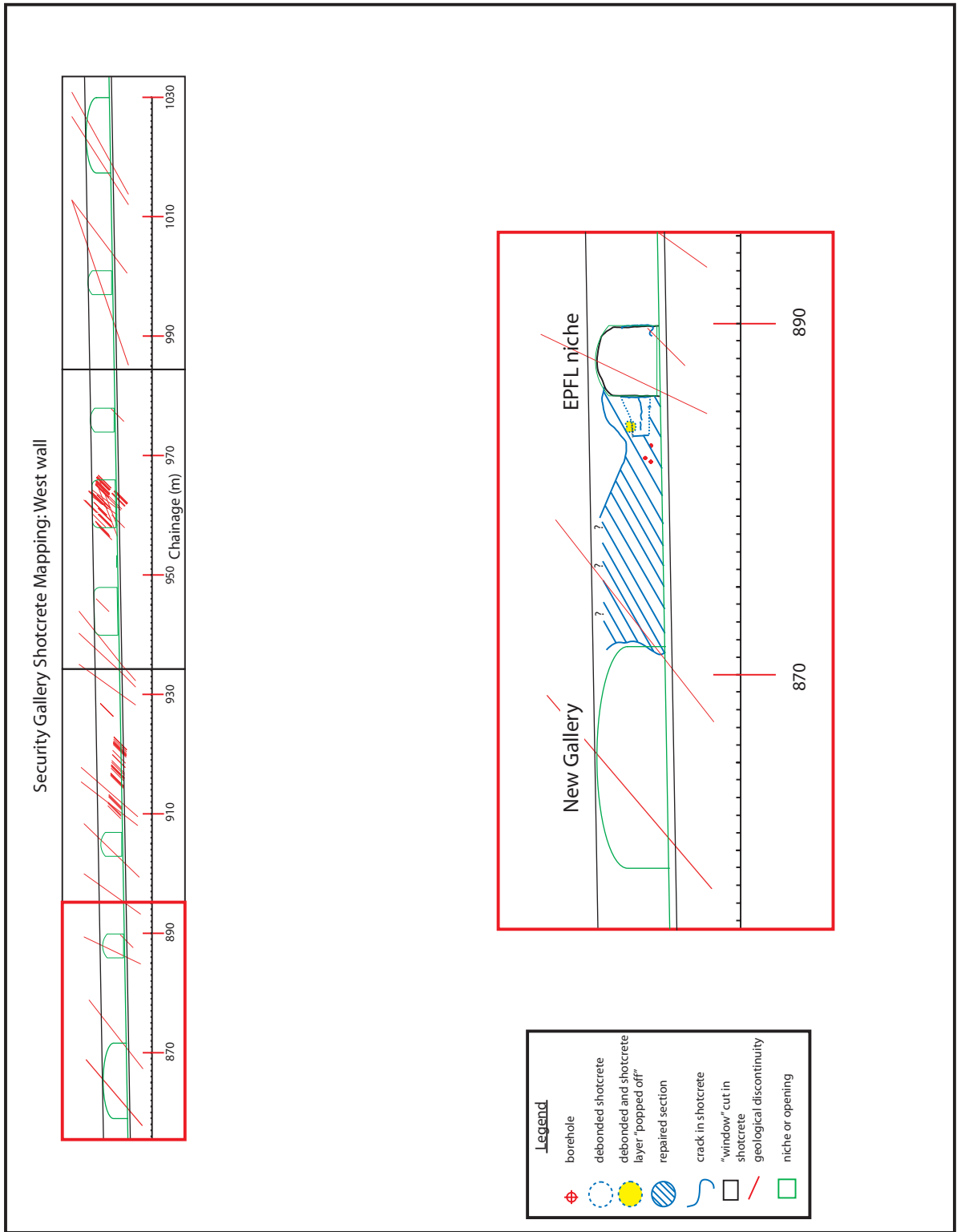


Figure E.5: Shotcrete mapping with geological structure overlay. West wall of Security Gallery, first mapping section.

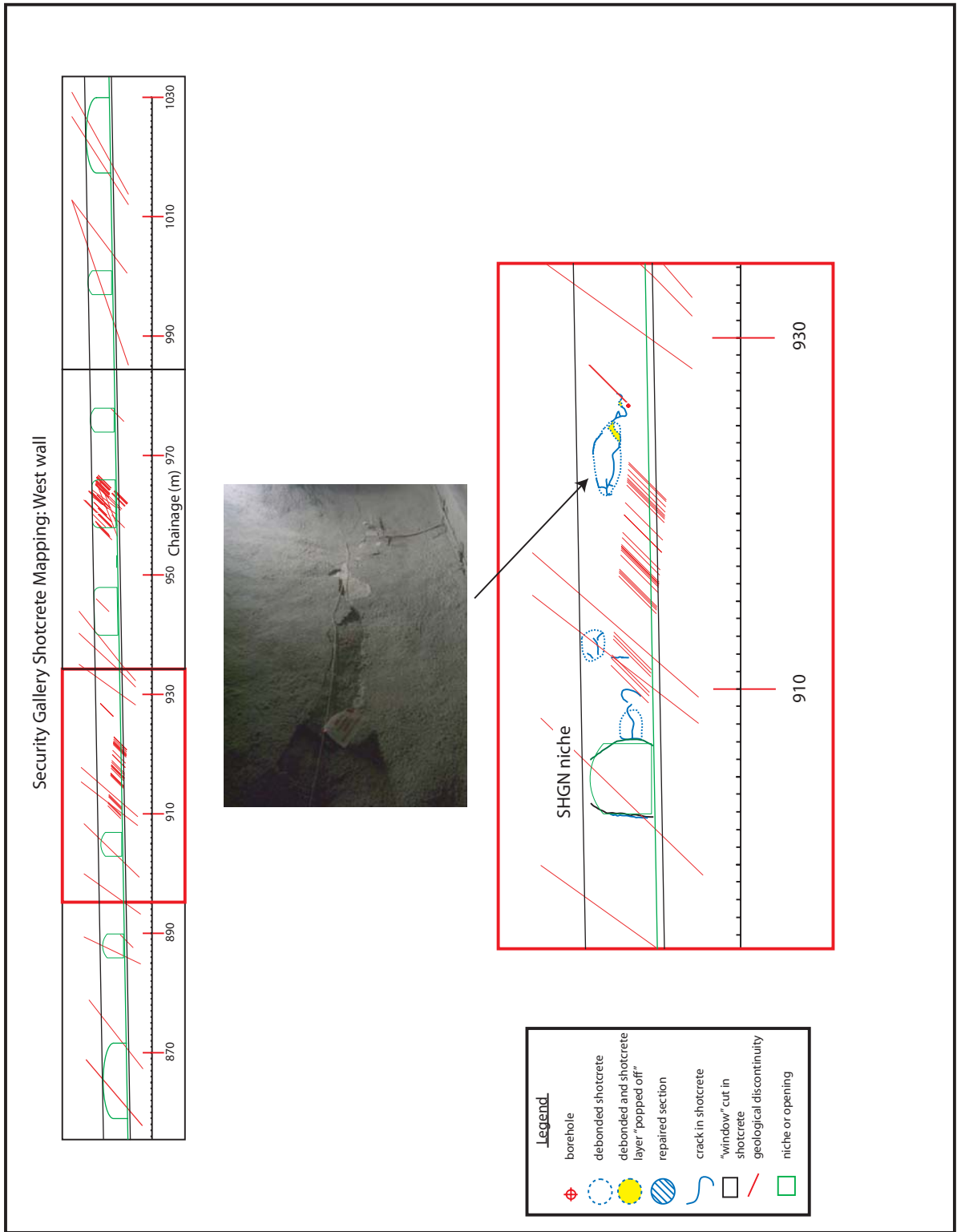


Figure E.6: Shotcrete mapping with geological structure overlay. West wall of Security Gallery, second mapping section.

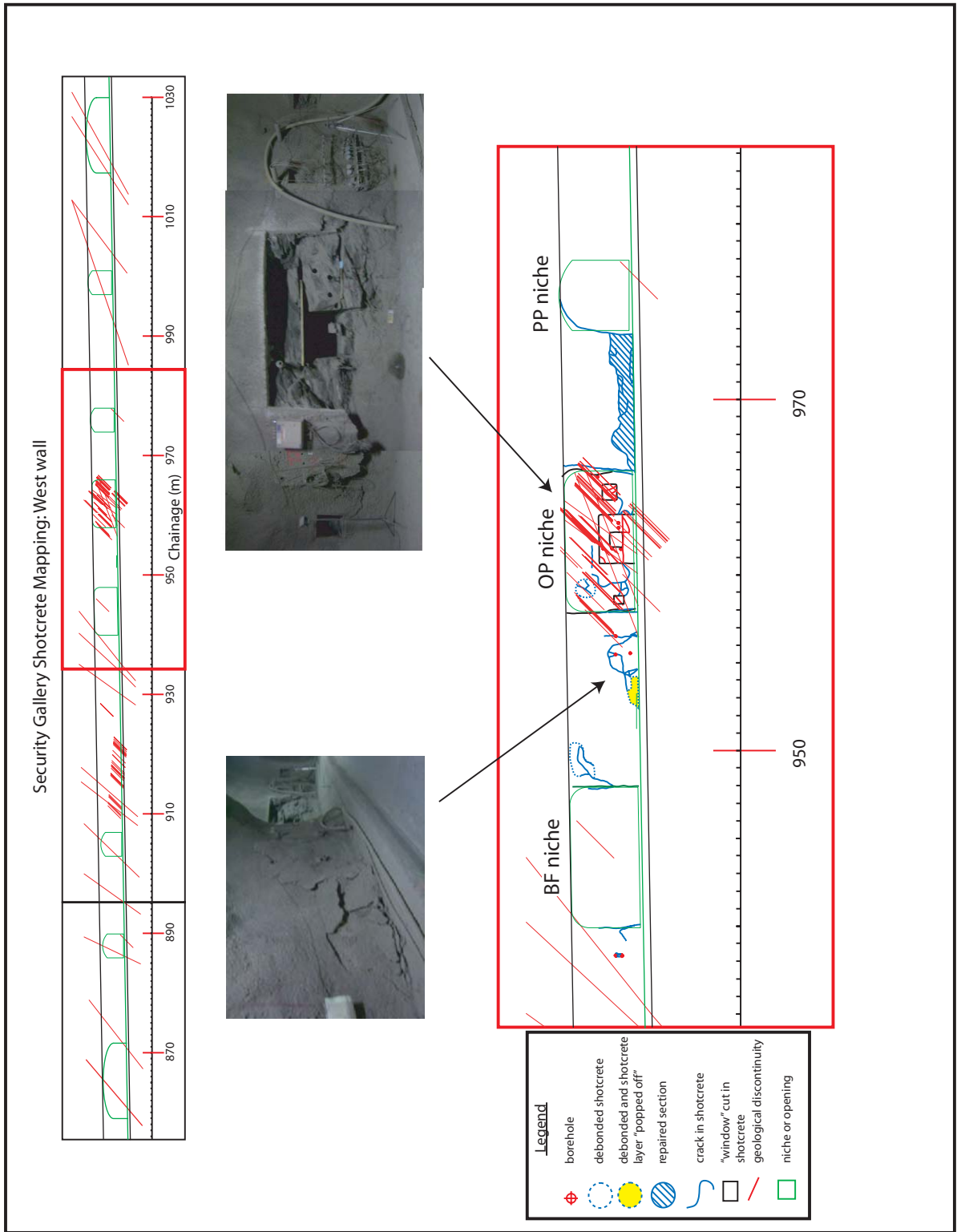


Figure E.7: Shotcrete mapping with geological structure overlay. West wall of Security Gallery, third mapping section.

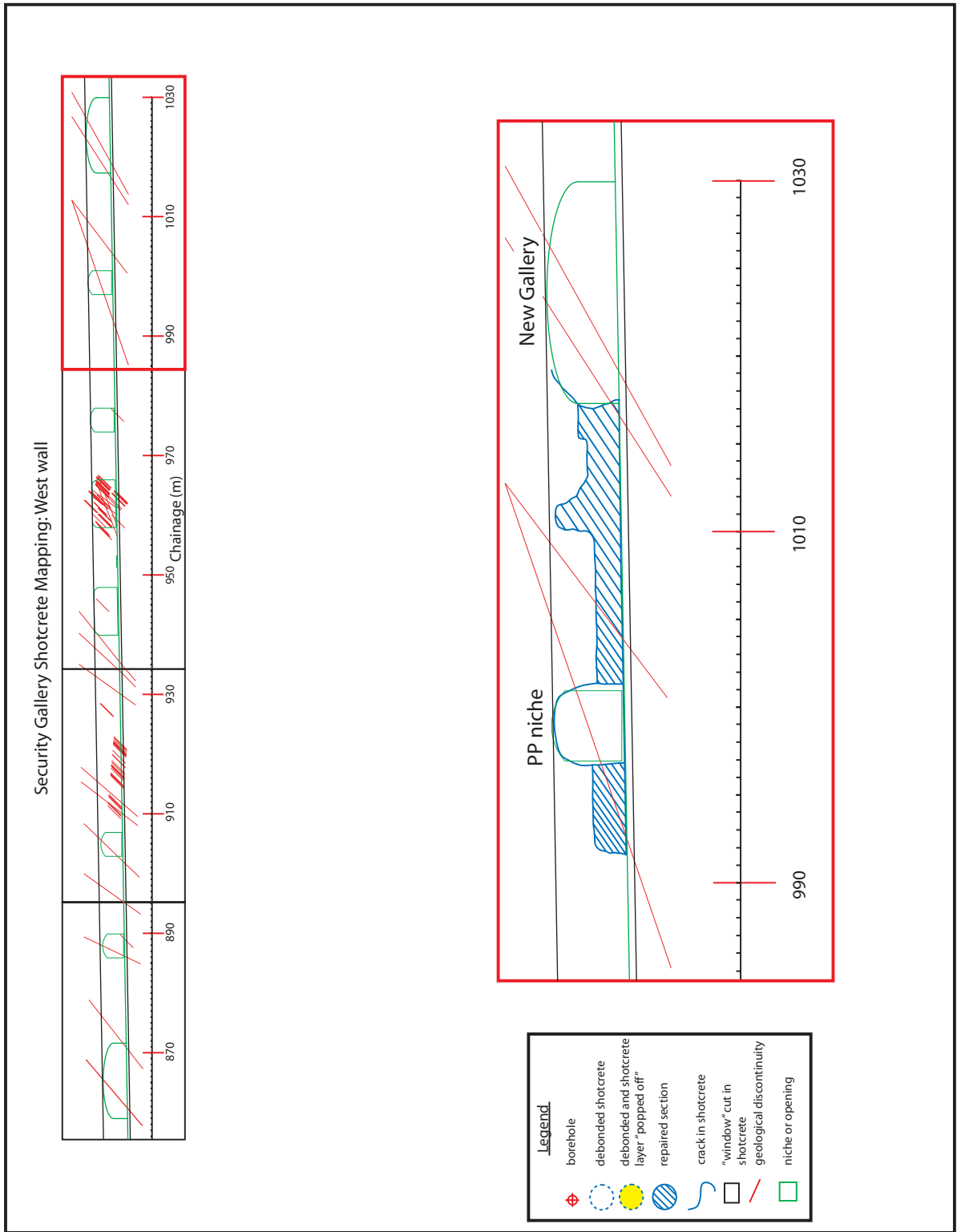


Figure E.8: Shotcrete mapping with geological structure overlay. West wall of Security Gallery, fourth mapping section.

## **Appendix F**

### **Field Program: Borehole Breakout Field Sketches**



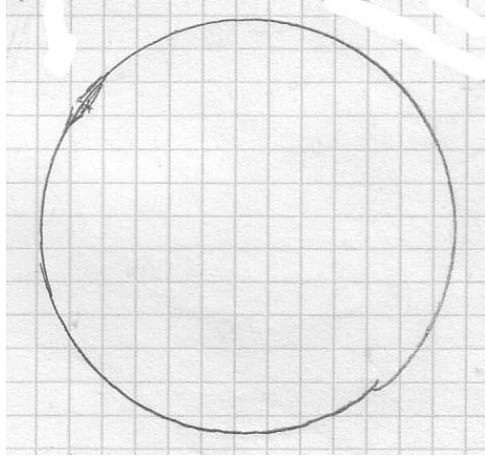


Figure F.1: Borehole: BCP-3, Diameter:110 mm

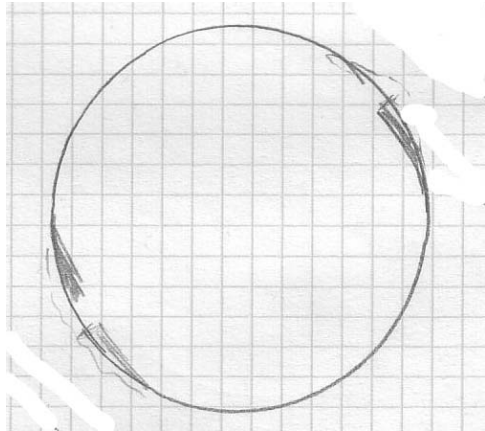


Figure F.2: Borehole: BCP-5, Diameter:110 mm

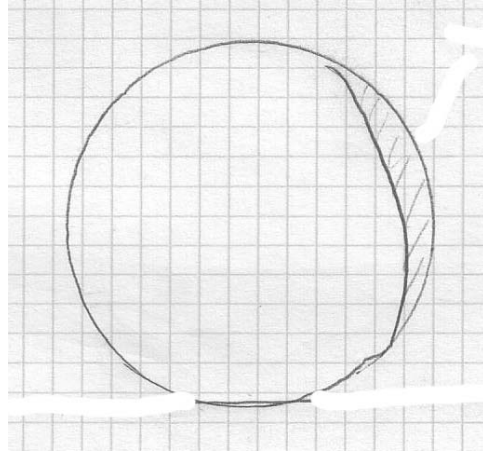
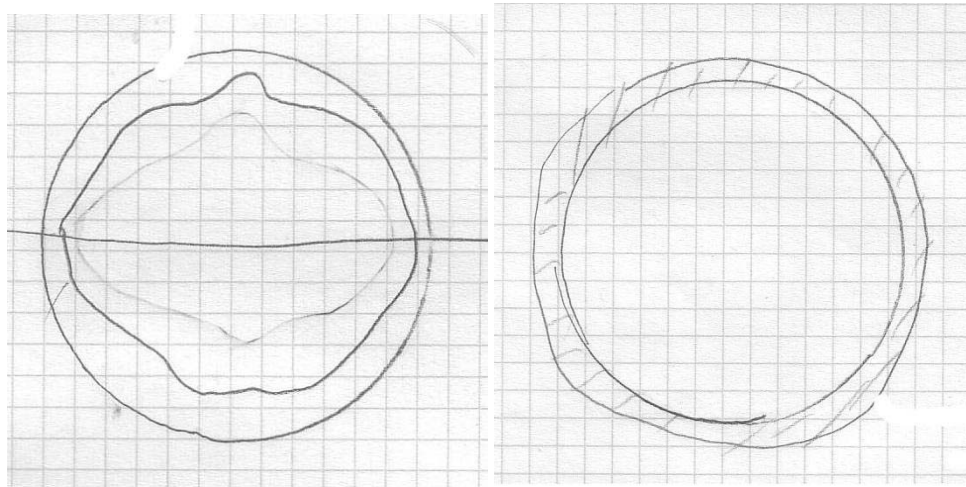


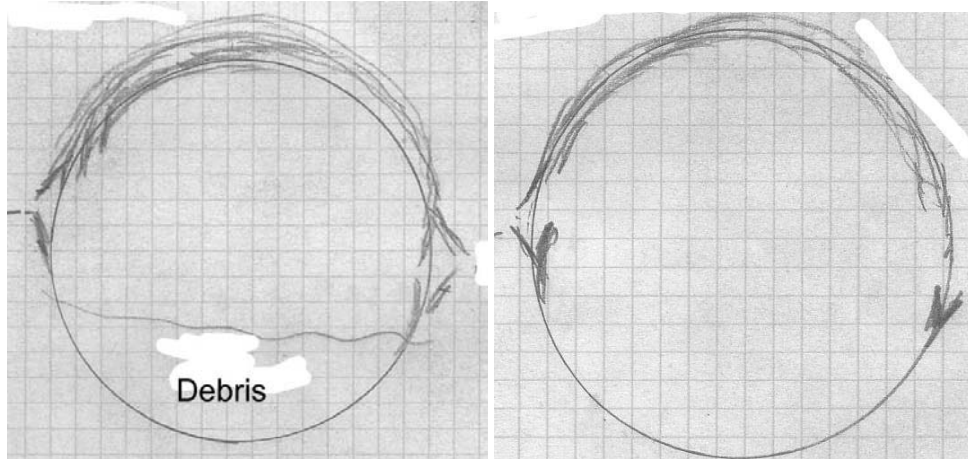
Figure F.3: Borehole: BDB-1, Diameter:110 mm



(a) From 0 m to 0.5 m.

(b) Beyond 0.5 m.

Figure F.4: Borehole: BDB-2, Diameter:110 mm.



(a) From 0 m to 0.6 m.

(b) Beyond 0.6 m.

Figure F.5: Borehole: BDT-1, Diameter:150 mm.

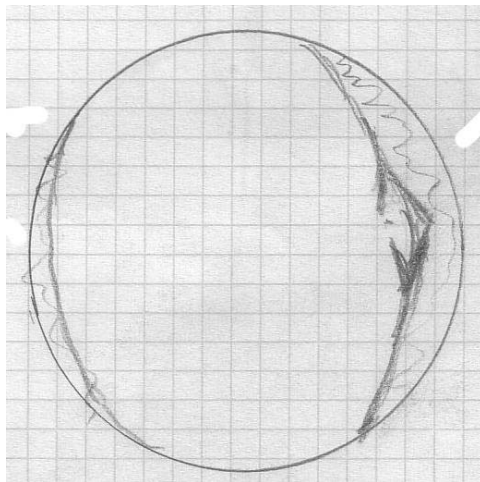


Figure F.6: Borehole: BDT-2, Diameter:95 mm

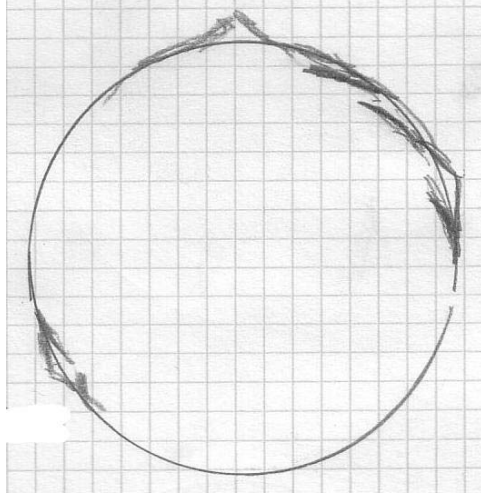


Figure F.7: Borehole: BED-B13, Diameter:110 mm

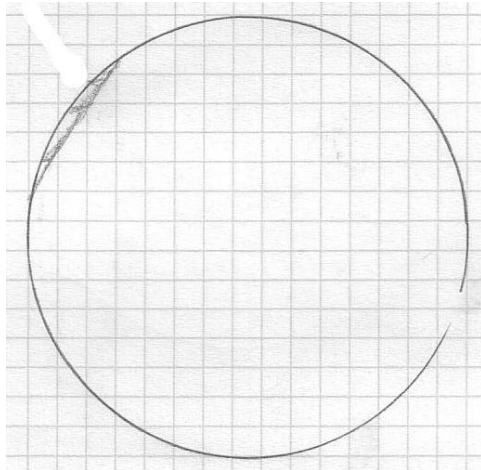
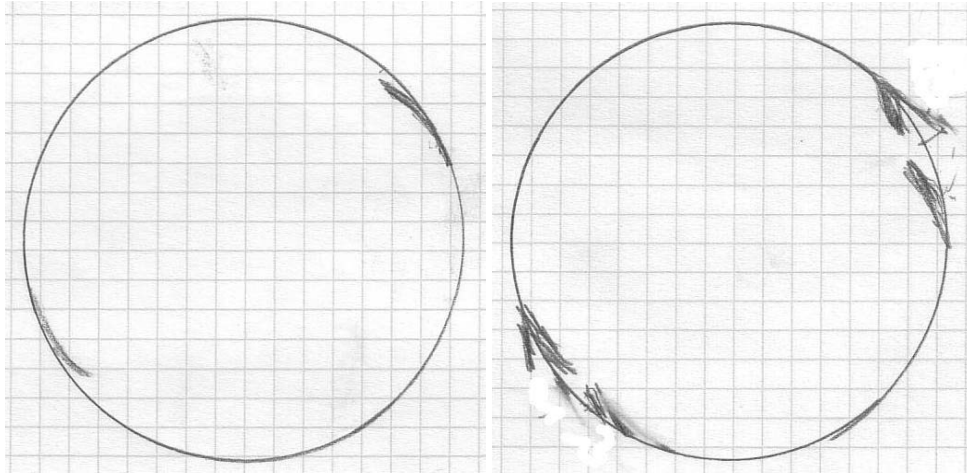


Figure F.8: Borehole: BED-C5, Diameter:110 mm



(a) From 0 m to 1 m.

(b) Beyond 1 m.

Figure F.9: Borehole: BED-C9, Diameter: 110 mm.

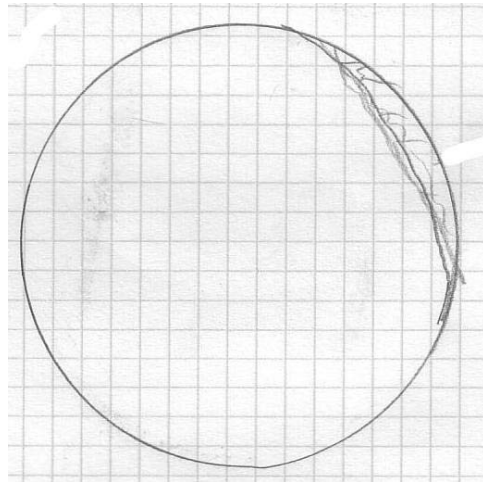


Figure F.10: Borehole: BED-C10, Diameter: 110 mm

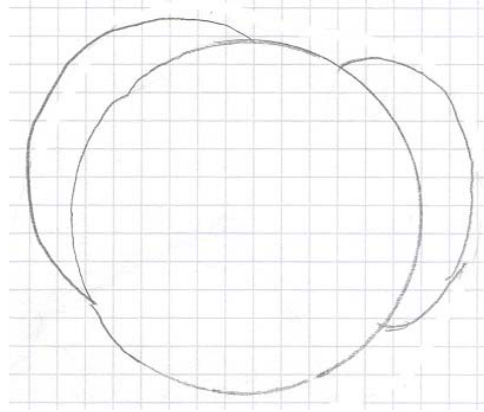
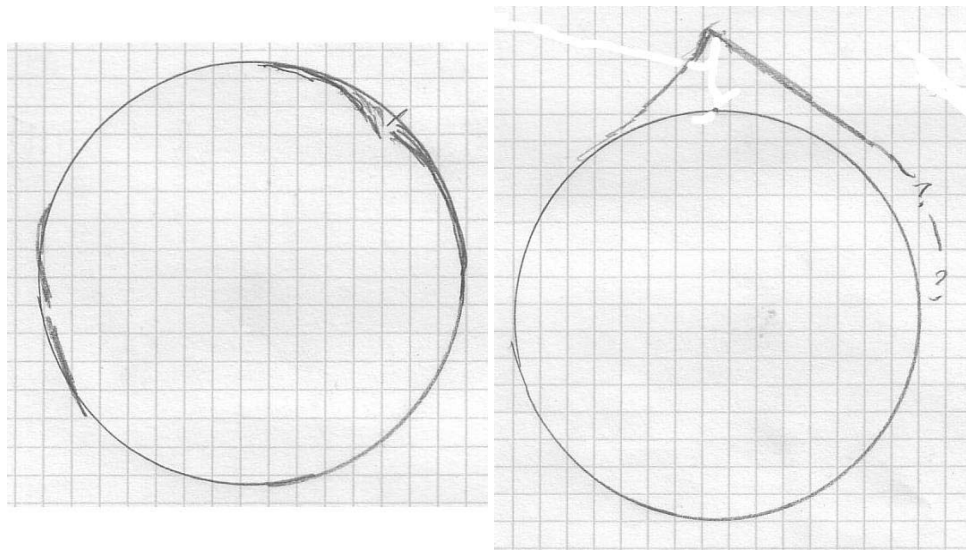


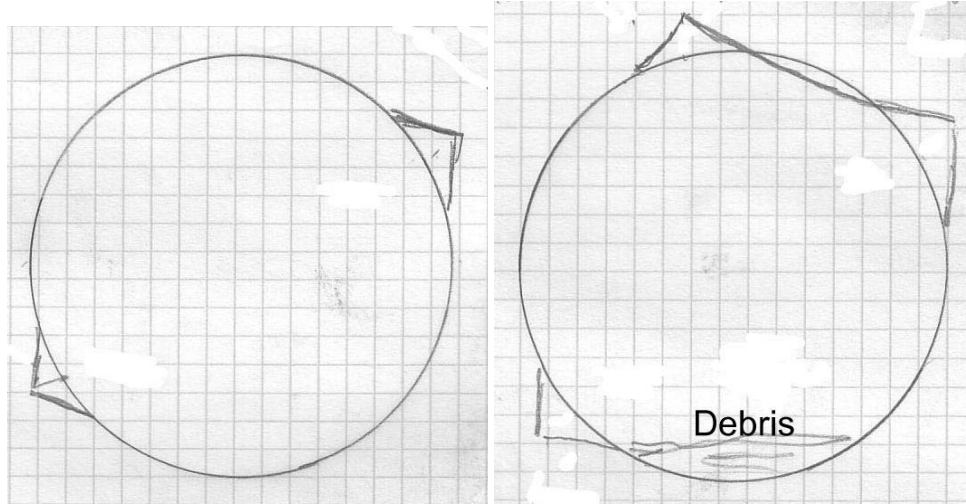
Figure F.11: Borehole: BEZ-A28, Diameter:110 mm



(a) From 0 m to 0.5 m.

(b) Beyond 0.5 m.

Figure F.12: Borehole: BFD-9, Diameter:250 mm.



(a) From 0 m to 0.7 m.

(b) Beyond 0.7 m.

Figure F.13: Borehole: BFD-B25, Diameter:250 mm.

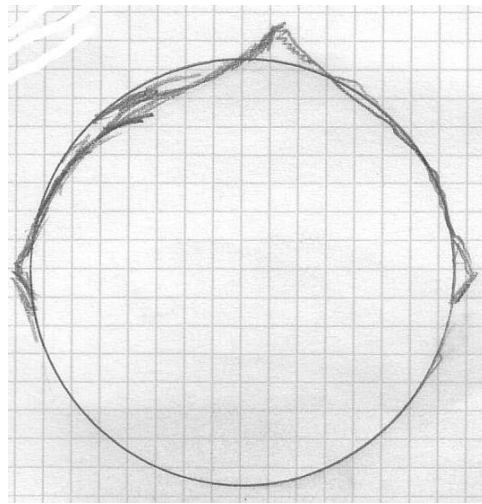


Figure F.14: Borehole: BFM-B2, Diameter:250 mm

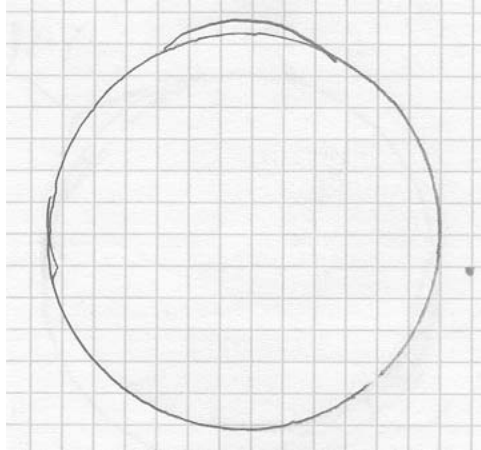


Figure F.15: Borehole: BFM-B6, Diameter:110 mm

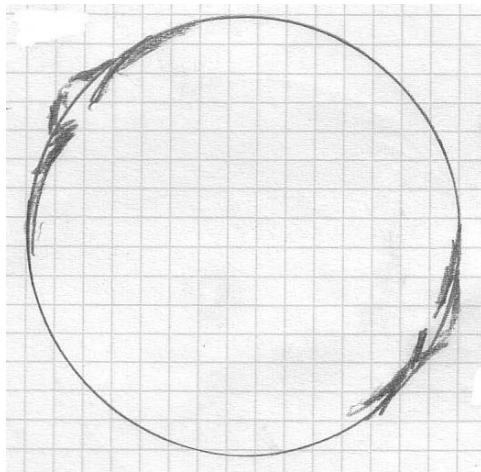
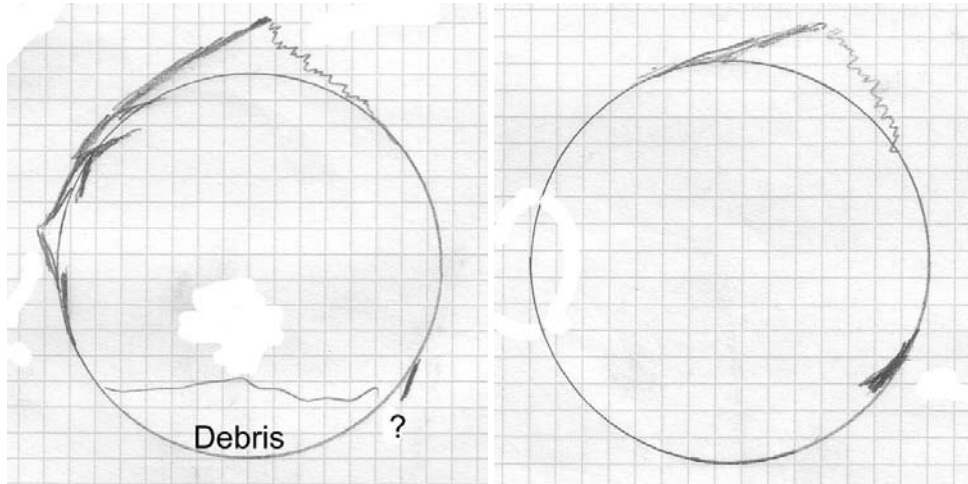


Figure F.16: Borehole: BFM-B8, Diameter:110 mm

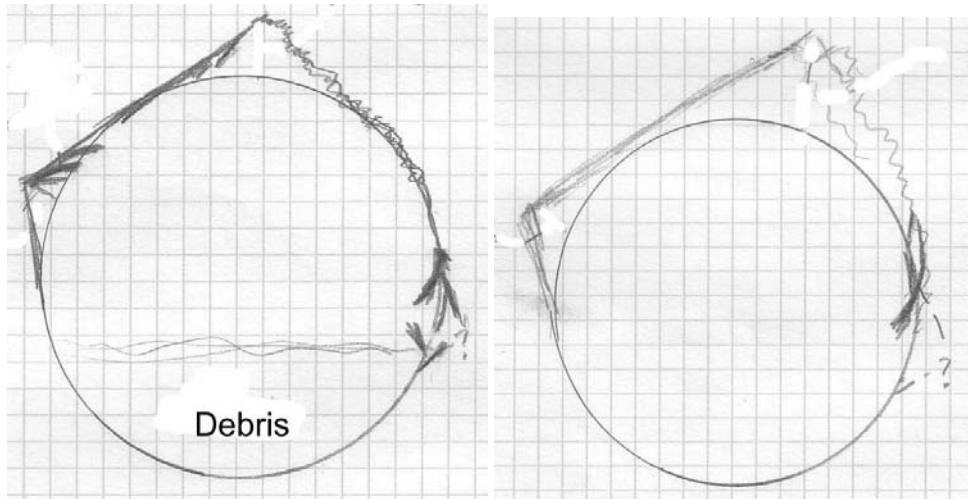




(a) From 0 m to 0.5 m.

(b) Beyond 0.5 m.

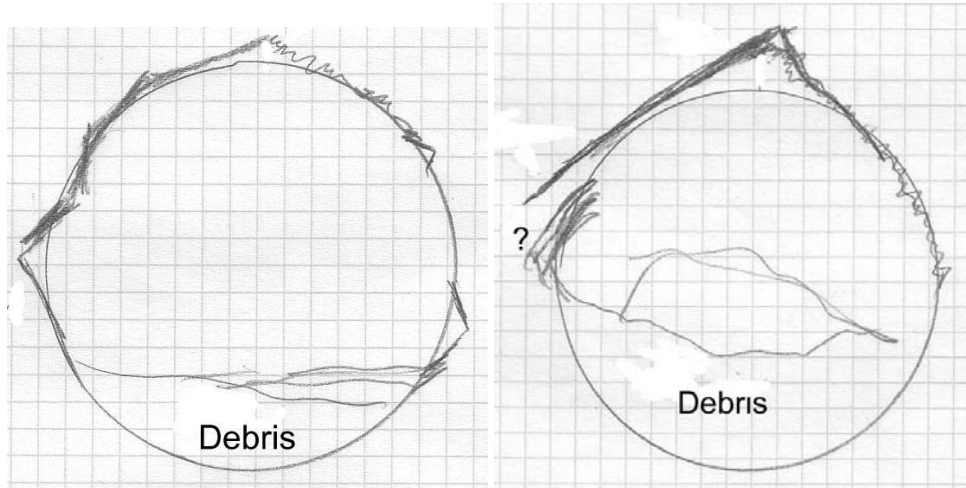
Figure F.17: Borehole: BFP-1, Diameter:250 mm.



(a) From 0 m to 1 m.

(b) Beyond 1 m.

Figure F.18: Borehole: BFP-3, Diameter:250 mm.



(a) From 0 m to 0.4 m.

(b) Beyond 0.4 m.

Figure F.19: Borehole: BFP-5, Diameter:250 mm.

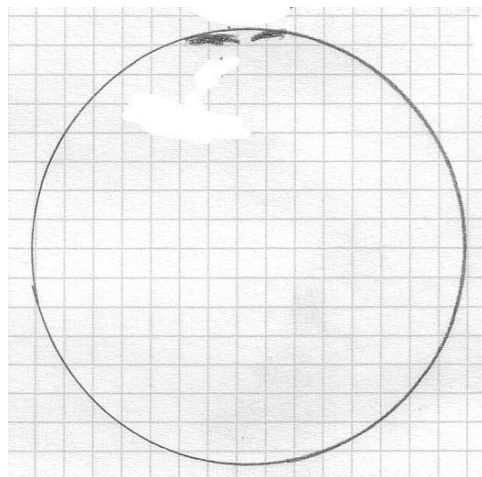


Figure F.20: Borehole: BFP-6, Diameter:250 mm

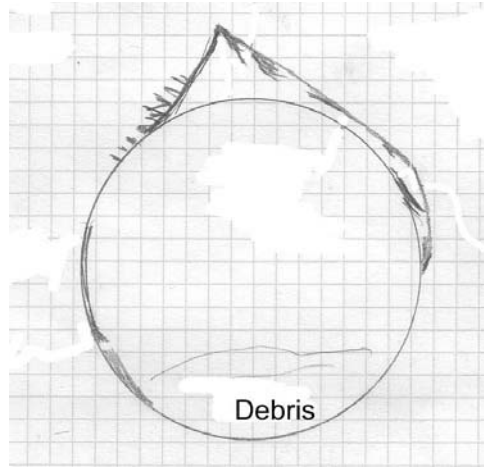


Figure F.21: Borehole: BFP-7, Diameter:250 mm

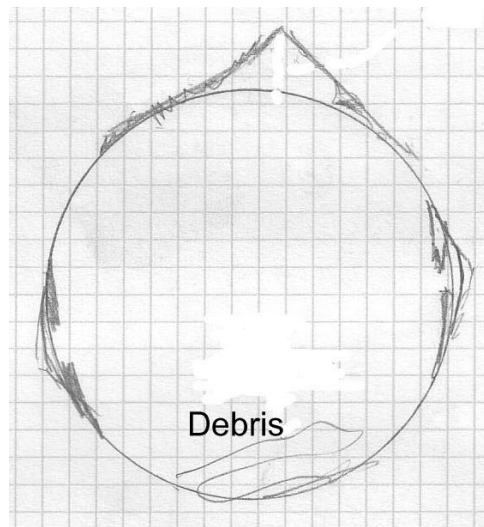


Figure F.22: Borehole: BFP-11, Diameter:250 mm

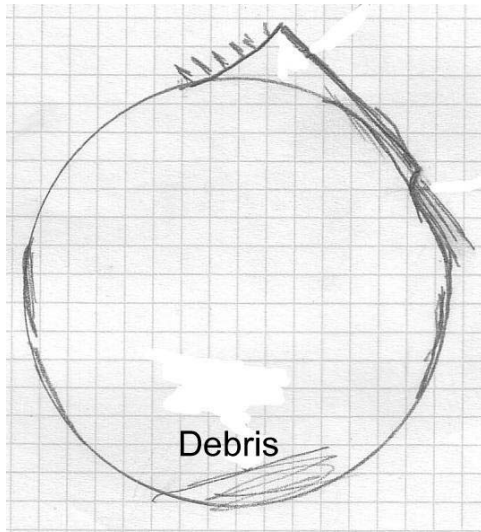


Figure F.23: Borehole: BFP-13, Diameter:250 mm

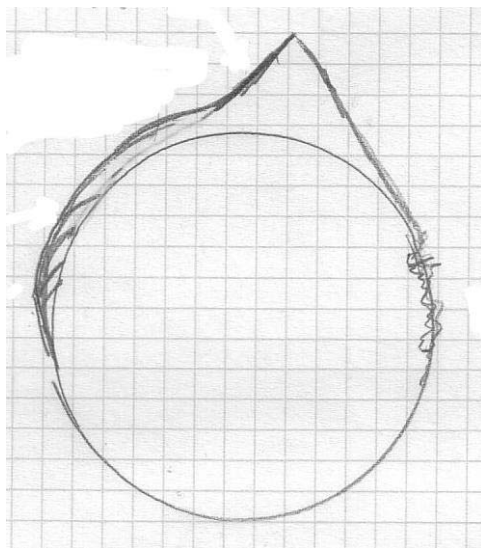
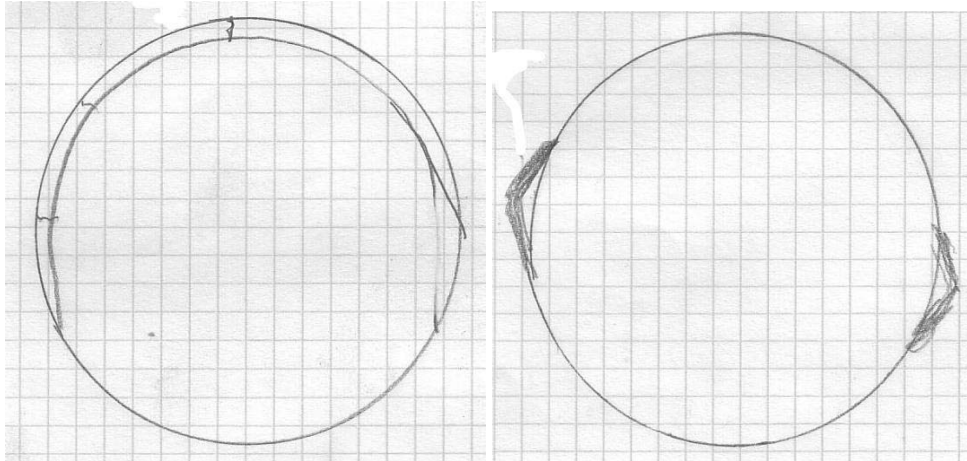


Figure F.24: Borehole: BFP-17, Diameter:250 mm



(a) From 0 m to 0.5 m.

(b) Beyond 0.5 m.

Figure F.25: Borehole: BIS-D8, Diameter: 110 mm.

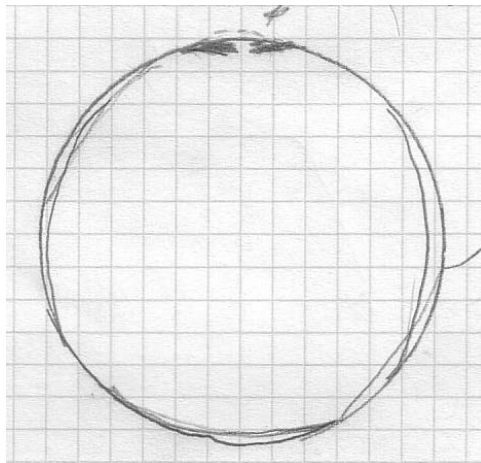


Figure F.26: Borehole: BLT-5, Diameter: 110 mm

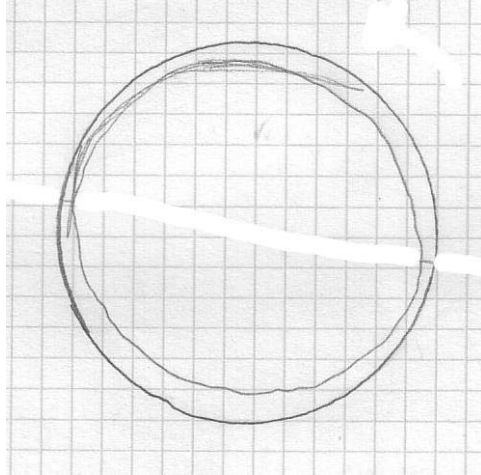
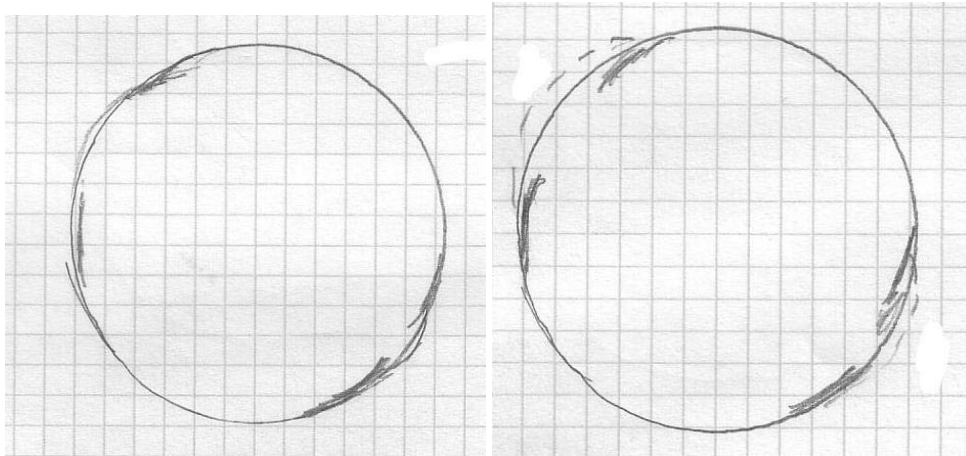


Figure F.27: Borehole: BLT-6, Diameter:110 mm



(a) From 0 m to 2 m.

(b) Beyond 2 m.

Figure F.28: Borehole: BLT-9, Diameter:110 mm.

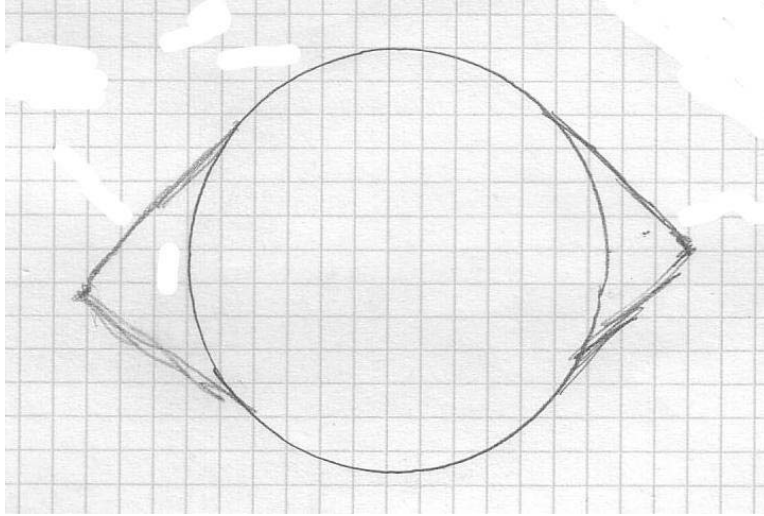


Figure F.29: Borehole: BPC-B3, Diameter:110 mm